NASA / CR—2001-210353

R2000AE114

Design, Fabrication, and Testing of an Auxiliary Cooling System for Jet Engines

Kevin Leamy and Jim Griffiths
GE Aircraft Engines, Cincinnati, Ohio

Paul Andersen, Fidel Joco, and Mark Laski
Honeywell, Inc., Torrance, California

January 2001

The NASA STI Program Office . . . in Profile

Since its founding, NASA has been dedicated to the advancement of aeronautics and space science. The NASA Scientific and Technical Information (STI) Program Office plays a key part in helping NASA maintain this important role.

The NASA STI Program Office is operated by Langley Research Center, the Lead Center for NASA's scientific and technical information. The NASA STI Program Office provides access to the NASA STI Database, the largest collection of aeronautical and space science STI in the world. The Program Office is also NASA's institutional mechanism for disseminating the results of its research and development activities. These results are published by NASA in the NASA STI Report Series, which includes the following report types:

- TECHNICAL PUBLICATION. Reports of completed research or a major significant phase of research that present the results of NASA programs and include extensive data or theoretical analysis. Includes compilations of significant scientific and technical data and information deemed to be of continuing reference value. NASA's counterpart of peer-reviewed formal professional papers but has less stringent limitations on manuscript length and extent of graphic presentations.

- TECHNICAL MEMORANDUM. Scientific and technical findings that are preliminary or of specialized interest, e.g., quick release reports, working papers, and bibliographies that contain minimal annotation. Does not contain extensive analysis.

- CONTRACTOR REPORT. Scientific and technical findings by NASA-sponsored contractors and grantees.

- CONFERENCE PUBLICATION. Collected papers from scientific and technical conferences, symposia, seminars, or other meetings sponsored or cosponsored by NASA.

- SPECIAL PUBLICATION. Scientific, technical, or historical information from NASA programs, projects, and missions, often concerned with subjects having substantial public interest.

- TECHNICAL TRANSLATION. English-language translations of foreign scientific and technical material pertinent to NASA's mission.

Specialized services that complement the STI Program Office's diverse offerings include creating custom thesauri, building customized data bases, organizing and publishing research results . . . even providing videos.

For more information about the NASA STI Program Office, see the following:

- Access the NASA STI Program Home Page at ***http://www.sti.nasa.gov***

- E-mail your question via the Internet to help@sti.nasa.gov

- Fax your question to the NASA Access Help Desk at 301–621–0134

- Telephone the NASA Access Help Desk at 301–621–0390

- Write to:
  NASA Access Help Desk
  NASA Center for AeroSpace Information
  7121 Standard Drive
  Hanover, MD 21076

NASA / CR—2001-210353

R2000AE114

Design, Fabrication, and Testing of an Auxiliary Cooling System for Jet Engines

Kevin Leamy and Jim Griffiths
GE Aircraft Engines, Cincinnati, Ohio

Paul Andersen, Fidel Joco, and Mark Laski
Honeywell, Inc., Torrance, California

Prepared under Contract NAS3–27395

National Aeronautics and
Space Administration

Glenn Research Center

January 2001

Available from

NASA Center for Aerospace Information
7121 Standard Drive
Hanover, MD 21076
Price Code: A09

National Technical Information Service
5285 Port Royal Road
Springfield, VA 22100
Price Code: A09

Available electronically at http://gltrs.grc.nasa.gov/GLTRS

Preface

In 1994, NASA began to investigate high-risk, high-payoff activities under the Advanced Concepts program. This report details the technical efforts of the GE Aircraft Engines and AlliedSignal (now Honeywell) team to design, fabricate, and test a jet engine auxiliary cooling system that expands the use of ordinary jet fuel as a heat sink. This activity was funded by the NASA Lewis Research Center (now NASA Glenn) under Contract NAS3–27395. Mr. Jeffrey Balser is the NASA Contracting Officer Technical Representative.

This report has been prepared in *Limited Rights* and *Industry* versions: Data and information deemed subject to *Limited Exclusive Rights* restrictions are omitted from the *Industry Version.*

Table of Contents

Table of Contents (Continued)

Table of Contents (Concluded)

List of Illustrations

List of Illustrations (Continued)

List of Illustrations (Continued)

List of Illustrations (Concluded)

List of Tables

Acronyms and Abbreviations

ACEP	Active cooling for enhanced performance
ACM	Air cycle machine
CBC	Coke-barrier coating
CDP	Compressor-discharge pressure (or plane)
ECM	Engine-cooling mode
ECS	Environmental control system
HPT	High-pressure turbine
HX	Heat exchanger
IRP	Intermediate-rated power
NCM	Nozzle-cooling mode
SCF	Specific fuel consumption (lbm/hr/lbf)
SLS	Sea-level static
T_C	Critical temperature

1.0 Summary

The ability to provide engine cooling air at temperatures well below conventional levels offers the opportunity to enhance aircraft and engine performance. Aircraft survivability can be improved by using the subcooled cooling air to reduce exhaust nozzle surface temperatures. Improved hot-section cooling offers the potential to increase engine specific thrust, enhance component life, mitigate combustor emissions, and reduce the need for advanced materials.

A turbocooler was designed, fabricated, and tested to provide cooled cooling air in either the exhaust nozzle or engine hot-section cooling modes. The turbocooler produces cooled cooling air by compressing main engine bleed air in an air cycle machine (ACM), cooling the ACM compressor discharge air in a fuel/air heat exchanger, and then further cooling the air as it expands across the ACM turbine. After functioning as coolant, the hot fuel is burned in the main engine combustor. Coke-barrier coating is used in the fuel system to allow the coolant-fuel to be heated beyond conventional temperatures in order to increase the useable heat-sink capacity of ordinary jet fuel.

The turbocooler system performance was successfully demonstrated in an integrated rig test and a separate ACM component test. The integrated rig test produced exhaust nozzle cooling air from 200° to –7°F. The fuel injection and combustion system provided stable operation with conventional liquid fuel and with high-temperature fuel up to 732°F — a maximum heat sink capacity of 360 Btu/s. There was no observed change in combustor dynamics or exit temperature profile and no evidence of flashback or autoignition due to hot fuel. Unburned hydrocarbons and carbon monoxide emissions were reduced 50% with hot fuel. The heat exchanger and fuel nozzles operated as predicted and were visually clean after the test.

The engine-cooling mode (ECM) configuration was successfully demonstrated during the ACM component test. The ECM test produced subcooled engine hot-section-cooling air at 524°F at simulated takeoff conditions. — approximately 400°F below conventional levels. In addition, the modified ACM air bearing thermal-protection configuration was successfully validated.

2.0 Introduction

The ability to provide engine cooling air at temperatures well below conventional cooling air sources offers opportunities to enhance aircraft and engine performance in a variety of ways. Cooling air, at temperatures well below fan discharge, can be used more effectively for engine exhaust nozzle system cooling to improve survivability. Improved engine hot-section cooling (a) permits higher core gas temperatures to increase engine specific thrust (at constant material temperatures), (b) enhances component life due to improved cooling, (c) reduces the need for advanced materials, and (d) improves combustor emissions by incorporating prevaporized fuel and/or reducing liner cooling/ dilution air. The key to improvements in these areas is enabling a significant increase in available heat sink capacity to produce sufficient quantities of cold air at the right pressures. The increased heat-sink capability with conventional jet fuels, typically limited to 300°F, is enabled by GE development of coke-barrier coating (CBC). CBC eliminates the deleterious effects of coke buildup and reduces gum adhesion in fuel systems.

The objective of this research program was to design, fabricate, and rig test an engine auxiliary cooling system that uses standard jet fuel as the primary heat sink. The first task defined the auxiliary cooling system (or turbocooler) and component requirements. A turbocooler consists of three primary components: (1) a high-temperature air cycle machine (ACM) driven by engine compressor discharge air, (2) a fuel/air heat exchanger that transfer energy from the hot air to the fuel, and (3) a high-temperature fuel injection system. The turbocooler cycle was integrated with an F404 engine cycle and designed for dual-mode capability. Dual-mode capability refers to the ability of the turbocooler component to operate in a nozzle-cooling mode (NCM) configuration or an engine cooling mode (ECM) configuration. The second task of the program completed the detailed design and fabrication of the turbocooler hardware. Integration and rig testing of the turbocooler system configured in the NCM, with the F404 full-annular combustor, was completed during task 3.

The full-scale integrated rig test demonstrated the ability of the turbocooler to generate pressurized, cooled cooling air; effectively transfer energy from the hot air to the jet fuel; and efficiently burn the hot fuel in a full-annular combustor. This project increased technical credibility in four areas: (1) high-temperature ACM, (2) direct fuel/air heat exchange (with CBC application in the heat exchanger), (3) high-temperature fuel injection system, and (4) combustion of high-temperature fuel in a full-annular combustor.

3.0 Component Design and Fabrication

3.1 Turbocooler System Design

3.1.1 Turbocooler System Description

The ability to provide engine cooling air at temperatures well below conventional cooling air sources offers opportunities to enhance aircraft and engine performance in a variety of ways. Cooling air, at temperatures well below fan discharge air, can be used for engine exhaust nozzle system cooling to improve survivability. Improved engine hot-section cooling permits: (1) higher core gas temperatures to increase engine specific thrust (at constant material temperatures), or (2) enhanced component life due to improved cooling, or (3) reduced need for advanced materials. The key to achieving improvements in these areas is enabling a significant increase in available heat sink capacity to produce sufficient quantities of cold air at the right pressures. Using fuel as the heat sink is the most efficient approach because the energy used to heat the fuel is returned to the cycle and thus avoids the negative performance impact associated with fan bypass air pressure drop when a fan duct air-to-air heat exchanger (HX) is used. GE development of coke-barrier coating provides the necessary increase in the heat sink capacity of conventional jet fuels (typically limited to 300°F).

The key objective of this research program was to design, fabricate, and rig test an engine auxiliary cooling system that uses standard jet fuel as the primary heat sink. An auxiliary cooling system, or turbocooler, consists of three primary components:

1. A high-temperature air cycle machine driven by engine compressor discharge air
2. A fuel/air heat exchanger that transfers energy from the hot air to the fuel
3. A high-temperature fuel injection system

The turbocooler performs a simple thermodynamic refrigeration cycle.

Exhaust Nozzle Cooling Mode – In the NCM mode shown in Figure 1, the ACM compresses engine bleed air and sends it the fuel/air heat exchanger where the air is cooled by rejecting heat to the fuel. The air is then further cooled as it expands across the ACM turbine, powering the ACM compressor. The ACM turbine discharge air is used to cool low-pressure components such as the engine exhaust system.

Engine Cooling Mode – In the ECM shown in Figure 2, the main engine compressor bleed air separately supplies the ACM compressor and turbine. This dual-stream arrangement enables the flows to be adjusted separately to power-balance the ACM while maintaining sufficient pressure to introduce the cooled cooling air into the gas turbine engine. The fuel/air heat exchanger cools only the ACM compressor discharge air. The ACM compressor boosts the pressure above the engine compressor discharge pressure (CDP) for cooling the high-pressure section of the engine: the last stages of the engine compressor, the combustor, and the high-pressure turbine. This configuration provides cooling air for rotating and static structures such as the blades, vanes, shafts, disks, and seals. In the engine cooling mode configuration, the turbocooler produces cold air at pressures greater than engine CDP and hundreds of degrees cooler than CDP air. The ACM turbine stream is not precooled; therefore, the turbine exit air, at temperatures comparable to conventional interstage compressor bleed air temperatures, can be used for cooling the low-pressure turbine.

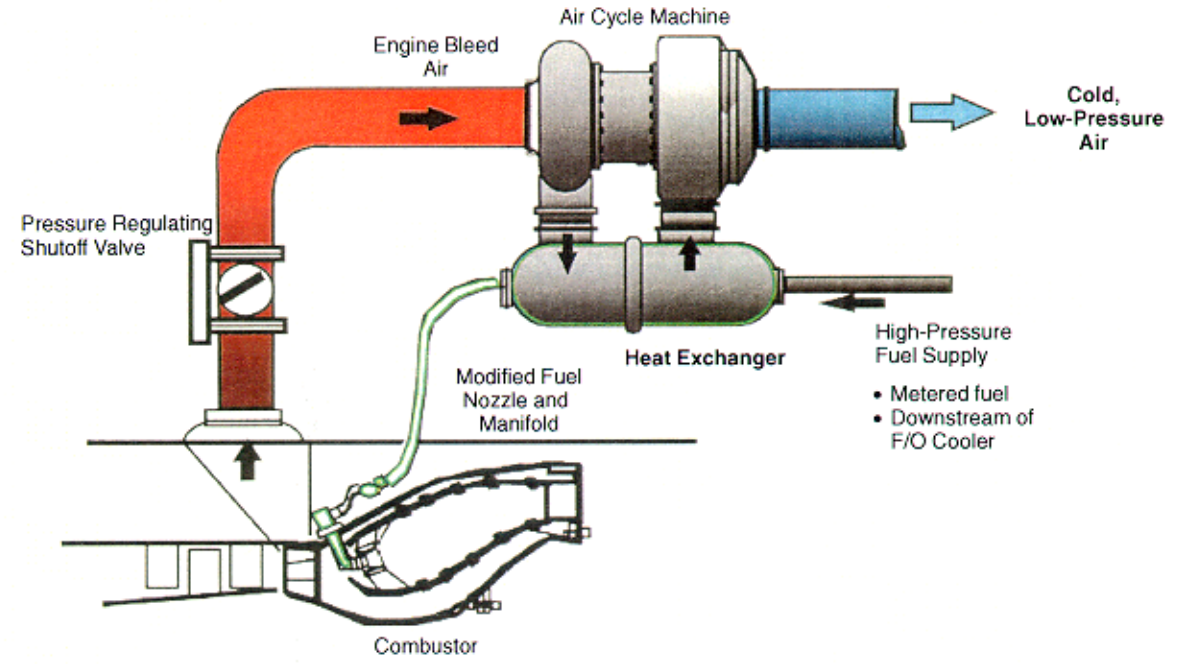

Figure 1. Turbocooler System Configured in a Nozzle-Cooling Mode (NCM)

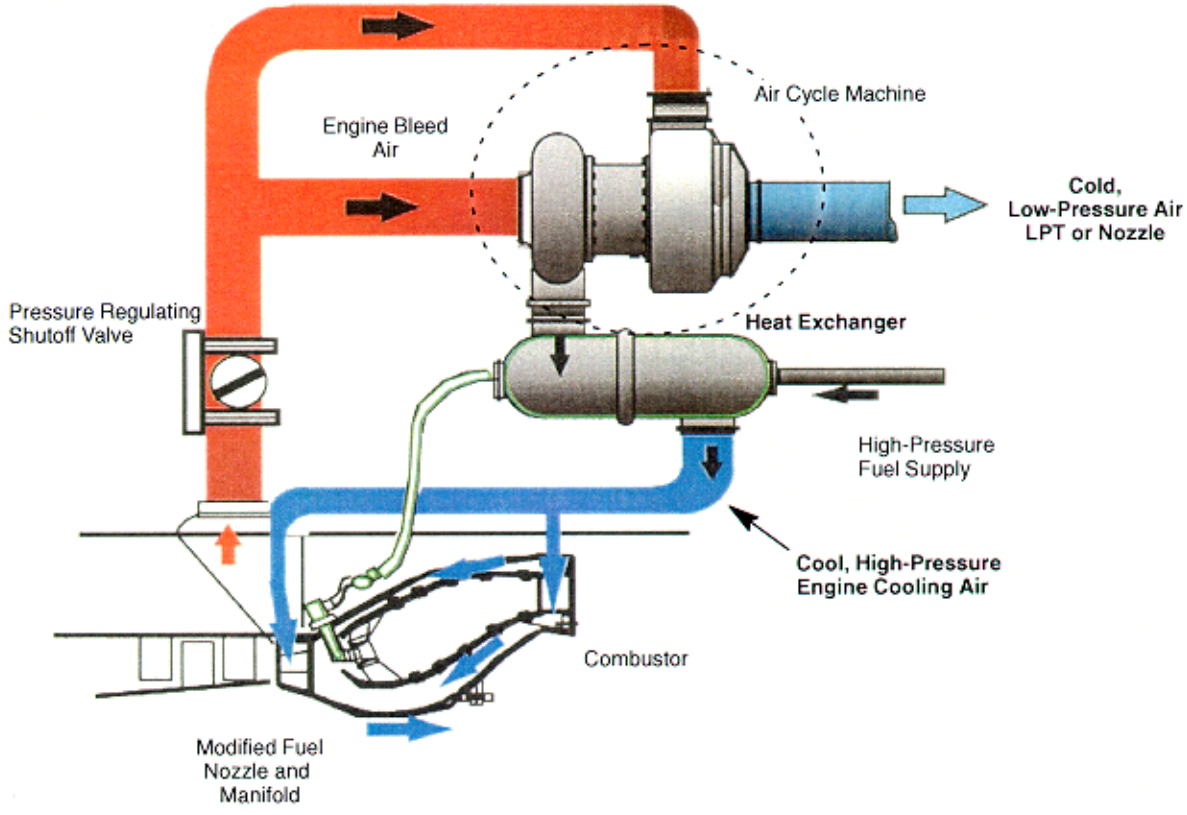

Figure 2. Turbocooler System Configured in a Engine-Cooling Mode (ECM)

3.1.2 Turbocooler System Design Criteria

The turbocooler system technical requirements are established on the basis of the following criteria:

- The turbocooler system must be capable of dual-mode operation. Dual-mode capability refers to the ability of the turbocooler components to operate in either an NCM configuration or an ECM configuration. This primarily dictates the air-side pressure drop through the heat exchanger.
- The ACM air bearing coolant supply is limited to 300°F (current production air bearing limitations). This is accomplished by extracting heat exchanger discharge air for bearing cooling and modulating turbocooler inlet pressure to limit flow to levels consistent with the required coolant temperature.
- The cooled cooling air must be returned to the engine at acceptable pressure in order to overcome any system air-side pressure losses and avoid icing conditions at the ACM turbine discharge.
- Fuel temperature was initially limited to approximately 650°F in order to minimize the changes to the F404 fuel system. However, early in the design phase it was decided to use the full fuel heat sink in order to maximize the amount of available cooling air. The maximum fuel temperature is driven beyond supercritical (> 772°F). The implications of this "high flow" design decision are discussed in Subsection 3.1.3.
- ACM power level is limited to 500 horsepower by the decision to employ an existing ACM aerodynamic and journal bearing designs for the demonstration.
- The system is sized at the design point to use available engine bleed air pressure (avoid pressure regulation) in order to minimize the ACM turbomachinery size and provide the maximum possible pressure drop for the heat exchanger air-side (typically the controlling factor in sizing the core) and for distribution of cooling air to the nozzle and expansion in the turbine.

3.1.3 High Flow Turbocooler System Impact

Increasing the fuel heat sink to include supercritical fuel provides additional nozzle cooling air. Exhaust nozzle heat transfer analysis indicated that increasing the turbocooler airflow rate would have a more significant effect than decreasing the air temperature. A greater portion of the divergent flap surface temperature was reduced below the target T_{Sbase} of 300°F. Therefore, it was decided to significantly increase the turbocooler delivery airflow rate. The implications of increasing the airflow rate are:

- Maximum fuel temperature is increased beyond critical temperature (T_c = 772°F) and may approach 900° to 1000°F.
- A larger air cycle machine is needed to accommodate the increased airflow (an F–15 class ACM versus F–16 class).
- Increased ACM horsepower is needed.
- ACM bearing cooling temperature must be increased to control heat exchanger growth.

- Larger fuel/air heat exchanger and structural complications are required due to the high fuel system pressures.
- Higher system pressure losses are induced in the exhaust nozzle cooling circuit.
- The operating envelope is more restricted due to the increased fuel temperature and the desire to maintain the basic F404 fuel nozzle features.

The high-flow turbocooler NCM configuration was ultimately tested on the F404 combustor rig.

3.1.4 Turbocooler System Model Development

Numerical representations of the turbocooler components were developed from existing component libraries and integrated into a steady-state, stand-alone, turbocooler model. The model features included:

- F–15 ACM performance maps, rotor dynamics, and recirculating air bearing cooling circuit and heat loads
- Heat exchanger performance characteristics and first-order transient lag
- High-temperature fuel system characteristics
- Exhaust nozzle cooling circuit pressure loss representation
- Engine bleed port losses and necessary pressure regulation
- Complete JP fuel thermodynamic properties

The model can be run in either exhaust nozzle or turbomachinery cooling mode. The turbocooler power balance is established in the following manner (exhaust cooling mode):

1. Once the fuel temperature limit is set, turbocooler airflow is initially established for a specific flight condition. Since the turbocooler uses fuel as the heat sink, the fuel flow delivered to the engine can be used to cool only a specific amount of air before the fuel temperature limit is reached. Turbocooler component requirements are defined from the engine cycle/interface conditions, air- and fuel-side pressure losses, and the design constraints previously noted.
2. The ACM turbine back pressure is defined by the exhaust nozzle cooling circuit. The exhaust nozzle cooling circuit, developed under a complementary program, is numerically represented by the flow curve presented in Figure 3. The exhaust nozzle cooling circuit pressure loss is plotted against the inlet flow function.
3. The ACM turbine inlet temperature is limited to 300°F — the maximum air bearing cooling supply temperature. The air bearing cooling flow is approximately 5% of the turbine inlet air. Roughly 50% of the bearing cooling air is restored at the ACM compressor inlet; the remaining portion is returned at the ACM turbine. The first two items, along with ACM mechanical efficiency and ACM turbine discharge temperature, set the power across the ACM turbine.
4. The heat exchanger air-side pressure drop must be acceptable for both exhaust nozzle cooling and engine cooling mode. A detailed engine cooling circuit is not being designed under the turbocooler program, but the cooling air must be

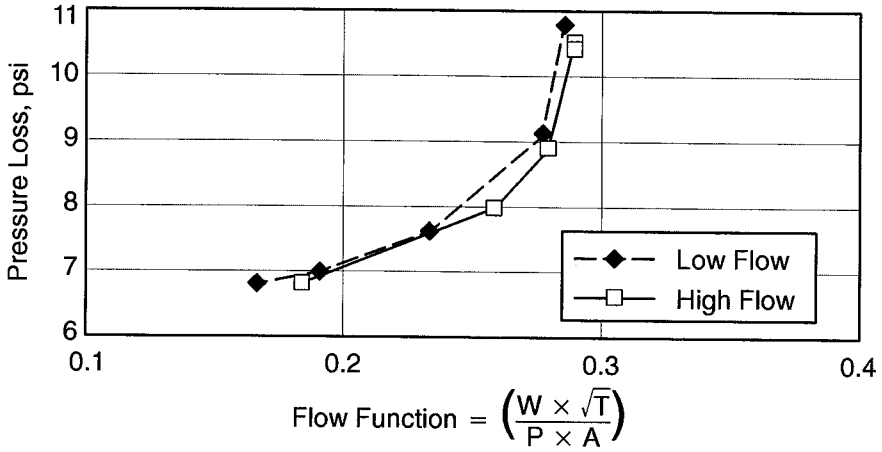

Figure 3. Exhaust Nozzle Cooling Circuit Flow Characteristic

returned to the engine at least 7.5% greater than the compressor discharge pressure. This pressure level is consistent with previous engine cooling studies.

5. The ACM compressor discharge pressure is established from the turbine and heat exchanger pressures. The compressor inlet conditions are set based on available horsepower (across the turbine). An engine compressor discharge bleed valve is incorporated to regulate the ACM supply pressure.
6. The engine power level angle (PLA) determines the engine fuel flow rate. At high fuel flow rates, the fuel delivery pressure is raised to accommodate the increased ΔP across the fuel nozzle due to the fuel density shift and to avoid two-phase flow during low-power applications.

The stand-alone turbocooler model was integrated into the F404 transient cycle model featuring:

- Combined engine and turbocooler power balancing across the flight envelope
- Existing ACM compressor and turbine maps
- Preliminary control algorithm to adjust engine bleed pressure
- ACM rotor dynamics and heat exchanger thermal lag
- Detailed modified F404 fuel nozzle characteristics

3.1.5 Summary of the Integrated Turbocooler Cycle Study Results

The combined F404 engine and turbocooler cycle model was run in the exhaust nozzle cooling mode configuration over the flight points of interest. The model iterations were set to maximize the turbocooler air delivered to the exhaust nozzle cooling system within the design constraints previously described.

3.1.5.1 Key Design Decisions for the Turbocooler Test Rig

A number of key design decisions were made regarding turbocooler system test configuration.

1. The full fuel heat sink capacity was used. The resulting system changes include:
   - Increasing the maximum fuel temperature beyond the fuel critical temperature (772°F).
   - Maximizing the amount of air available for exhaust nozzle cooling or engine cooling modes. For exhaust cooling, this translated into an additional 50° to 200°F surface-temperature reduction.
   - Increasing the air cycle machine from an F–16 class to an F–15 class (larger flow, diameter, and horsepower).
   - Enlarging the fuel/air heat exchanger.
2. The turbocooler heat exchanger was a conventional tube-and-shell design in order to minimize manufacturing and schedule risks.
3. Fuel flowed over the tubes and air flowed through the tubes. This provides the added benefit of being able to more readily verify the coating process and enhance safety. Potential fuel leaks can be detected.
4. The turbocooler rig test employed a slow start-up transient to minimize thermal differentials.
5. The F–15 air cycle machine aerodynamic design was used without any trimming or scaling. This minimized any ACM performance risk and schedule.
6. The modifications to the F404 fuel injectors was minimized to maintain compatibility with the test rig and reduce technical and schedule risk.
7. A high-temperature barrier filter was incorporated downstream of the turbocooler heat exchanger to protect the fuel nozzle flow divider valve.
8. The turbocooler test envelope was restricted due fuel nozzle operability limits. Again the primary concerns was to avoid vaporization in the secondary circuit and reduce the maximum fuel pressure required at high power.

3.1.5.2 Nozzle Cooling Mode (NCM)

Key aspects of the NCM configuration include:

- Cold air (5–6% of the main engine compressor flow rate) was supplied to the exhaust nozzle at all flight conditions studied.
- Exhaust nozzle heat transfer analysis indicated that 1/3 of the divergent metal surface temperatures were 300°F or more below baseline surface temperatures.
- At military power (maximum nonafterburning) steady-state fuel temperatures approached 950°F.
- Transient analyses indicate that sufficient control over fuel temperature and manifold pressure was effected by the control system using fuel temperature and pressure measurements to adjust the turbocooler air supply. However, due to the increased fuel temperature (lower density), the available operating envelope was more restrictive with the modified F404 fuel nozzle.

- No changes were made to the F404 control system to optimize performance with the turbocooler operating. The model did not account for any thrust benefit for introducing the cooling air upstream of the exhaust nozzle throat. Consequently, the cycle incurs a performance penalty (specific fuel consumption and thrust) due to the increased engine bleed flow.

The turbocooler cycle performance prediction at sea level static (SLS)/military intermediate-rated power (IRP) is presented in Figure 4 — which illustrates component performance characteristics, bleed air modulation, and ACM bearing cooling-flow distribution.

The effects of the amount of engine bleed air modulation (or pressure regulation) on the turbocooler power balance were also evaluated. At SLS the engine bleed (Figure 4) air is modulated approximately 25% in order to limit ACM power to approximately 500 hp. Decreasing bleed air modulation to 21.6% increases the available cooling air by about 6% but also raises the ACM power requirements to 576 hp — exceeding the design limit.

The turbocooler cycle performance for a typical altitude condition (30,000-ft, Mach 0.9, IRP) is presented in Figure 5. At altitude, ACM horsepower is not an issue. In this case, the quantity of available cooling air to the exhaust nozzle is increased 29% by setting the bleed valve full open. All of the fuel heat sink is used.

3.1.5.3 Engine Cooling Mode

The combined F404 engine and turbocooler cycle model was run in the ECM configuration over the flight points of interest. The model iterations were set to maximize the turbocooler air delivered to the engine hot-section cooling system but within the design constraints previously described. This analysis was limited to aerothermal study only; no additional detailed heat transfer or mechanical analyses were conducted.

Two approaches to engine hot-section cooling were explored. The first approach evaluated potential life enhancements by reducing high-pressure turbine (HPT) blade metal temperature while holding thrust constant. In this study the conventional turbine blade cooling air was replaced with subcooled turbocooler air. This approach is the basis of the *Active Cooling for Enhanced Performance* (ACEP) dual-mode design criteria. The results from the ECM (life enhancement) analysis indicate that a 250°F reduction in HPT blade metal temperature is achievable at comparable engine thrust levels, with a 2.5% specific fuel consumption (SFC) penalty associated with the separate ACM turbine air stream.

The second approach was to push the engine power level (thrust) while maintaining a constant HPT blade metal temperature. Again the HPT blade cooling air is replaced with the subcooled turbocooler air. The results of this ECM study (throttle push) indicate:

- 6% to 8% takeoff thrust increase without major engine changes.
- 4% increase in SFC.

It should be noted that this was strictly an analytical aerothermal study. Evaluation of the throttle push cases at constant HPT blade temperatures resulted in excessive engine shaft torque, reduced stability margins, and higher temperatures downstream of the HPT. The key message from the engine cooling mode study is that turbocooler air can be used to either significantly enhance engine hot-section life or throttle-push the engine.

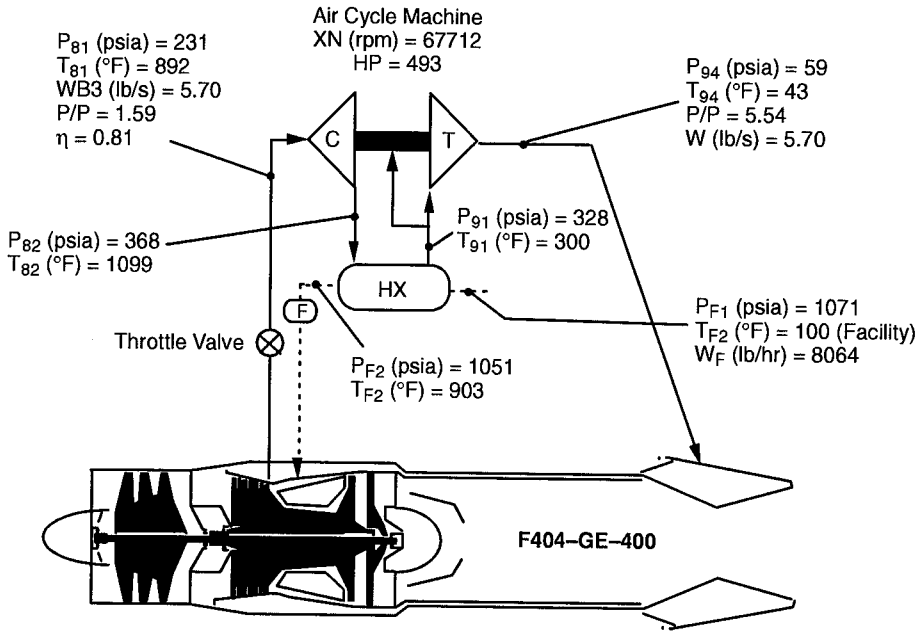

Figure 4. Turbocooler Predicted Performance at Sea Level Static, IRP

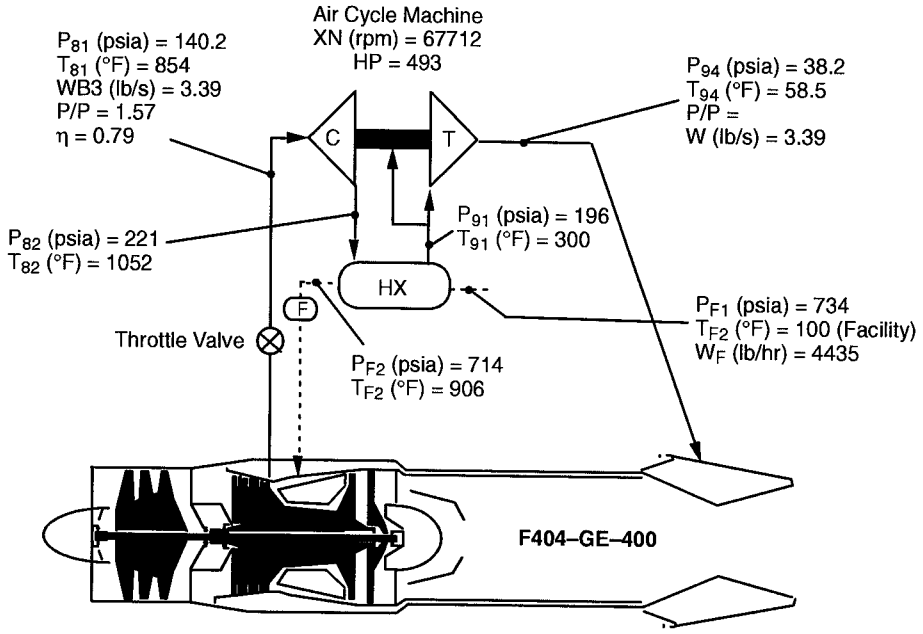

Figure 5. Turbocooler Predicted Performance at 30,000-ft, Mach 0.8, IRP

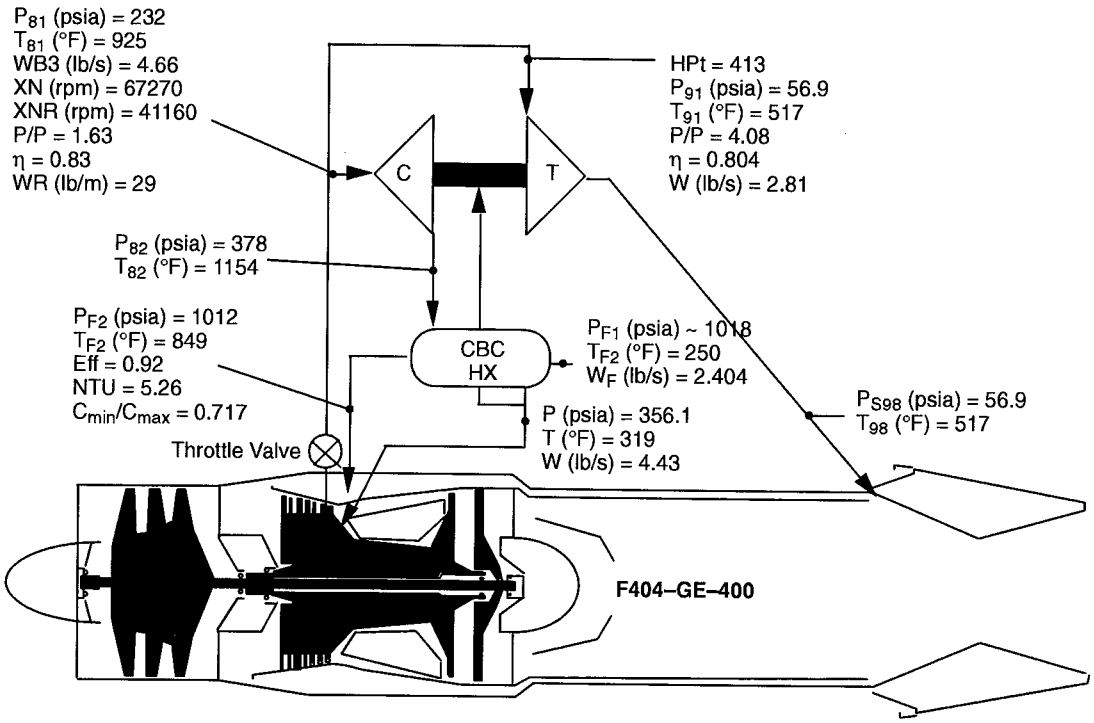

Figure 6. Turbocooler Predicted Performance in the Engine Cooling Mode at SLS/IRP

The turbocooler performance prediction in the engine cooling mode at SLS/IRP is presented in Figure 6. For engine cooling, the bleed air is divided into two streams: one for the compressor and the other for the turbine. The compressor discharge air is cooled by the fuel/air heat exchanger before it is returned to the high-pressure section of the engine. The turbine air is used to power-balance the turbocompressor and is returned to the engine cycle through the exhaust nozzle cooling circuit. Figure 6 shows the impact of modulating both the compressor inlet air and the turbine inlet air in order to maintain the ACM neat 500 hp. Note that the engine bleed air is modulated to limit the ACM horsepower to less than 500-hp.

The next sections describe the detail design of the key turbocooler components.

3.2 Air Cycle Machine Design

The F–15 environmental control system (ECS) ACM aerodynamic design was suitable for use as the ACEP air cycle machine due to similar airflow and performance requirements. This reduced the technical risk associated with ACM development since the performance was well understood. Two ACM's were manufactured for the ACEP program — one fully instrumented with internal sensors and the other without internal sensors.

During the course of the ACEP program, several ACM failures occurred at AlliedSignal and at GEAE. These failures prompted two design modifications. The first enhanced start capability and the second addressed compressor journal bearing cooling flow. Only the original compressor journal bearing cooling flow configuration was tested at GEAE. The modified bearing cooling flow configuration was successfully tested at AlliedSignal in both cooling modes (nozzle and engine).

This section describes the detailed design analyses associated with the original bearing cooling configuration and, later, the design modifications.

3.2.1 ACM Description

The ACEP ACM is a turbocompressor that functions as a cooling turbine in the ACEP turbocooler system. In conjunction with an advanced air-to-fuel heat exchanger and a high-temperature fuel system, this ACM supplies cold pressurized air for cooling exhaust nozzle or engine hot-section components. The ACM will be integrated into the complete turbocooler assembly and tested with the full-annular F404 combustor.

The single-stage ACEP ACM turbocompressor rotor is supported by air-cooled foil bearings in the radial as well as the axial direction. The design consists of existing geometry (F–15 ECS ACM) radial wheels such as a centrifugal compressor impeller and a radial inflow turbine. The compressor relies on a vaned diffuser for dynamic pressure recovery and the turbine (a 50% reaction machine) uses a drilled conical nozzle ring. The stationary diffuser and nozzle ring are designed to contain wheel tri-hub bursts at overspeed conditions. A cross section of the machine is shown in Figure 7.

Limited Rights information has been omitted from this Industry-Version report.

Figure 7. ACEP Air Cycle Machine Cross Section (Modified ACM Bearing Configuration)

3.2.1.1 ACM Performance

The ACEP ACM uses the F–15 ECS ACM aero design "as is" with the exception of reducing the number of turbine blades from 20 to 18 to accommodate manufacturing difficulties associated with machining the turbine wheel. Manufacturing difficulties arose due to the use of stronger, more temperature-resistant material. It was anticipated that this change would have a negligible impact on turbine performance, and that assumption was latter verified during the ACM acceptance test. The F–15 performance characteristics satisfy the specified operating requirements very well, yielding excellent efficiencies and an adequate compressor stall margin. Basic compressor and turbine performance are shown in Figures 10, 11, and 12. The ACEP ACM specific performance operating at the three exhaust cooling points, as well as the engine cooling mode point, is given in Table 1.

Table 1. ACEP ACM Predicted Performance

Parameter	Exhaust System Cooling			Engine Cooling
	Sizing Point	Test Point E	Test Point C	Test Point G
Compressor Inlet Pressure (P_{1C}) psia	215	221	149	212
Compressor Discharge Press (P_{2C}) psia	355	337	266	354
Engine Bleed Air Temperature, °F	923	923	872	923
Compressor Inlet Temperature (T_{1C}), °F	908	910	859	902
Compressor Discharge Temp (T_{2C}), °F	1141	1118	1122	1134
Engine Bleed Flow Required (W_e), lb/min	329.8	332.4	237.8	240.1
Compressor Inlet Flow (W_C), lb/min	338.4	340.8	244.8	250.2
Compressor Efficiency (η_C)	0.786	0.752	0.808	0.823
Turbine Inlet Pressure (P_{1T}), psia	333	316	249	212
Turbine Discharge Pressure (P_{2T}), psia	54	53.5	38.6	39.4
Turbine Inlet Temperature (T_{1T}), °F	377	285	434	923
Turbine Discharge Temperature (T_{2T}), °F	81	25	116	496
Turbine Discharge Flow (W_T), lb/min	329.8	332.4	237.8	164.3
Turbine Efficiency (η_T)	0.880	0.880	0.880	0.822
Turbine Power (PW_T), hp	0518	0456	410	377
Mech. Efficiency (η_M)	0.979	0.979	0.975	0.972
Overall Efficiency ($\eta_C \times \eta_T \times \eta_M$)	0.677	0.648	0.693	0.658
Turbine Speed (N), rpm	70,950	67,580	74,460	67,910
Note: Test Point E is the ground demonstration point; C is an altitude (flight) point.				

Table 1 shows the machine performance as affected by the internal cooling flow and the thrust bearing cooling flow return to the compressor inlet. Also taken into account is the mechanical efficiency associated with this air-bearing machine design.

Limited Rights information has been omitted from this Industry-Version report.

Figure 8. ACM Cooling Flow Connections (Original ACM Bearing Configuration)

Limited Rights information has been omitted from this Industry-Version report.

Figure 9. ACEP ACM, Exhaust Cooling Mode (Original ACM Bearing Configuration)

Nomenclature

N = Compressor Rotational Speed, rpm

P_{5T} = Compressor Inlet Air Total Pressure, in. Hg A

P_{6T} = Compressor Outlet Air Total Pressure, in. Hg A

T_5 = Compressor Inlet Air Temperature, °R

T_6 = Compressor Outlet Air Temperature, °R

W_C = Compressor Inlet Airflow Rate, lb/min

$\theta_5 = T_5/T_0$ (T_0 = 519°F)

$\delta_5 = P_{5T}/P_0$ [P_0 = 29.92 in Hg (Absolute)]

η_c = Compressor Adiabatic Efficiency, percent

$$\eta_c = \frac{100\,T_5}{(T_6 - T_5)}\left[\left(\frac{P_{6T}}{P_{5T}}\right)^{0.283} - 1\right]$$

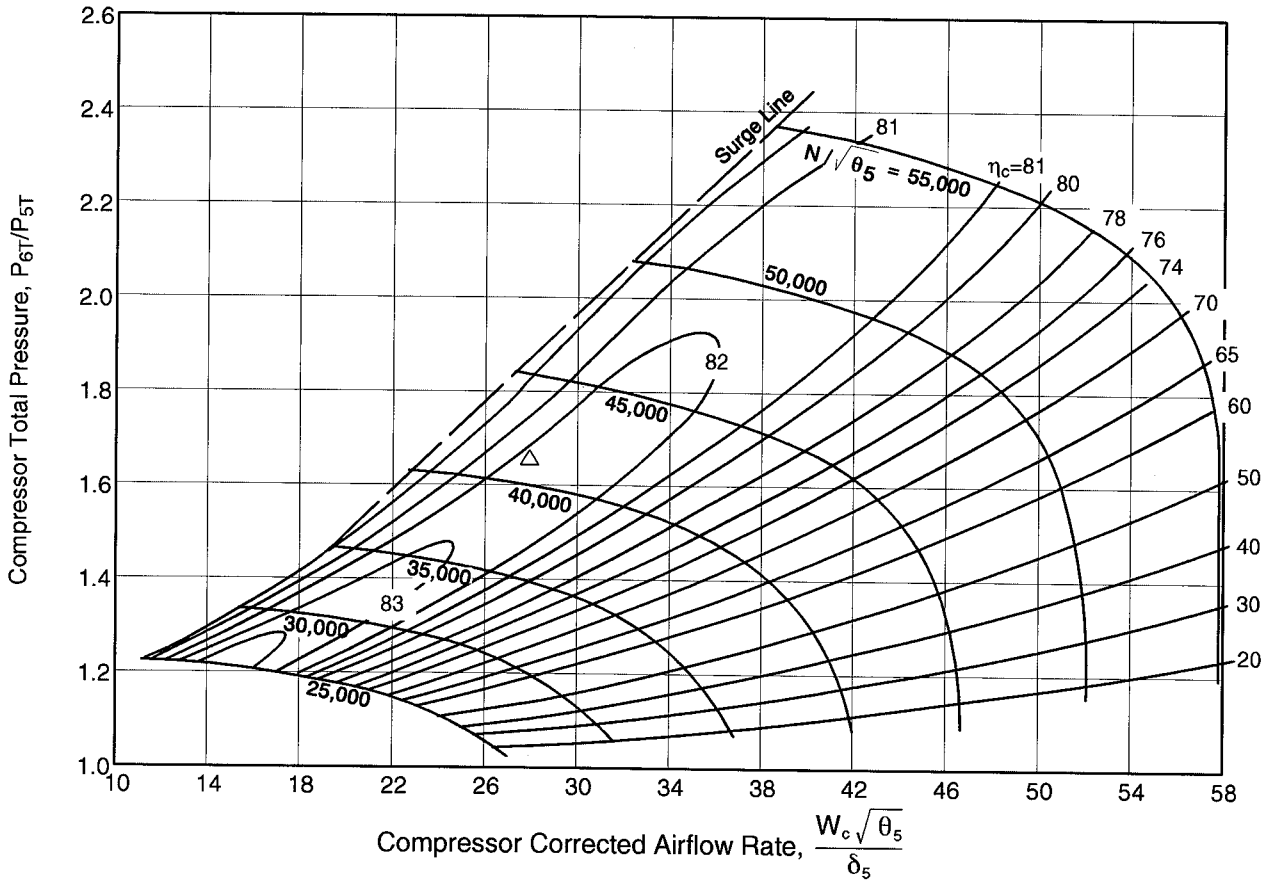

Figure 10. F–15 ECS ACM Compressor Performance

Nomenclature

N = Turbine Shaft Speed, rpm

P_{2T} = Turbine Inlet Air Total Pressure, in. Hg A

P_{3T} = Turbine Outlet Air Total Pressure, in. Hg A

T_2 = Turbine Inlet Air Temperature, °R

T_3 = Turbine Outlet Air Temperature, °R

$$\eta_t = \frac{T_2 - T_3}{T_2\left(\frac{Y}{Y+1}\right)} \times 100, \text{ percent} \qquad \text{Where } Y = \left[\left(\frac{P_{2T}}{P_{3T}}\right)^{0.283} - 1\right]$$

$$F_v = \frac{N}{3760\sqrt{\Delta T_1}} \qquad \text{Where } \Delta T_1 = T_2\left(\frac{Y}{Y+1}\right)$$

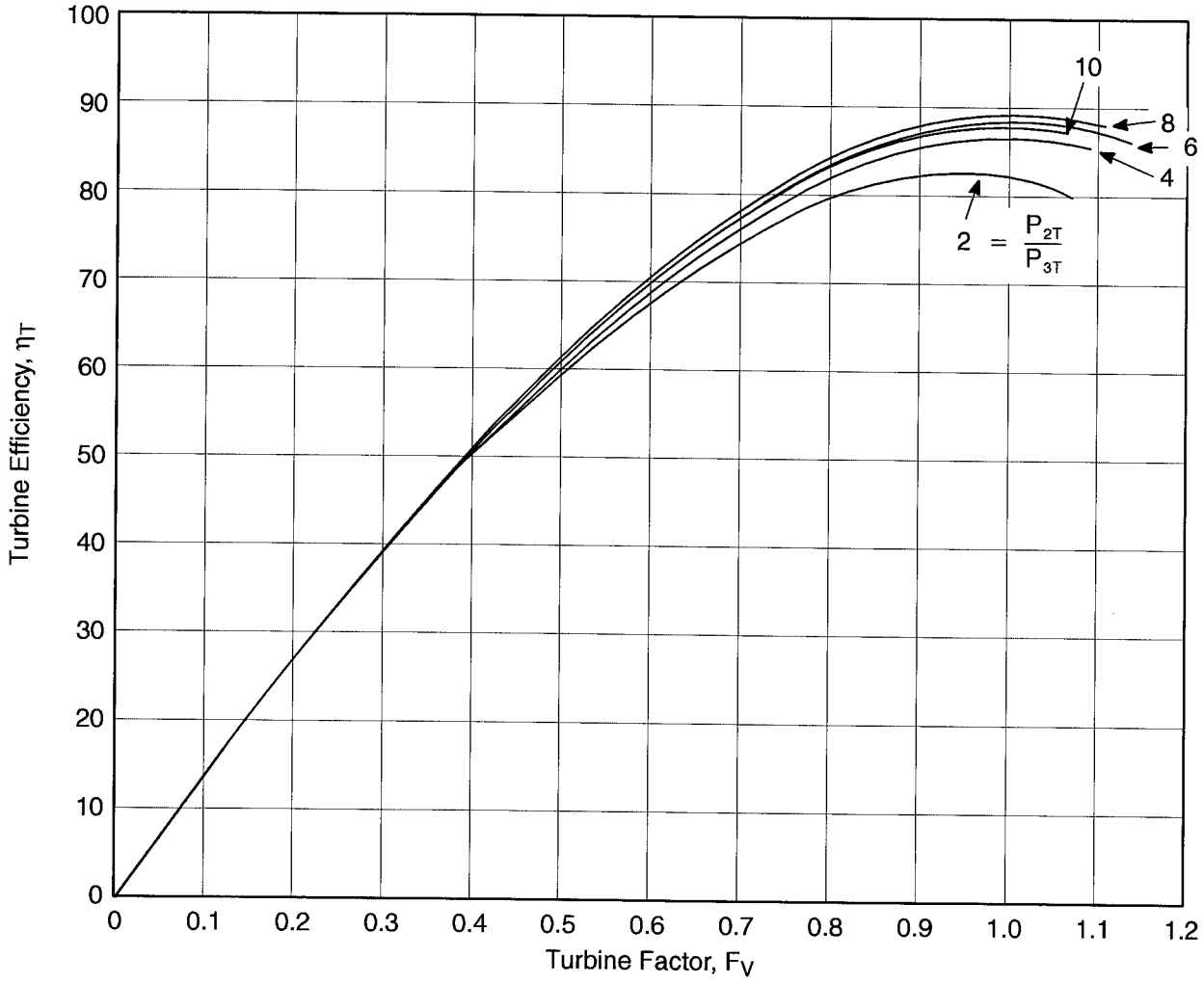

Figure 11. F–15 ECS ACM Turbine Performance

Nomenclature

$F_F = \frac{A_E}{A_N}$

A_E = Effective Nozzle Area, $in^2 = \frac{W_T\sqrt{T_2}}{15.64\ P_{2T}}$

Where: W_T = Turbine Inlet Airflow, lb per min

P_{2T} = Turbine Inlet Air Total Pressure, in. Hg A

T_2 = Turbine Inlet Air Temperature, °R

A_N = Nominal Effective Area, $in^2 = 0.98\ A_G$

A_N = 0.884 in^2 for Test Unit

A_G = Geometrical Nozzle Area, $in^2 = 0.902 \pm 0.012\ in^2$

P_{3T} = Turbine Outlet Air Total Pressure, in. Hg A

N = Turbine Shaft Speed, rpm

$\theta_2 = \frac{T_2}{519}$

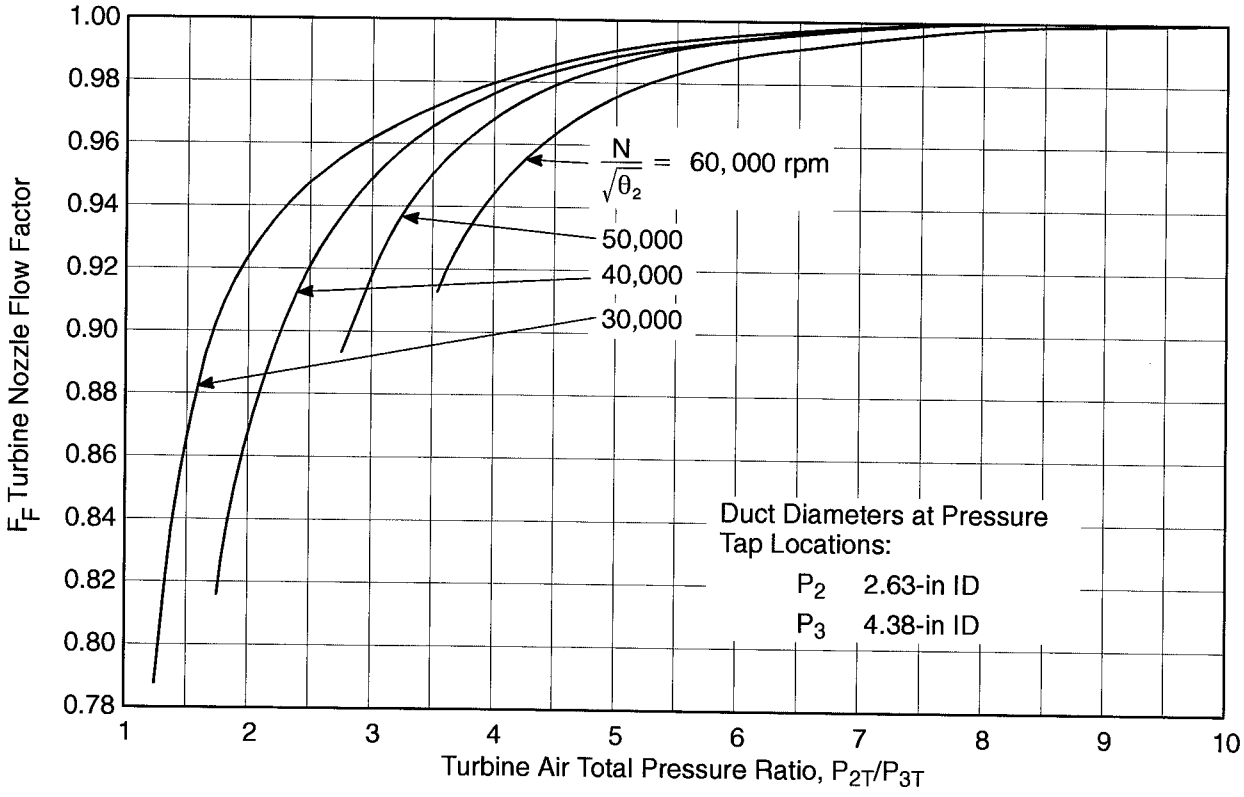

Figure 12. F–15 ECS ACM Turbine Nozzle Calibration

3.2.1.2 Bearing Power Loss and Cooling

Limited Rights information has been omitted from this Industry-Version report.

Table 2. ACEP Bearing and Bearing Cooling Data

Limited Rights information has been omitted from this Industry-Version report.

3.2.2 Thermal Analysis

The thermal design of the ACM consists of the following features:

Cooling of the gas bearings – Cooling air is provided for the journal and thrust bearings to maintain operating temperatures below safety limits dictated by the coating material of the bearing foil (650°F).

Cooling of the rotor/shaft – Adequate air is provided for cooling the rotor/shaft in the area between the hot wheel and the journal bearing. This will prevent bearing overheating during the soakback on shutdown.

Thermal insulation between the manifold and the housing – A high-strength/low-conductivity material (Mycalex) is applied between the hot manifold and the cold bearing housing to prevent the bearing housing from being heated during operation and soakback on shutdown.

Heat shield between wheel and housing – A thermal blanket made of extremely low thermal conductivity material (Min-K) is placed between the wheel and the housing to restrict heat energy radiating from the hot wheel to the adjacent housing.

3.2.2.1 Thermal Network Model

Limited Rights information has been omitted from this Industry-Version report.

3.2.2.2 Thermal Analysis Results

Steady-State Temperature Distributions of ACM – The steady-state temperature distributions of three operation modes (sizing point, altitude flight, and engine cooling) are presented respectively in Figures 14 through 16.

- The maximum temperatures of the manifold and the wheel occur in the sizing point mode on the compressor side, while on the turbine side they occur in the engine cooling mode. This is because the maximum gas temperatures of the compressor and the turbine occur at these operating modes.

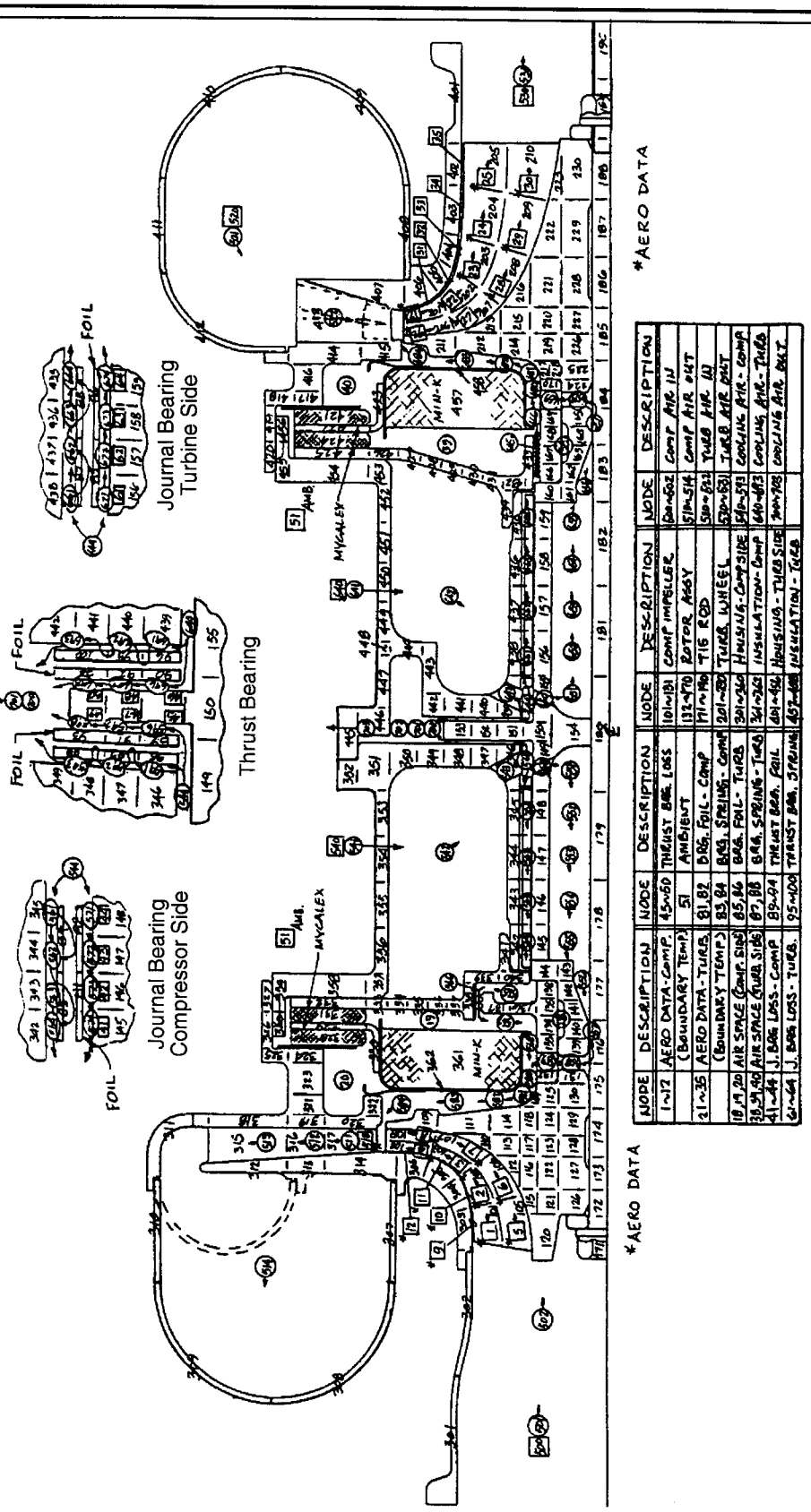

NODE	DESCRIPTION
1~12	AERO DATA - COMP.
	(BOUNDARY TEMP)
21~35	AERO DATA - TURB.
	(BOUNDARY TEMP.)
18,19,20	AIR SPACE (COMP. SIDE)
38,39,40	AIR SPACE (TURB. SIDE)
41~44	J. BRG. LOSS - COMP
61~64	J. BRG. LOSS - TURB.

NODE	DESCRIPTION
45~60	THRUST BRG. LOSS
51	AMBIENT
81,82	BRG. FOIL - COMP
83,84	BRG. SPRING - COMP
85,86	BRG. FOIL - TURB.
87,88	BRG. SPRING - TURB.
89~94	THRUST BEAR. FOIL
95~100	THRUST BRG. SPRING

NODE	DESCRIPTION
101~134	COMP IMPELLER
135~170	ROTOR ASSY
171~180	TIE ROD
201~220	TURB. WHEEL
301~320	HOUSING - COMP SIDE
321~340	INSULATION - COMP
401~436	HOUSING - TURB SIDE
437~488	INSULATION - TURB

NODE	DESCRIPTION
600~602	COMP. AIR. IN
513~514	COMP AIR. EXIT
530~532	TURB AIR IN
533~535	TURB. AIR. EXIT
510~512	COOLING AIR - COMP
660~663	COOLING AIR - TURB
700~705	COOLING AIR EXIT

Figure 13. Thermal Network Model, ACEP Turbocooler ACM

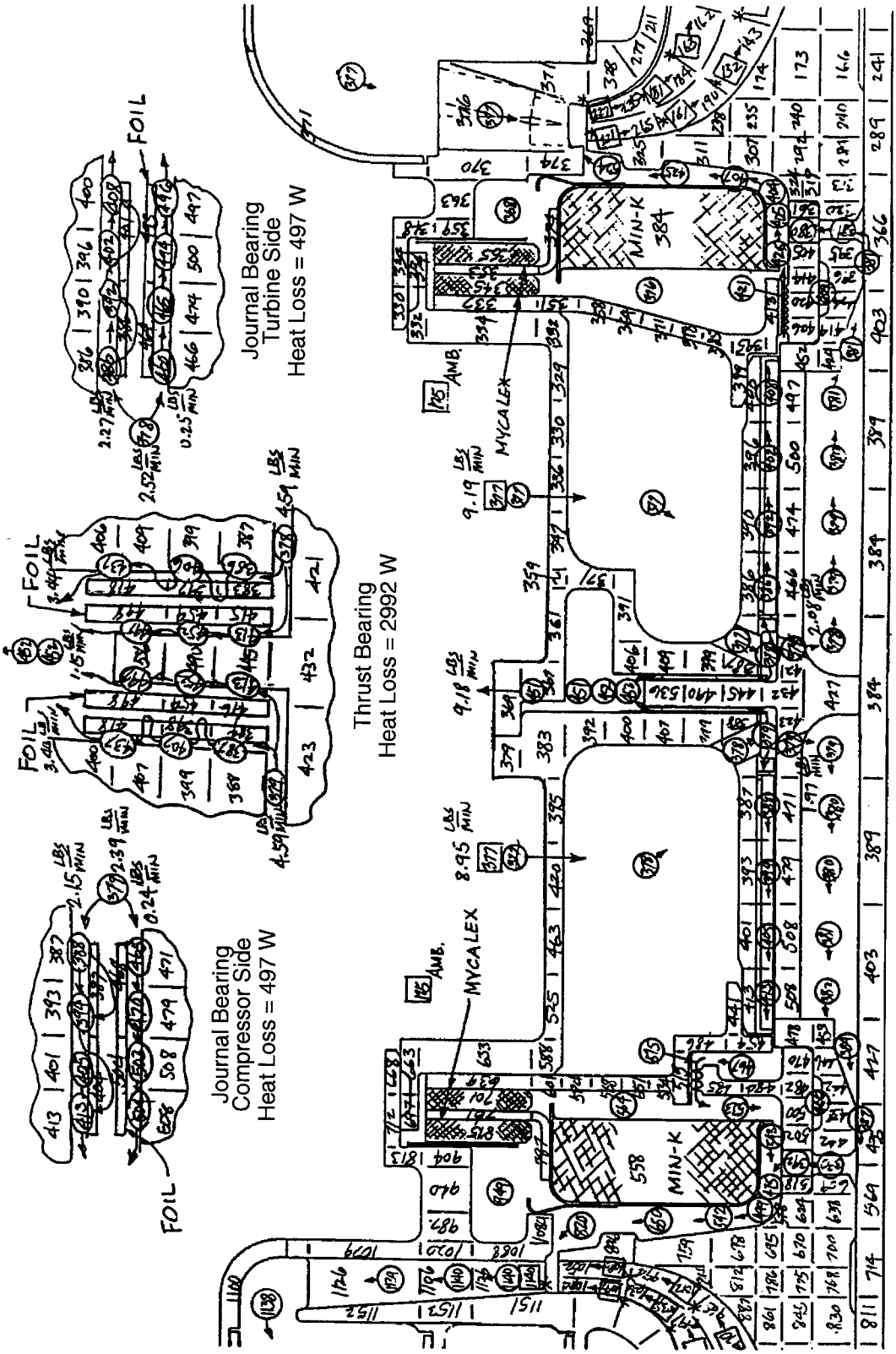

Figure 14. Steady-State Temperature Distribution (Degrees F), Sizing Point Mode

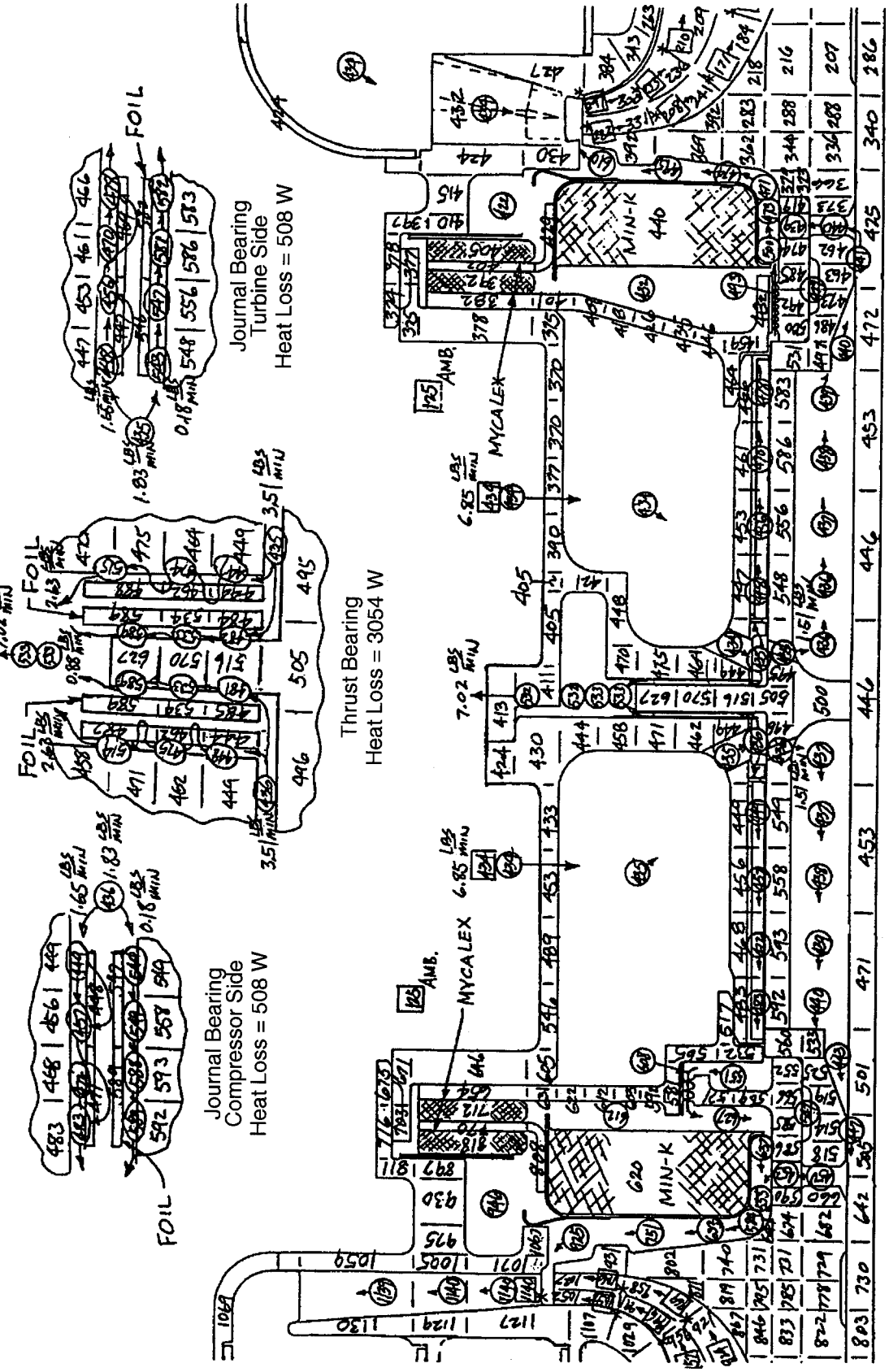

Figure 15. Steady-State Temperature Distribution (Degrees F), Altitude Flight Mode

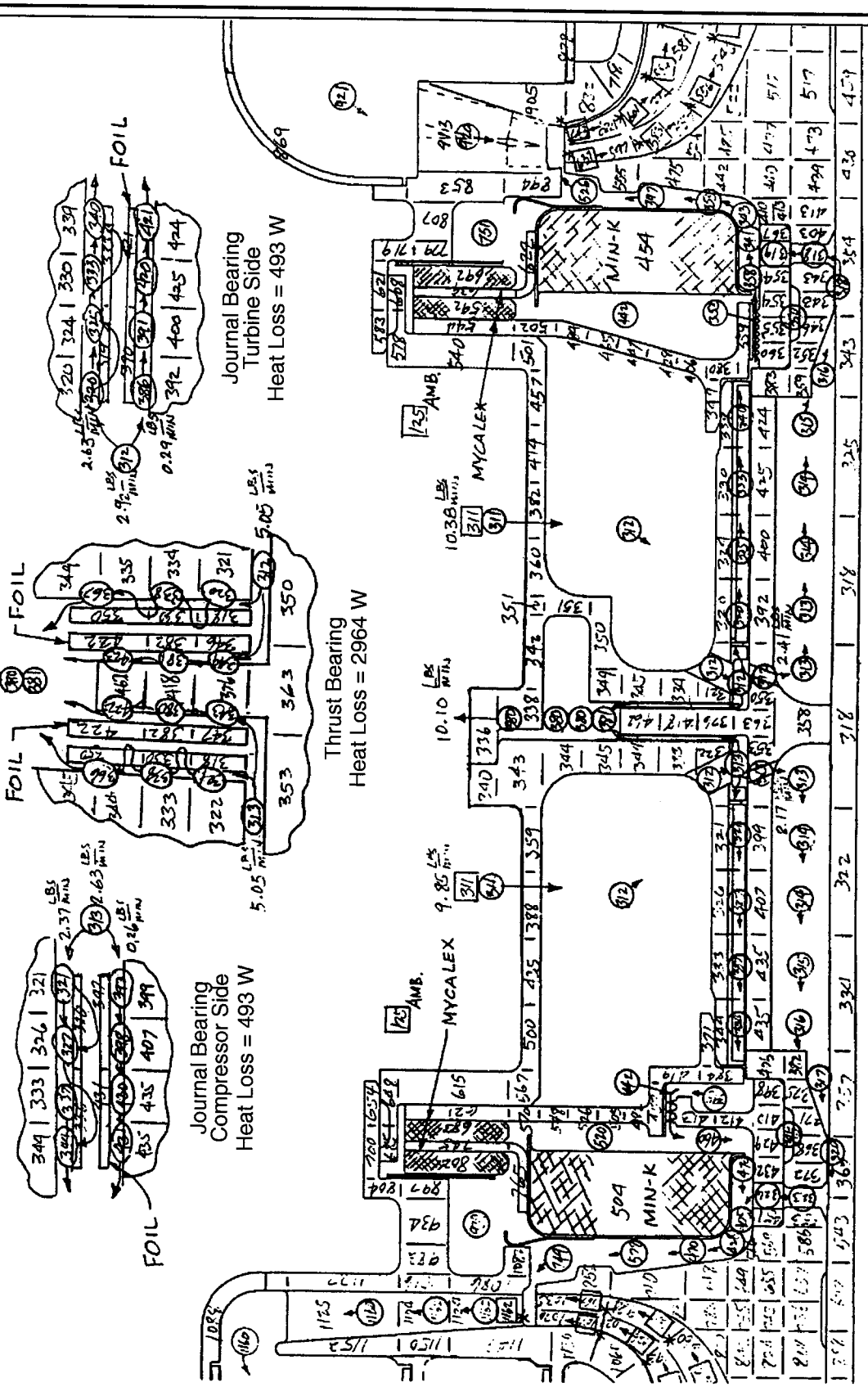

Figure 16. Steady-State Temperature Distribution (Degrees F), Engine Cooling Mode (E or F)

- The maximum temperature of the bearing foil (538°F) occurs in the thrust bearing (node 93) at altitude flight mode (test condition C, see Figure 15). This occurs because, among the three operating modes, the cooling air for the altitude flight has the lowest flow rate and the highest temperature.
- The Mycalex insulation between the manifold and the housing effectively prevented the housing from being heated up. A maximum temperature difference of 265°F occurs across the insulation on the compressor side (Figure 14) and 235°F on the turbine side (Figure 16).

Histories of Compressor and Turbine Wheel Temperature Gradients – The maximum temperature gradient in a turbomachinery wheel tends to occur at the beginning of a startup. The blade temperature rapidly approaches the gas temperature while the hub remains in its initial condition. The temperature gradients along the radial direction of the compressor and the turbine wheel, with time as a parameter, are presented in Figures 17 (altitude flight) and 18 (engine cooling). The initial temperature of the wheels is assumed to be 120°F. Both wheels show the same trend, except for the temperature levels, which are dictated by the relative total temperature of the air in the wheels.

Temperature Histories of Gas Bearings During Soakback

Limited Rights information has been omitted from this Industry-Version report.

3.2.3 Rotor Dynamics

3.2.3.1 Description of Structure

The ACEP ACM rotor comprises a shaft assembly, an impeller, a shaft, a thrust desk, a turbine, and a tie rod. The various rotor components are piloted to each other and held together with the tie rod. The tie rod is preloaded to prevent separation or relative rotation of the mating components. The rotor is supported by two compliant-foil bearings and operates between 41,400 and 74,460 rpm. Because of the high damping of the compliant-foil bearings, resonances of the second rigid body mode almost disappear. The shaft bending mode will be 141% of the maximum operating speed. Rotor dynamics and stress analyses were conducted to assure structural integrity of the ACM prior to final design and fabrication.

3.2.3.2 Material Data

Limited Rights information has been omitted from this Industry-Version report.

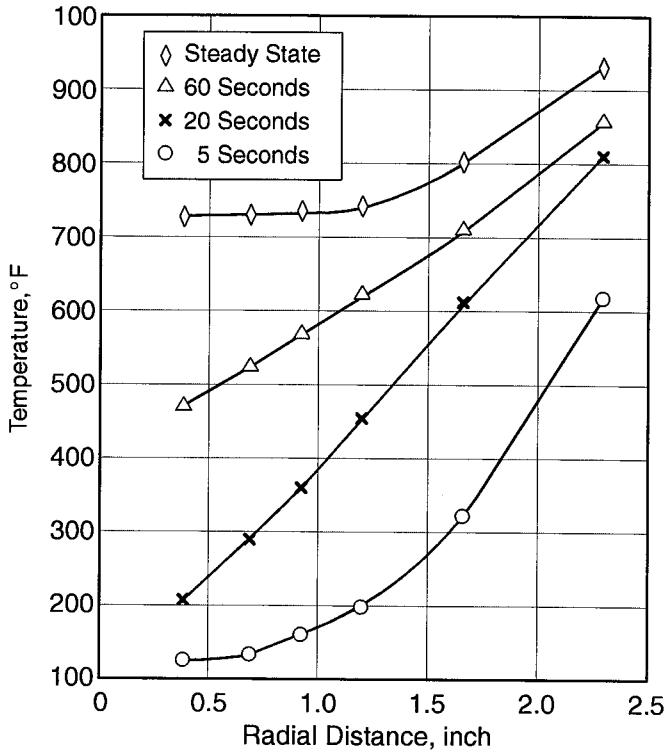

Figure 17. Temperature Gradient Histories of Compressor Hub in Radial Direction, Test Condition – Initial Temperature = 125°F

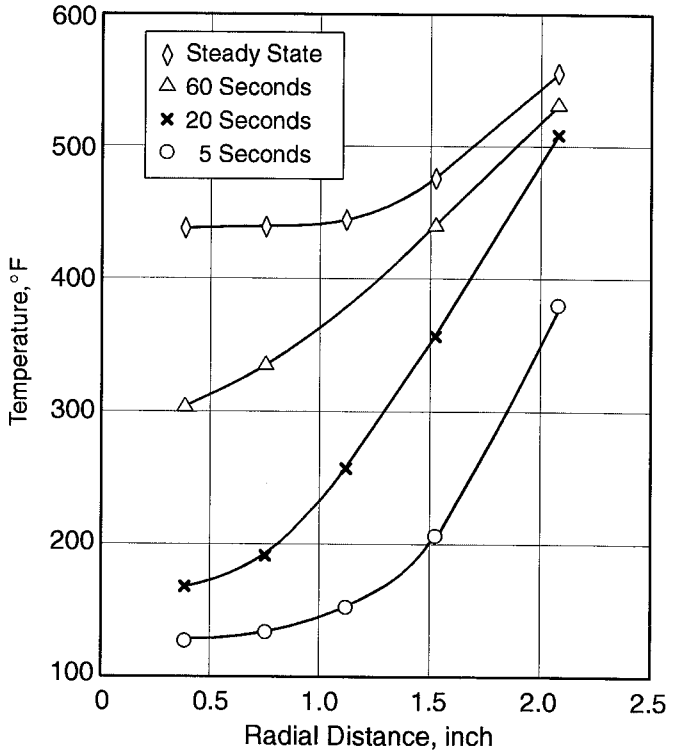

Figure 18. Temperature Gradient Histories of Turbine Wheel Hub in Radial Direction, Engine Cooling Mode – Initial Temperature = 125°F

Figure 19. Temperature Histories of Gas Bearings During Soakback Shutoff at Steady-State Operation, Sizing Point – Ambient =125°F

Limited Rights information has been omitted from this Industry-Version report.

Figure 20. Temperature Histories of Gas Bearings During Soakback Shutoff at Steady-State Operation, Altitude Flight – Ambient = 125°F

Figure 21. Temperature Histories of Gas Bearings During Soakback Shutoff at Steady-State Operation, Engine Cooling – Ambient = 125°F

Table 3. Rotor Material Data (MIL–HDBD–5, Except as Noted)

Limited Rights information has been omitted from this Industry-Version report.

3.2.3.3 Analysis Methods

Limited Rights information has been omitted from this Industry-Version report.

3.2.3.4 Analysis Results

Limited Rights information has been omitted from this Industry-Version report.

Table 4. Natural Frequencies

Limited Rights information has been omitted from this Industry-Version report.

Figure 22. Rotor Dynamic Model of ACEP ACM

Limited Rights information has been omitted from this Industry-Version report.

Figure 23. Undamped Natural Frequency

Figure 24. First Mode Shape (4,929 cpm)

Limited Rights information has been omitted from this Industry-Version report.

Figure 25. Second Mode Shape (10,989 cpm)

Figure 26. Third Mode Shape (104,840 cpm)

Limited Rights information has been omitted from this Industry-Version report.

Figure 27. Bearing Reaction Load Versus Spin Speed

Limited Rights information has been omitted from this Industry-Version report.

Figure 28. Amplitude Versus Spin Speed (e=0.0001-inch)

Table 5. Dynamic Analysis of the ACEP ACM

Limited Rights information has been omitted from this Industry-Version report.

3.2.4 Stress Analysis

3.2.4.1 Compressor Wheel

The compressor wheel is machined from a 3.0-in long, 6.0-in diameter, low-carbon, PM (powder metal) Astroloy pancake. HIP (hot isostatic pressing) is used to consolidate the powder. This process results in a more homogeneous structure than that obtained by conventional forging and produces more uniform metallurgical properties throughout the material. Mechanical properties are:

- Ultimate strength = 190 ksi (70°F), 174 ksi (1110°F)
- Yield strength = 117 ksi (70°F), 106 ksi (1110°F)

An ANSYS two-dimensional, finite-element model was constructed to evaluate the hub stress. The hub was modeled with two-dimensional axisymmetric elements, and the blade was modeled by two-dimensional plane stress elements with equivalent thickness input. The blade elements were used to transfer blade centrifugal loading to the hub.

A linear finite-element analysis was first performed by applying maximum rotational speed (74,460 rpm) combined with worst-case transient or steady-state thermal loading. The maximum steady-state temperature of the wheel is 1100°F at the blade exit area. The results of the linear analysis are shown in Figures 29 and 30. In this analysis, linear material properties are used; the effect of the wheel preassembly production overspeed spin (to 102,000 rpm to lock in compressive hoop stress in the bore area) was not considered.

The maximum bore stress calculated by linear finite-element analysis is 174 ksi, as shown in Figure 29. The apparently high local stress is misleading in assessing the wheel margin of safety caused by the large radial stress gradient in the hub. Experience indicates that wheel burst speed can be evaluated by equating the average hub tangential stress to the average material ultimate strength. The average hub tangential stress is an area-weighted tangential stress of the entire hub section or, in mathematical form:

$$S_{avg.tan} = \frac{e^{s_i A_i}}{e^{A_i}}$$

where s_i and A_i are the element tangential stress and element area of the finite-element model, respectively. The summation is taken over the entire hub. The average tangential hub stress was calculated to be 69.1 ksi. By the same method, the cross-sectional average temperature corresponding to the worst-case transient thermal loading was calculated to be 288°F. At this temperature, the material ultimate strength is 179 ksi. By applying this method, the estimated wheel burst speed is calculated as follows:

$$N_{burst} = 74460 \times \sqrt{\frac{179}{69.1}} = 74460 \times 1.61 = 119,840 \text{ rpm}$$

The burst speed is estimated to be 119,840 rpm, and the corresponding margin-of-safety burst is +0.61 (61%).

The benefit of the production overspeed spin can be seen in Figure 31 (Goodman diagram). Without production overspeed spin, the start/stop fatigue life is less than the required 10,000 cycles. With production overspeed, the wheel fatigue life increased to approximately 110,000 cycles. The difference is due to the residual compressive hoop stress of 87 ksi in the bore area, as shown in Figure 32.

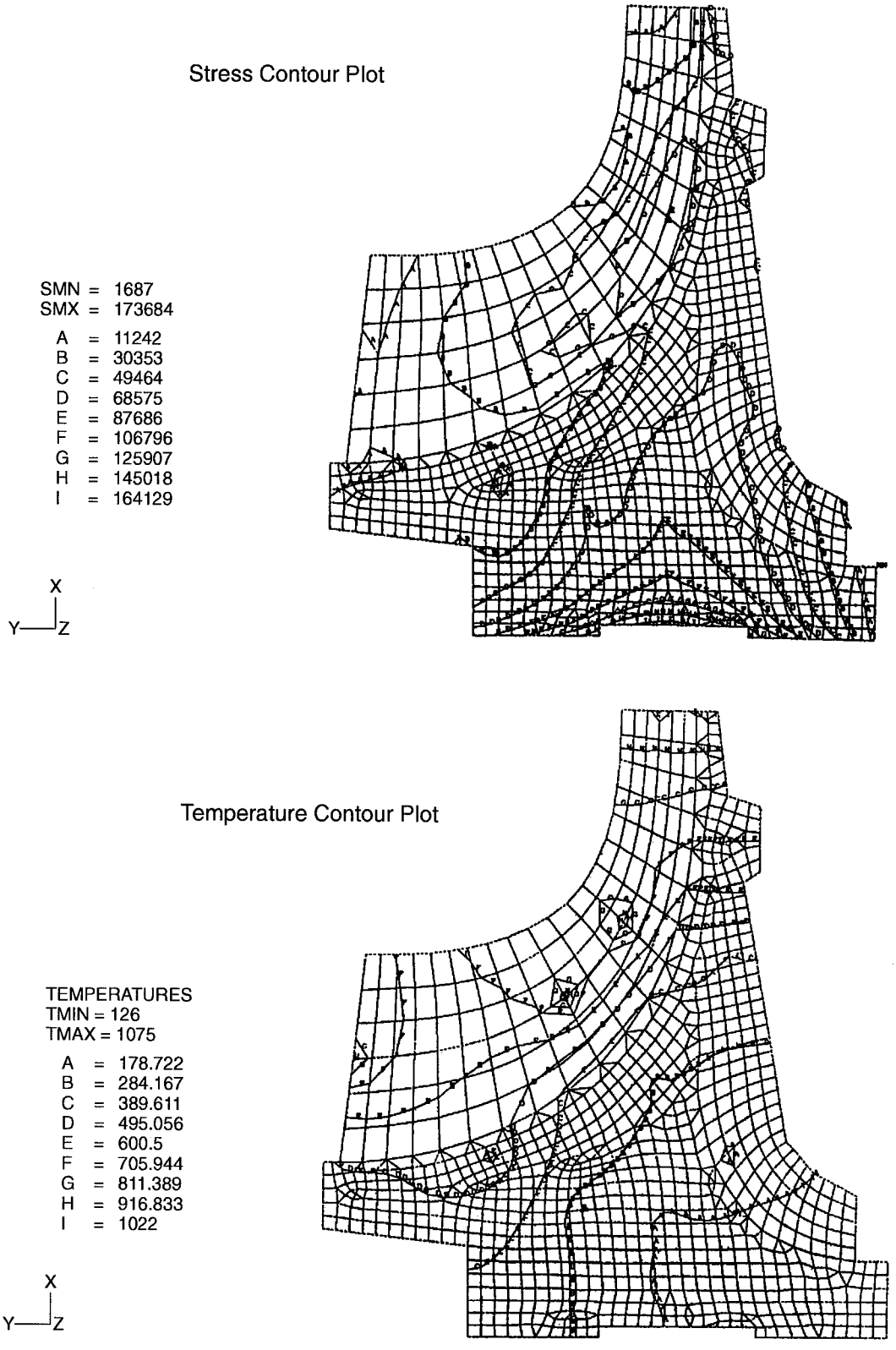

Figure 29. ACEP Compressor Wheel Linear Stress Analysis, Worst-Case Transient Thermal

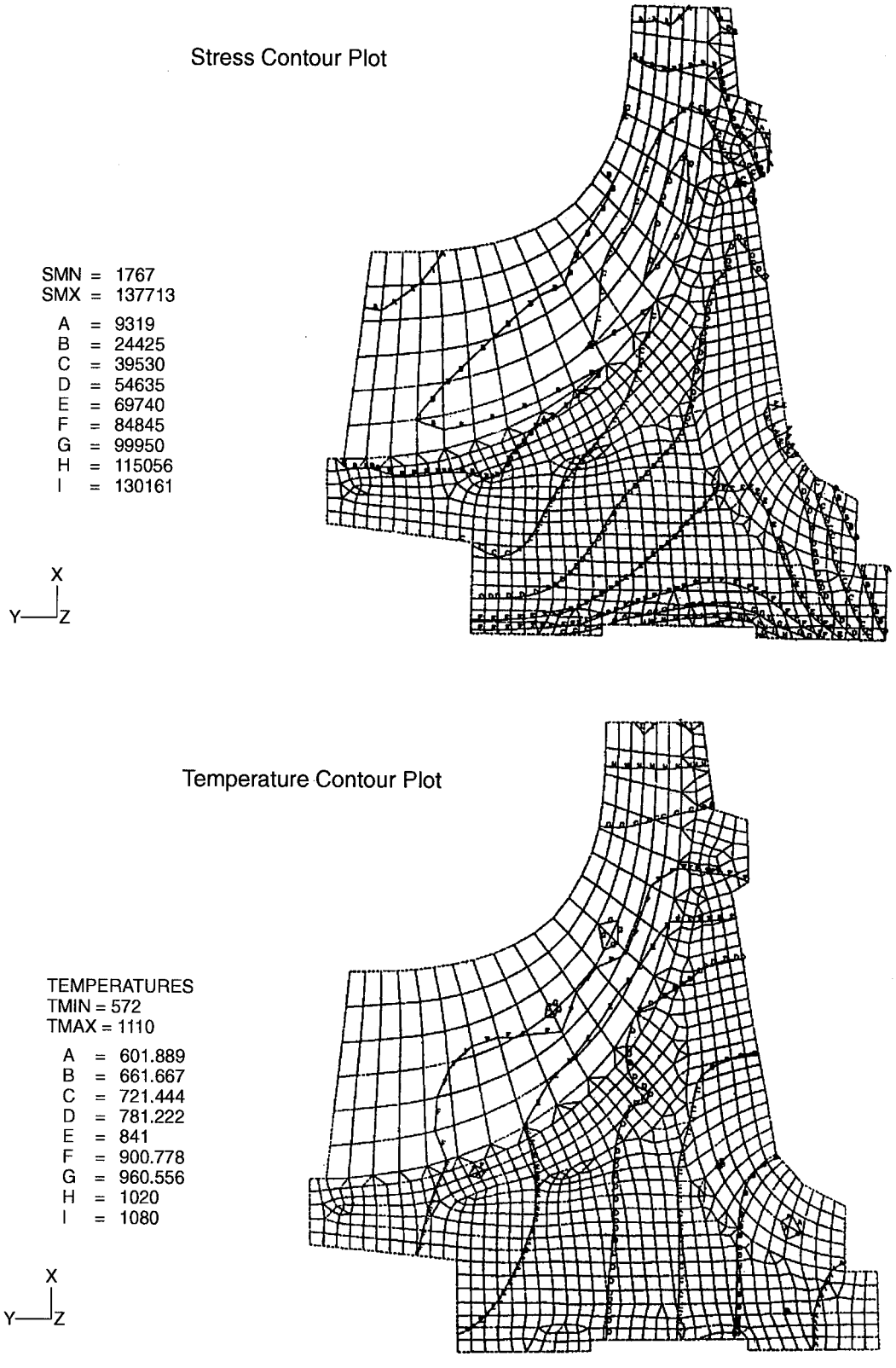

Figure 30. ACEP Compressor Wheel Linear Stress Analysis, Steady-State Thermal

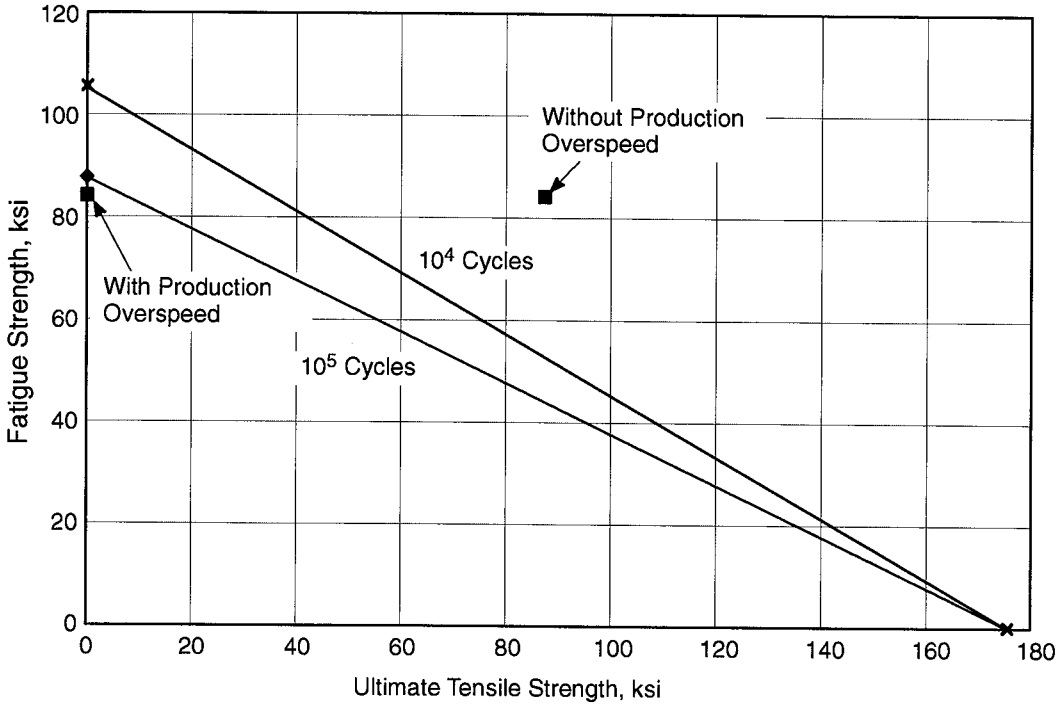

Figure 31. ACEP Compressor Goodman Diagram

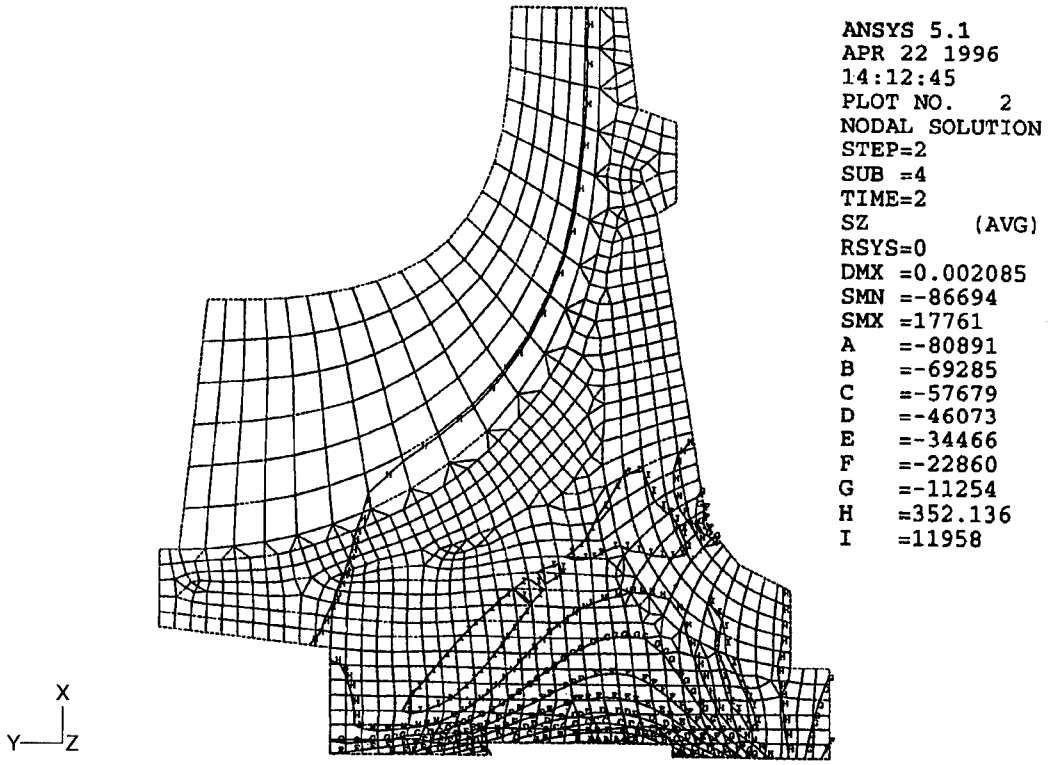

Figure 32. ACEP Compressor Residual Stress Caused by 102,000 RPM Overspeed

The compressor blade stress analysis was performed by using a three-dimensional ANSYS solid-finite-element model, as shown in Figure 33. The compressor wheel has 15 curved blades, equally spaced in the hub. The solid-element model is a curved sector model containing one-fifteenth of the wheel. The blade is located in the center of the sector, and symmetry boundary conditions were applied to the two hub cut boundaries. The maximum calculated blade stress is 97 ksi (Figure 34), which is less than the calculated hub stress.

3.2.4.2 Turbine Wheel

The turbine wheel is machined from wrought Inconel alloy 718. The mechanical properties, as specified by AMS 5662, are as follows:

- Ultimate strength = 180 ksi (70°F), 165 ksi (640°F)
- Yield strength = 150 ksi (70°F), 132 ksi (640°F)

An ANSYS two-dimensional, finite-element model was constructed to evaluate the hub stress. The hub was modeled with two-dimensional axisymmetric elements, and the blade was modeled by two-dimensional plane stress elements with equivalent thickness input. The blade elements were used to transfer blade centrifugal loading to the hub.

A linear finite-element analysis was first performed by applying the maximum rotational speed of 74,460 rpm combined with worst-case transient or steady-state thermal loading. The maximum steady-state temperature of the wheel is 637°F at the blade inlet area. The results of the linear analysis are shown in Figures 35 and 36. In this analysis, linear material properties are used; the effect of the wheel preassembly production overspeed spin (to 105,000 rpm to lock in compressive hoop stress in the bore area) was not considered.

The maximum bore stress calculated by linear finite-element analysis is 158 ksi, as shown in Figure 35. The apparently high local stress is misleading in assessing the wheel margin of safety caused by the large radial stress gradient in the hub. From experience, the wheel burst speed can be evaluated by equating the average hub tangential stress to the average material ultimate strength. The average hub tangential stress is an area-weighted tangential stress of the entire hub section:

$$S_{avg.tan} = \frac{e^{s_i A_i}}{e^{A_i}}$$

where s_i and A_i are the element tangential stress and element area of the finite-element model, respectively. The summation is taken over the entire hub. The average tangential hub stress was calculated to be 64 ksi. By the same method, the cross-sectional average temperature corresponding to the worst-case transient thermal loading was calculated to be 288°F. At this temperature, the material ultimate strength is 172 ksi. By applying this method, the estimated wheel burst speed is calculated as follows:

$$N_{burst} = 74460 \times \sqrt{\frac{172}{64}} = 74460 \times 1.64 = 122,110 \text{ rpm}$$

The burst speed is estimated to be 122,110 rpm and the corresponding margin-of-safety burst is +0.64 (64%).

The benefit of the production overspeed spin can be seen in Figure 37 (Goodman diagram). Without production overspeed spin, the start/stop fatigue life is less than the required 10,000 cycles. With

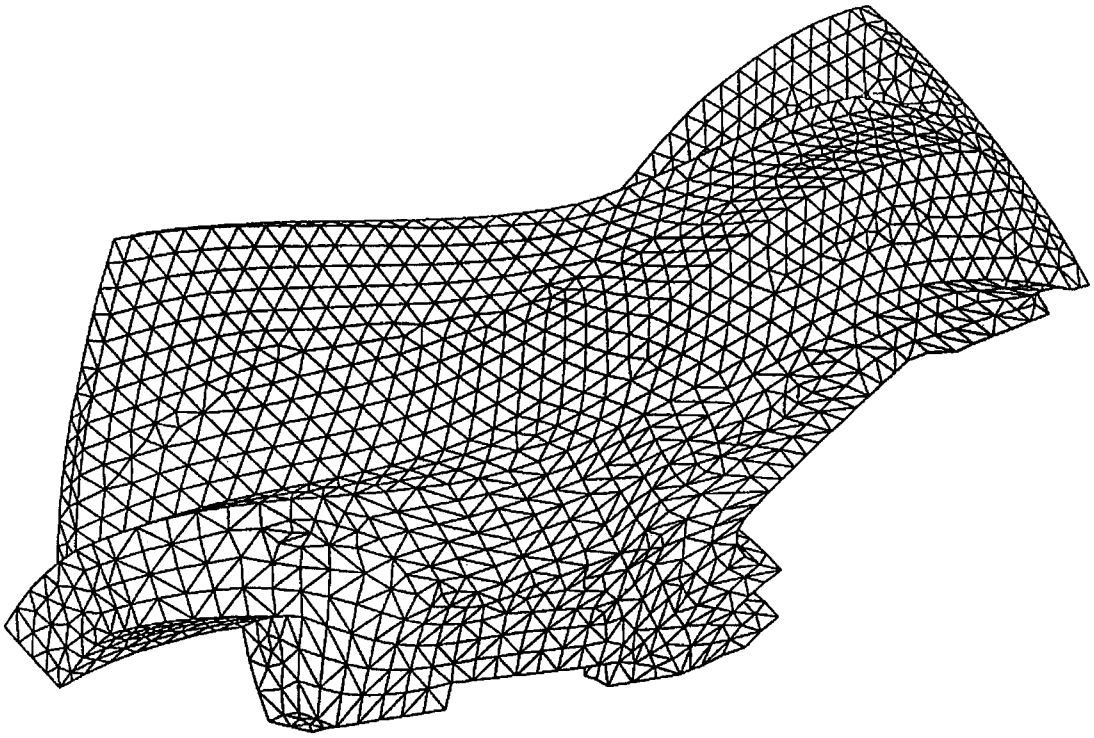

Figure 33. ACEP Compressor Three-Dimensional Solid-Element Finite-Element Model

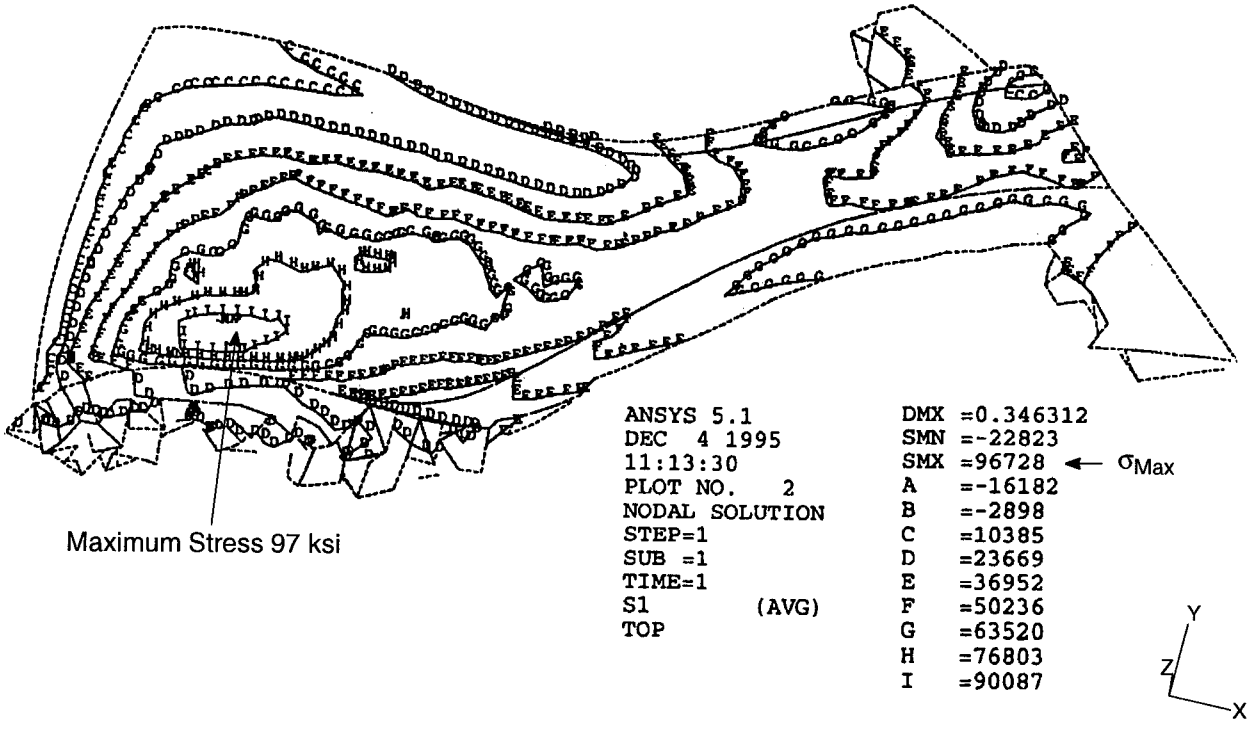

Figure 34. ACEP Compressor Blade Stress Contour Plot at 74,460 RPM

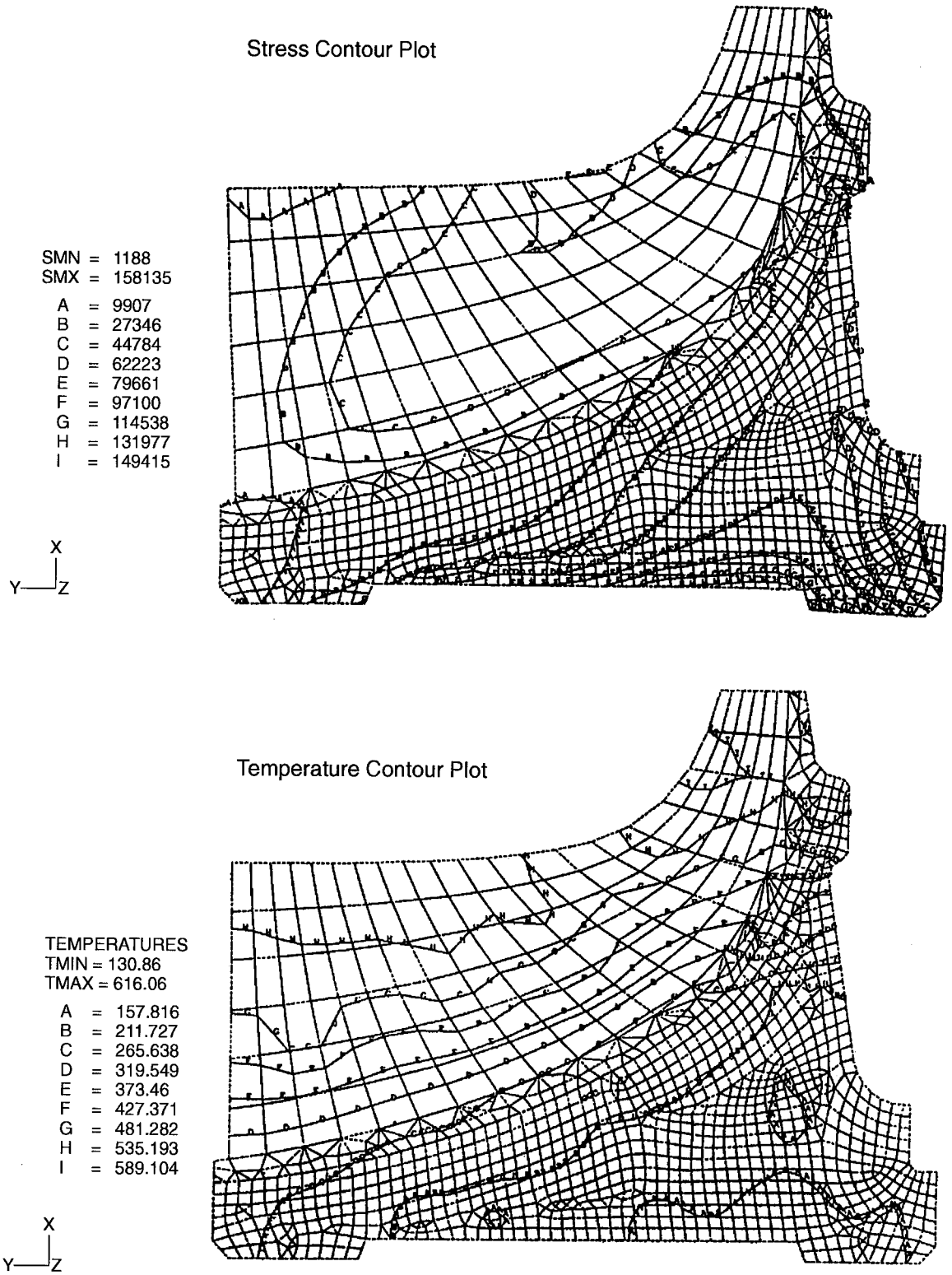

Figure 35. ACEP Turbine Wheel Linear Stress Analysis, Worst-Case Thermal

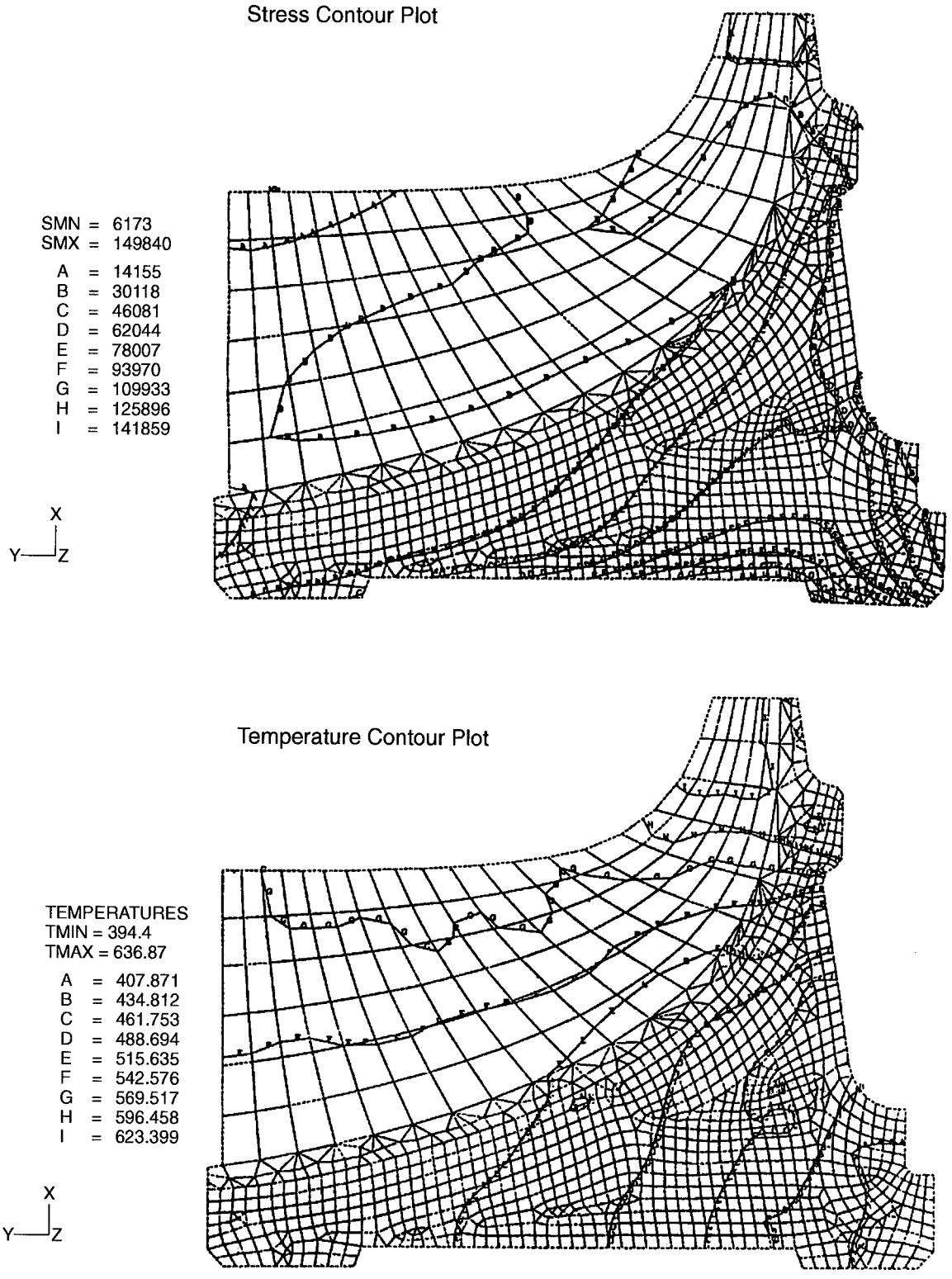

Figure 36. ACEP Turbine Wheel Linear Stress Analysis, Steady-State Thermal

production overspeed, the wheel fatigue life increased to about 400,000 cycles. The difference is caused by the residual compressive hoop stress of 79 ksi in the bore area, as shown in Figure 38.

The turbine blade stress was analyzed by using a three-dimensional ANSYS shell-element model. The blade shell model is shown in Figure 39, along with a shell elements thickness contour plot. The blade is constrained in all directions at the hub, and loading is at the maximum operating speed of 74,460 rpm. The maximum calculated blade stress is 53 ksi at the blade root near the exit area (Figure 40). This calculated maximum blade stress is less than the calculated hub stress.

3.2.5 ACM Design Modifications

The ACEP ACM underwent two phases of modification. It was first modified to improve the start capability. The second modification relates to improving cooling air flow through the compressor journal bearing.

3.2.5.1 Start-Related Modification

Limited Rights information has been omitted from this Industry-Version report.

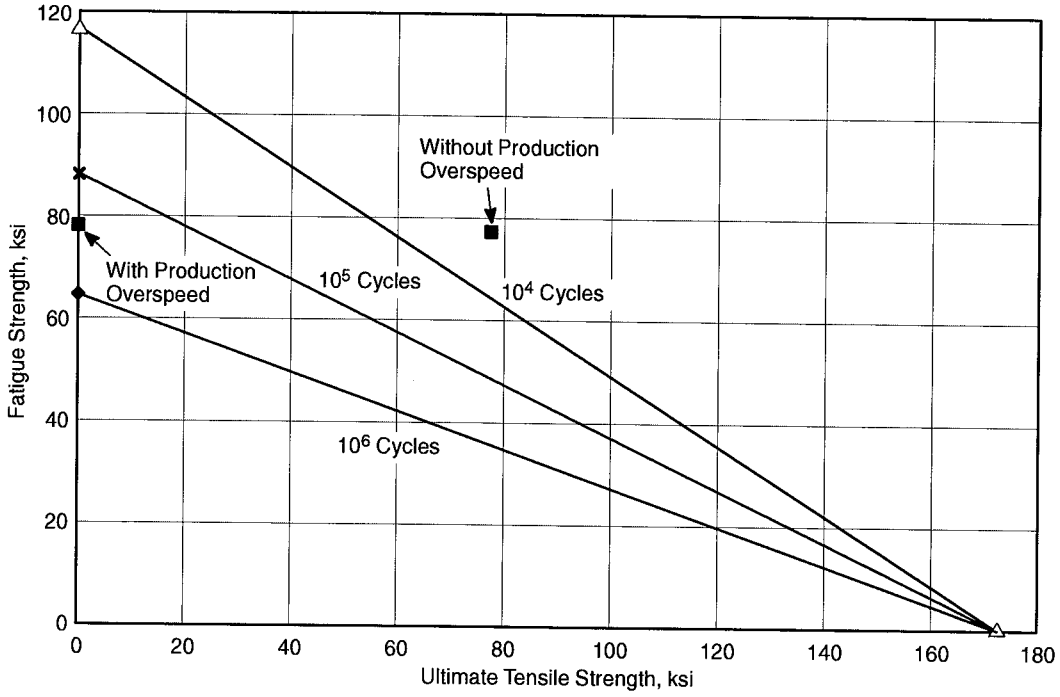

Figure 37. ACEP Turbine Goodman Diagram

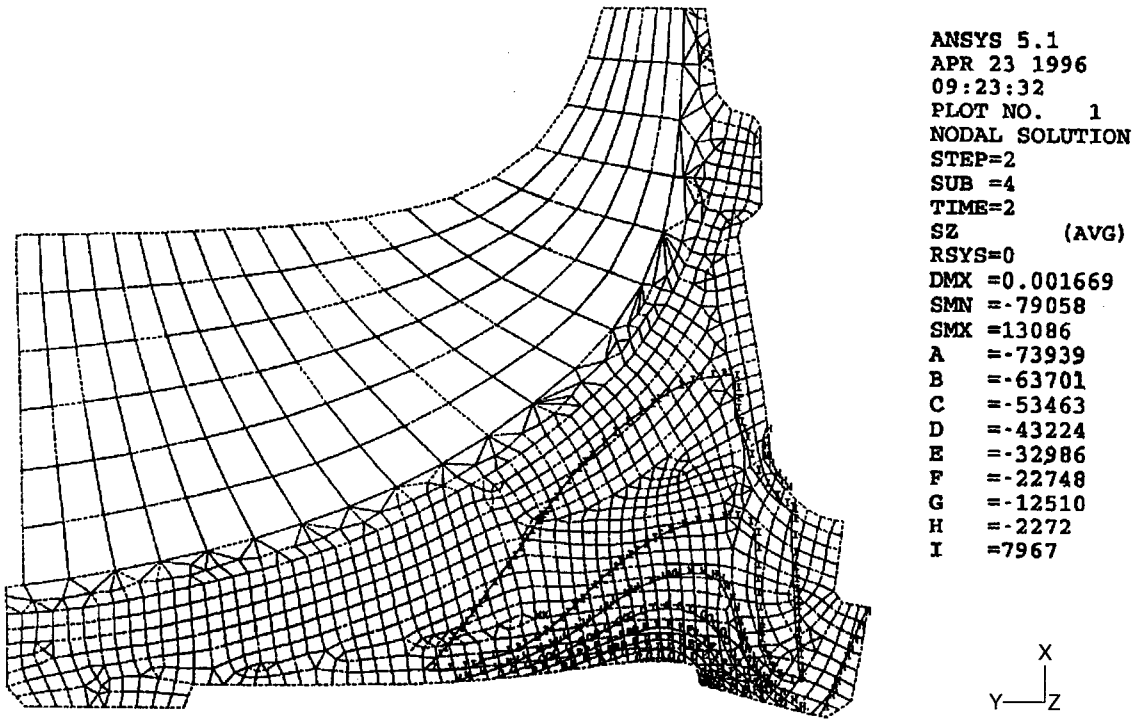

Figure 38. ACEP Turbine Residual Stress Caused by 105,000 RPM Overspeed

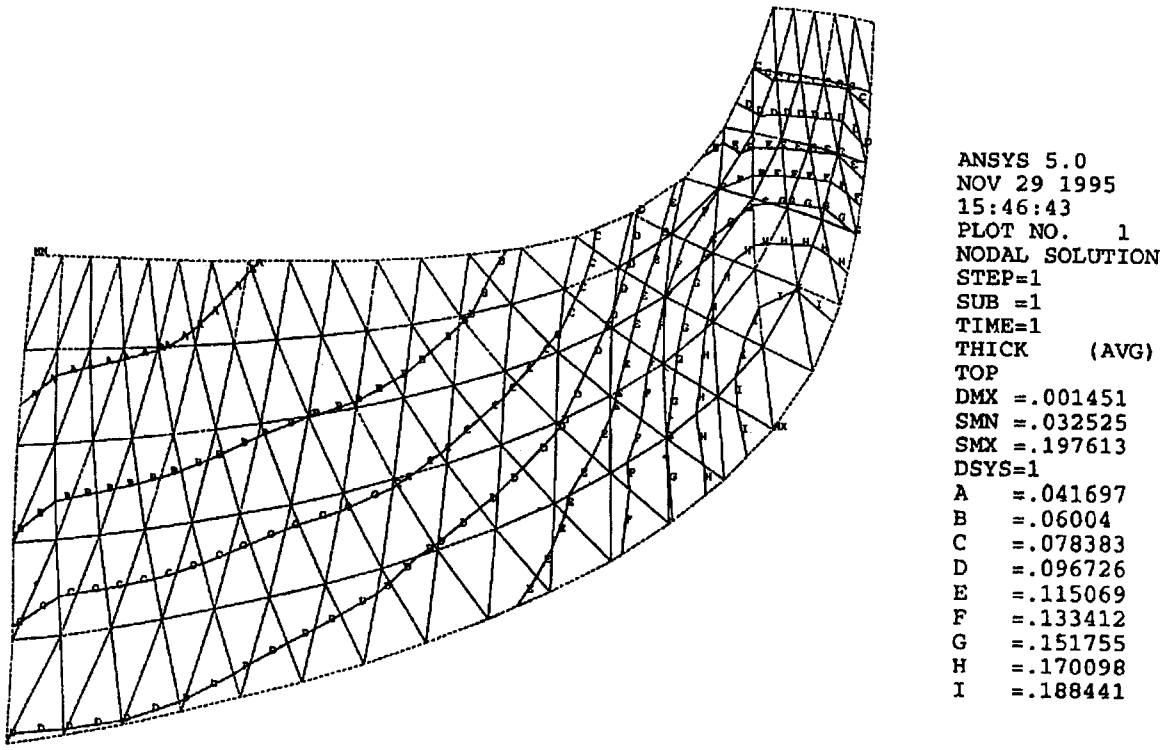

Figure 39. ACEP Turbine Three-Dimensional Shell Element Finite-Element Model: Thickness Contour at 74,460 RPM

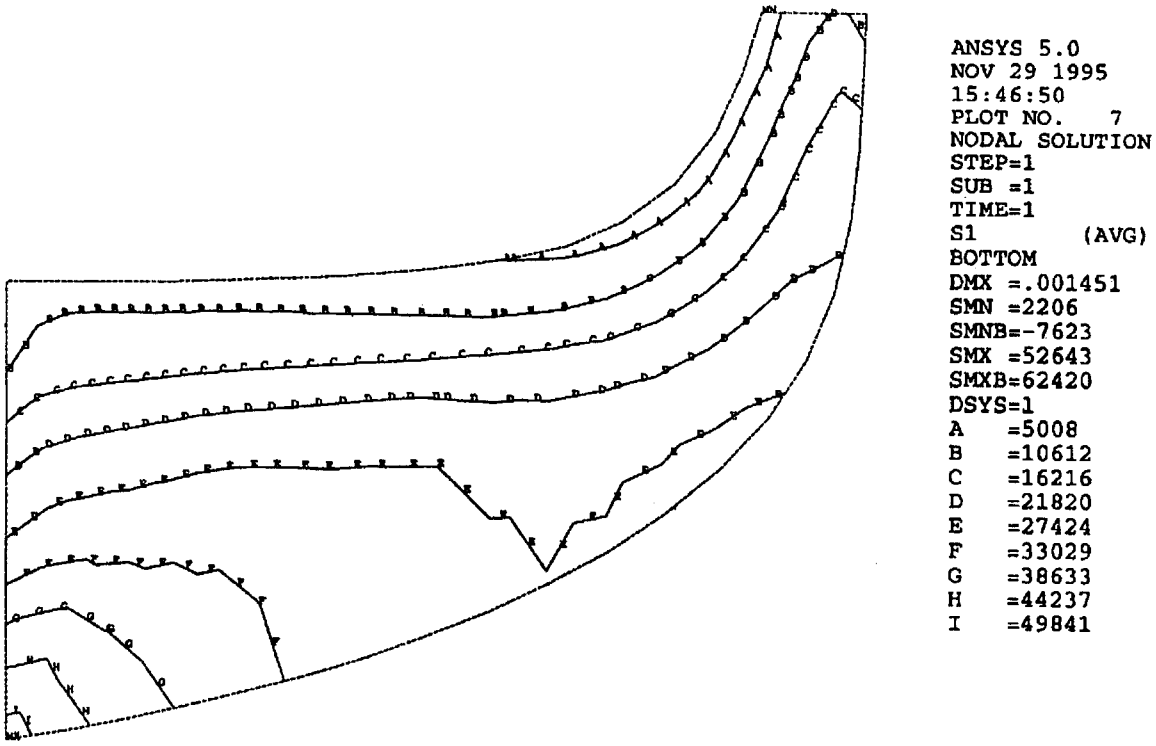

Figure 40. ACEP Turbine Blade Stress Contour Plot at 74,460 RPM

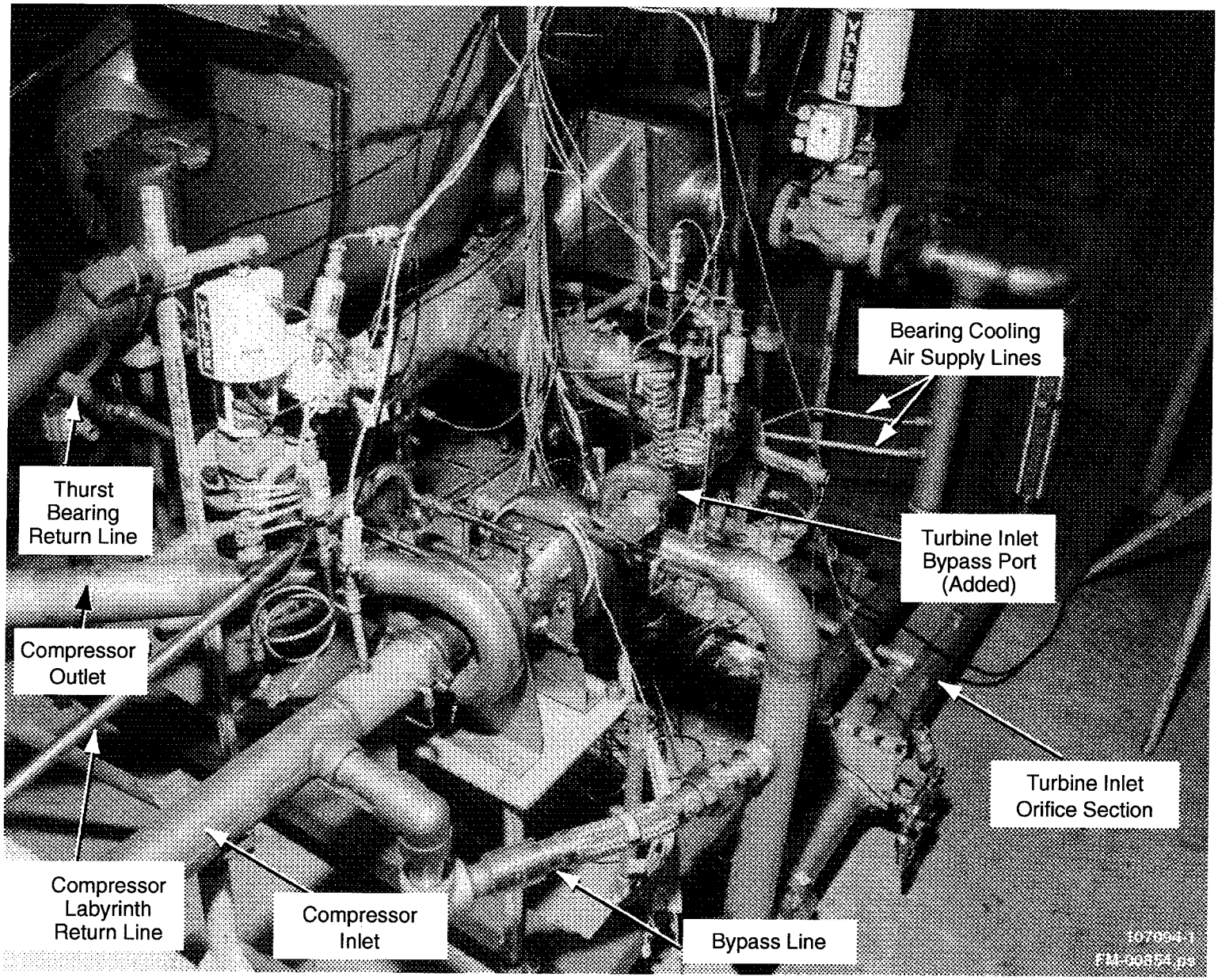

Figure 41. Exhaust Cooling Mode Test Setup (Actual)

Limited Rights information has been omitted from this Industry-Version report.

Figure 42. Deflector Ring

Limited Rights information has been omitted from this Industry-Version report.

Figure 43. ACEP ACM Bearing Cooling Modification

3.2.5.2 Compressor-Journal Bearing Airflow-Related Modification

Limited Rights information has been omitted from this Industry-Version report.

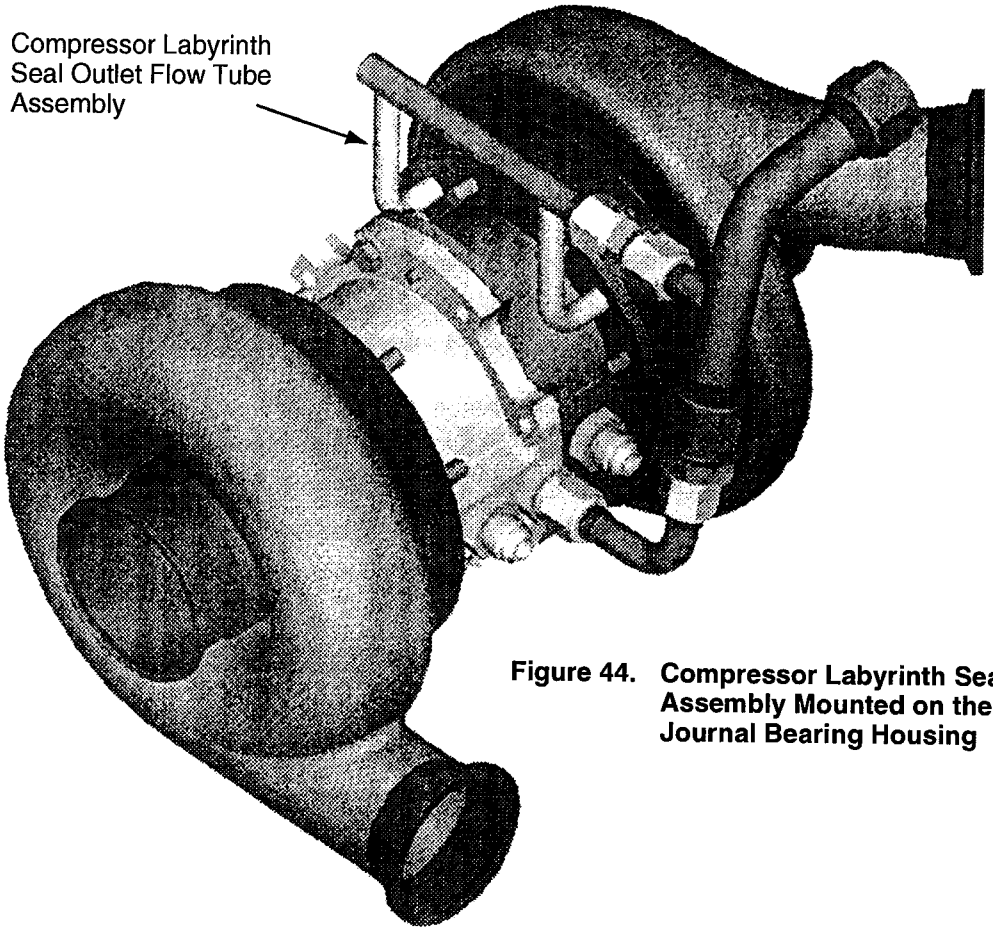

Figure 44. Compressor Labyrinth Seal Outlet Flow Tube Assembly Mounted on the Compressor Journal Bearing Housing

3.2.6 ACM Acceptance Test

The ACM development tests included an acceptance test, the exhaust nozzle cooling-mode test, and the engine cooling-mode test.

3.2.6.1 Test Setup

Two setups were used to facilitate the ACEP ACM tests, one for exhaust nozzle cooling mode and acceptance tests and the other for engine cooling mode tests.

The exhaust nozzle cooling mode test requires a closed-loop setup where the hot compressor discharge air is cooled as it passes through the heat exchangers and is further cooled as it expands through the turbine wheel. This is similar to the boot-strap configuration used on conventional environmental control systems.

The engine cooling mode test requires a two-line setup where the turbine inlet air comes from the same source as the compressor inlet air. The turbine air is cooled as its expands through the turbine wheel. The compressor discharge air, which was directed to the turbine inlet during the exhaust cooling mode test, is now dumped overboard after a small amount is recovered for bearing cooling.

The test facility at AlliedSignal uses dryers to supply air containing less than ten grains of water per pound of air. If the water is not removed, the effect of condensation at the turbine discharge must be accounted for when assessing the ACM performance. Figure 41 is a photo of the test setup, and it is shown schematically in Figure 45.

The ACM acceptance test setup used two heat exchangers (in series) capable of accommodating the high airflow, pressure, and temperature. The two heat exchangers (commercial aircraft ECS precoolers) leaked during the leak test. However, the leak was small, and the heat exchangers were deemed satisfactory for the development test. The test sequence was arranged to progress from low-power (pressure) conditions to high-power conditions to minimize further damage to the heat exchangers. Two ACM's were fabricated for the ACEP program. One unit was fully instrumented with internal sensors to monitor bearing cooling and thrust load.

Safety precautions were implemented to alleviate hazards during the test. Specific parameters were instantaneously displayed to provide real-time verification of unit condition (Figure 46). Specific signals were incorporated to provide audible and visible warnings when the limits of selected parameters were reached:

- Thrust bearing exit temperature > 500°F
- Compressor journal bearing exit temperature > 500°F
- Turbine journal bearing exit temperature > 500°F
- Turbine inlet temperature > 350°F (irrelevant during engine cooling mode test)
- Compressor inlet temperature > 1000°F

3.2.6.2 ACM Modification-Related Setup

Start-Related Modification – A bypass line was added between the compressor inlet and the turbine inlet to improve the start characteristics of the unit. The bypass line includes a 12-in long flex line. A flex line was used to accommodate the thermal expansion of the unit during and after operation. This bypass line also includes a checkvalve to check the high pressure/flow when the unit is running. During the ACM acceptance test, as a convenience, the bypass line was connected at the turbine supply line instead of the port added to the turbine torus. Figure 41 shows the unit with the turbine inlet bypass port (plugged) and the bypass line in the test setup.

Compressor-Journal Bearing Airflow-Related Modification – A tube assembly was fabricated and attached to the compressor bearing housing flange to direct the air from the compressor low-pressure cavity to the compressor inlet return line. A gasket also was fabricated and used to prevent air leaks between the compressor bearing housing and this tube assembly. A provision was made for the tube assembly to accommodate an orifice plate in the flow restricter for airflow control, and a tube assembly for the thrust bearing outlet airflow was fabricated only for testing at GEAE. This tube assembly connects to the compressor tube assembly. It also has a provision to accommodate an orifice plate in the flow restricter for airflow control (as required).

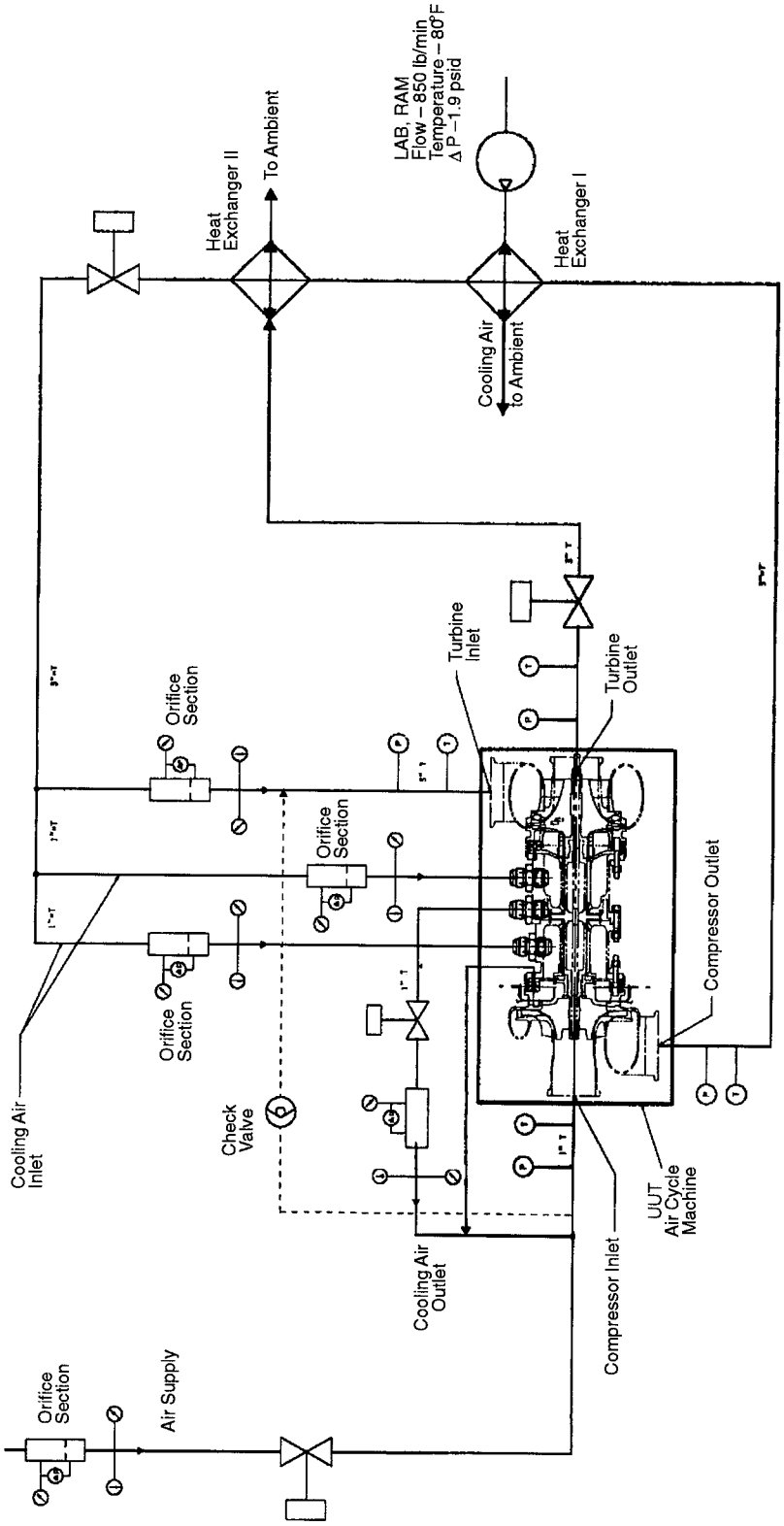

Figure 45. ACEP ACM Exhaust Cooling Mode Test Setup Schematic

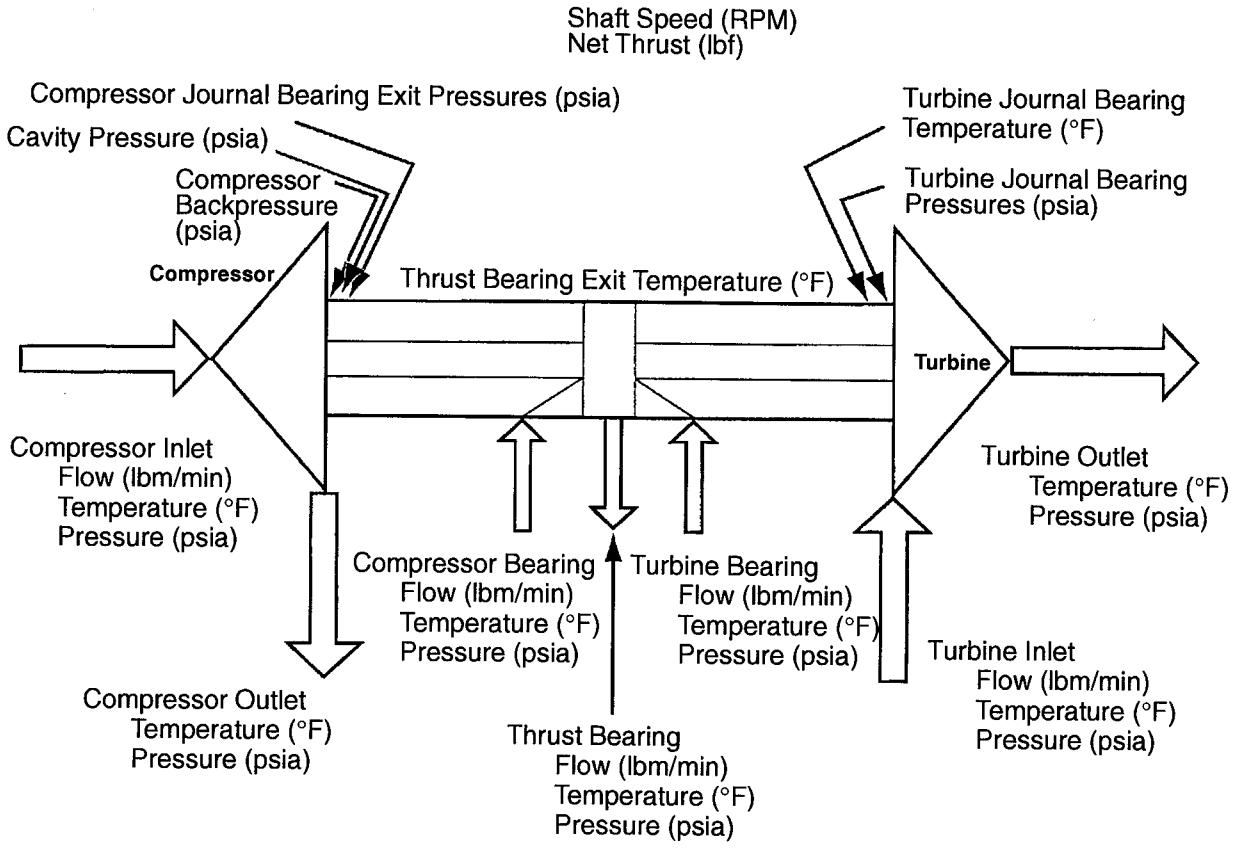

Figure 46. ACEP ACM Test Unit Parameters Instantaneously Displayed and Monitored

3.2.6.3 Test Setup Instrumentation

The test setup included instrumentation to control the specific test conditions, measure the performance characteristics of the test unit, and determine pressures and temperatures at selected locations for unit condition monitoring. Measurements included internal pressure and temperature distribution. Figure 47 shows the various parameters instrumented in the unit. Evaluation of the relationships among the observed parameters (from the unit instrumentation together with the unit performance-related instrumentation) provided verification of correctness of instrumentation and the unit condition during the test start.

3.2.6.4 Data Acquisition

Both discrete and real-time data were obtained during the test. Instantaneous data during startup were also recorded to measure and correlate various parameters. Instantaneous data were also recorded during each test condition to assess the sensitivity of the recorded parameter with time.

Pressure Sensor Location

P_1 Back of Compressor Wheel by the Tip

P_2 Back of Compressor Wheel by the Tip

P_3 Back of Compressor Wheel by the Midsection, Between Tip and Hub

P_4 Back of Compressor Wheel by the Midsection, Between Tip and Hub

P_5 Back of Compressor Wheel by the Lower Section, Near Hub

P_6 Back of Compressor Wheel by the Lower Section, Near Hub

P_7 Back of Turbine Wheel by the Lower Section, Near Hub

P_8 Back of Turbine Wheel by the Lower Section, Near Hub

P_9 Back of Turbine Wheel by the Tip

P_{10} Back of Turbine Wheel by the Tip

P_{11} Back of Turbine Wheel by the Midsection, Between Tip and Hub

P_{12} Back of Turbine Wheel by the Midsection, Between Tip and Hub

P_{15} Compressor Journal Bearing Exit

P_{16} Compressor Labyrinth Low-Pressure Cavity

P_{17} Turbine Journal Bearing Exit

P_{18} Turbine Journal Bearing Exit

P_{21} Thrust Bearing Outlet Cavity

P_{22} Thrust Bearing Outlet Cavity

Temperature Sensor Location

T_{15} Compressor Journal Bearing Exit

T_{16} Compressor Labyrinth Low-Pressure Cavity

T_{17} Turbine Journal Bearing Exit

T_{18} Turbine Journal Bearing Exit

T_{21} Thrust Bearing Outlet Cavity

T_{22} Thrust Bearing Outlet Cavity

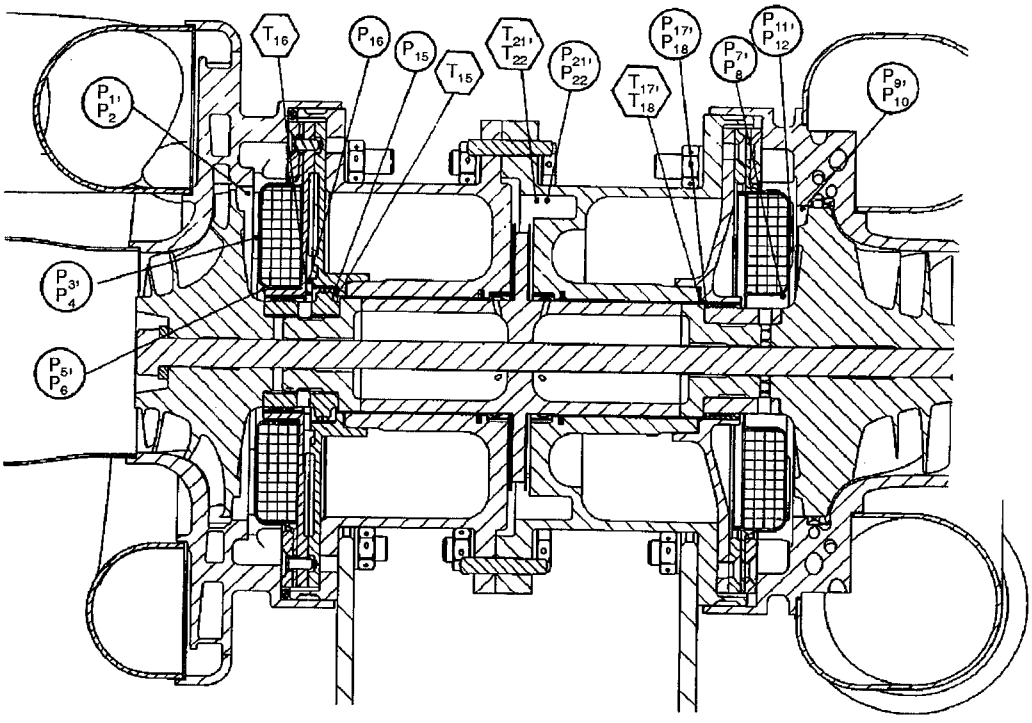

Figure 47. Test Unit Instrumentation

3.2.6.5 Test Conditions

The ACEP ACM exhaust nozzle cooling mode acceptance test was conducted to satisfy the F–15 acceptance test conditions and the ACEP exhaust cooling mode conditions. These test conditions are as follows:

Test A – Verifies the operation and aerodynamic performance of the ACM (condition derived from F–15 cooling turbine ATP performance test).

Test B – Simulates the structural integrity test of the F–15 cooling turbine (derived from the F–15 cooling turbine ATP integrity test, later deleted as part of ACM ATP).

Test C – Lower power ACEP ACM exhaust cooling mode condition.

Test D – Reduced Test E condition (intended for extrapolating ACEP ACM performance during worst engine cooling mode condition, if the condition is not achieved).

Test E – most severe ACEP ACM exhaust cooling mode condition.

3.2.6.6 ACM Acceptance Test Results

A series of ACM acceptance tests were conducted as a result of component failures, design modifications, and physical reconfiguration of the test setup to support the exhaust cooling mode. The acceptance test events are summarized as follows.

Baseline ACM Configuration – The instrumented ACM (serial number R1) was assembled and installed in the exhaust nozzle cooling mode test assembly. The unit failed during start, due to high start torque. An attempt to start the unit by gradually increasing the compressor inlet pressure resulted in a start but under excessive thrust load that failed the thrust bearings and destroyed the thrust disk.

Modified Start ACM Configuration – The ACM design was modified to enhance start capability by incorporating the turbine nozzle flow deflector, turbine inlet bypass, and housing interface O-rings. The ACM R1 unit was retested but failed due to instrumentation installation error. Teardown of the unit showed that the thrust bearing tip temperature sensor potting interfered with the movement of the thrust bearing, making the bearing rigid (no flexibility), thus causing the thrust bearings to fail. The ACM R1 unit was rebuilt without the thrust bearing tip temperature sensor. The unit was retested at the F–15 ATP conditions, and the ACEP exhaust cooling mode test conditions were completed.

The second ACM (R2, without internal instrumentation) was assembled, acceptance tested, and sent to GEAE for installation into the turbocooler assembly. The ACM R2 unit failed during the turbocooler rig test. A plugged thrust bearing outlet port blocked cooling flow; the thrust bearings failed due to overheat, and the thrust disk was destroyed.

The instrumented ACM (R1) was sent to GEAE to continue the turbocooler test. When the bearing cavity pressures were found inadequate to ensure sufficient journal cooling, an independent source of bearing coolant (shop air) was added to the integrated turbocooler rig setup. However, at cavity pressures sufficient to ensure positive flow over the compressor journal bearing, the thrust bearing failed either due to a flow disruption (overtemperature) or an axial thrust imbalance. This failure curtailed the integrated turbocooler rig test at GEAE before supercritical fuel temperatures could be achieved (see Section 4).

Modified Compressor Journal Bearing Cooling Configuration – Only one ACM (R1) was modified to improve compressor journal-bearing cooling. The modified unit successfully completed the acceptance test (F–15 performance test condition and low-power ACEP exhaust cooling mode test condition) and was shipped to GEAE to be installed for a planned second turbocooler rig test (funded by a complementary program). The objective of the second turbocooler rig test was to complete the supercritical fuel test segment. Unfortunately, due to complications with the combustor test rig, the second turbocooler rig test could not be conducted.

Exhaust Nozzle Cooling Mode ACM Test Data – ACM acceptance test data for the exhaust nozzle cooling mode configuration test runs are summarized in Table 6. There were five primary test conditions of interest: cases A, B, C, D, and E. Cases A and B are specific to the baseline F–15 ACM; cases C through E are specific to the ACEP requirements. For comparative purposes, data from both ACM units (R1 and R2) are presented. In addition, data from both the ACM design modifications (start and compressor labyrinth) are shown.

Case C closely approximates the target test conditions. Section 3.2.6.5 shows minor differences between results with the original unit and the modified compressor labyrinth seal configuration, implying that the high-power test condition (Test E) results with the ACM with original compressor labyrinth configuration are applicable to the modified unit.

Due to facility limitations, test condition E could not be fully assessed. Therefore, based on the recorded pressure distribution and the required compressor inlet pressure, test condition E was extrapolated to estimate ACM performance at the high-power exhaust cooling mode condition. Estimated ACM performance per test condition E closely approximates the target test results.

The ACEP ACM employs recirculation of the bearing parasitic flows. In the original compressor bearing configuration, the recirculating system restored the thrust bearing coolant at the compressor inlet, and journal components were restored respectively at the compressor diffuser and turbine rotor inlets. This places a significant constraint on heat exchanger air-side pressure drop to ensure positive flow over the compressor journal. The facility heat exchanger employed in the acceptance tests had lower air-side resistance than the fuel/air units designed for the turbocooler rig tests. Analysis of the acceptance tests with the original compressor bearing configuration indicated that pressure losses well in excess of those for the tested unit were consistent with reliable bearing cooling. When the bearing cavity pressures were found to be inadequate to assure journal cooling (ACM compressor discharge air flowing over the journal) attempts to provide a cooling source independent of the machine, but at cavity pressure sufficient to ensure positive flow over the compressor journal, apparently resulted in a failed thrust bearing. Development of the low-pressure cavity between the compressor wheel and the journal bearings significantly improved the bearing cooling robustness and reduced sensitivity to the heat exchanger air-side pressure drop — as demonstrated on the latter acceptance tests and the engine cooling mode demonstration.

3.2.7 ACM Engine Cooling Mode Test

An objective of this program was to demonstrate that the turbocooler has dual-mode capability. "Dual mode" means that the turbocooler can operate in either a nozzle cooling mode or an engine cooling mode. The engine cooling mode operation is demonstrated by testing only the ACM in the engine cooling mode configuration since the ACM is the component directly effected by the mode change. The ACM tested in the engine cooling mode test included compressor labyrinth seal modification.

Table 6. Nozzle-Cooling Mode Acceptance Test Data

		ACM UNIT #	R1	R2	R1	R2		R1	R2		R1	R1	R2		R1		R1
ACM CONFIGURATION #			START MOD	START MOD	START MOD	START & COMP. LAB SEAL MOD		START MOD	START MOD		START MOD	START MOD	START & COMP. LAB SEAL MOD		START MOD		START MOD
MEASUREMENTS	**UNITS**	A	1	2	3	4	B	5	6	C	7	8	9	D	10	E	11
COMPRESSOR																	
COMP–PIN	PSIA	42	44.4	42	41.5	41.92	75	73.7	74.7	147	146.5	146	147.18	189	192.9	243	211
COMP–TIN	F	263	264.1	262.4	266.4	262.4	508	486.3	497.8	859	876	880.4	878.65	881	862.2	881	866.3
COMP–PEX	PSIA	76	79.8	68.1	76.4	66.75	165	149.1	154	220	214	213.6	208.22	300	285.8	385	312.7
COMP–TEX	F	424	423	388	423.2	383.08	801	734.3	746.6	1049	1052.7	1057.6	1041	1099	1044.3	1099	1048.2
TURBINE																	
TURB–PIN	PSIA	74	73.7	64.4	71.8	61.01	158	136.3	142.6	194	198.3	197.8	188	266	264.3	341	288.3
TURB–TIN	F	186	184.1	186.7	188.7	177.37	334	307.2	308.1	289	287.6	288.3	291.33	300	301.6	300	303
TURB–PEX	PSIA	19	18	18.8	14.5	19.54	18	21	21.1	39	37.9	37.7	39.07	48	50.6	61	55.3
TURB–TEX	F	12	5.3	42.6	4	34.38	11	12.8	11.7	45	57.4	58	68.28	46	66.8	46	68.1
XN – SPEED	RPM		54480	48352	55338	48073		68727	69309		63487	63778	61247		64070		64070
PERFORMANCE																	
COMP–PR		1.810	1.797	1.621	1.841	1.592	2.200	2.023	2.062	1.497	1.461	1.463	1.415	1.587	1.482	1.584	1.482
TURB–PR		3.895	4.094	3.426	4.952	3.122	8.778	6.490	6.758	4.974	5.232	5.247	4.812	5.542	5.223	5.590	5.213
ETACOMP	%	82.1%	82.2%	84.3%	87.3%	84.3%	82.6%	84.2%	87.5%	83.9%	85.6%	86.0%	85.1%	85.9%	85.4%	85.6%	0.859
ETATURB	%	84.4%	84.4%	75.7%	78.2%	81.4%	88.6%	93.4%	92.4%	89.3%	82.3%	82.2%	82.7%	87.1%	82.5%	86.7%	0.825
COMP–HP	HP	75.6	79.8	50.6	75.3	52.5	290.1	217.4	229.7	225.8	197.7	202.1	209.2	355.2	296.4	455.2	333.2
TURB–HP	HP	76.8	81.9	57.0	81.9	55.2	310.7	249.5	255.4	281.6	230.0	274.6	249.8	402.4	402.4	515.9	402.6
POWER BALANCE FACTOR		98.5%	0.974	0.888	0.919	0.951	93.4%	0.871	0.899	80.2%	0.859	0.736	0.837	88.3%	0.737	88.2%	0.828
HXPLOSS	%	2.6%	7.6%	5.4%	6.0%	8.6%	4.2%	8.6%	7.4%	11.8%	7.3%	7.4%	9.7%	11.3%	7.5%	11.4%	7.8%
FLOWS																	
COMP INLET	LB/MIN	83	88.8	71.2	84.9	76.9	175	154.9	163.2	210	197.7	201.6	227.7	288	287.7	369	323.7
TURB INLET	LB/MIN	78.0	81.0	69.9	78.4	68.2	170.0	149.8	152.3	204.0	176.6	210.7	197.9	280.0	302.9	359.0	302.9

3.2.7.1 Test Setup

AlliedSignal converted the ACM acceptance test rig from the exhaust nozzle cooling mode configuration to the engine cooling mode test setup. The ACM test setup in the engine cooling mode configuration is similar to the facility used for the exhaust nozzle cooling mode. However, in this test setup, although separate lines supply the turbine inlet air and compressor inlet air independently, the flows are extracted from the same source. Figure 48 is a photo of the setup, and it is schematically shown in Figure 49.

Because the high-pressure bleed air is fed directly to the turbine inlet, the bypass line (used to boost start during the exhaust cooling mode test) is no longer required. Bearing cooling is facilitated by the same bearing cooling inlet and outlet duct assemblies as used during the exhaust cooling mode test. The same heat exchangers were also used to cool the bearing cooling air (to 300°F or less) extracted from the compressor discharge air. A valve was added downstream of the heat exchangers to regulate the pressure into the ACM bearing cooling circuit. The purpose of this valve was to accurately simulate the air-side pressure drop across the ACEP heat exchangers. The remaining compressor discharge air, normally cooled and returned to the engine for cooling the hot section, is dumped during this rig test. Only the instrumented ACM with the compressor labyrinth seal modification was tested in the engine cooling mode configuration.

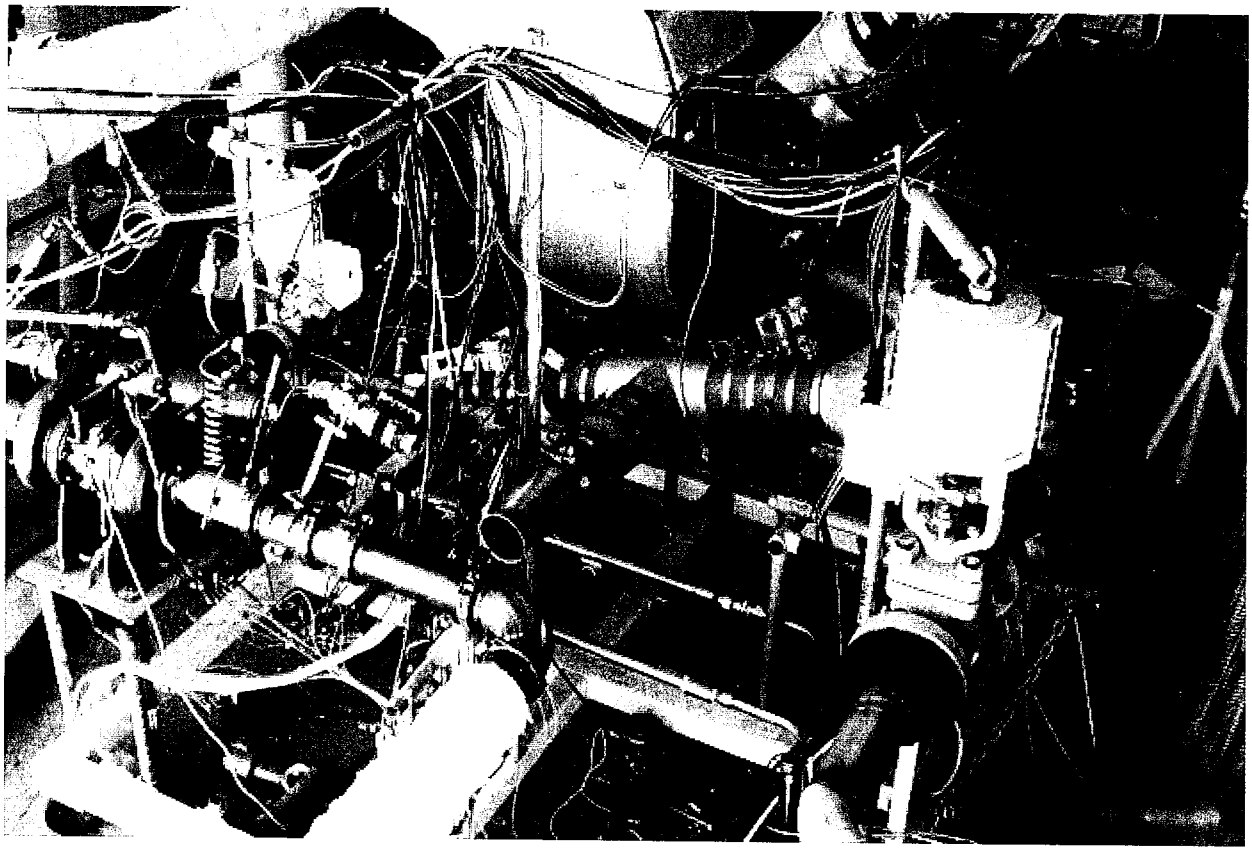

Figure 48. Engine Cooling Mode Test Setup

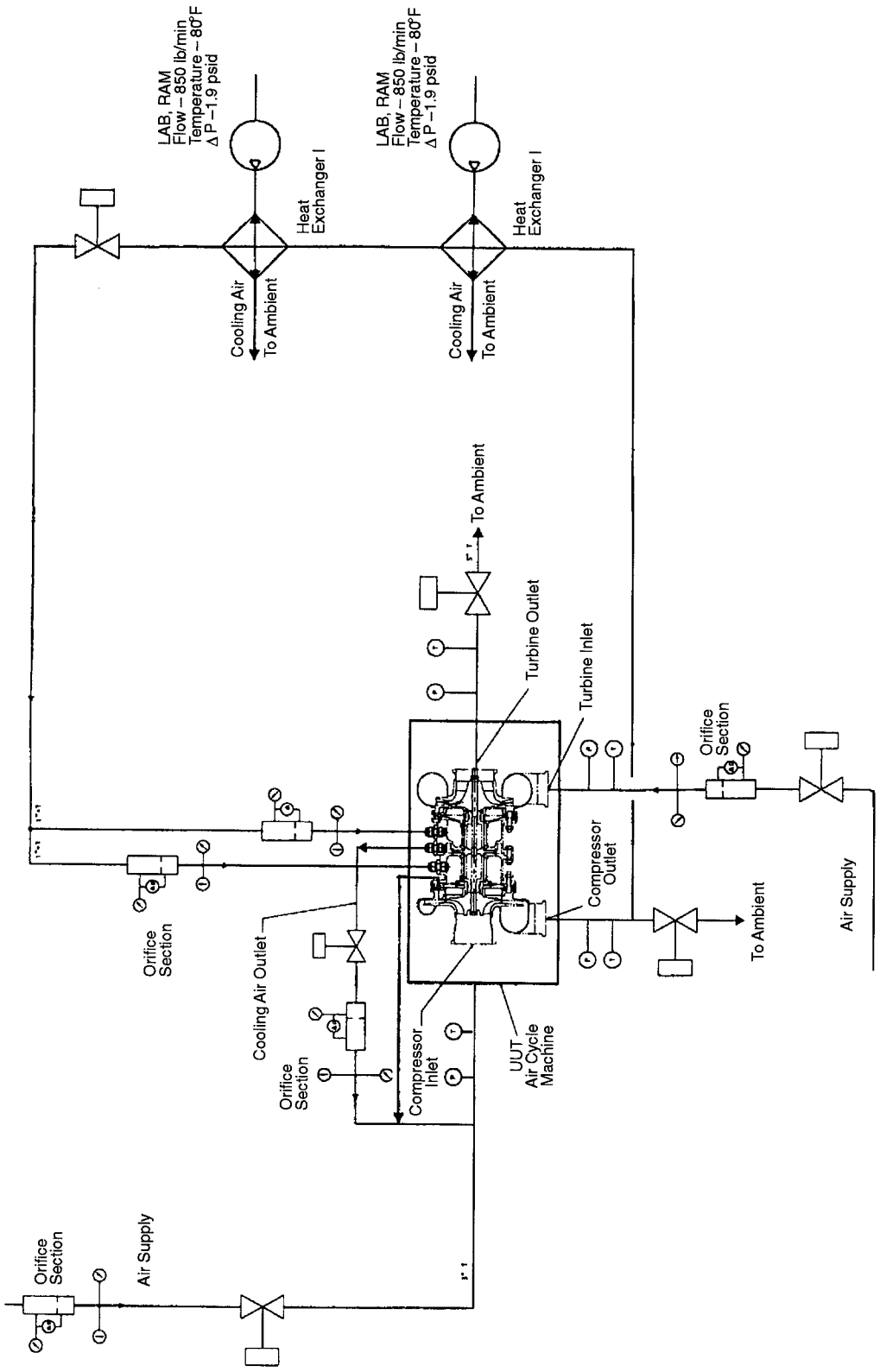

Figure 49. ACEP ACM Engine Cooling Mode Test (FM00856.ps)

The test setup included instrumentation to control the specific test conditions, evaluate performance characteristics of the test unit, and measure pressures and temperatures at selected locations for unit condition monitoring (similar to the exhaust nozzle cooling mode setup). Both discrete and real-time data were obtained during the test.

3.2.7.2 Test Conditions

The ACEP ACM engine cooling mode development test conditions are summarized in Table 7. Test condition F simulates the high-power engine cooling mode configuration associated with an engine throttle push and conventional fuel inlet temperatures (about 250°F). Test condition G simulates a low-power engine cooling mode condition associated with an engine life enhancement cooling approach and typical test cell fuel inlet temperatures (about 100°F).

3.2.7.3 Test Results

ACM acceptance test data for the engine cooling mode configuration summarized in Table 7 identifies the two primary test conditions of interest (F and G) and compares predicted versus measured results. Test condition G was adjusted to provide sufficient surge margin. Test condition F could not be reached because of the facility air limitation. The maximum achievable test condition commensurate with the same pressure ratios and required test temperatures was evaluated.

The measured test parameters closely approximate the target test conditions. Modification of the compressor labyrinth seal configuration, creating a low-pressure cavity between the back side of the compressor wheel and the compressor side journal bearing, provides sufficient cooling flow through the bearing cavity with air-side pressure drops comparable to those of the ACEP heat exchangers.

3.2.8 ACM Acceptance Test Performance Summary

Results of the ACM exhaust nozzle cooling mode acceptance tests, with the start and compressor labyrinth seal modifications, demonstrated the capability of the ACM to satisfy the intended application. The unit successfully operated at the maximum temperature and maximum achievable pressure and airflow (within the facility limits). Table 7 compares test results with the predicted performance of the unit. These results show that the ACEP ACM meets the required performance and is capable of dual-mode operation. The performance calculations relate to the latest test unit configuration (ACM modified for improved compressor journal bearing cooling).

Bearing Cooling – The air bearings used for the ACEP ACM can operate up to 500°F satisfactorily and without distress. The thermal capability of the bearing coating is limited to 650 F. To provide sufficient thermal margin, the bearing condition inlet air temperature is limited to a maximum of 300°F, and the bearing cooling flow area is sized to provide ample airflow to absorb the heat generated by the bearings. Instrumentation in the unit enabled verification of ample bearing cooling. Internal unit pressures and temperatures provided deductions of the adequacy of bearing cooling which was later improved by providing a low-pressure cavity between the compressor wheel and the compressor journal bearing exit.

Table 7. Engine Cooling Mode ACM Test Data

MEASUREMENTS	UNITS	ACM UNIT						
		R1	R1	R1		R1	R1	R1
		CASE F	START & COMP. LAB. SEAL MODS	START & COMP. LAB. SEAL MODS	EXTRAPOLATED	CASE G	START & COMP. LAB. SEAL MODS	START & COMP. LAB. SEAL MODS
COMPRESSOR								
COMP–PIN	PSIA	259	222	224	259	213	188.3	226.9
COMP–TIN	F	880	924	906	924	881	890	897
COMP–PEX	PSIA	381	334.3	336.3	390	357	306.5	368.5
COMP–TEX	F	1068	1115	1097	1115	1119	1119	1132
TURBINE								
TURB–PIN	PSIA	259	227.4	227.9	265	213	191.2	227.9
TURB–TIN	F	894	902	899	902	894	890	901
TURB–PEX	PSIA	53	47	47.1	55	48	42.6	51.2
TURB–TEX	F	519	524	524	524	525	523	531
SPEED	RPM	62780	63621	63328		66442	65675	65675
PERFORMANCE								
COMP–PR		1.47	1.51	1.50	1.51	1.68	1.63	1.62
TURB–PR		4.89	4.84	4.84	4.82	4.44	4.49	4.45
COMP–TR		1.14	1.14	1.14	1.14	1.18	1.17	1.17
TURB–TR		1.40	1.36	1.36	1.41	1.32	1.30	1.35
XNR	RPM	100906	103923	102769	0	106831	105952	106226
WAR	LB/M	34.02	37.76	38.57	36.99	26.07	29.79	29.24
ETACOMP	%	0.82	0.89	0.87	0.89	0.89	0.87	0.85
YFAC		0.57	0.56	0.56	0.56	0.52	0.53	0.53
DTi		489.78	490.22	489.15	489.19	465.87	467.34	469.05
ETATURB	%	0.77	0.77	0.77	0.77	0.79	0.79	0.79
Fv		0.75	0.76	0.76	0.00	0.82	0.81	0.81
COMP–HP	HP	396.77	377.27	391.43	431.20	316.46	306.57	371.11
TURB–HP	HP	420.12	350.12	356.04	408.51	338.23	276.60	320.10
POWER BALANCE FACTOR		0.94	1.08	1.10	1.06	0.94	1.11	1.16
HXPLOSS	%	10.7%	9.2%	9.3%	9.6%	5.2%	5.9%	10.6%
EST. BRG. FLOW PRES	P	40.767				18.564		
FLOWS								
COMP INLET	LB/MIN	373	349.1	362.2	399	235	236.6	279.1
TURB INLET	LB/MIN	198	163.7	167.8	191	162	133.2	152.9
BEARING LOADS, ACTUAL PRESSURE								
COMP IN THRST	LBF	5701	4892	4925	N/A	4874	4215	5081
COMP BK THRST	LBF	–5955	–5075	–5088	N/A	–5398	–4488	–5411
COMP LAB THRST	LBF	1	–3	–5	N/A	–11	–15	–12
TURB BK THRST	LBF	1846	1092	971	N/A	1569	1025	1202
TURB OUT THRST	LBF	–1217	–988	–985	N/A	–1074	–890	–1070
COMP MOMENTUM	LBF	45	48	50	N/A	22	25	29
TURB MOMENTUM	LBF	–37	–28	–30	N/A	–27	–21	–23
TURB LAB SEAL	LBF	–21	–17	–18	N/A	–20	–16	–19
NET THRUST	LBF	364	–80	–179	N/A	–66	–165	–223
THRUST LOAD ESTIMATES								
COMP IN THR EST.	LBF	5769	4982	5022	5813	4956	4337	5222
COMP BK THR EST.	LBF	–5867	–5110	–5146	–5962	–5287	–4578	–5507
COMP LAB THR EST.	LBF	0	–2	–1	–2	0	–1	0
TURB OUT THR EST.	LBF	–1640	–1446	–1449	–1689	–1412	–1260	–1508
THRB BK THR EST.	LBF	1830	1611	1615	1880	1551	1387	1658
COMP IN MOMENTUM	LBF	45	48	50	53	22	25	29
TURB OUT MOMENTUM	LBF	–37	–28	–30	–33	–27	–21	–23
PTH, TURB LABY SEAL	LBF	–16	–14	–14	–17	–13	–12	–14
NET THR EST.	LBF	85	40	47	44	–211	–122	–144

Thrust Load – The net thrust load acting on the rotating assembly affects the thrust bearing load during start and operation. Excessive thrust load makes it difficult for the unit to start, and when the unit is forced to start it subjects the thrust bearing to a brake-like wear and immediate failure. The unit was modified to induce lower start inlet pressure. During operation, the thrust load is affected mostly by the available pressure behind both wheels (compressor and turbine) and the pressure acting on the labyrinth seals (compressor, compressor bearing, and turbine). The compressor labyrinth seal was designed to reduce the thrust load during start and during the worst thrust-load-related operating condition (considering that both compressor wheel and turbine wheel diameters were fixed by their required performance). Various seals were assessed to optimize the ACM thrust during all operating conditions. Commensurate with acceptable thrust load during operation, reasonable start thrust load and redesign envelope (compressor wheel labyrinth seal diameter of 1.7245 inches), a compressor-journal bearing labyrinth seal diameter of 2.05 inches was chosen.

A summary of the ACM thrust loads during the engine cooling mode rig test is presented in Table 7. The objective is to keep the thrust load under 500 lbf with a maximum limit of 700 lbf. A negative sign indicates that the thrust load is toward the compressor wheel, and a positive sign indicates that the thrust load is toward the turbine wheel.

A start/stop cycle test also was conducted to demonstrate the capability of the unit to handle multiple start/stops. The unit (with original compressor labyrinth seal configuration) was tested for 130 cycles. Test results showed that the start pressure gradually increased and stabilized to about 27 psig after 80 start/stop cycles.

3.3 Fuel/Air Heat Exchanger

3.3.1 Heat Exchanger Trade Studies

The purpose of the heat exchanger is to transfer energy efficiently from the hot compressor discharge air to the fuel. Design constraints must be satisfied for heat transfer capacity, air- and fuel-side pressure losses, and ease of manufacturing (including CBC application after the unit is manufactured). The baseline heat exchanger configuration proposed for this application was a conventional shell-and-tube type due to the high fuel and air side pressures. The high-pressure fuel is placed on the shell side of the heat exchanger — flowing over the tubes while air flows through the tubes. The design requirements summarized in Table 8 are based on the exhaust nozzle cooling mode (Test condition E).

Table 8. Heat Exchanger Thermal Performance Requirements

Requirement	Hot Side	Cold Side
Fluid	Air	JP Fuel
Flow, lbm/s	5.64	2.246
Inlet Temperature, °F	1154	250
Inlet Pressure, psia	354.6	1200
Outlet Temperature, °F	396.8	912.6
Pressure Drop, psi	20.0	11.3
Heat Load (Ref only), Btu/s	1100	—
Effectiveness (Ref only)	0.84	—

Heat exchanger trade studies were conducted to select a preferred configuration. Initially, seven configurations of tube OD (outer diameter) and wall thickness were considered, as summarized in Table 9. Two of the configurations used inserts (turbulators) to enhance the air-side heat transfer.

Preliminary size estimates are also listed in Table 9. Six of these configurations had equilateral triangular tube patterns with 0.060-in spacing between the tubes; configuration 7 had 0.030-in tube spacing. Tube spacing of 0.030-in is quite conventional, and the contractor has experience with tube spacing as low as 0.023-in on production units. The first tube size, in configuration 1, was used as a starting point. The second configuration was an attempt to reduce the heat exchanger weight. The third was an attempt to reduce tube count. The fourth was an attempt to reduce the tube length. The fifth was an attempt to reduce the shell diameter, overall volume, and weight. The sixth was to determine the effect of small tube diameter on heat exchanger volume. Configuration 7 reduced the shell diameter and overall heat exchanger volume.

Table 9. Preliminary Heat Exchanger Sizing

Tube Configuration	Number of Tubes	Shell ID (in)	Tube Length (in)	Core Volume (ft^3)	Tube Bundle Weight (lbm)	Turbulators
1. 0.1228-in OD, 0.0184-in Wall	1350	7	48	0.93	117	
2. 0.125-in OD, 0.010-in Wall	925	6	64	0.86	64	
3. 0.250-in OD, 0.020-in Wall	225	5	150	1.3	146	
4. 0.150-in OD, 0.012-in Wall	5260	16	18	1.78	148	Dog-ears
5. 0.150-in OD, 0.010-in Wall	1187	8	29	0.78	44	Moderate
6. 0.0625-in OD, 0.010-in Wall	4321	8.7	21	0.67	34	
7. 0.0625-in OD, 0.008-in Wall with 0.030-in Tube Spacing	4332	6.5	21	0.38	34	

The normalized results shown in Table 10 indicate that the shell inner diameter, tube length, and tube count are greatly affected by the selected tube configuration. This is caused primarily by the flow and pressure-drop characteristics of the airflow inside the tubes. Allowable pressure drop was initially 20 psid. The heat exchanger air-side pressure drop is dictated by the engine cooling mode system balance. In this operating mode, the heat exchanger air discharge pressure cannot be less than 7.5% above P_3 (engine compressor discharge pressure) in order for the cooling to be reintroduced to the engine cooling system.

A qualitative assessment of the various heat exchanger configurations is presented in Table 11. As indicated, configuration 2 is considered the baseline design, primarily because it produces the best compromise between shell diameter, tube length, tube count and weight. Structural considerations drive the design toward smaller shell diameters. Packaging considerations drive the design toward smaller tube lengths. Manufacturing considerations drive the design toward smaller tube counts.

The dog-eared turbulator inserts, configuration 4, produce significantly higher pressure drop than smooth tubes. Thus, more tubes with less flow per tube (and larger shell diameter) are required to achieve the 20 psid. The large shell diameter is unacceptable from a structural standpoint; the shell

Table 10. Normalized Heat Exchange Sizing

Tube Configuration	Tubes	Shell ID	Volume	Weight	Tube Length	Turbulators
1. 0.1228-in OD, 0.0184-in Wall	1.5	1.17	1.08	1.83	0.75	
2. 0.125-in OD, 0.010-in Wall	1.0	1.00	1.00	1.00	1.00	
3. 0.250-in OD, 0.020-in Wall	0.2	0.83	1.51	2.28	2.34	
4. 0.150-in OD, 0.012-in Wall	5.7	2.67	2.07	2.31	0.28	Dog-ears
5. 0.150-in OD, 0.010-in Wall	1.3	1.33	0.91	0.69	0.45	Moderate
6. 0.0625-in OD, 0.010-in Wall	4.7	1.45	0.78	0.53	0.33	
7. 0.0625-in OD, 0.008-in Wall with 0.030-in Tube Spacing	4.7	1.08	0.44	0.53	0.33	

Table 11. Qualitative Heat Exchanger Assessment

Characteristic/Issues	Configuration						
	1	2	3	4	5	6	7
Tube Length	–	– –	– –	+ +	+	+ +	+ +
CBC Compatibility	+	+	–	–	+	–	–
Ease of Fabrication	+	+ +	–	–	+	– –	– –
Shell Thickness	+	+ +	+ +	– –	– –	– –	+
Performance Confidence	+	+	+	+	–	+	+
Weight/Volume	– –	–	– –	– –	+	+ +	+ +
Relative Score	***+1***	***+3***	***–3***	***–3***	***1***	***0***	***3***

and header thickness increase dramatically. Configuration 5 attempted to provide an intermediate solution between the baseline and dog-eared insert configurations. In other words, reduce the shell diameter from configuration 4 but try to maintain the shorter tube length. The "moderate" turbulation is theoretically based on extrapolation of dimpled-tube heat transfer and pressure drop characteristics. Although the sizing results of configuration 5 are very favorable, the theoretical turbulator required additional development and was deemed high risk. Configurations 6 and 7 use 0.0625-in diameter tubes to reduce the overall heat exchanger volume. Configuration 7 produces the best overall heat exchanger solution relative to volume, tube length, and shell diameter — by virtue of the closer packed tubes. However, the contractor team felt that the combination of low tube diameters, quantity of tubes, and high operating pressure and temperature levels would introduce significant heat exchanger development risks. Therefore, the 0.0625-in tube OD solutions were dropped from consideration.

The preferred heat exchanger arrangement is configuration number 2. To reduce the overall tube length for configuration 2, the heat exchanger could be divided into modules connected in series flow, so the shell diameter would remain the same at approximately 6 inches, but the length of each module would be reduced to about 32 inches (excluding manifolds and fittings). Structurally, this should be the same as one 64-in module. Flow-wise, there would be an additional pressure drop due to two sets of manifold losses rather than one.

3.3.2 Design Description

This subsection describes the final configuration and detailed design characteristics of the fuel/air heat exchanger. The heat exchanger is an Inconel alloy assembly consisting of a brazed tubular core with welded air-side manifolds. It is a cross-counterflow heat exchanger with air flowing through the tubes and fuel flowing over the tubes in an 11-pass configuration. The tube bundle is contained by a cylindrical outer shell, brazed at each end to the headers and supported by a series of baffles. The baffles channel flow for the multipass configuration in addition to providing longitudinal support for the tubes. The tubes are polished to a smooth finish. The cooler shell has a 6.43-in inside diameter with a single convolute bellow to help minimize stress due to the difference in thermal expansion between the shell and tubes during the transient "cold start" design condition. CBC is applied to the fuel-side components after the unit is fully assembled.

Fuel makes 11 passes over the baffles and through the tube bundle. In the other circuit, airflow is contained at both ends by semispherical manifolds. Airflow enters through a 2.75-in duct, flows through the tubes, and exits through another 2.75-in duct at the opposite end. The air-side interface consists of two 20°, high-pressure/temperature flanges. The heat transfer surface consists of 946 tubes arranged in a 0.185-in equilateral triangle pattern. The tubes have 0.125-in OD with 0.013-in wall thickness, and the length between headers is 29 inches. The heat exchanger material and calculated weight are summarized in Table 12.

Table 12. Heat Exchanger Material and Weight Estimate

Part	Material	Quantity	Weight, lbm	Total Weight, lbm
Shell	Inconel 625	1	30.12	30.12
Header	Inconel 625	2	10.675	21.35
Tube	Inconel 625	946	0.04247	40.17
Baffle	Inconel 625	10	0.52	5.20
Rail	Inconel 625	4	0.1905	0.762
Ring	Inconel 625	1	0.436	0.436
Boss, Fuel	Inconel 625	2	0.686	1.372
Boss, Instrumentation	Inconel 625	4	0.077	0.308
Manifold Assembly	Inconel 625	2	1.29	2.58
Flange	Inconel 625	2	0.37	0.74
Miscellaneous (+5%)				5.152
Total Dry Weight				**113.60**

3.3.3 Thermal Performance

The heat exchanger sizing point is defined as the exhaust system cooling mode. These conditions are summarized in Table 13.

Table 13. Heat Exchanger Thermal Performance Requirements

Parameter	Hot Side	Cold Side
Fluid	Air	JP Fuel
Flow, lbm/s	5.64	2.246
Inlet Temperature, °F	1154	250
Inlet Pressure, psia	354.6	1200
Outlet Temperature, °F	396.8	912.6
Pressure drop, psi	20.0	11.3
Heat Load (Reference only), Btu/s	1100	—
Effectiveness (Reference only)	0.84	—

The performance predictions for heat transfer and pressure drop are summarized in Figures 50, 51, and 52. Fluid properties and analyses methods are described in the following paragraphs.

3.3.3.1 Fluid Properties

Air Properties – The properties used in the analysis of the heat exchanger are from the standard air tables in the AlliedSignal library. The particular data set is for air at 20 bars (290 psia); the inlet pressure for the design point is 355 psia. Since the transport properties of air do not vary greatly with pressure, the use of the 20-bar data was deemed acceptable.

Fuel Properties – The JP–5 fluid properties for the analyses were defined especially for the high-pressure operating condition of 1200 psia, see Table 14). Two sets of reference data were used. Standard AlliedSignal data for saturated liquid data up into the critical region were combined with shell development tables for the range of 800° to 1500°F.

3.3.3.2 Heat-Transfer and Pressure-Drop Analyses

The fuel/air heat exchanger was initially designed using a generalized technique for tube-and-shell heat exchangers. This technique is based on experience and correlations developed in the chemical process industry. It employs fluid properties evaluated at average temperatures and many simplifying assumptions. The technique is useful for providing a first-cut design.

3.3.3.3 Design-Point Performance Prediction

This step was carried out by means of a detailed program using finite-difference techniques. The program, HXT5, is set up for a heat exchanger that has a rectangular tube bundle. The rectangular shape is well suited to being divided into many finite-difference elements. In order to use HXT5, the round tube-and-shell bundle was "mapped" into a rectangular shape. In addition, the two heat exchangers were combined into one device for this analysis. The dimensions of the resulting "equivalent-rectangular-platform" HX are:

- JP–5 Single-Pass Length: 5.287 in
- Airflow Length: 58.000 in
- "No Flow" Height: 5.362 in

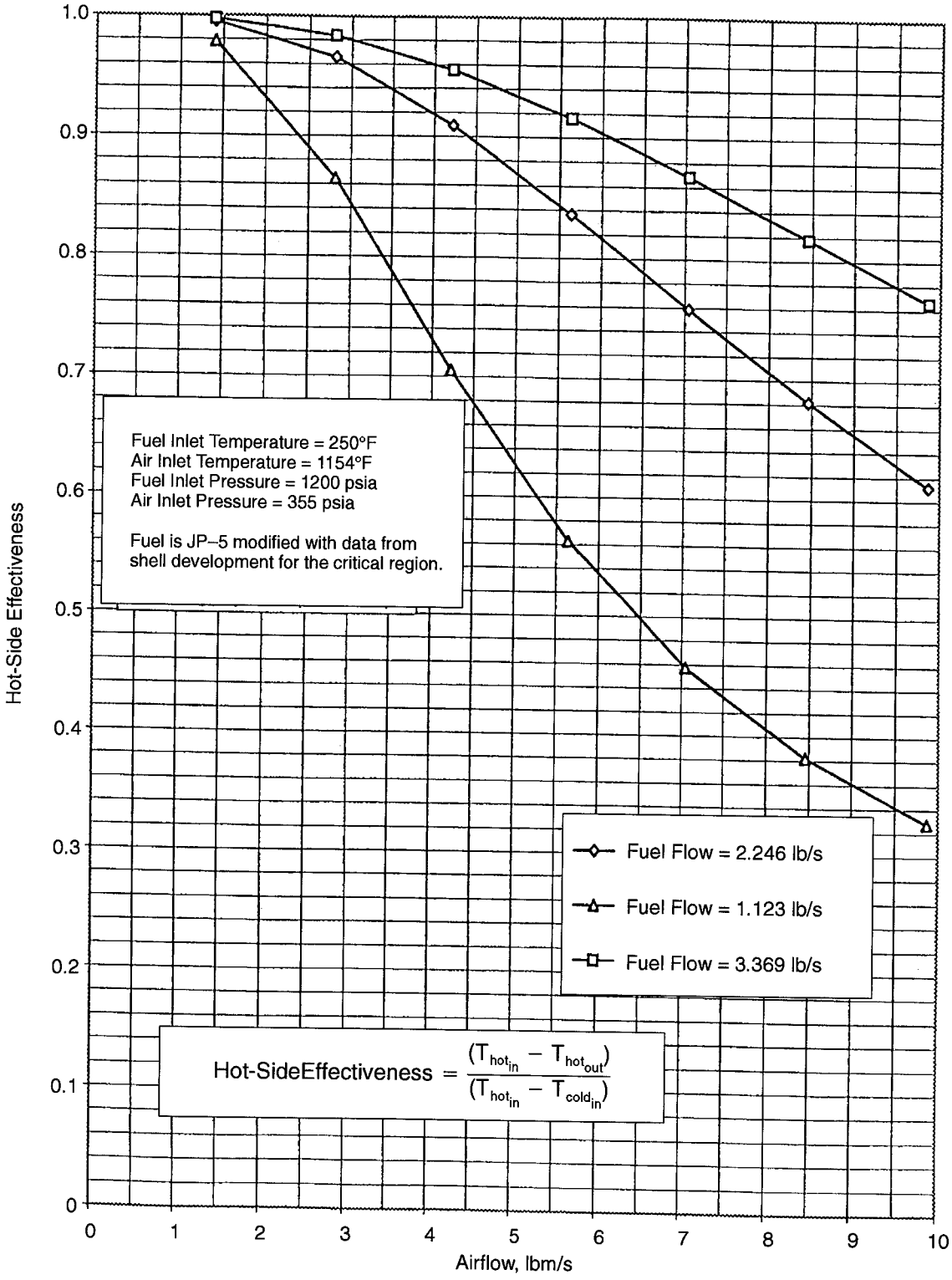

Figure 50. Calculated Heat Transfer Performance

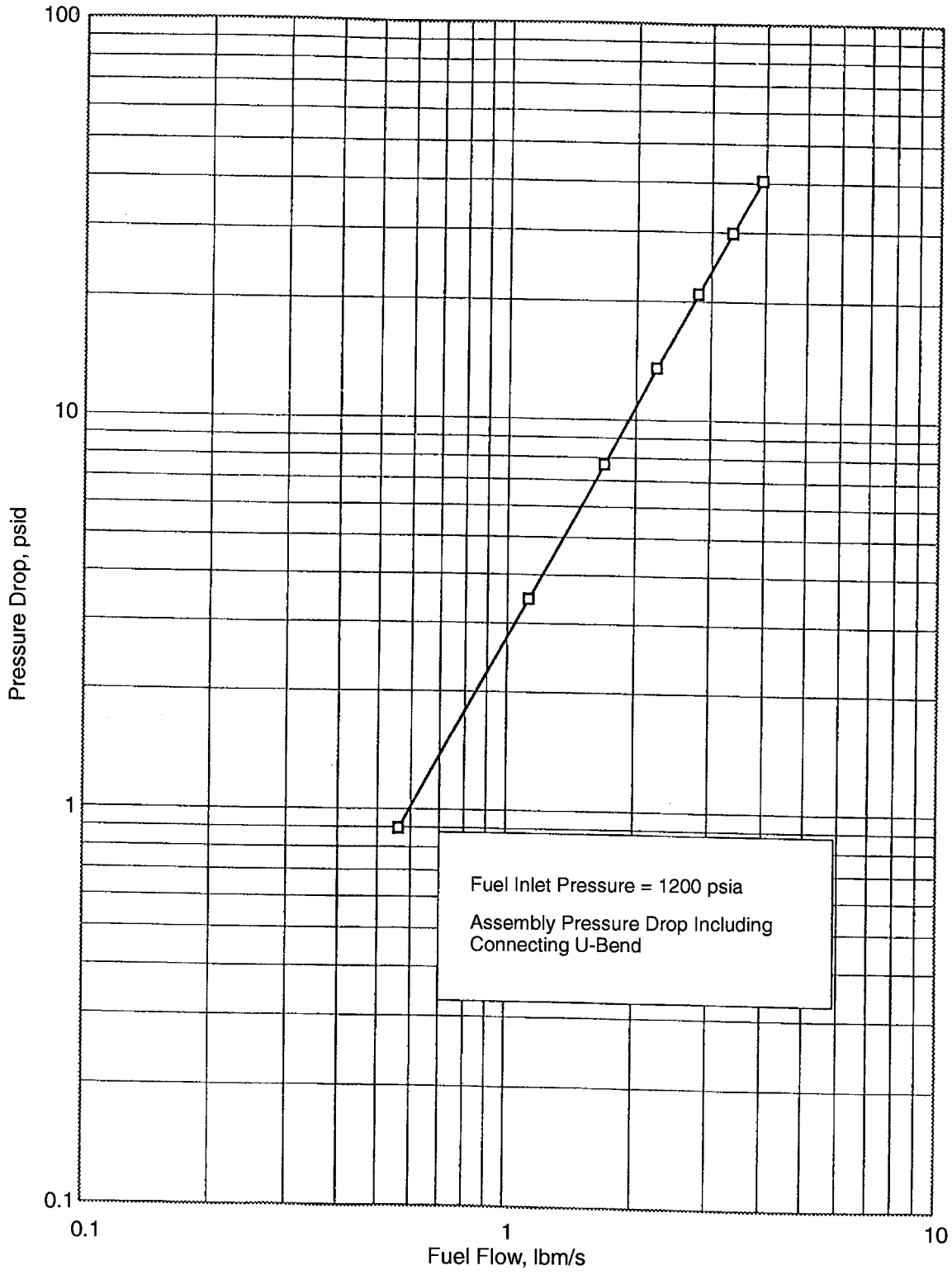

Figure 51. Fuel-Side Pressure Drop

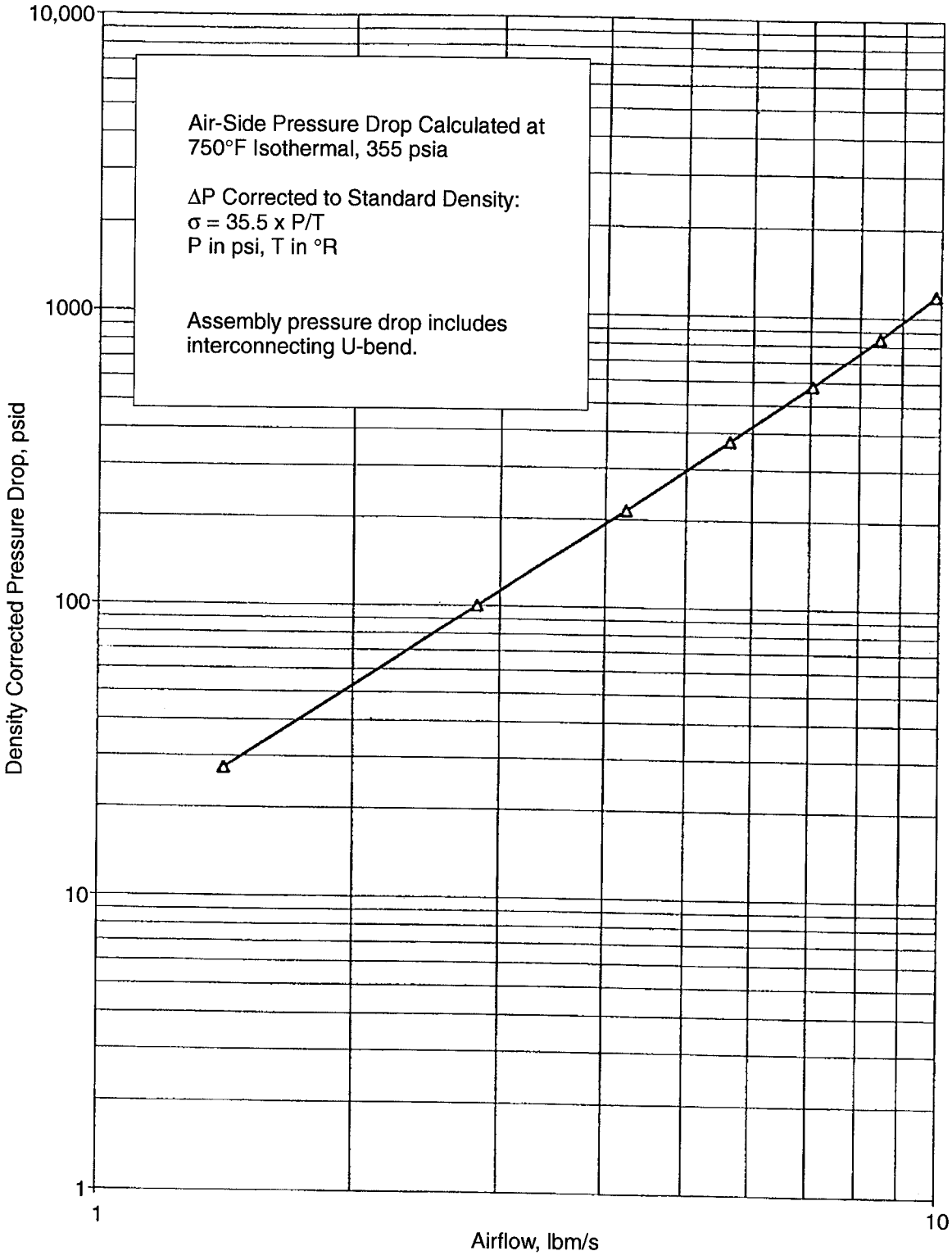

Figure 52. Air-Side Pressure Drop

Table 14. JP–5 Fluid Properties at 1200 Psia

Temperature, °F	Density, lbm/ft^3	Specific Heat, Btu/lbm–°F	Viscosity, lbm/hr–ft	Prandtl Number
0	52.5	0.393	13.0	63.0
50		0.424	5.8	32.2
100	50.7	0.455	3.35	21.3
150		0.486	2.16	15.8
200	48.7	0.521	1.55	12.7
250		0.553	1.17	10.9
300	46.8	0.585	0.95	9.4
350		0.622	0.78	8.3
400	44.6	0.656	0.66	7.5
450		0.694	0.56	6.8
500	42.4	0.730	0.475	6.23
550		0.755	0.404	5.63
600	39.7	0.775	0.352	5.1
650		0.792	0.299	4.6
700	36.5	0.810	0.248	3.98
750		0.815	0.190	3.66
800	32.33	0.8256	0.1587	3.174
850	29.72	0.8266	0.1349	2.807
900	27.12	0.8278	0.1199	2.506
950	24.64	0.8287	0.1057	2.234
1000	22.20	0.8291	0.0932	1.981
1050	19.92	0.8287	0.0833	1.770
1100	17.94	0.8276	0.0761	1.603
1150	16.26	0.8259	0.0709	1.472
1200	14.85	0.8240	0.0672	1.369
1250	13.65	0.8219	0.0646	1.287
1300	12.62	0.8187	0.0627	1.219
1350	11.73	0.8174	0.0613	1.167
1400	10.97	0.8164	0.0604	1.124
1400	10.33	0.8154	0.0598	1.091
1500	9.79	0.8144	0.0594	1.064

It can be seen that this rectangular bundle shape is not greatly different from the actual tube bundle in the circular shell. The tube bundle configuration (tube pitch and alignment) remained the same as in the actual heat exchanger.

The finite-difference computations matrix was 6×66, for a total of 396 elements. That is, 6 elements across the heat exchanger and 66 elements along the length. The program has the capability of evaluating fluid properties and heat transfer coefficients based on the average temperature of a fluid (average from inlet and outlet) or optionally using the local fluid temperature at each and every finite-difference element. For the ACEP fuel/air heat exchanger, the latter computation mode of local evaluation was used because it is more accurate than average-temperature evaluation as the fuel properties vary significantly from inlet to outlet.

The pressure-drop computations in the program always use local properties (viscosity and density) and local friction factors. For each element, the friction and flow acceleration (or deceleration) losses are evaluated rigorously. For liquid flow outside of the tube bundle, the friction and heat transfer data of Bergelin were used. The evaluations of friction factor and j factor for the liquid involve corrections involving the ratio of the free-stream viscosity to that at the tube wall. For the airflow within the tubes, standard tubular f and j data were used.

The pressure-drop computations involve the frictional/accelerational losses within the heat-transfer matrix, the various entrance and exit losses into the matrix, and the losses associated with the pans (or headers) at the ends of each unit. The HXT5 pressure drop computations had to be augmented to include the additional pressure losses in the air-side exit pan of the first unit, the inlet pan of the second unit, and the connecting piping between the two units. This was done via a spreadsheet computation. The pressure-drop computation for the interconnecting piping includes special considerations for the pipe bends in these tubes.

The program considers heat conduction within the heat transfer matrix. For a tubular unit, there is usually little conduction across the unit (via the baffles); thus, the matrix is limited to longitudinal conduction in the tube walls. This is considered automatically for the ACEP fuel/air heat exchanger with its very long tubes, and it is judged that there is very little effect due to this conduction.

The conduction in the tube header plates is considered, but that of the baffles within the shell is not. The effect of the lateral conduction in the baffles is not expected to be great, especially since the contact between tubes and baffles is, by design, minimal.

3.3.3.4 Effect of Coating on Heat Exchanger Performance

The performance predictions are for clean, noncoated tubes. The heat exchanger analysis program can accommodate the effects of a coating in the form of a "fouling factor" and a "fouled-layer thickness" (both built-in options). Very little performance change due to coating is expected since it is very thin (5000 Å), is only applied on the fuel side (outside the tubes), and the heat-transfer conductance is far greater on the outside of the tubes than that on the inside of the tubes. The pertinent conductances are approximately 91,000 Btu/hr–°F outside the tubes and 34,000 Btu/hr–°F inside the tubes. Clearly the performance is dominated by the air-side heat transfer.

3.3.4 Structural Analysis

The analysis described in this section addresses key structural design areas including the header, manifold, collars, and tubes. All of these items respond to pressure and thermal load. The structural

analysis for the heat exchanger requires thermal and pressure loading. The shell design includes a convolution that significantly reduces thermally induced loading from the heat exchanger tubes and shell. The major components are shown in Figure 53.

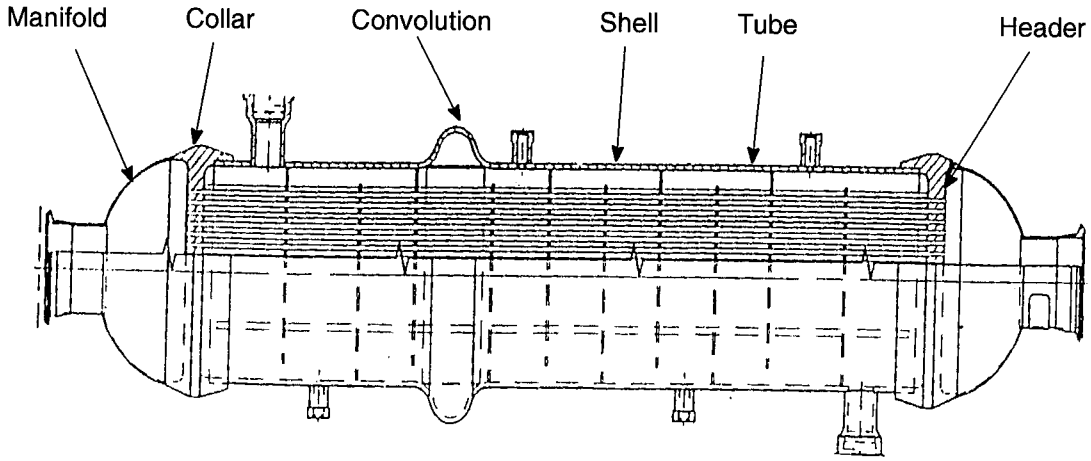

Figure 53. Fuel/Air Heat Exchanger Components

The following subsection (3.3.4.1) addresses analysis results based on the start-up transient devised in the initial stages of the program. It involves establishment of full fuel flow through the heat exchanger well before any air is admitted to the unit. Then, over a 60-second period, the airflow is increased to the full flow rate.

Subsection 3.3.4.2 describes low-cycle fatigue analysis using ANSYS.

3.3.4.1 Start-Up Transient Structural Analysis

The start-up transient, devised in the initial stages of the program, involves establishment of full fuel flow through the heat exchanger well before any air is admitted to the unit. The initial stress analysis indicated a shell thickness of 0.14 inch using Inconel 625 as the heat exchanger material. This was set primarily by the 1200-psia fuel pressure in the shell and tube and shell steady-state temperature distributions. However, transient startup conditions are more severe than steady-state conditions in terms of tube-to-shell temperature differences. Prior to startup, cold fuel flows through the heat exchanger (over the tubes), but no air is flowing through the tubes. At startup, hot air is introduced to the heat exchanger over a 60-second period. The thin-walled tubes quickly heat up while the shell temperature lags behind. This produces a tube-to-shell temperature difference larger than the steady-state condition (as high as 400°F). The tubes expand faster than the cooler shell which, in turn, restrains the tubes. The greatest thermal stresses are expected during the startup of the unit, so this special type of startup transient was envisioned to limit such stress. This stress situation is only experienced by the heat exchanger immediately downstream of the ACM compressor. Originally the stress analysis was to be based on a transient involving a "cold soak" of 250°F (representing the initial fuel temperature in the aircraft). However, test conditions on the ground, involving a fuel storage facility at 60°F, changed the cold-soak initial condition to the latter temperature. The primary fix for this classic condition is placement of one or more bellows in the shell so that the shell will flex with the expanding tubes. To accommodate this, the shell thickness (and therefore the shell diameter) should be kept to a minimum so the bellows will have approximately the same thickness

as the shell. The bellows must provide the same hydrostatic restraint against the 1200-psia fuel pressure and still provide adequate flexibility.

HXT5 was used to compute the transient response of the fluids and the heat transfer matrix during the 60-second startup. This was done for both the 250°F and 60°F initial conditions. HXT5 is a fully functional, transient-analysis program. When used to obtain steady-state results, as discussed in previous sections, the boundary conditions (flow rates, inlet temperatures, and inlet pressures) are held constant with time and the performance prediction is continued until steady conditions are attained.

For a shell-and-tube heat exchanger, HXT5 does not compute the shell and pan temperatures. (They are not considered part of the active thermal matrix.) Because of the relative mass of the shell, headers, and manifold — and the typically poor heat-transfer coefficients associated with them — these parts of the heat exchanger will lag significantly behind the fluid and tube temperatures. This lag can introduce considerable stresses within the heat exchanger.

To compute the shell, header, and manifold temperatures during the transient, it is necessary to use a separate analysis using a thermal analyzer program. For the start-up transient, HXT5 is first run; at specified time intervals, the temperatures of all finite-difference elements (metal and the two fluids) are printed out (or alternatively written to an external file). These transient fluid and tube-wall temperatures form the boundary conditions for the transient thermal analyzer computations. This approach is based upon the assumption that the fluid and tube-wall temperatures are minimally affected by the presence of the massive shell, header, and manifold; thus, the separate computation can be made using the stand-alone, finite-difference program. This approach has been verified in many previous projects that involve heat exchangers.

Design Point Assumptions – For the steady-state loads, the pressures and temperatures were assumed to be:

- Air inlet pressure: 354.6 psia
- Air inlet temperature: 1154°F
- Fuel inlet pressure: 1200 psia
- Fuel inlet temperature: 250°F

For the transient analysis, it was assumed the system will reach steady conditions after 60 seconds.

Material Properties – The material properties of Inconel 625 listed in Table 15 were used in the stress calculations.

Table 15. Inconel 625 Properties (Annealed), from MIL HDBK–5G

Minimum Properties	70°F	300°F	600°F	1100°F
Ultimate Strength, ksi	120	112.8	106.8	98.4
Yield Strength, ksi	54	45.4	40.0	36.7

Steady-State Analysis – The 2D, axisymmetric, finite-element model developed for the steady-state analysis is shown in Figure 54. The model consists of the header, manifold, collar, shell, and tubes. The requirements for operating, proof, and burst pressures and temperatures are summarized in Table 16.

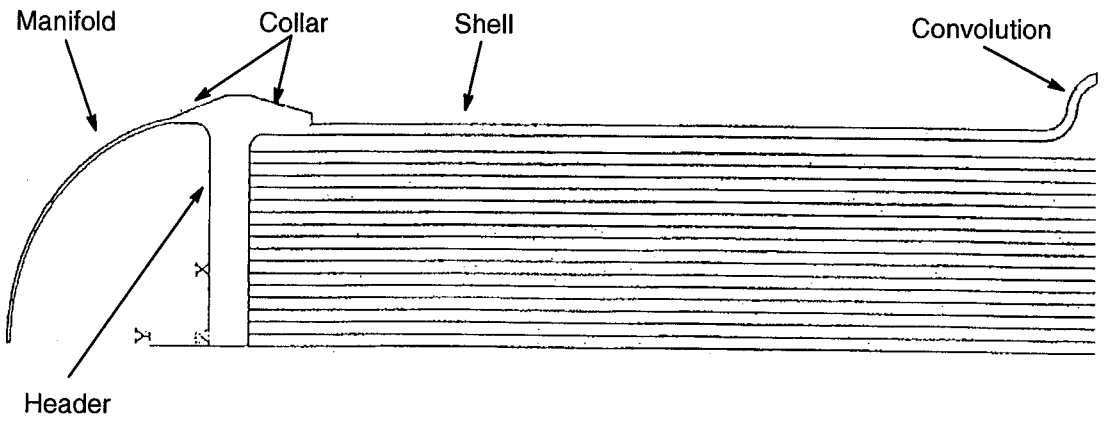

Figure 54. Finite-Element Model of Heat Exchanger

Table 16. Steady-State Condition Requirements

Location	Operating		Proof		Burst	
	psia	°F	psia	°F	psia	°F
Air Inlet	354.6	1154	532.0	1154	886.5	1154
Fuel Inlet	1200	935	1800	935	3000	935

Transient Analysis – Temperature distribution for the analysis was provided by transient gradients generated by the finite-difference thermal models are shown in Appendix A. A thermal-cycle stress analysis was performed with a tubular heat exchanger program. The results were reviewed, and the peak stress regions were identified. Life estimates are obtained from the low-cycle fatigue analysis for the most severe conditions of temperature and stress.

Summary of Transient Analysis – The results indicate that the heat exchanger is structurally satisfactory for the steady-state and transient conditions. The expected life to crack initiation is 1400 cycles. The results for the steady-state conditions and for the transient fatigue life are listed in Tables 17 and 18, respectively. The boundary conditions and stresses at steady state are shown in Figures 55 and 56.

Table 17. Margin of Safety for Steady-State Conditions

Critical Area	Material	Loads, psi		Temperature (°F)	Calculated Stress (ksi)	Allowable Stress (ksi)	Margin of Safety
		P_{fuel}	P_{air}				
Header	Inco 625	1185	335	1150	5.40	40.8	+5.20
Collar	Inco 625	1185	335	935	10.60	36.7	+2.50
Shell	Inco 625	1185	335	935	23.8	36.7	+0.50
Collar	Inco 625	1185	335	1150	10.60	40.8	+2.85
Manifold	Inco 625	1185	335	1150	10.60	40.8	+2.85
Tube	Inco 625	1185	335	1040	8.08	41.0	+4.07

Table 18. Predicted Minimum Life for Transient Conditions (Includes Scatter Factor of 10)

Critical Area	Material	Stress, ksi			Estimated Life (Cycles)
		30 Seconds	40 Seconds	60 Seconds	
Header	Inconel 625	14.0	15.0	12.3	4.8×10^{10}
Collar	Inconel 625	121.0	125.4	95.3	5.0×10^{3}
Shell	Inconel 625	45.5	47.4	37.2	5.1×10^{7}
Collar	Inconel 625	155.0	157.5	110.0	1.4×10^{3}
Manifold	Inconel 625	20.0	19.1	12.3	7.1×10^{9}
Tube	Inconel 625	9.1	9.3	9.1	3.7×10^{12}

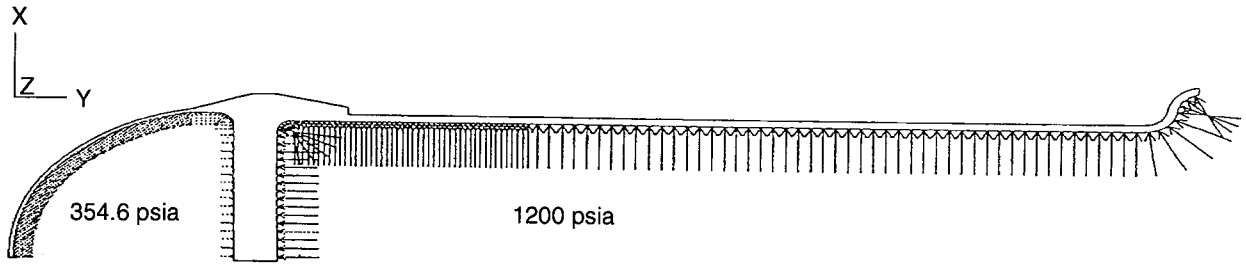

Figure 55. ACEP Fuel/Air Cooler Steady-State Boundary Conditions

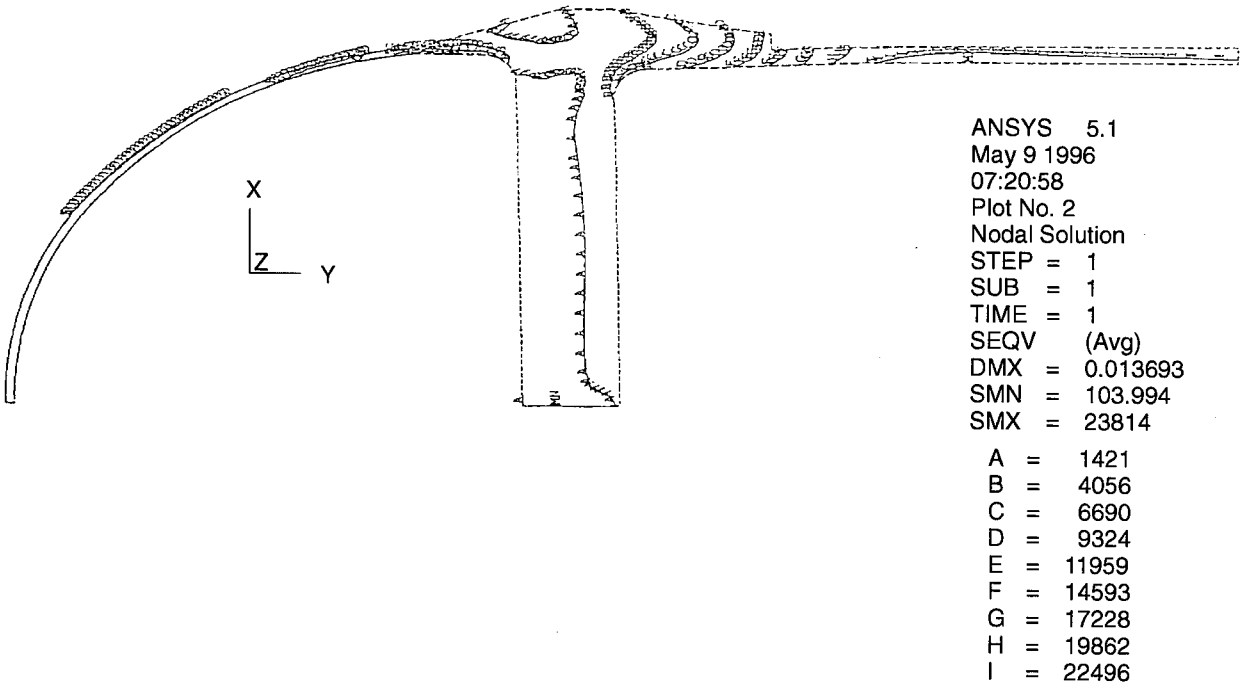

Figure 56. ACEP Fuel/Air Cooler Equivalent-Stress Plot at Steady-State Conditions

3.3.4.2 Low-Cycle Fatigue Structural Analysis

A thermal cycle stress analysis was performed with an ANSYS finite-element model of the fuel/air heat exchanger. Stresses were calculated for several transient temperatures. The thermal maps used for this analysis are shown in Appendix A.

Life estimates were made from low cycle fatigue life prediction methodology (Mason-Halford Universal Slope) for the most severe conditions of temperature and stress. The analysis results show that the heat exchanger is structurally satisfactory for the operating conditions. The expected life to crack initiation is 10,550 cycles, which greatly exceeds the 1,000 cycle requirement. Table 19 is a summary of the results.

Table 19. Estimated Life Based on ANSYS Analysis (Includes Scatter Factor of 10)

Location	Stress (Thermal + Pressure Loads), ksi				Estimated Critical-Area Life (Cycles)
	20 Seconds	35 Seconds	50 Seconds	60 Seconds	
Location A	57.2	100	105	96.2	10,550
Location B	45.1	66	69.6	62.7	170,000
Convolution	106	77.5	45.8	29.3	13,860

Finite-Element Model – To capture the local behavior of the heat exchanger at the header-to-collar and collar-to-manifold junctions, a detailed finite-element model with fine mesh was created (shown in Figure 57).

Material – The heat exchanger is constructed of Inconel 625. The material properties used for analysis, per MIL-HDBK-5G, are listed in Table 15 and illustrated in Figure 58.

Loads – The finite-element model was loaded with 354.6 psi on the air side and 1200 psi on the fuel side with the transient temperature distribution at various intervals. The temperatures were provided by transient gradients generated by finite-difference thermal models using the H0298 Thermal Analyzer. They are shown in Appendix A.

Summary of Results – Stresses and estimated life at the critical areas are summarized in Table 19 and Figure 59. Stresses and temperature plots are shown in Appendix A.

3.3.5 Manufacturing

The fuel/air heat exchanger is a welded and brazed assembly. There were a number of manufacturing challenges associated with the fabrication of the heat exchanger. Brazing of the long Inconel unit was the biggest challenge. The brazing is performed in accordance with the contractor's internal procedures (AES specification WBS27 using braze alloy in accordance with AMS4778). The first major assembly that takes place in fabrication of the heat exchanger is brazing of the core assembly. The components included in this brazed assembly are listed in Table 20.

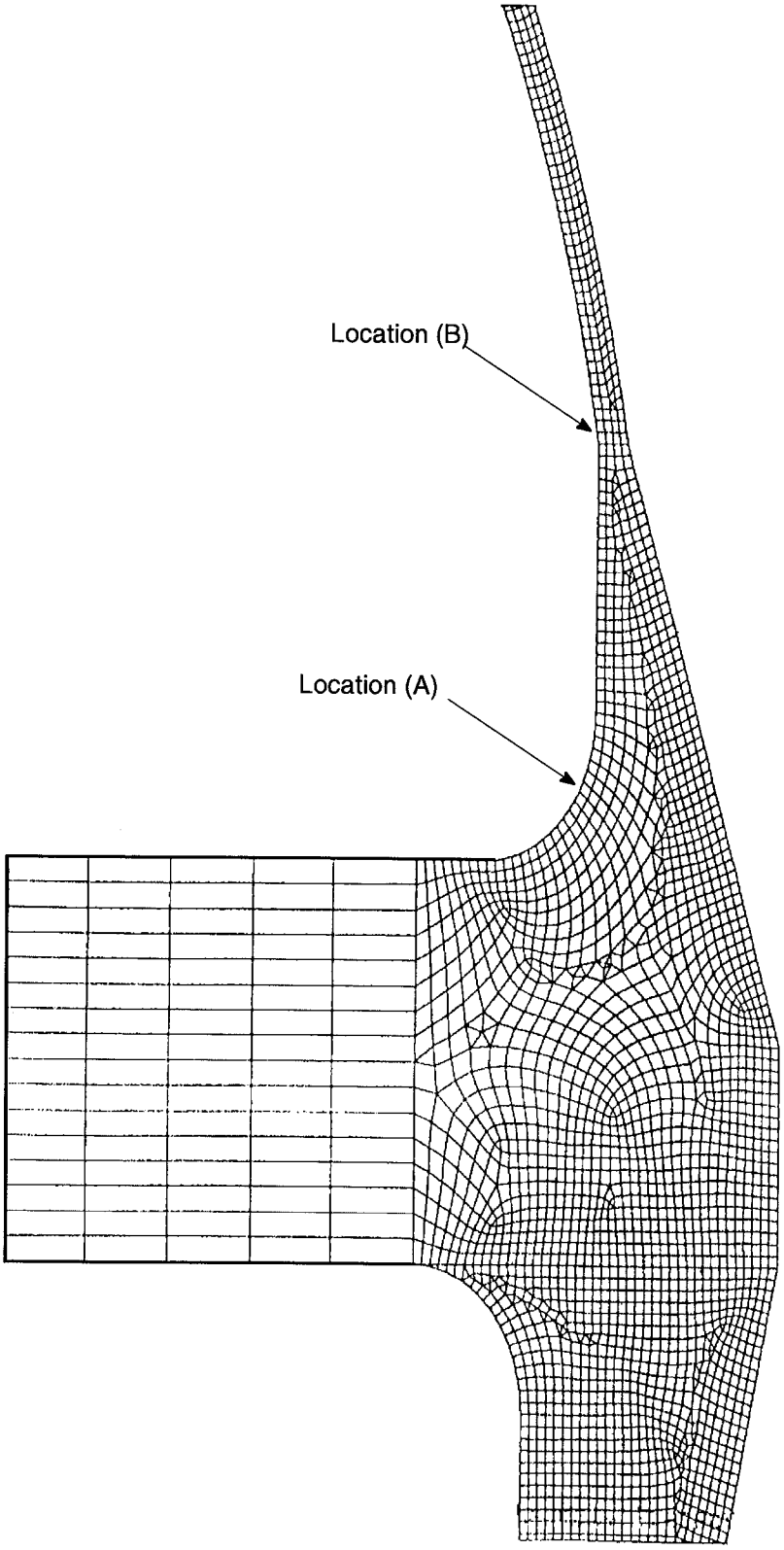

Figure 57. Finite-Element Model

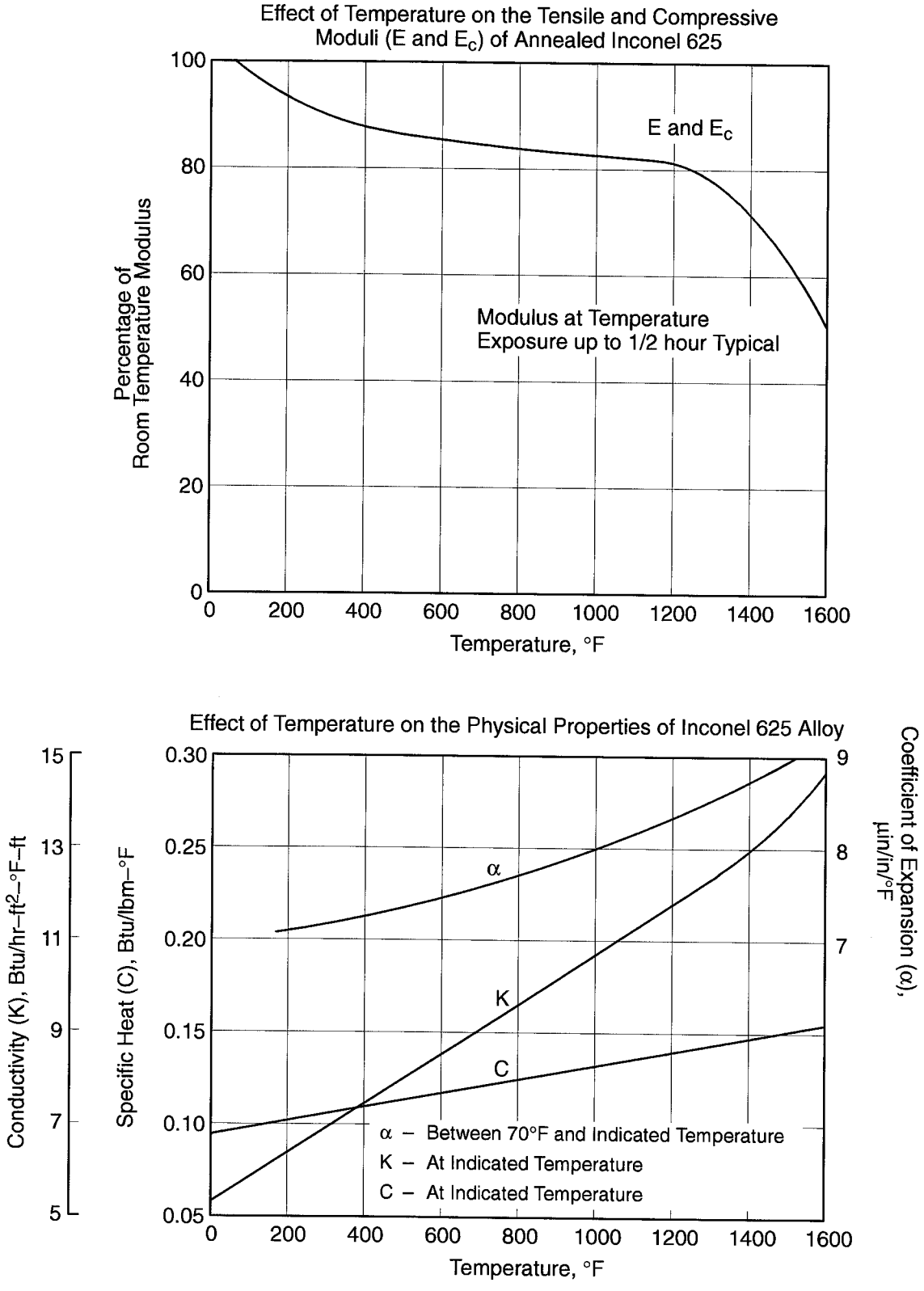

Figure 58. Inconel 625 Material Properites

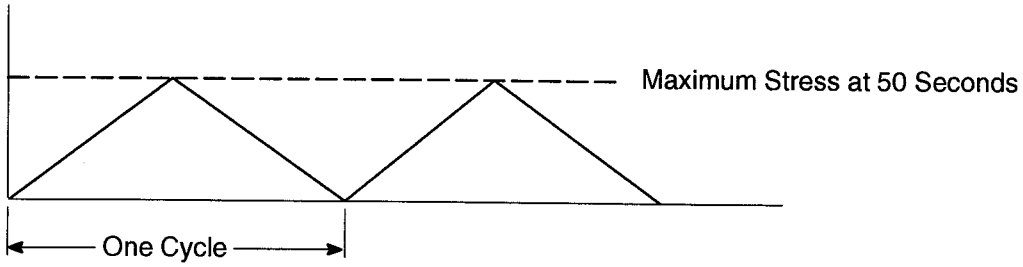

$$N = \left(\frac{2 \times \epsilon_p'}{\Delta\epsilon_p}\right)^{\frac{1}{0.6}}$$

$\Delta\epsilon_p$: Plastic Strain Range

$\epsilon_p' = D$ (Tensile Cyclic Ductility)

Figure 59. Cyclic Life Prediction (Manson–Halford Universal-Slope Method)

Table 20. Braze Assembly Components

Part Number	Description	Qty
2372587-1	Shell Assembly	1
2372589-1	Headers	2
2372592-1	Tubes	946
2372590-1	Baffles	10
2372591-1	Diverter Rails	4
2372593-1	Ring	1

Brazing occurs at the joints between the shell assembly and the headers (two places) and between the headers and each end of the 0.125-in tubes. All other joints are unbrazed to allow thermal growth induced by the temperature differential between the tubes and the shell at transient conditions. Following the braze operation, the air-side manifolds and flanges are arrached via full-penetration butt welds (AES internal weld specification WBS28).

3.3.5.1 Brazing Issues

Prior to brazing a full-scale unit, a number of braze samples were tested. These samples represented the same tube diameter and header thickness as the full-scale heat exchanger. The objective was to determine the optimum tube-to-header gap, the optimmum braze alloy, and the ideal orientation for placing the full-scale unit into the furnace. All of these tests were performed in the vacuum braze furnace.

At the conclusion of this testing, it was determined that the unit would be brazed in a two-step process in the vertical orientation. Vertical orientation was chosen because of the tendency of the braze alloy to run-off when brazed in a horizontal position. A generous amount of braze alloy must be applied to ensure adequate wicking down the 0.68-in thick tube-to-header joint. Initially, use of AMS4779

braze alloy was considered because it offers good consistency at braze temperature. (It tends to be thicker when melted, thereby reducing the tendency of the alloy to run through the tube/header joint and down the length of the tubes.) However, initial braze tests indicated that AMS4779 did not flow adequately across the surface of the header, and ability to "wick" around the tubes and form braze fillets was inadequate. The braze testing also answered a number of other issues including:

- The smooth tube surface was not adversely effected by the braze process.
- The smooth tube surface had no effect on the ability of the braze alloy to "wick" and adhere to the tubes to create quality braze joints.
- Although difficult, machining the 0.125-in tube holes through the 0.68-in Inconel header material was achieved by initially drilling undersized and then reaming to the final tolerance.

In the first braze, the unit is oriented with the tube-to-header joint facing upward. The lower shell-to-header joint is alloyed using AMS4778 powder mixed with a binder to create a slurry. The shell-to-header joints are "bridge" tack welded to hold the details in place during braze. A graphite spacer is used at the bottom of the unit to register the tubes in proper location during braze. The unit is then loaded into the furnace, and the furnace is ramped up to the braze temperature of 1920°F. The same procedure is repeated with the unit oriented in the opposite direction (see Figure 60).

After the first braze of the subject unit, the brazing looked acceptable. Brazing alloy flowed nicely in the tube-to-header and shell-to-header joints, forming the desirable braze fillets. During the second braze, the temperature and resultant thermal expansion differential (approximately 600°F and 0.135 inch) between the tubes and the shell produced an undesirable result. After removing the

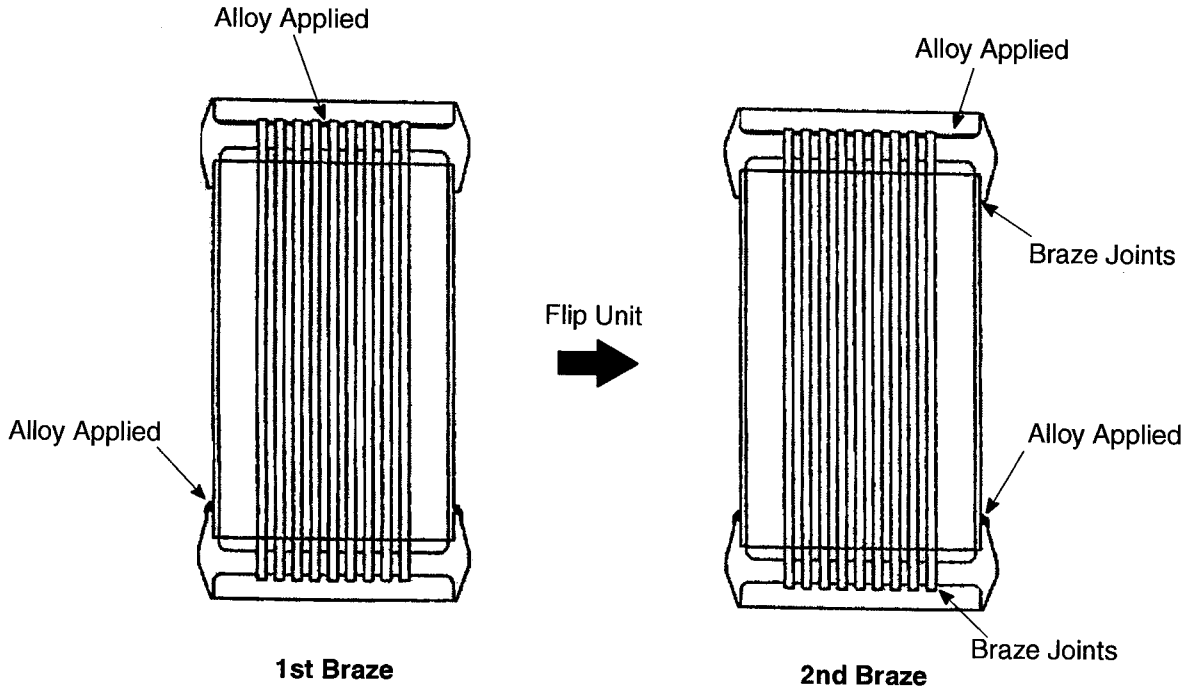

Figure 60. Two-Step Braze Process

heat exchanger from the furnace, it was observed that the tubes were pulled below the surface of the header, allowing alloy to spill in and plug approximately 5% of the tubes. In addition, at the opposite-end shell-to-header joint, the shell had pulled out of the header by the same amount (see Figure 61).

It was also observed that the braze alloy on both joints (second braze) did not flow properly, indicating the possibility of surface contamination prior to the second braze. A subsequent pressure test validated the already obvious problem. The joints formed in the first braze cycle showed no leakage, and those brazed in the second cycle showed an unacceptable amount of leakage. The following actions were taken to resolve the braze issue:

- The failed heat exchanger was instrumented with thermocouples and run through several mock braze cycles to quantify the thermal differentials. The center tube and the shell experience a 600°F ΔT during the heat-up and cool-down segments. This is the reason the tubes pulled below the header surface on the second braze.
- A shroud placed on the cooler during braze cycle to provide a radiation heat shield and more uniform heat-up was evaluated but not implemented. It was determined that it would help but not make a big difference in the 600°F ΔT between the shell and tube bundle.
- The header-to-shell overlap was machined to allow the header to slide over the shell an additional 0.10 inch and increase the protrusion of the tubes by the same amount. This was implemented immediately because, if it had been prepared in this fashion, the first cooler would have been salvageable. (The tubes pulled

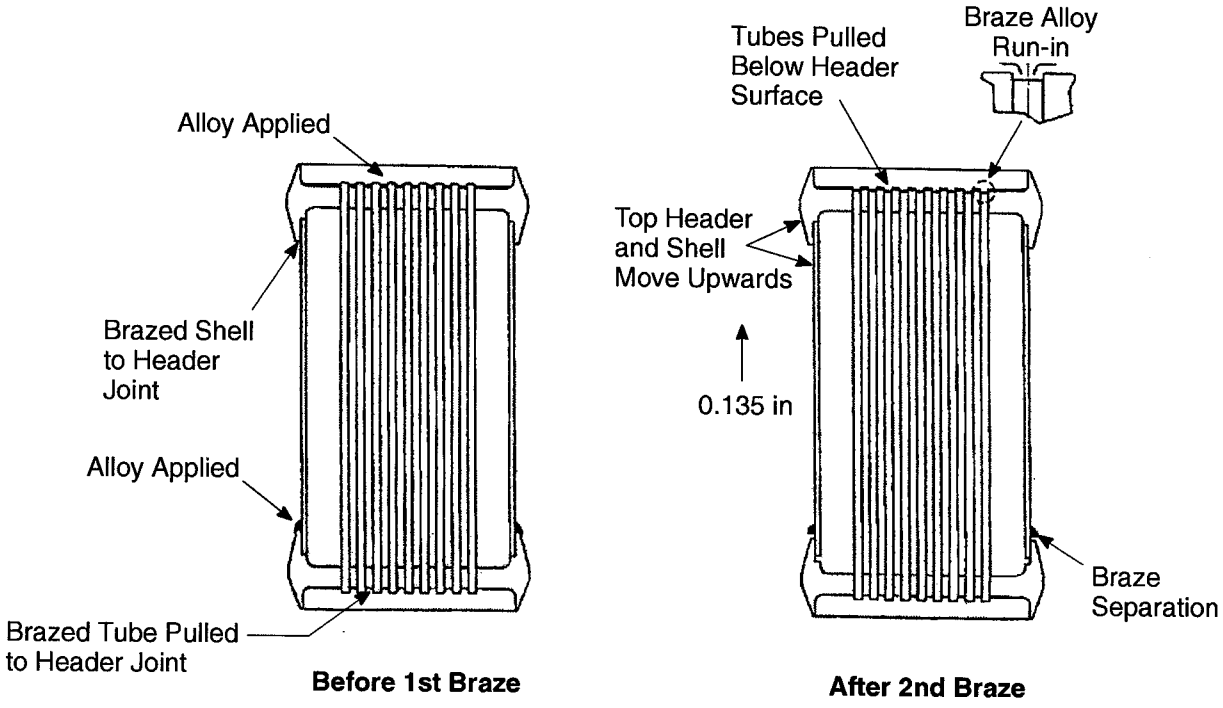

Figure 61. Failure of Heat Exchanger During Second Braze Step

below the header surface and alloy was able to plug approximately 5% of the tubes; the increased protrusion would have prevented this plugging.)

- The ramp rate was slowed, and an addition soak was included in the braze cycle where the maximum ΔT occurred. A mock braze cycle indicated the double-soak braze cycle reduced the ΔT by only 100°F, from 600° to 500°F.
- Hydrogen furnace brazing was investigated to take advantage of enhanced convection and decrease the thermal lag between core components. A mock braze cycle in the hydrogen braze furnace showed that the effect of convection could decrease the ΔT between the tube bundle and shell to 225°F with a resultant growth Δ of 0.06 inch.

Given the size of the unit, the thick outer shell, and the dense tube bundle, it is not surprising that thermal lag was a challenge. After running a number of "mock" braze cycles, it was also obvious that the hydrogen furnace presented the brazing process of choice. The unit would still undergo a two-step process and be brazed with the same ramp-up and cool-down rates. The convective nature of the hydrogen furnace also presented the lowest risk solution.

All three deliverable units were brazed in the hydrogen furnace. In all three cases, the units went through an additional braze cycle above the two-step base process. This was performed to add alloy into the shell-to-header joint. The additional braze operation was necessary due to the diameter and the gap between the shell and header — and the fact that the amount of alloy that can be applied prior to brazing is limited. During braze, the alloy wicks down into the joint, consuming all the alloy. An ideal braze joint does "wick" in this manner; however, a generous braze fillet at the top of the joint is desirable. This third braze cycle is designed to ensure this filleting. Small leaks in the tube-to-header joints were also repaired at the same time.

3.3.6 Acceptance test

The fuel/air heat exchanger was subjected to various in-process inspections (core pressure test, x-ray of the manifold and flange welds, workmanship, etc.) culminating in a final inspection and acceptance test. Final inspection included a detailed visual examination, dimensional inspection, and review of the manufacturing history to verify prior inspections and tests. The acceptance test was performed in accordance to the plan provided in Appendix A and included the following:

- Visual Examination
- Fuel-side proof pressure
- Air-side proof pressure and leakage
- Fuel-side internal leakage (using helium)
- Fuel-side external leakage (using helium)
- After-test examination

The three heat exchangers successfully passed the acceptance test, and (with the quality control heat exchanger) all four units were provided to GEAE for coating application. The quality control heat exchanger was used to verify the coating process prior to coating the three acceptable units. Two of the heat exchangers are required for the turbocooler rig test; the third is a spare.

3.4 High-Temperature Fuel Injection System

The goal for integrating a high-temperature fuel system into the ACEP program is to define and implement a technical approach that satisfies the turbocooler rig test requirements and at the same time retains many of the F404 production fuel nozzle characteristics.

3.4.1 Design Description

Precise and highly responsive control of fuel flow is the most important aspect of the overall engine control strategy. The fuel-delivery system for current military engines typically contains:

- A main fuel pump that pressurizes the fuel
- A bypass valve to set the metering valve ΔP to establish the demand fuel flow
- A fuel/oil heat exchanger to transfer lube oil heat load
- A pressurizing valve at the head of the combustor fuel nozzle assembly to maintain the pressure in the fuel manifold (prevents leakage at shutdown and minimizes ignition delay at engine start–up)

Gas turbine combustors must supply uniformly mixed hot gases to the turbine while providing stable and efficient operation over a wide range of operating conditions and must be capable of starting and accelerating the engine. To satisfy the combustor requirements, typical pressure-atomizing fuel nozzle designs employ a dual fuel circuit. The primary circuit is for low-power/starting operation. The secondary circuit opens (via the flow-divider valve), when the fuel system pressure is increased, to provide good fuel atomization at high-fuel-flow operating conditions. The primary and secondary circuits both contain spin chambers that swirl the liquid fuel and produce fine spray after the fuel passes through the final orifice. Modern fuel-delivery systems are designed to maintain fuel temperatures below 300°F. To accommodate the high-temperature fuel (>900°F) associated with the turbocooler rig test, a production F404 full-annular fuel injection system was modified. Four fundamental issues dictated the fuel injection system modifications:

1. Fuel vaporization due to the increased fuel temperature
2. Fouling due to fuel deposition
3. Complications associated with particulates suspended in the fuel
4. Thermal stresses

3.4.1.1 Vaporization and Fuel System Pressure

Fuel system pressure must be sufficient to provide acceptable fuel atomization and eliminate the adverse effects of vaporization in the fuel nozzle. To avoid vaporization within the fuel system, the pressure level should be maintained above the fuel vapor pressure. The vapor curve for JP–5 fuel is illustrated in Figure 62. If the fuel condition is below the vapor pressure curve (to the right-hand side), vaporization is likely. Once the critical pressure is achieved (330 psia), the fuel is supercritical and will no longer vaporize, although fuel density will continue to decrease with temperature. Vaporization is a key concern in the secondary fuel passage because, at low-fuel flow conditions, the secondary circuit fuel pressure is established primarily by the combustor operating conditions. The problems associated with two-phase flow are:

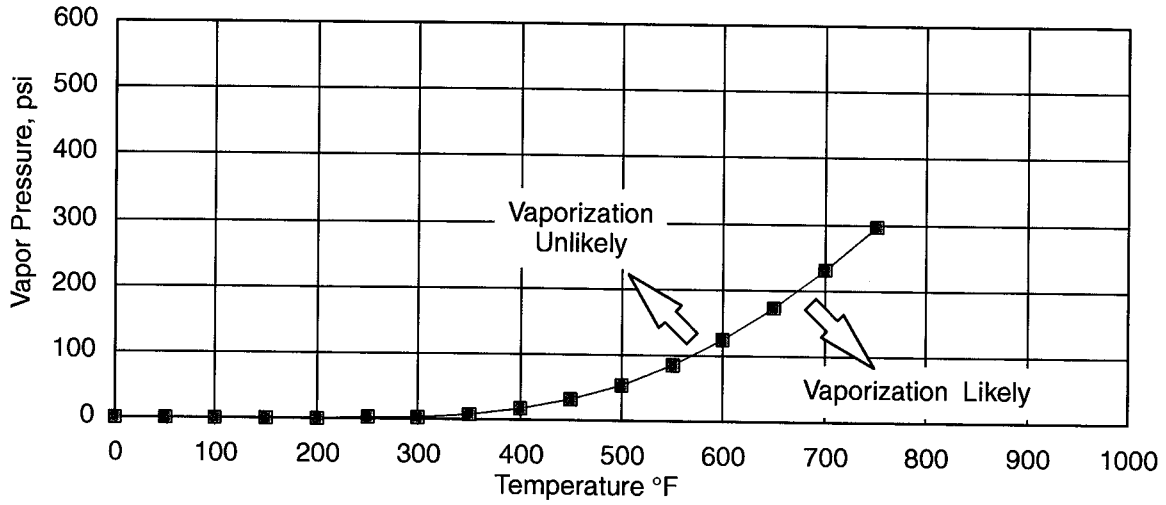

Figure 62. JP–5 Vapor Pressure as a Function of Temperature

- Maldistribution of fuel flow in the fuel manifold leading to nonuniform flow to the fuel nozzles
- Combustor instability associated with the large density changes
- Inability to predict and reproduce heat transfer and ΔP characteristics in the heat exchanger

At low-altitude/high-power flight conditions, combustor operating pressure is typically above critical pressure for JP–5, so vaporization is less likely. At high-altitude, low-power conditions, the combustor operates below critical pressure, and fuel vaporization may be an issue.

A dynamic simulation representing the turbocooler/F404 engine system was developed to evaluate and define an acceptable rig test envelop in order to avoid potential vaporized fuel conditions. The model includes detailed component representations (ACM, heat exchangers, fuel-delivery components, and fuel nozzles), complete fuel and air thermodynamic properties, and was integrated with a dynamic engine model.

Fuel system pressure is set by the combustor operating pressure plus the pressure drop across the fuel nozzle. The F404 engine uses pressure-atomizing fuel nozzles designed with small orifices and consequently large pressure drops across the fuel nozzle (approximately 500 psid at maximum flow). Contributing to the overall fuel nozzle pressure drop is the flow-divider valve and the secondary tip orifice. As the turbocooler heats the fuel, the density of the fuel will decrease dramatically as shown in Figure 63.

The reduction in fuel density directly affects the overall fuel nozzle pressure drop characteristic due to the increase in the volumetric flow rate. The effect of fuel temperature on the production F404 fuel nozzle flow characteristic is illustrated in Figure 64. If the fuel nozzle flow-through areas are not increased to accommodate the volumetric flow as temperature increases, fuel system pressure becomes excessive. The goal was to keep the maximum fuel system pressure under 1200 psia due to the heat exchanger design limitations and also to avoid vaporization.

A detailed analytical model of the fuel nozzle was created and integrated into a turbocooler transient simulation. Predicted fuel nozzle pressures, temperatures, and vaporization margins were observed

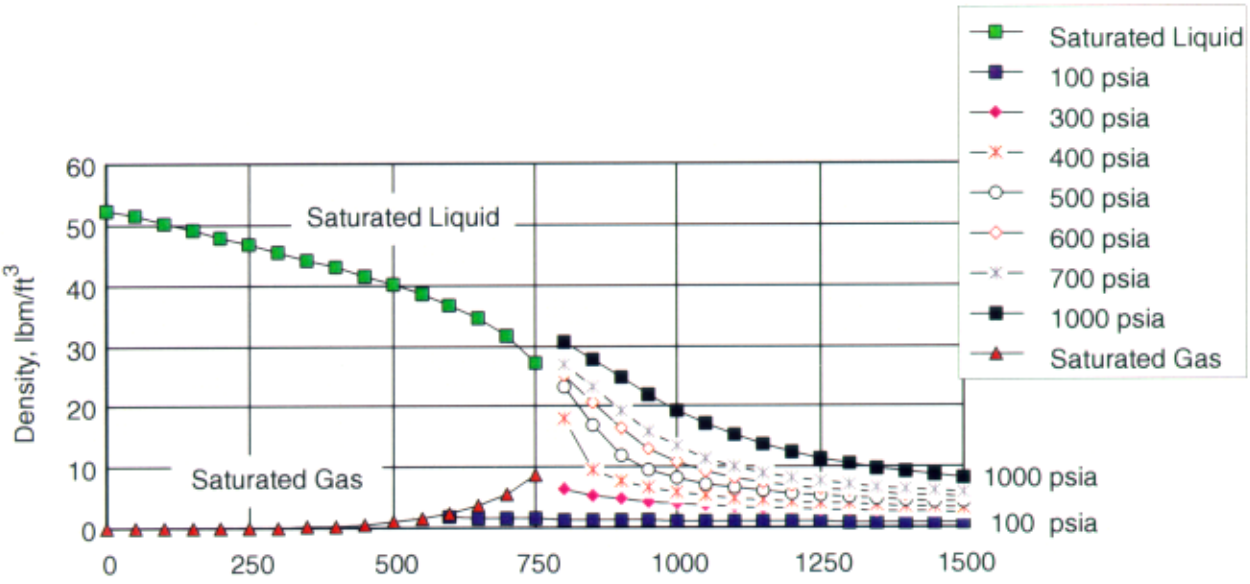

Figure 63. Fuel Density as a Function of Temperature

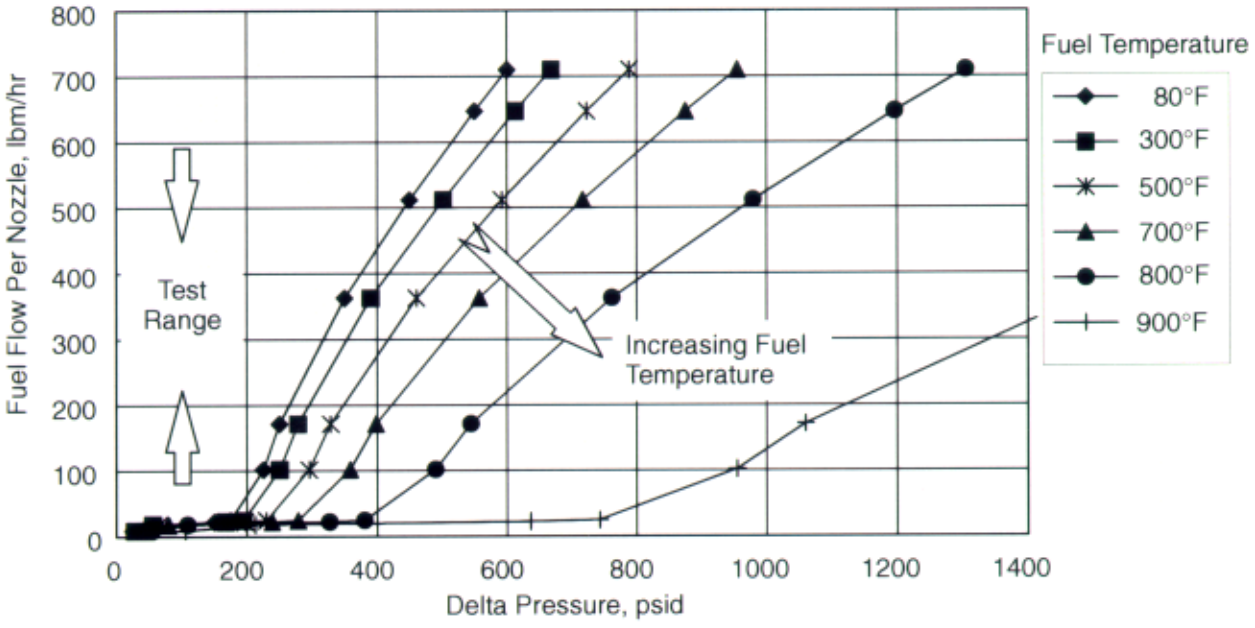

Figure 64. F404 Fuel Nozzle (Baseline) Flow Characteristic Versus Fuel Temperature

during operations throughout the flight envelope in order to identify potential concern areas in the flight envelope, define operational boundaries for the rig demonstration test, and analytically evaluate potential modifications to the fuel nozzle. The fuel nozzle performance characteristics for a sea-level static power hook (or full throttle movement) are presented in Figure 65. As the engine power level angle (PLA) is increased from 40 to 102 (military power), the pressure in the combustor and fuel nozzle circuits increases.

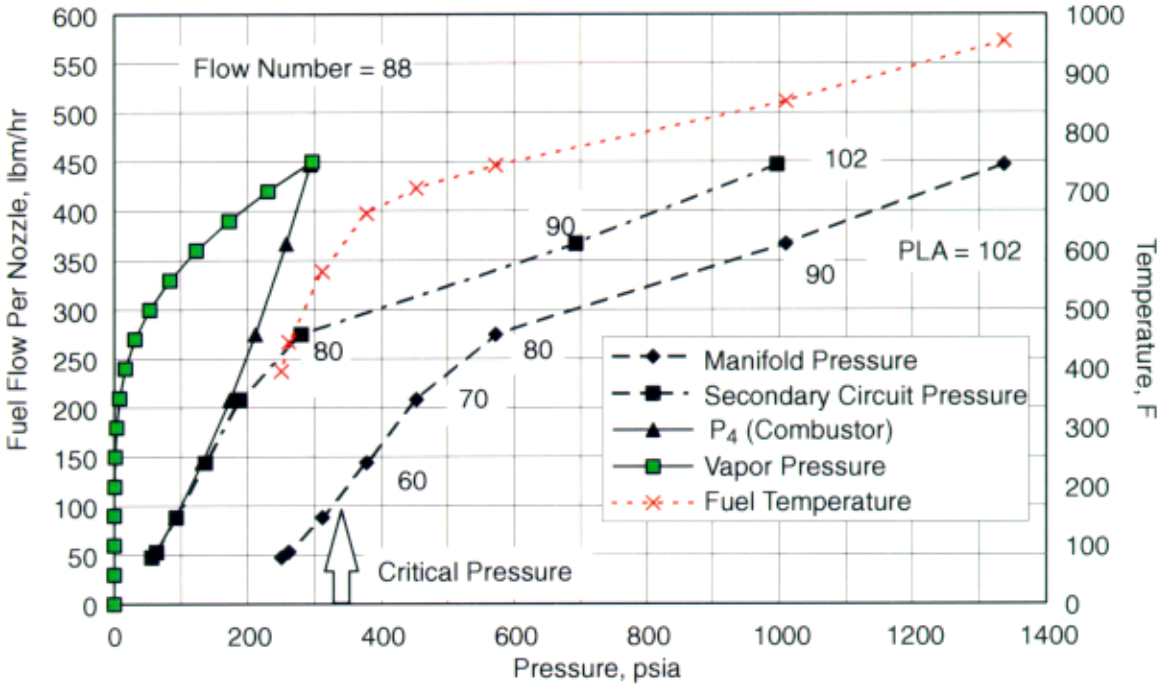

Figure 65. F404 Fuel Nozzle Flow Characteristic Over a Sea-Level Static Throttle Hook

The estimated turbocooler fuel temperature is also shown on Figure 64. The objective of the fuel nozzle modifications is to always maintain fuel system pressure above the fuel vapor pressure and above the fuel critical pressure (P_c = 334 psia), when the fuel temperature exceeds 770°F, but to limit the maximum fuel pressure below 1200 psia in the fuel manifold and heat exchangers.

A similar fuel nozzle performance analysis is presented in Figure 66 for the altitude power hook condition (30,000 ft, Mach 0.9). By varying the fuel nozzle slot sizes in the secondary spin chamber and in the flow divider valve, a final overall flow number of 80 or 76 was selected for the final fuel nozzle configuration.

3.4.1.2 Suspended Fuel Particulates

Regular petroleum distillate fuels, when heated, may undergo chemical changes that precipitate solid matter, depending on fuel quality and the conditions of heating. Carbon-barrier coating will be used to prevent adhesion of deposits to the surfaces of the tube walls. Narrow passages and stagnant regions where suspended particulate might accumulate should be avoided downstream of the heat exchangers. The flow divider valve, made of 440C for erosion resistance, is an underfeed, spring-loaded, spool-and-sleeve assembly calibrated to distribute the fuel uniformly as a function of fuel manifold pressure and combustor pressure. The spool-and-sleeve assembly is a matched set with clearances on the order of 0.0003 to 0.0005 inch. The flow divider valves are located in the fuel nozzle bodies downstream of the fuel/air heat exchangers but outside of the main engine air stream. In this region, no additional heat load is applied to the fuel. Due to the lack of additional heat load, fuel deposits were not considered an issue. From the onset of the program it was decided that a high-temperature fuel filter would be installed downstream of the heat exchangers to protect the fuel injectors and flow-divider valves from the potential problems of suspended particulates. In related

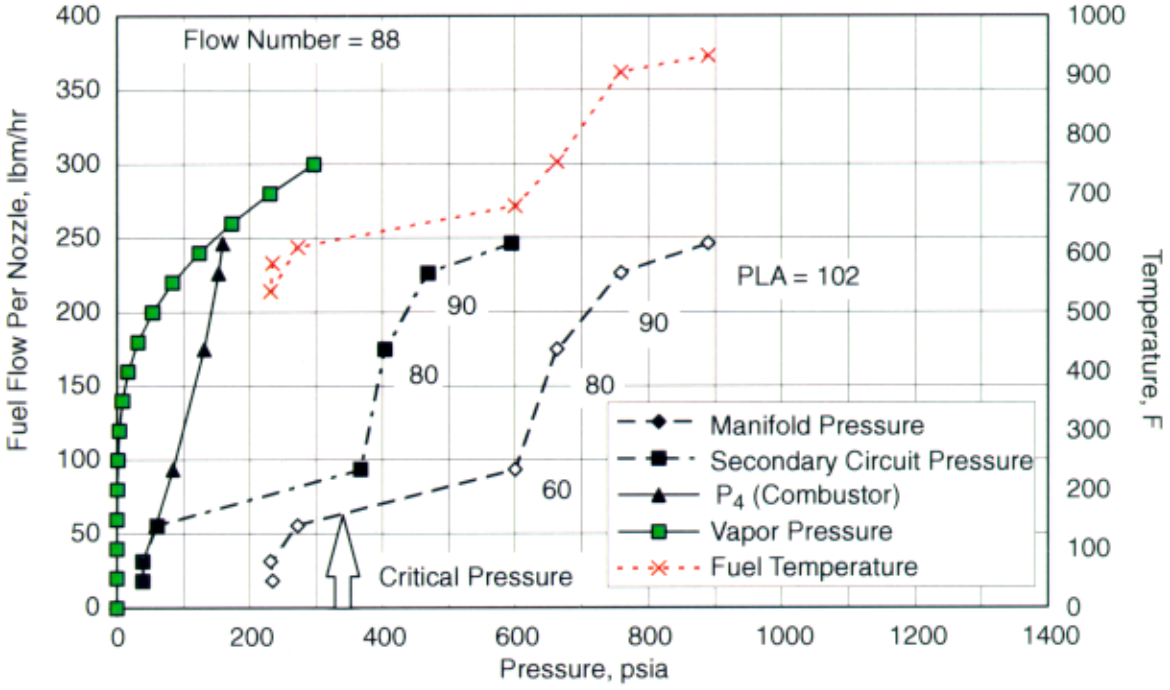

Figure 66. F404 Fuel Nozzle Flow Charateristic over a 30,000-ft/Mach 0.9 Mach Throttle Hook

single-cup combustor tests of high-temperature fuel (up to 1000°F), although the contractor did not use a fuel filter or apply CBC to the flow divider valve, no operational problems were encountered.

3.4.1.3 Deposition

Deposition within the fuel nozzle passages will be mitigated by applying CBC to the interior surfaces of the fuel nozzles. This was incorporated into the manufacturing process.

3.4.1.4 Thermal Stresses

Thermal stresses are actually reduced in the fuel nozzle because hotter fuel lowers the ΔT between the engine compressor discharge air and the fuel.

3.4.2 Fuel Nozzle Manufacturing

Modifications to the F404 production fuel nozzle to support high-temperature fuel operation include the following:

1. Increase the secondary circuit orifice to a flow number of 76. Flow number is defined as the fuel flow divided by the square root of the overall fuel nozzle pressure drop: $FN = W_F/\sqrt{\Delta P}$. Fuel flow is in lbm/hr/nozzle; ΔP is lb/in^2.
2. Machine additional slots in the flow divider valve spool and sleeve assembly.
3. Replace the steel springs of the flow-divider valve with high-temperature Inconel springs.
4. Change the fuel inlet fitting to accommodate a local braze filet for leak protection (see subsection 3.4.4).

5. Apply CBC to the fuel nozzle support surfaces (the flow-divider valve will be uncoated).
6. Install a high-temperature fuel filter downstream of the fuel/air heat exchangers to preclude the potential adverse effects of suspended particulates.

An updated drawing, including modified fuel fitting, of the high-temperature fuel nozzle is presented in Figure 67. Photographs of a modified flow divider spool piece are presented in Figures 68 and 69. The top spool piece in Figure 67 shows the normal production valve slot. The bottom spool piece in Figure 68 shows the increased-flow slot in the same radial location. Two of these slots are located on each spool piece 180° apart. Figure 69 shows the added slot located 90° from the normal production slot. Two auxiliary slots were added to the spool piece (total of four slots per spool piece).

3.4.2.1 Application of CBC to the Flow-Divider Valve

Two risks were associated with applying CBC to the flow-divider valve. The initial concern was over fuel deposits in the region. The contractor's test experience indicated that areas in the system without heat addition to the fuel are less susceptible to fuel deposits. Since the flow-divider valve is located outside the main engine air stream, this risk was judged acceptable; fuel deposits would not likely form at the valve location. Also, the use of a fuel filter downstream of the fuel/air heat exchangers eliminated the concern over suspended particulates getting trapped on the valve sliding surfaces.

The second risk concerned the effect of the coating process on the current production valve material (CRES 440C). The coating application temperature is high enough that valve material, which is normally hardened to a RHc of 55–60 for wear/galling resistance, is annealed and the hardness reduced to RHc 38–40. The failure mode for a valve with softer material properties is potential galling of the two sliding units as a result of material deformation in the spool and essentially locking the valve in a fixed position. Switching the valve material, for example to Inconel 718, would mitigate the hardness-reduction associated with the coating process. However, Inconel 718 is not used in any of contractor's fuel nozzles and would require some additional development. In addition, the potential dimensional changes of the flow-divider valve spool and sleeve assembly as a result of the coating process (either thermally induced or as a result of the coating thickness) created assembly problems: the spool would not fit correctly into the sleeve. The dimensional clearances on the spool and sleeve assemblies are small (0.0003 to 0.0005 inch on the diameters) and are processed as matched sets. One alternative would be to increase the clearance to account for the thermal-induced dimensional changes and coating thickness. Launching a flow-divider valve development (either new materials or optimizing clearances) was outside the scope of the program.

To better understand the issues associated with coating the flow-divider valves, a simple endurance cycle test was performed with contaminated fuel on a coated fuel nozzle valve cartridge. Similar data were already available on the production flow-divider valve. Prior to the test, the valve (CRES 440C material) was modified/machined to account for the additional coating thickness. The coated valve cartridge was assembled into a fuel nozzle support and exposed to 5000 cycles that ranged from a low-pressure of 0 to 50 psig (valve closed) to a high pressure of 350 to 400 psig (1000 lb/hr to simulate valve full-stroke). The fluid (ambient temperature) is the typical media used to perform accelerated life testing in the design assurance phase of new fuel nozzle designs. The acceptance criteria for the assembly was a comparison of the flow rate between a pretest flow and a posttest flow plus visual examination. After 5000 cycles, there was essentially no flow difference between the pretest flow recordings and the posttest flow recordings. Upon visual examination of the valve

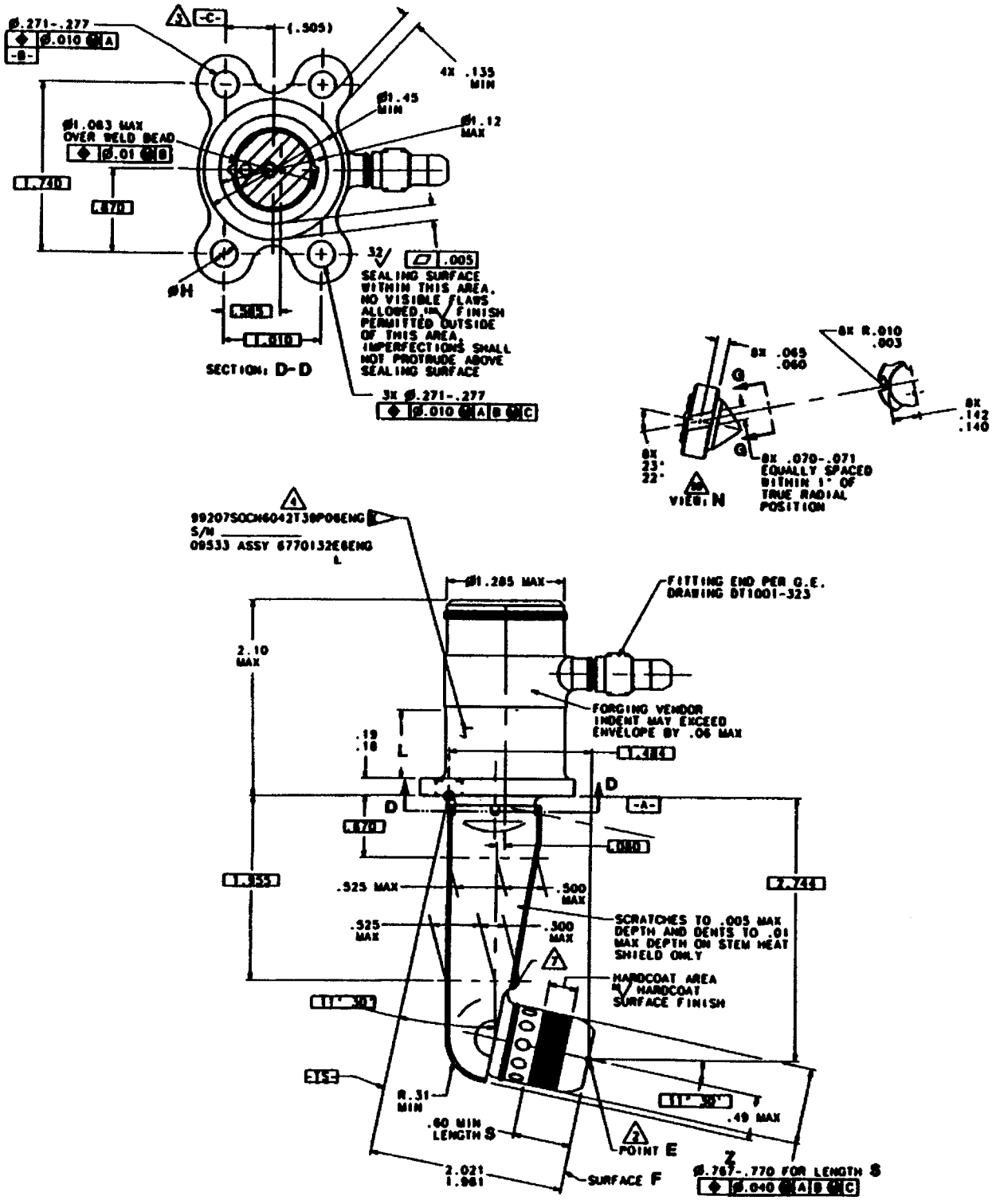

Figure 67. High-Temperature Fuel Nozzle Drawing

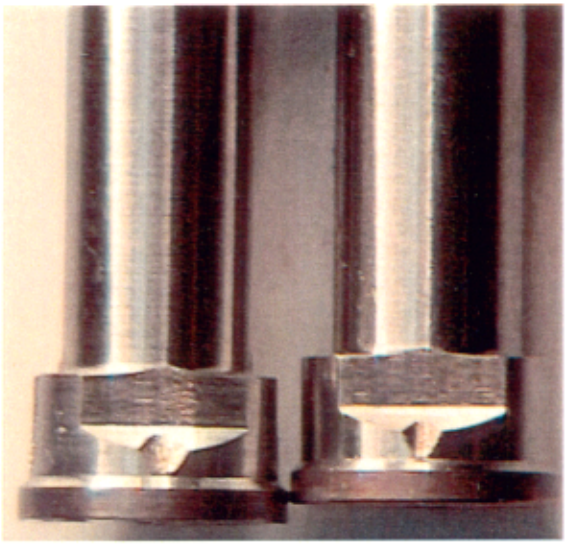

Figure 68. Modified Flow Divider Valve

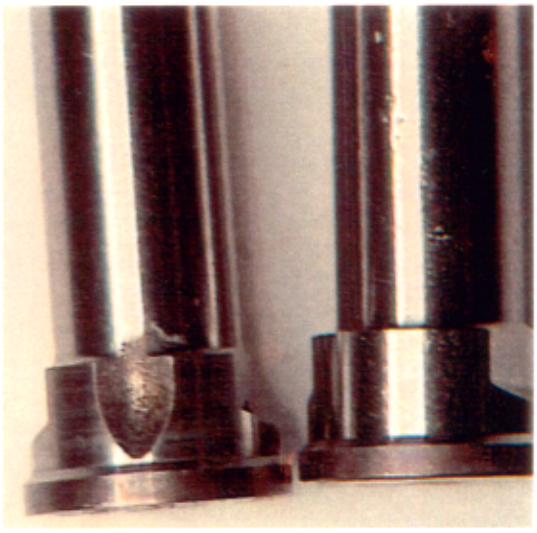

Figure 69. Modified Flow Divider Valve: Additional Slot

cartridge spool and sleeve, the only notable finding was a discoloration on the spool. This discoloration appears to be the result of the mechanical forces of the spool sliding inside the sleeve, or the abrasive effects of the contaminated fluid flowing past this surface, or a thinning of the CBC. These results indicate that the coated valve cartridge could perform adequately for the test program. In related high-temperature fuel single-cup combustor testing, no operational issues were encountered with uncoated flow divider valves or by not using a fuel filter. The potential for less than optimum clearances and softening of the valve material leading to potential valve failure prompted the decision not to coat the valve cartridge.

Standard vendor processes were used in fabrication/assembly of the fuel nozzles. The only exception was that CBC was applied to the fuel nozzle support (everything but the flow-divider valve) prior to installation of the flow-divider valve and welding of the cap piece. Twenty-four fuel nozzles were manufactured: 18 required for the F404 full-annular combustor plus spares.

3.4.3 Fuel Nozzle Acceptance Test

Each fuel nozzle was subjected to a four-point flow check (including hysteresis at 225 psig) and a six-port patternation test. Fuel nozzle patternation accuracy is a measure of the nozzle spray pattern or cone shape and is defined as the maximum flow sector minus the minimum flow sector divided by the maximum flow sector. The fuel nozzle acceptance test data are presented in Table 21. Note that 3 of the 24 nozzles are slightly outside the production patternation limit of 30%. This is attributed to opening up of the secondary flow slots to accommodate the increased volumetric flow requirements.

In related high-temperature, single-cup combustor testing (funded by a complementary program), the final ACEP fuel nozzle configuration was successfully tested. The fuel nozzle flow-divider valve was uncoated, and no fuel filter was used to capture suspended particulates. Fuel temperatures up to 1000°F were evaluated at combustor operating conditions exceeding the planned ACEP test conditions. There was no discernible change in combustor operation between cold and hot fuel. The only notable difference was a 50°F increase in the tip of the combustor venturi with hot fuel.

Table 21. Fuel Nozzle Acceptance Test Flow Rates (lbm/hr)

Test Point	Inlet Fuel Pressure, psi				Hysteresis (Δ Flow)	Patternation (%)
	25	225	350	600		
1: A91691	9.47	280	707	1226	2.5	15
2: A94230	9.4	279	707	1242	2.2	17
3: A96160	9.7	288	728	1290	0.3	25
4: A91626	9.4	286	719	1278	1.1	17
5: A91125	9.8	272	713	1264	0.5	19
6: A90110	9.3	292	700	1225	3.7	28
7: A70141	9.7	283	694	1220	1.2	29
8: A95640	9.4	285	726	1292	0.3	24
9: A96095	9.4	268	719	1263	0.1	20
10: A92957	9.03	270	701	1249	2.4	21
11: A90063	9.2	282	685	1199	0.5	15
12: A95959	9.08	284	720	1287	1.6	31
13: A71072	9.2	287	718	1272	2.1	29
14: A91265	9.7	280	704	1256	0.5	32
15: A90284	9.2	272	707	1257	2.9	26
16: A83567	9.2	288	712	1264	0.1	29
17: A90019	9.2	274	704	1257	1.9	33
18: A93681	9.7	271	700	1242	1.4	26
19: A95411	9.5	280	711	1263	2.5	9
20: A90574	9.6	275	706	1268	0.9	15
21: A90199	9.6	272	707	1267	2.7	24
22: A87195	9.8	277	710	1262	0.5	28
23: A71140	9.2	277	713	1264	0.1	27
24: A90999	9.6	281	718	1264	2.7	8
Average	9.54	280.5	712.5	1245		
Low Tolerance	9.0	266.5	684.0	1195.2		
High Tolerance	10.0	294.5	741.0	1294.5		

During single-cup combustor testing, thermocouples were installed at three axial locations on the venturi (see Figure 70) to evaluate flash-back and autoignition issues. The outside of the venturi is covered in counterswirling combustor inlet air. The inside of the venturi is bathed in fuel exiting from the fuel nozzle. During hot-fuel operation, the aft section of the venturi was approximately 50°F hotter. This result was expected and did not pose any risk to the integrated rig test.

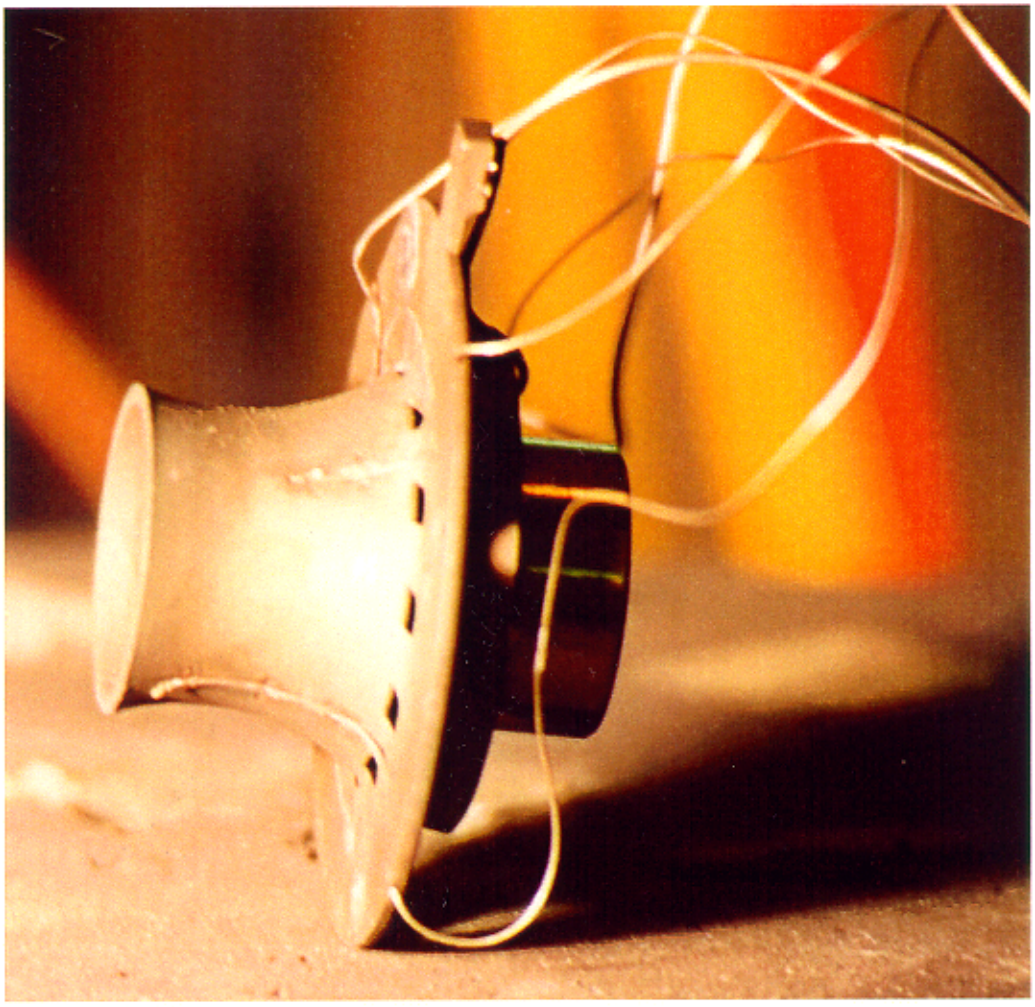

Figure 70. Single-Cup Venturi Instrumented with Thermocouples

3.4.4 Hot Fuel Connectors

To minimize the possibility of fuel-system leaks during rig testing, the high-temperature fuel connectors were modified in one of two ways. On the turbocooler skid, all of the fuel connectors were selected to accommodate a "C seal." Shown in Figure 71, this is a high-temperature, pressure-energized, self-aligning seal that provides leak-proofing protection on typical fuel fittings.

The second method, used on the combustor fuel manifolds, pigtails, and fuel injectors, modified the fuel fittings to incorporate a local braze fillet joint. This approach allowed the combustor and fuel injection system to be fully assembled before the braze joint was locally heated. Figure 72 is a cross section of the pigtail-to-fuel-nozzle connector. The braze joint is fused prior to the B-nut assembly as shown in Figure 73.

Both of these techniques proved to be 100% effective. There were no fuel leaks during the rig test.

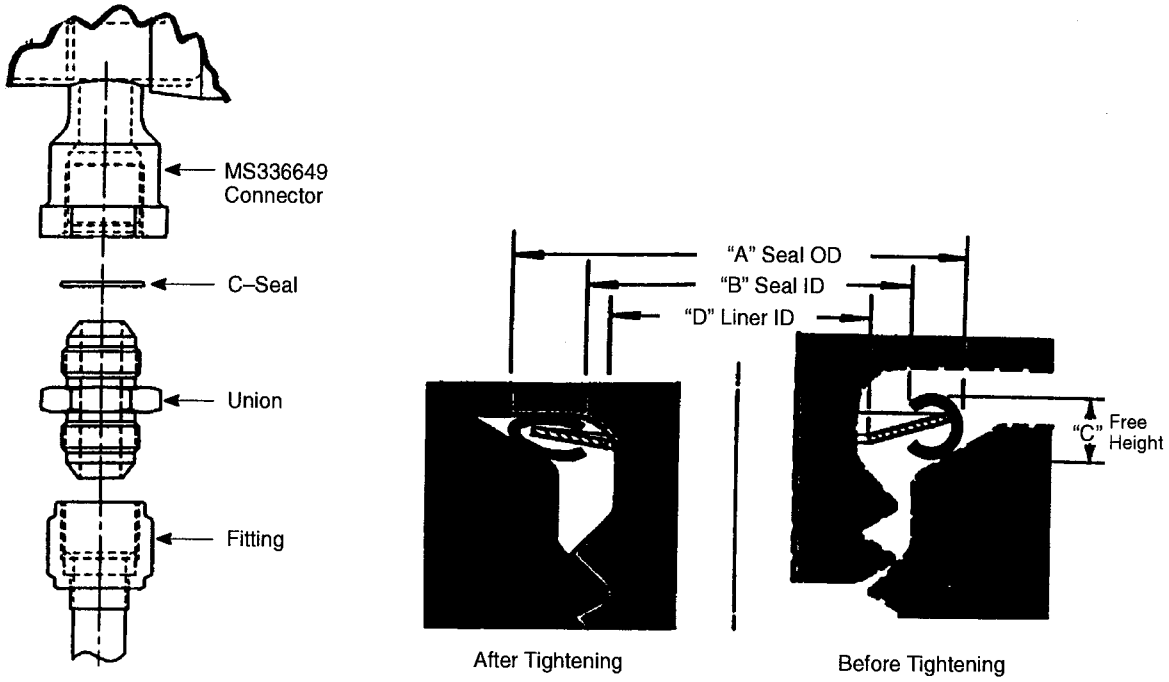

Figure 71. Fuel-Side Fitting with C-Seal

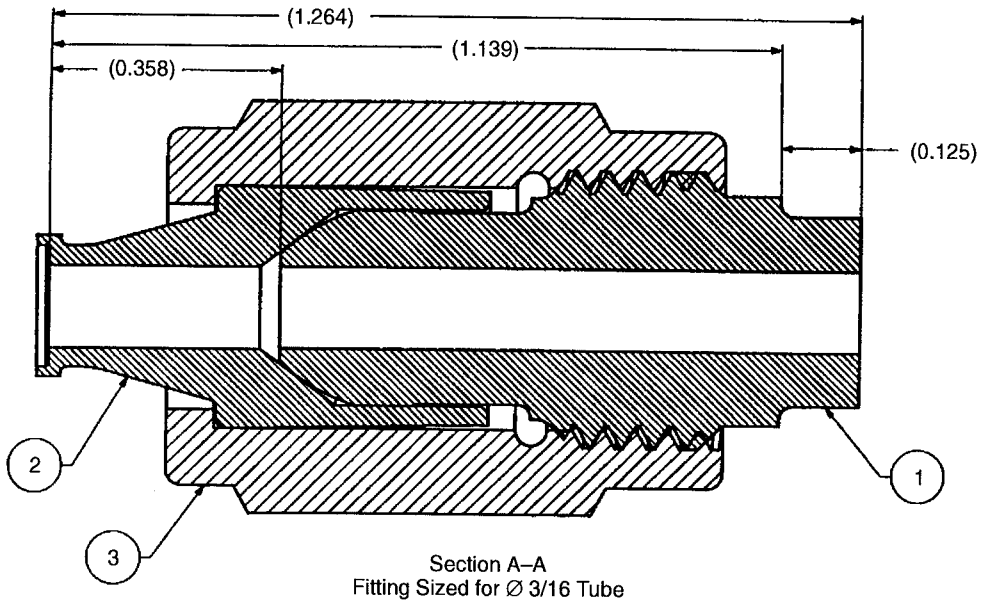

Figure 72. Local Braze Joints Used on Fuel Injection System (Diassembled Pigtail-to-Fuel-Nozzle Connector)

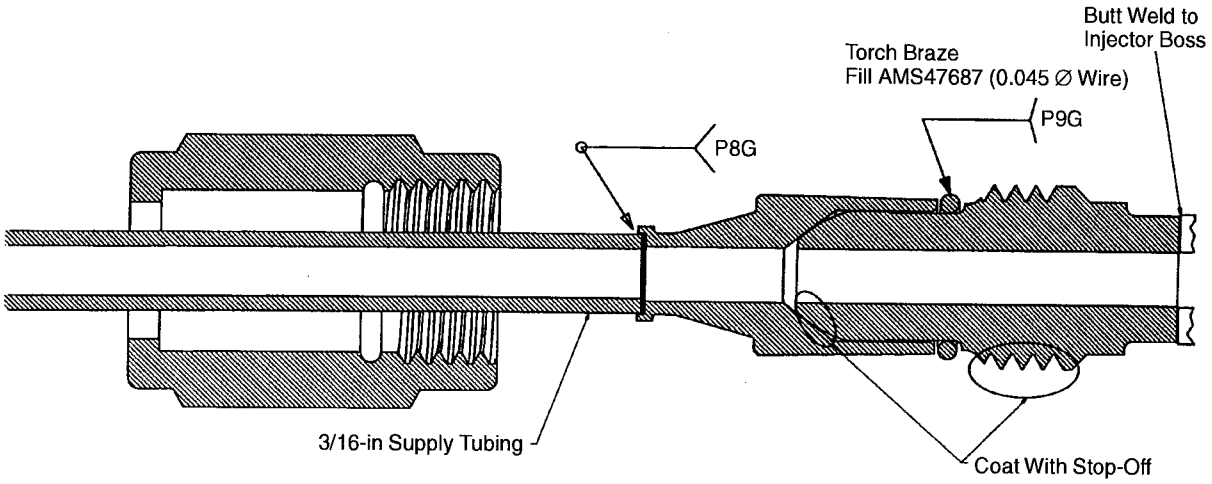

Figure 73. Assembled Connector Used on the Fuel Injection System

4.0 Turbocooler System Rig Test

4.1 Test Setup and Procedures

The objectives of the test program are to verify the technical feasibility and performance of the turbocooler and the F404 full-annular combustor system arranged in an exhaust nozzle cooling-mode configuration. Key figures of merit for the primary system components are:

1. Combustor performance with both cold and hot fuel operation
   - Efficiency
   - Exit temperature profile
   - Liner, dome, and venturi metal temperatures
   - Dynamic pressure characterization
   - Fuel nozzle operation (modified F404)
   - Emissions (secondary objective)
2. Air cycle machine performance
   - Efficiency
   - Operability
   - Air bearing operation and cooling
3. Heat exchanger performance
   - Effectiveness
   - Air-side ΔP
   - Fuel-side ΔP
   - Hot-fuel filter ΔP
   - Coating effectiveness

4.1.1 Test Approach

The test approach to accomplish the program objectives is illustrated in the test flow chart (Figure 74). The prime objectives for each phase are summarized as follows:

Phase A – Conduct a combustor facility functional checkout. The combustor test rig and facility are evaluated before any fired tests occur. The objective of the checkout runs is to verify the integrity of the facility and combustor hardware before any fired testing. These tests also blow-down the facility — minimizing the potential for foreign-object damage to the ACM. These checkout runs first provide airflow to the combustor at the maximum operating pressure, unheated, and without the fuel delivered to the combustor (unfired). Next, airflow is supplied to the combustor rig at high temperature and high pressure with the combustor unfired.

Phase B – Conduct low-power combustor mapping, at SLS and 30,000-ft/Mach 0.9 power-hook test points with cold fuel.

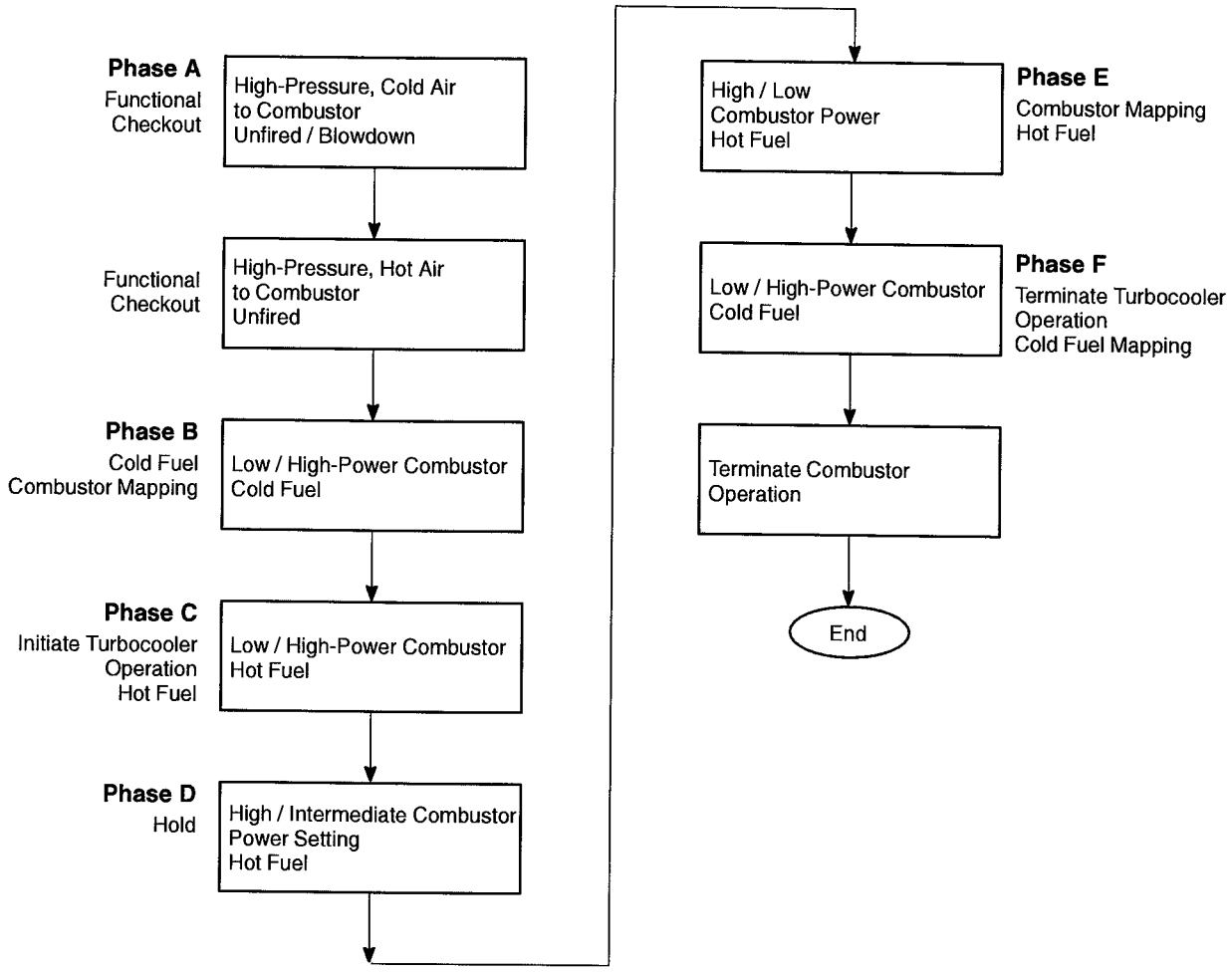

Figure 74. NASA ACEP Test Flow Chart *Turbocooler test plan begins with unfired combustor checkout and proceeds to cold-fuel mapping and turbocooler operation (hot fuel).*

Phase C – Initiate turbocooler operation and map the turbocooler system in a similar manner as Phase B (with hot fuel). Turbocooler operation will be initiated at low to intermediate power levels.

Phase D – Hold steady-state conditions with the turbocooler operating (hot fuel).

Phase E – Conduct combustor and turbocooler performance mapping with hot fuel.

Phase F – Conduct combustor performance mapping with cold fuel.

4.1.2 Test Point Conditions and Operating Procedures

The planned test point conditions are listed in Table 22.

Table 22. Planned Test Point Conditions

Test Point	Test Cycle		Air Flow (pps)			W_{F36MV} (pph)	ACM Inlet, P_{T81AA} (psia)	P_{cntrl} (psia)	ACM Exit, P_{T92AA} (psia)	Estimated T_{fulex} (°F)
	T_{T30A} (°F)	P_{Tcom} (psia)	Facility, W_{Amain}	Bleed, W_{AACM}	Combustor, W_{Acom}					
Phase B – Cold-Fuel Combustor Mapping										
100	650	90	30.9	0	24.7	1633	Amb.	Amb.	Amb.	100
101	650	125	36.7	0	29.3	2070	Amb.	Amb.	Amb.	100
1011	650	117	36.7	0	29.3	2455	Amb.	Amb.	Amb.	100
102	650	125	36.7	0	29.3	2070	Amb.	Amb.	Amb.	100
102	650	141	46.7	0	37.3	2593	Amb.	Amb.	Amb.	100
103	750	139	42.1	0	33.6	3148	Amb.	Amb.	Amb.	100
104	750	186	58.8	0	46.9	3750	Amb.	Amb.	Amb.	100
105	750	227	69.1	0	55.1	4944	Amb.	Amb.	Amb.	100
106	860	164	47.8	0	38.1	4075	Amb.	Amb.	Amb.	100
107	860	170	48.2	0	38.5	4435	Amb.	Amb.	Amb.	100
108	860	275	80.5	0	64.2	6604	Amb.	Amb.	Amb.	100
Phase C – Hot-Fuel Combustor Mapping										
200	650	90	31.3	1.5	23.8	1685	65.3	41	24.4	708
201	650	117	39.7	2.0	30.1	2455	86.0	48	28.3	778
202	650	141	49.4	2.7	37.3	2593	105.8	56	38.8	728
203	750	139	44.6	2.5	33.6	3148	104.8	56	31.9	822
204	750	186	62.8	3.0	47.7	3750	122.0	58	38.6	811
205	750	227	72.8	3.8	55.1	4944	152.3	69	44.4	832
206	860	164	52.0	3.2	38.9	4075	131.3	70	37.3	864
207	860	170	51.6	3.3	38.5	4435	140.5	74	37.5	906
208	860	275	86.3	4.8	65.0	6604	196.1	85	53.1	869
Phase D – Hot-Fuel Hold Condition										
300	750	227	72.8	3.78	55.1	4944	152.3	69	44.4	832
Phase E – Post Endurance Hot-Fuel Combustor Mapping – Repeat 200 Series Points										
400	650	141	49.4	2.7	37.3	2593	105.8	56	38.8	728
401	860	275	86.3	4.8	65.0	6604	196.1	85	53.1	869
450	860	275	86.3	4.1	65.6	6604	156.0	75	53.1	740
451	860	275	86.3	3.4	66.1	6604	130.0	65	53.1	614
452	860	275	86.3	2.6	66.8	6604	105.0	55	53.1	469
453	860	275	86.3	1.9	67.4	6604	79.0	45	53.1	334
Phase F – Post Endurance Cold Fuel Combustor Mapping – Repeat 100 Series Points										
500	650	141	46.7	0	37.3	2593	Amb.	Amb.	Amb.	100
501	650	141	46.7	0	37.3	**2830**	Amb.	Amb.	Amb.	100
502	860	275	80.5	0	64.2	6604	Amb.	Amb.	Amb.	100
503	860	275	80.5	0	64.2	**7120**	Amb.	Amb.	Amb.	100

Typical start-up and shut-down procedures are as follows:

Normal F404 Combustor/Turbocooler Start-Up

- Ensure combustor bleed valve to ACM is closed.
- Initiate airflow to F404 combustion system and establish light-off conditions.
- Initiate cold-fuel flow to the combustor rig (through the turbocooler heat exchangers).
- Establish low/idle power conditions on the combustor.
- Bleed a small amount of fuel from the heat exchangers to remove any trapped air on the fuel side.
- Establish desired power conditions on the combustor.
- Open combustor bleed valve to initiate turbocooler operation (initiate hot fuel operation). To minimize the thermal gradients on the heat exchanger, the turbocooler start-up is staged over a 60-second period.
- Set/trim test conditions to desired level.

Normal F404 Combustor/Turbocooler Shut-Down

- Establish low/intermediate power setting on the combustor and turbocooler.
- Terminate airflow to the ACM — close bleed valve.
- Continue combustor operation (cold fuel) until all external heat exchanger thermocouples are less than 200°F.
- Terminate fuel flow to the combustor (fuel system is not purged).
- Cool down facility.

Emergency F404 Combustor/Turbocooler Shut-Down

In the event of a high-temperature fuel leak or other observed problems, the following emergency procedures are followed:

- Terminate airflow to the ACM — close bleed valve.
- Terminate fuel flow.
- Purge fuel system (pulse).

4.1.3 General Safety Considerations

The intent of this subsection is to describe the general approach to safety for the ACEP test program.

1. No personnel are allowed in the test cell when the turbocooler is operating (hot fuel and ACM rotation).
2. Pressure relief valves are include in the fuel supply system to prevent any fuel-side overpressurization.
3. Nitrogen purge is installed for normal shut-down procedures (if required), leak checking, and emergency operation.

4. All ACEP turbocooler components are anchored to prevent any movement or shifting that might contribute to a leak. The turbocooler skid is designed to accommodate thermal growth.
5. Valves are designed for fail-safe operation on loss of power. The combustor bleed valve fails close, terminating the turbocooler operation. The back-pressure valve fails close, terminating the turbocooler operation. A flow-measuring orifice in the ACM turbine discharge line is sized to prevent ACM overspeed.
6. Operating limits are established on critical parameters to provide early warning of potential problems.
7. Leak and fire detection devices (CO and HC sensors) are installed and continuously monitored.
8. The local CO_2 deluge system is installed near the turbocooler skip to augment cell deluge. The local CO_2 deluge does not bypass the normal cell CO_2 system.
9. The fuel system, including the heat exchangers, is leaked-checked each day prior to testing.
10. Video cameras monitor critical hardware. At a minimum, cameras are located on both sides of the combustor rig, viewing the fuel manifold, and one camera on the turbocooler skid.

4.2 Turbocooler Performance and Test Results

Test demonstration of the turbocooler systems and the F404 combustor with the turbocooler system, configured in an exhaust nozzle cooling mode, was successful. A maximum fuel temperature of 732°F was achieved along with subcooled cooling air as low as –7°F. A heat sink capacity of 360 Btu/s was achieved with conventional JP fuel. The turbocooler and F404 combustor demonstrated safe, stable operation throughout the operating range of this study. There was no observed change in combustor operation with hot or cold fuel and no evidence of combustor instability, flashback, or any change in the combustor exit temperature profile. Observed performance levels of the primary components, air cycle machine, heat exchangers, and fuel injection system, agreed with predicted levels. Heat exchanger and fuel injector performance was on target, and the units were visually clean at the end of the test.

4.2.1 Turbocooler Performance

The first two test runs were associated with the system shakedown and checkout, primarily focusing on the combustor rig. Detailed descriptions of the operational procedures and test instrumentation are provided in Section 4.3. There were some unexpected problems getting started: power outages and community-wide power curtailment. Critical instrumentation problems were identified during this time and corrected. Control and safety valves were cycled, and positions were checked. The combustor discharge rake assembly was successfully rotated. Data analysis programs were updated.

During run 3, cold-fuel combustor mapping was initiated. Combustor operability with the modified fuel injectors was as expected relative to lightoff capability, stability, emissions, and temperature profiles on the combustor liners and at the combustor discharge plane. At test point 106, reference Table 22 (page 94), the packing material (rope seals) that help form air seals on the combustor rig modules disintegrated and had to be reapplied to plug several leaks.

The turbocooler system was operated during runs 4 through 8. Figure 75 shows the transient response of key turbocooler parameters during a typical startup. The F404 combustor is stabilized at test point 200. As the turbocompressor inlet pressure increases to approximately 30 psia, the turbocompressor starts to rotate and within seconds is operating at approximately 40,000 rpm. The turbocompressor turbine discharge drops nearly 300°, to less than 0°F, in 60 seconds. Fuel temperature smoothly increases to 350°F in the same time period. At no time was there any indication of unstable behavior in the turbocooler or combustor. The transition was smooth and well controlled. The temperature differential between the heat exchanger header and the dome never exceeded 400°F — an acceptable thermal difference.

Key turbocooler rig operating test points are presented in Figures 76 through 79 for readings 48, 54, 121, and 131. In these test points, fuel temperature varies from 408° to 732°F and turbine discharge air varies from 123° to approximately 0°F. The test point data are summarized in Table 23. A maximum heat sink point of 360 Btu/s was achieved during reading 54 as presented in Figure 77. In this test point, 749°F combustor bleed air is cooled to 123°F at sufficient pressure to significantly cool a gas turbine exhaust nozzle structure as compared to conventional cooling schemes.

Measured ACM compressor performance is compared to pretest predictions in Figure 80. The compressor test performance agrees with the pretest predictions. It should be noted that the ACM speed measurement proved unreliable in the GEAE test facility, although it is successfully used on most ACM acceptance/development tests. This may be attributed to the lead length from the sensor to the control room. The measured speed does not agree with the predicted speed lines.

ACM turbine performance (efficiency) is compared to pretest predictions in Figure 81. The turbine efficiency of the R1 unit is as predicted. The turbine efficiency of the R2 unit is degraded as compared to the predicted turbine efficiency — down approximately 7 points. The performance lapse in R2 was also observed to some extent during the ACM acceptance testing. The root cause of R1 performance degradation is not fully known, but the degradation may be due to such factors as turbine clearances, turbine nozzle geometry, and turbine blade aerodynamics.

Measured heat exchanger air-side pressure drop is compared to pretest performance predictions in Figure 82. The air-side pressure drop, including the interconnecting U-tube, is as predicted. The pressure drop data presented in Figure 82 has been corrected to standard density. Proper prediction of air-side pressure drop is critical to adequately accommodating air bearing cooling distribution and thrust balance. The ACEP ACM employs a recirculation of the bearing parasitics — not a conventional cooling means. Typically the bearing coolant is discharged to ambient (as a predictable system loss). In the recirculating system the thrust bearing coolant is restored at the compressor inlet, and journal components are restored respectively at the compressor diffuser and the turbine rotor inlet. This places a significant constraint on the heat exchanger air-side pressure drop to ensure positive flow over the compressor journal. This proved detrimental to the original bearing cooling design but was modified and validated on the ACM engine cooling mode acceptance test.

The thermal performance of the heat exchangers exceeded expectations with respect to air-side cooling capability. A contributor to the thermal performance was the heat loss from the fuel to ambient. The heat exchanger performance was simulated by reducing the fuel inlet temperature to the heat exchanger in order to match the observed turbine inlet temperature. The heat exchangers were not insulated during the test so that potential fuel leaks could be visually detected.

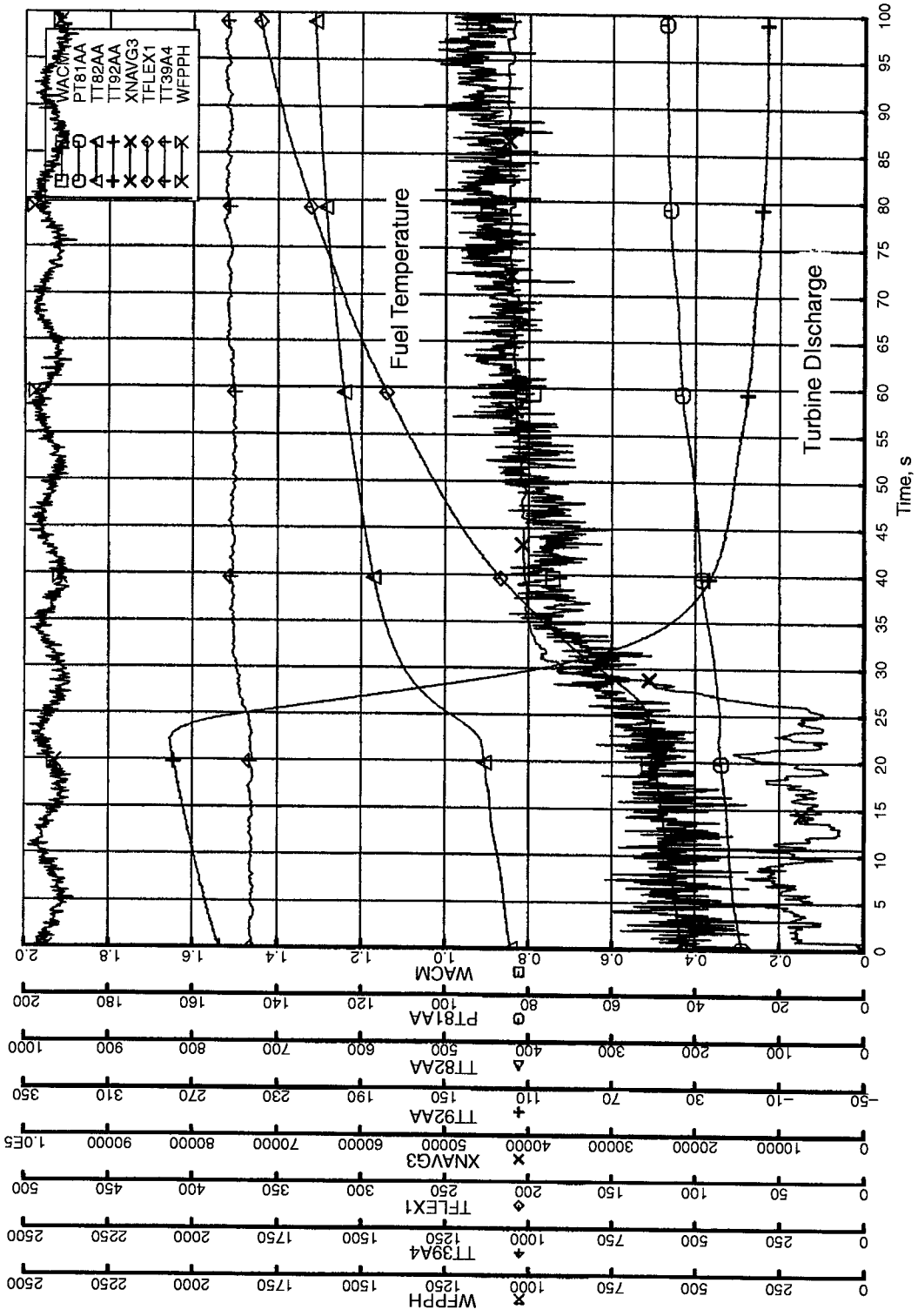

Figure 75. NASA ACEP Rig Test ACM Start-Up Transient

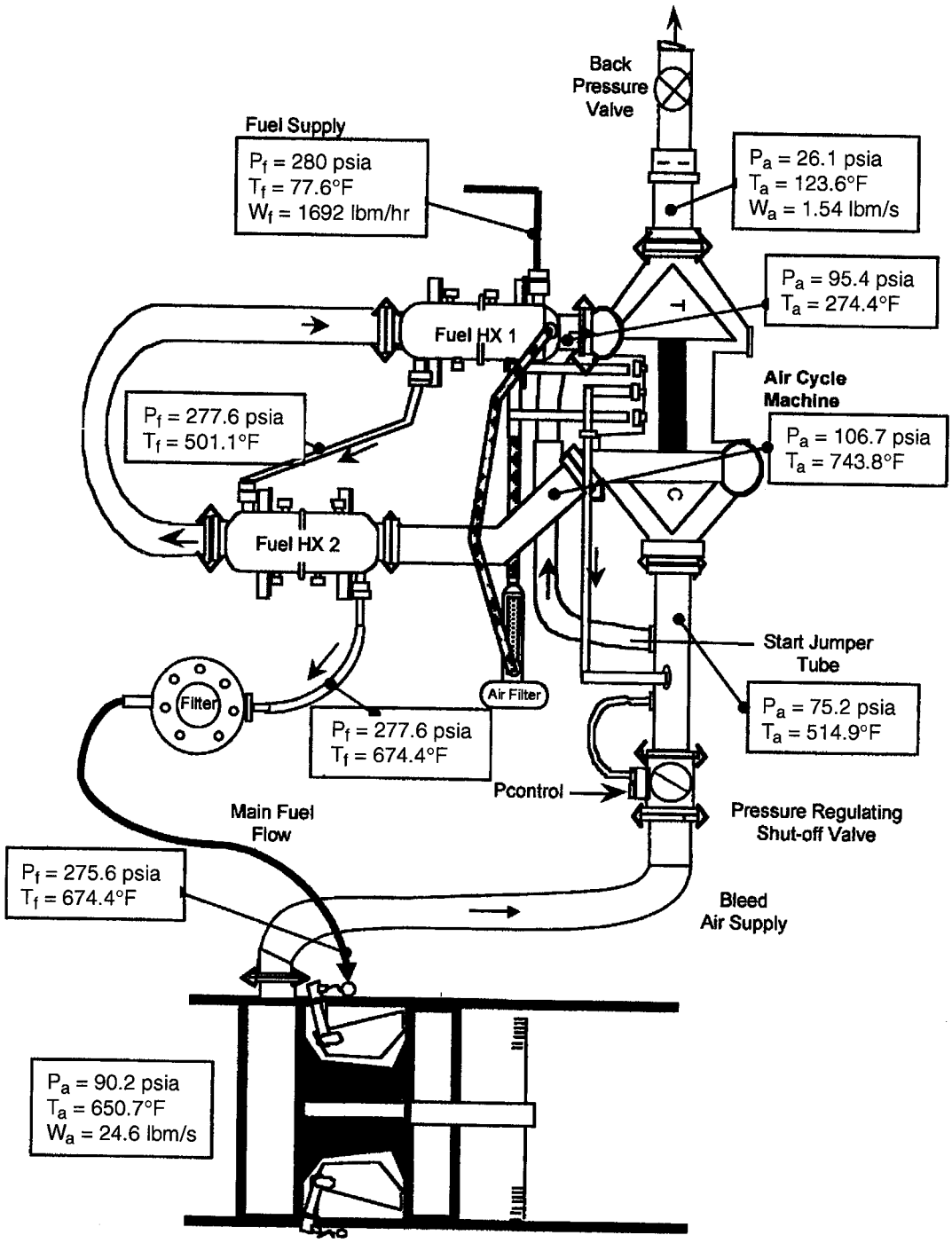

Figure 76. F404 Full-Annular Combustor Rig: Reading 48, Test Point 200

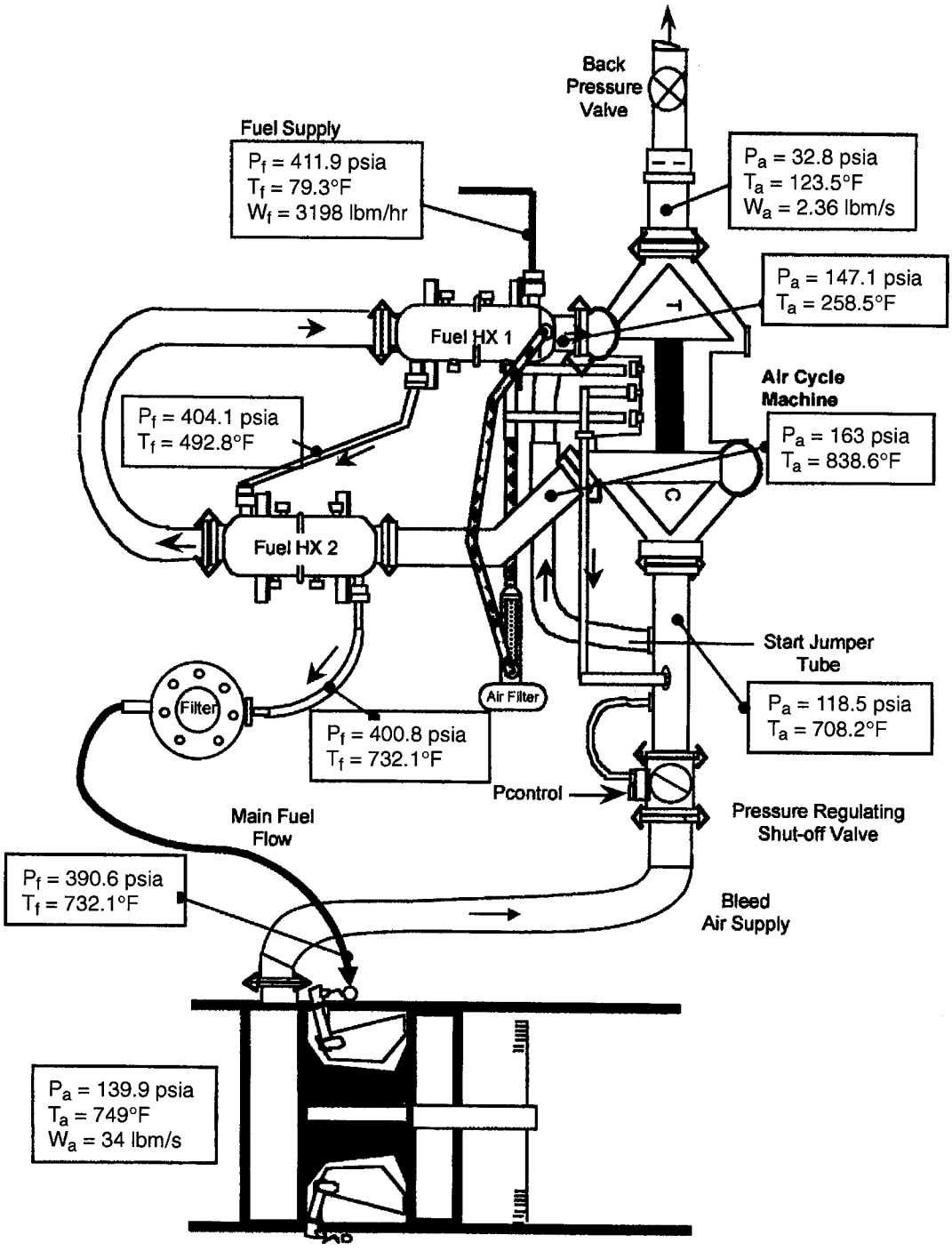

Figure 77. F404 Full-Annular Combustor Rig: Reading 54, Test Point 203 (Maximum Heat Sink Test Point)

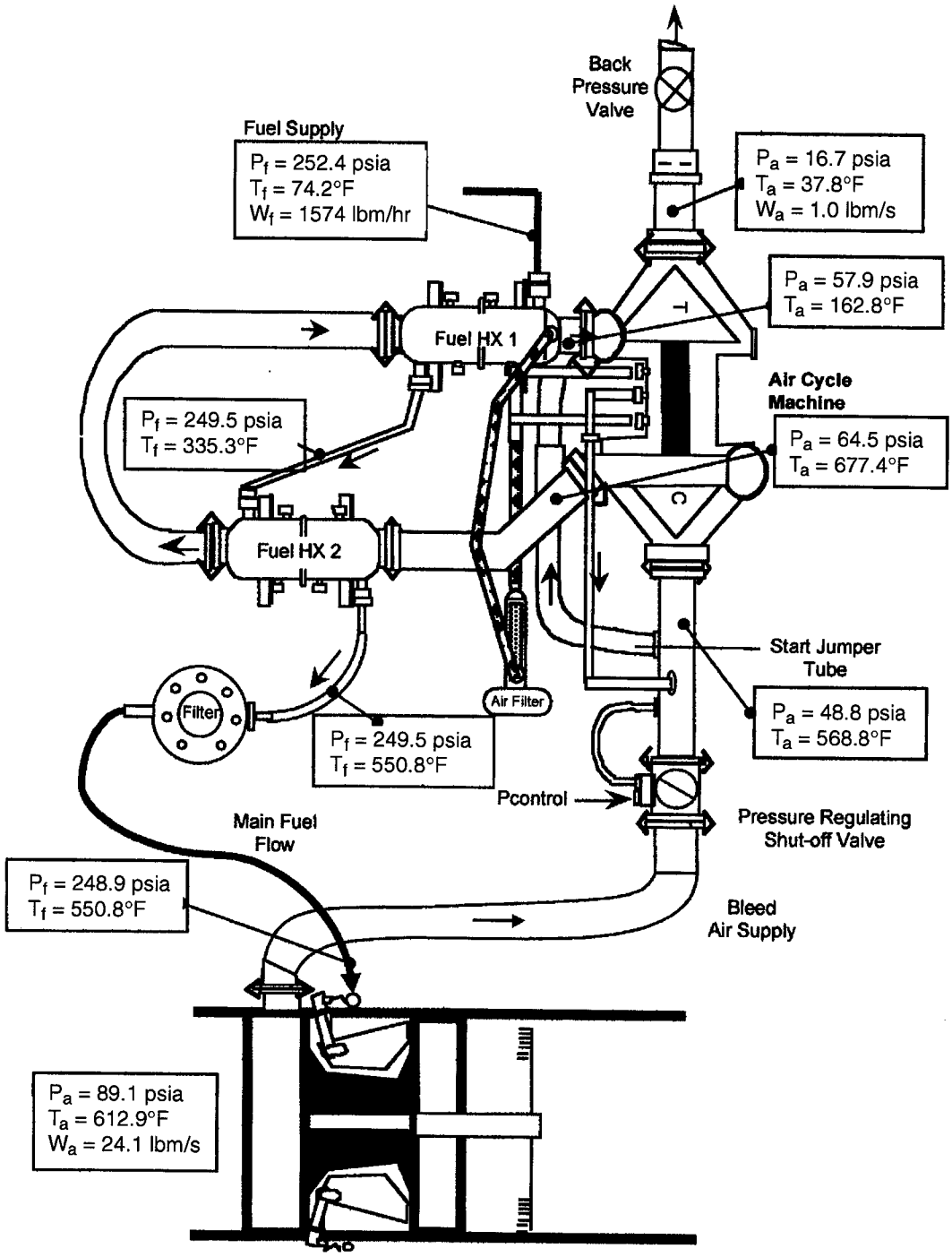

Figure 78. F404 Full-Annular Combustor Rig: Reading 121, Test Point 202

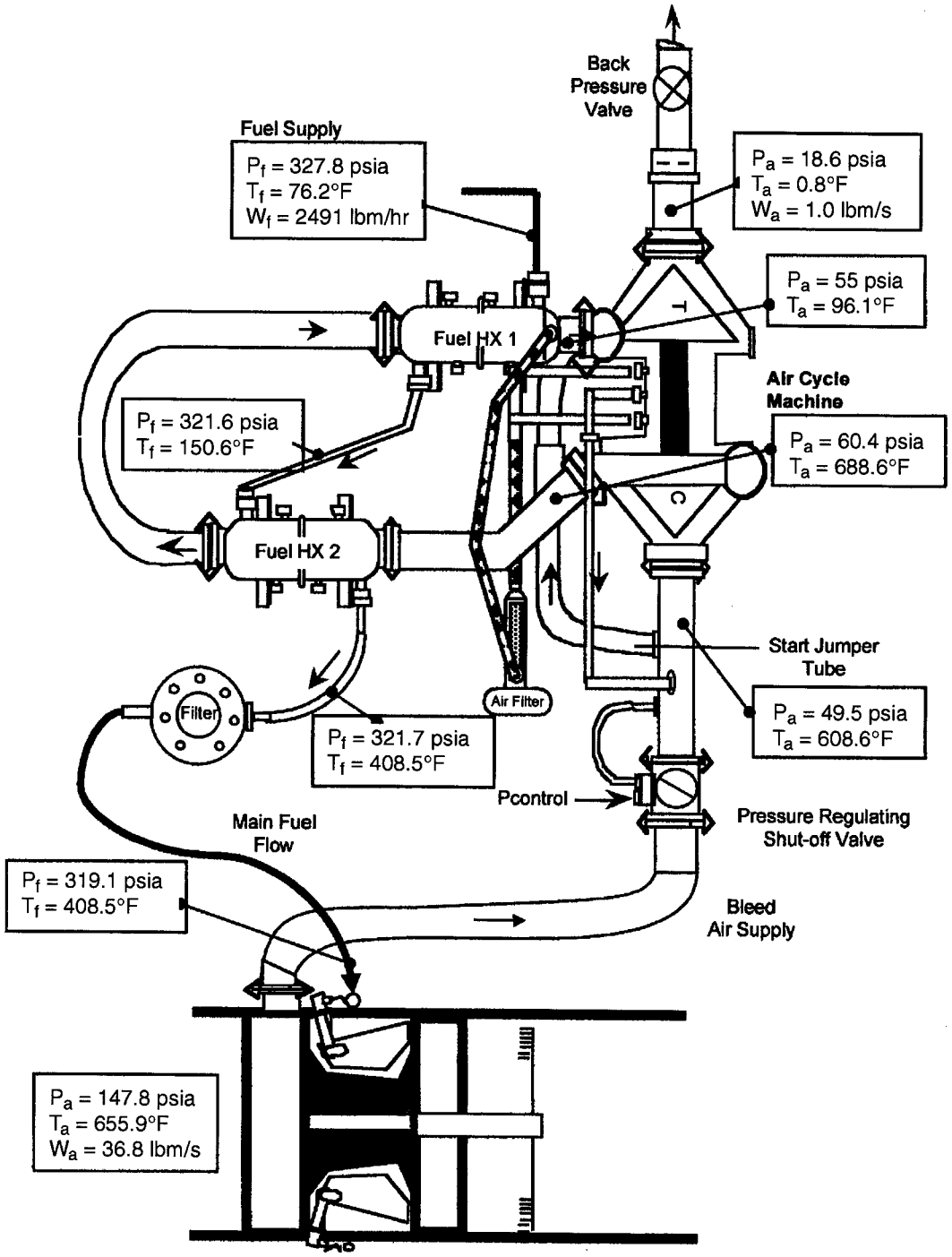

Figure 79. F404 Full-Annular Combustor Rig: Reading 131, Test Point 202

Table 23. Summary of Key Turbocooler Test Points

Reading Number / Test Point ➧		48 / 200	54 / 203	121 / 202	131 / 020
ACM Unit ➧		R2	R2	R1	R1
Compressor	P_{in}, psia	75.2	118.5	48.8	49.5
	P_{ex}, psia	106.7	163	64.5	60.4
	T_{in}, °F	514.9	708.2	568.8	608.6
	T_{ex}, °F	743.8	838.6	677.4	688.6
	Pressure Ratio	1.42	1.38	1.32	1.22
	Speed, RPM*	63394	51782	33887	50413
	Flow, lbm/s	1.54	2.36	1	1
	Efficiency, %**	0.83	0.73	0.77	0.74
Turbine	P_{in}, psia	95.4	147.1	57.9	55
	P_{ex}, psia	26.1	32.8	16.7	18.6
	T_{in}, °F	274.4	258.5	162.8	96.1
	T_{ex}, °F	123.6	123.5	37.8	0.8
	Pressure Ratio	3.65	4.49	3.46	2.95
	Efficiency, %***	0.66	0.56	0.72	0.76
Heat Exchanger Air Side	P_{in}, psia	105.6	157.2	63.6	59.6
	P_{ex}, psia	95.4	147.1	57.9	55
	T_{in}, °F	738.1	841.5	662.6	683.1
	T_{ex}, °F	274.4	258.5	162.8	96.1
	ΔP, %	9.6	6.4	9.1	7.6
	Effectiveness	0.7	0.77	0.85	0.97
	Heat Load, Btu/s	182.2	357.3	127.7	148.2
	ΔT Header–Shield, °F	55	70.1	75.7	253.5
Heat Exchanger Fuel Side	P_{in}, psia	280	411.9	252.4	327.8
	P_{ex}, psia	277.2	400.8	249.5	321.7
	T_{in}, °F	77.6	79.3	74.2	76.2
	T_{ex}, °F	674.2	732.1	550.8	408.5
	ΔPressure, psid	3.6	11.1	2.7	6.1
	Heat Load, Btu/s	167.9	360.3	120.6	128.6
	Fuel Flow, lbm/hr	1692	3198	1574	2491
Fuel Nozzle	P_{in}, psia	275.5	390.6	248.9	319.1
	T_{in}, °F	674.2	732.1	550.8	408.5
	Fuel Flow / Nozzle, lbm/hr	94	177.7	87.4	138.4
	Fuel Nozzzle ΔP, psid	193.8	265.3	170.9	192.8
	Filter ΔP, psid	1.6	10.2	0.8	2.6

* Speed sensor was intermittent
** Corrected for recirculated bearing flow
*** Corrected to dry-air conditions

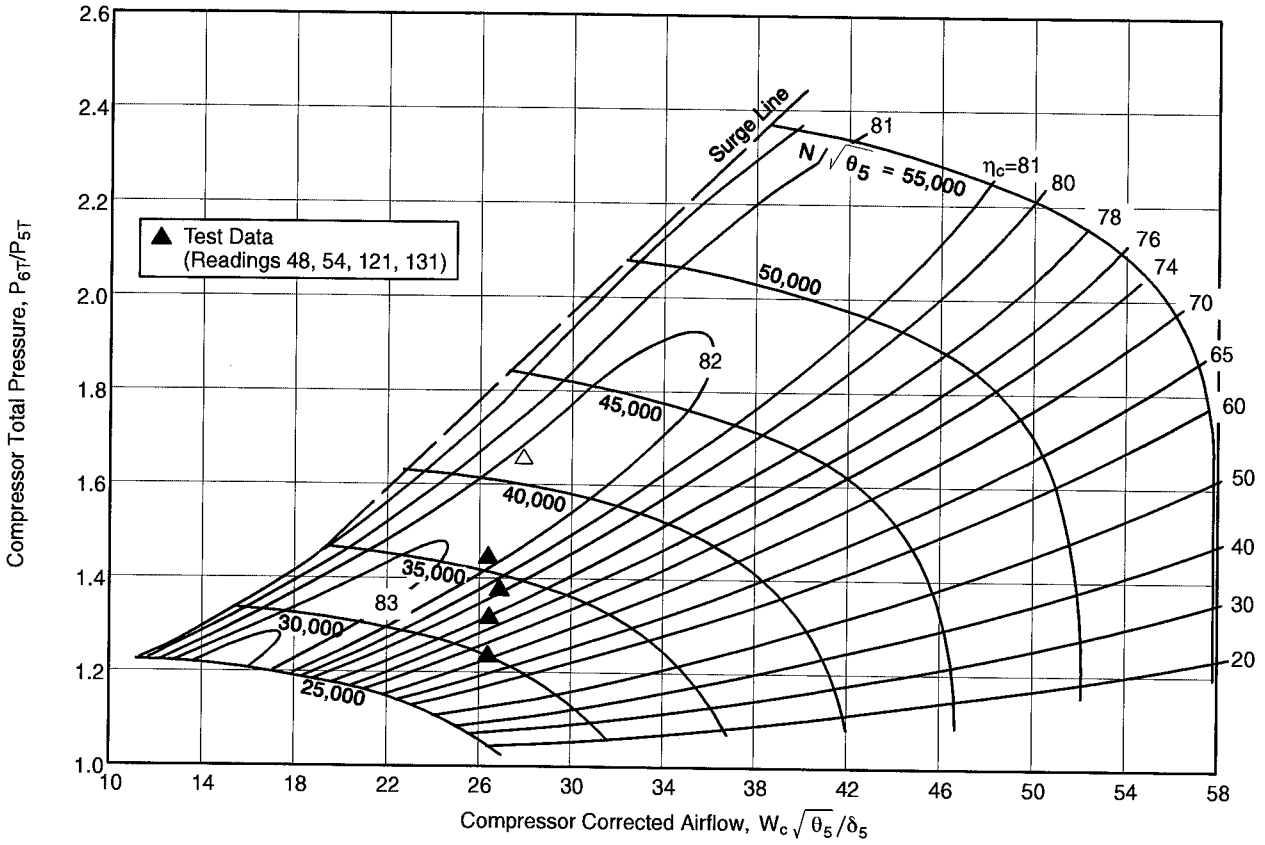

Figure 80. Comparison of ACM Compressor Performance with Pretest Predictions

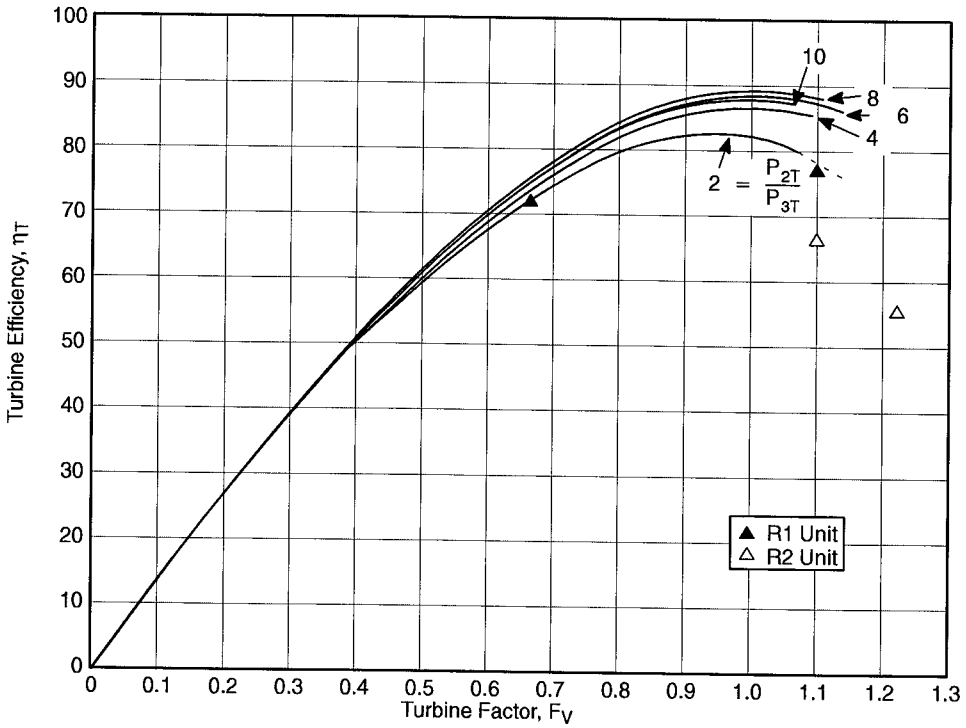

Figure 81. Comparison of ACM Turbine Performance with Pretest Predictions

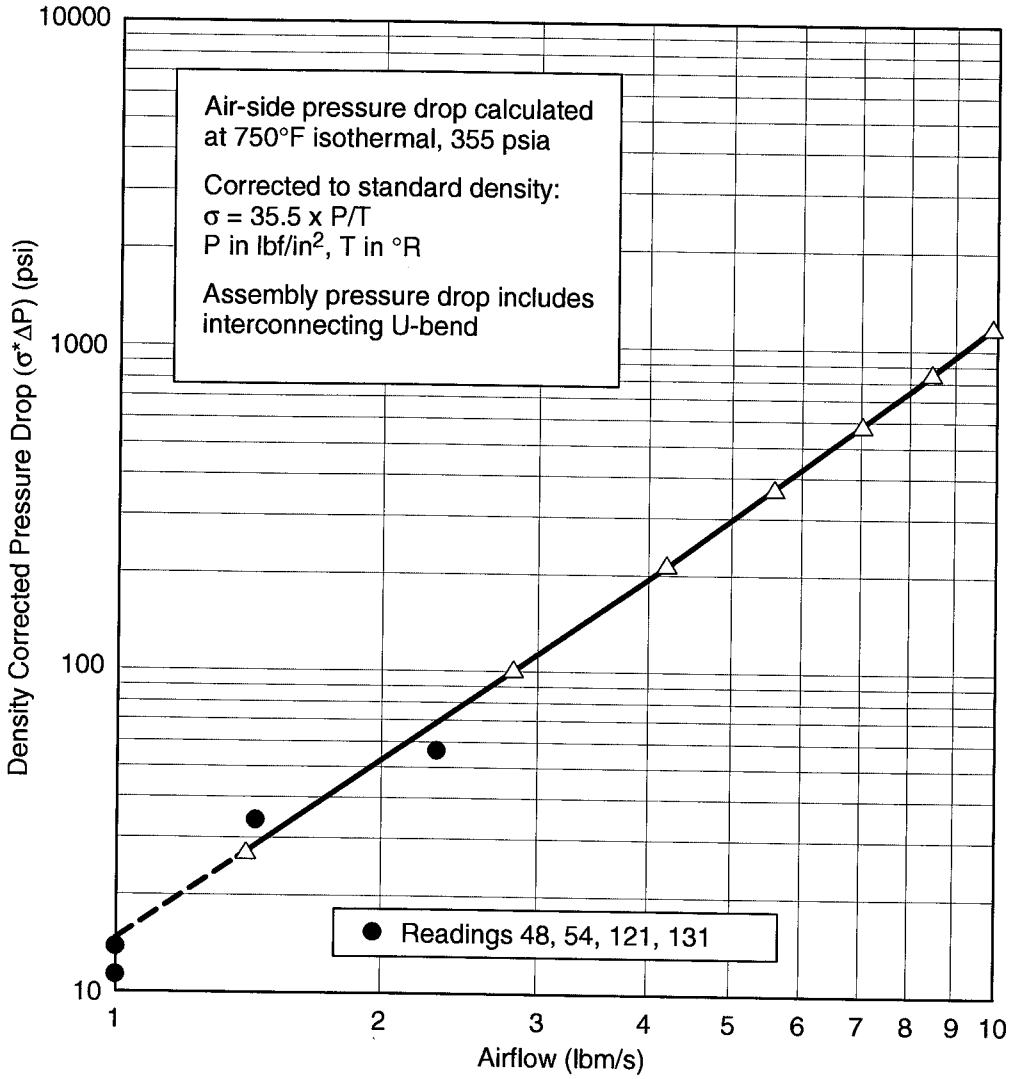

Figure 82. Heat Exchanger Air-Side Pressure Drop Performance Matches Pretest Predictions

Measured heat exchanger fuel-side pressure drop is compared to pretest performance predictions in Figure 83. The measured fuel-side pressure drop is higher than predicted. Alhough the measured differs considerably from the predicted levels, the consequence of this error is small. The fuel control system in a gas turbine engine will increase overall fuel system pressure to deliver the fuel demand.

The fuel-side surfaces of the heat exchangers were visually inspected by means of a small, flexible borescope at the end of the test program. The fuel-side surfaces in both heat exchangers appeared clean, shiny, and free of debris. Photographs of the fuel-side surfaces of the heat exchangers are presented in Figure 84.

4.2.2 Combustor and Fuel Injector Performance

The F404 full-annular combustor and modified fuel injection system operated the same with either hot or cold fuel. No combustor instability was observed during the test. The exit temperature profile,

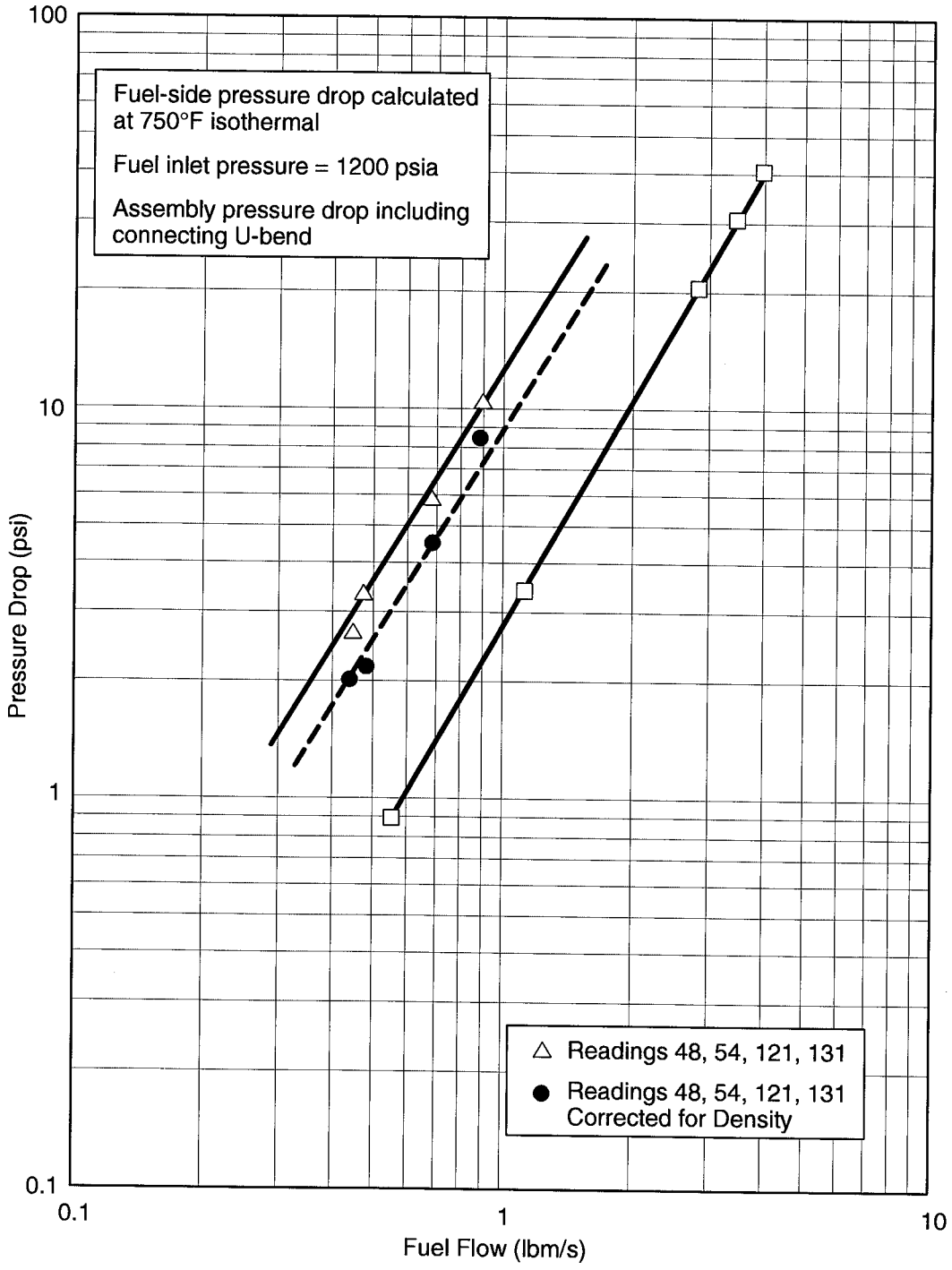

Figure 83. Fuel Side Pressure Drop

The fuel-side surfaces of the heat exchangers appeared clean, shiny, and free of debris at the end of the test

Figure 84. Fuel-Side Surfaces of the Heat Exchangers

combustor dynamics, and axial location of the flame front (flashback) were unchanged between hot- and cold-fuel operation. Normalized exit temperature profiles, as measured from the discharge rake, for hot- and cold-fuel operation are presented Figure 85. The combustor was operating at similar conditions for the comparison. The hot-fuel temperature was 674°F, and the cold fuel temperature was approximately 100°F. Normalized temperature or profile factor is calculated as:

$$Profile\ Factor = (T_{probe} - T_{3avg}) / (T_{4avg} - T_{3avg})$$

where T_{3avg} is the average combustor inlet temperature and T_{4avg} is the average combustor exit temperature. The profile factor with hot fuel has a similar shape and general magnitude as with cold-fuel operation. The temperature profile that would be experienced by a turbine nozzle/rotor in an engine is essentially unchanged; no change would be required in the turbine cooling arrangement.

Combustor liner metal temperatures with hot- and cold-fuel operation are presented in Figure 86. Metal temperatures for the upper liner and the lower combustor liner are shown. During hot-fuel operation, the fuel temperature reached 732°F. As indicated in the plot, there is essentially no difference in the liner metal temperatures due to fuel heating.

Combustor exhaust gas emission levels with hot and cold fuel are presented in Figure 87. At this combustor operating condition, emission of CO and unburned hydrocarbons is reduced over 50% with hot fuel. Nitrous oxide (NO_2) and other nitrogen products (NOx) appear to increase with fuel temperature; however, when plotted against average combustor discharge temperature, NOx emissions appear comparable or slightly lower with hot fuel than with cold fuel (see Figure 88).

Posttest inspection of the fuel nozzles found them clean in appearance. A comparison of the pre- and posttest fuel nozzle flow checks indicated no change in the fuel nozzle flow characteristics. Figure 89 shows the results of the pre- and posttest fuel nozzle flow checks at four fuel pressure levels. The fuel nozzle flow ranges overlap, and there are no statistical differences in the variances.

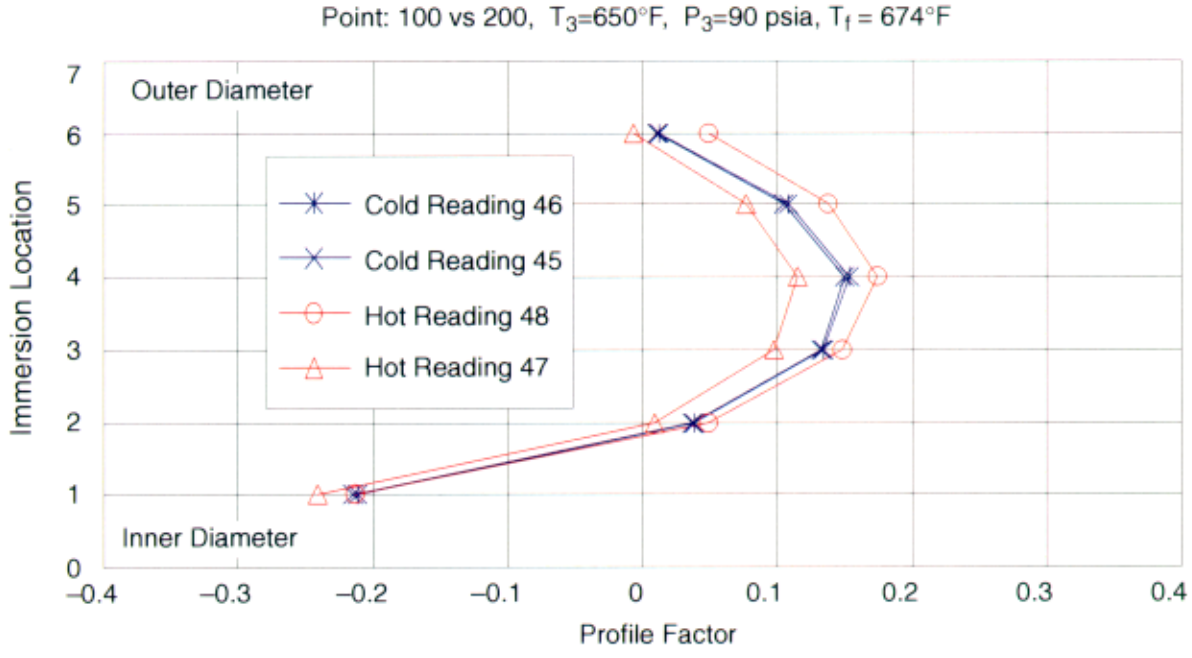

Figure 85. Combustor Temperature Profile With Hot- and Cold-Fuel Operation *Normalized exit temperature profiles are similar in shape and level with both hot and cold fuel.*

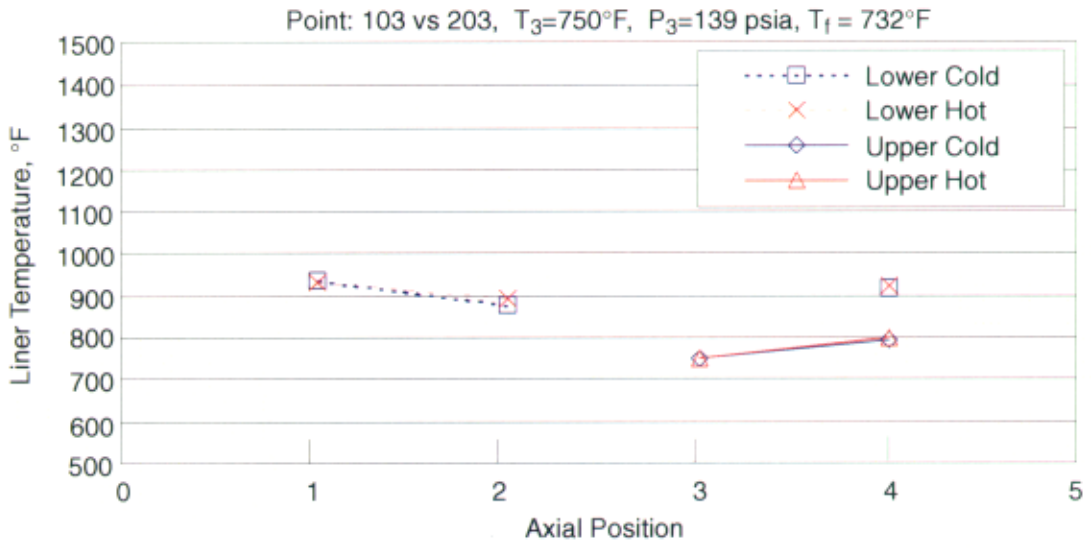

Figure 86. Combustor Liner Metal Temperatures With Hot and Cold Fuel *Combustor liner metal temperatures are unchanged with hot-fuel operation.*

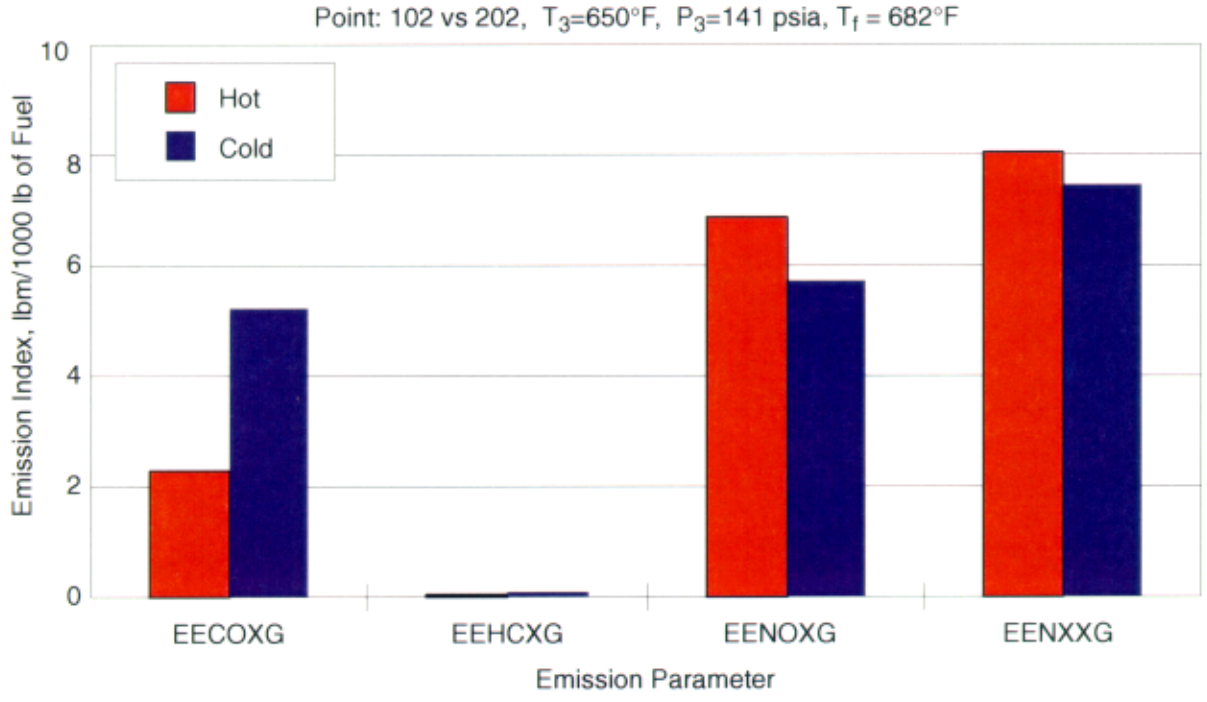

Figure 87. Combustor Emissions With Hot and Cold Fuel *Combustor emission levels, CO and unburned HC, are significantly reduced with hot fuel.*

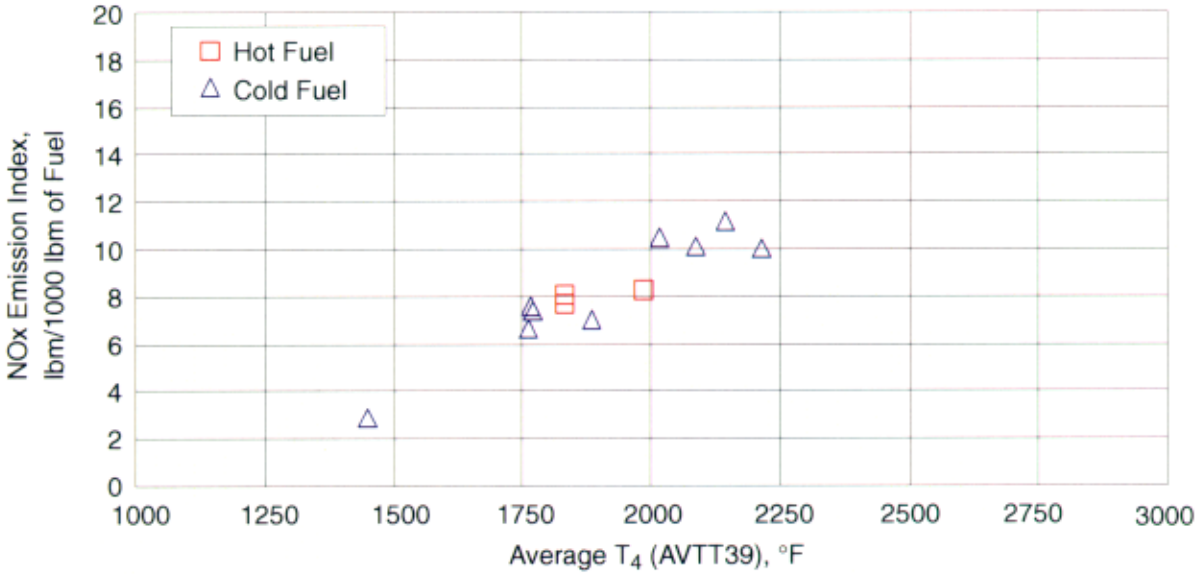

Figure 88. NOx Emissions for Hot and Cold Fuel as a Function of Combustor Discharge Temperature *NOx emissions with hot fuel are unchanged when evaluated against combustor discharge temperature.*

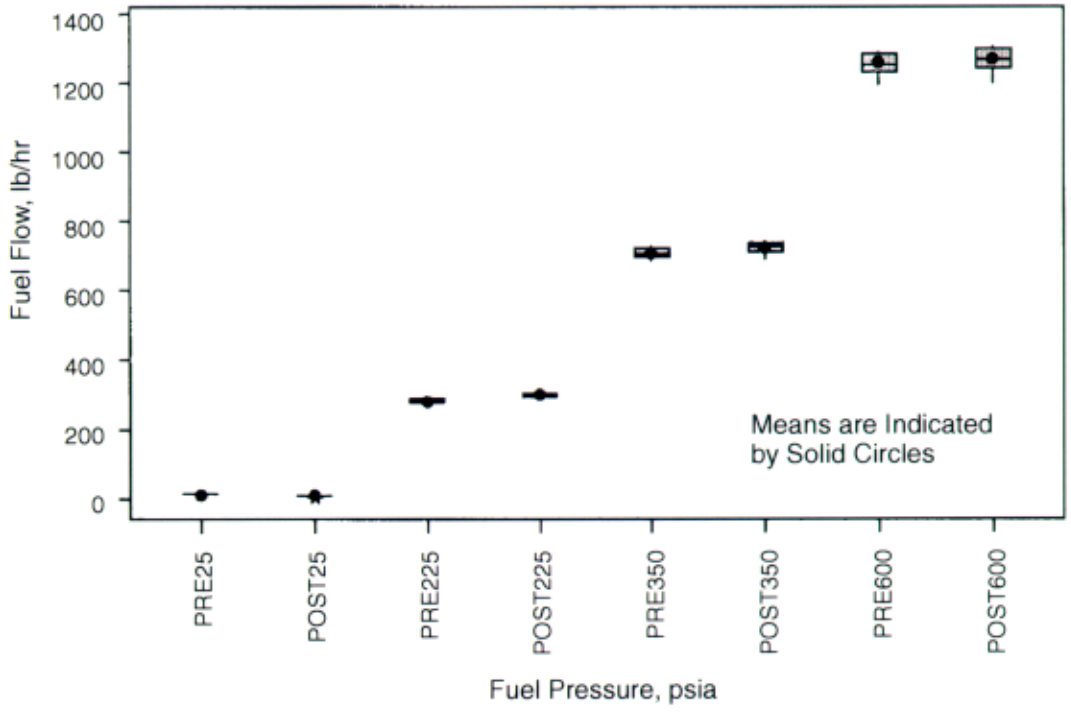

Figure 89. One-Way Analysis of Fuel Nozzle Flow Variance *Pre- and posttest fuel nozzle flow check indicated that fuel nozzle performance did not deteriorate with hot fuel operation*

4.3 ACEP Test Rig System Description

The turbocooler system with the F404 full-annular combustor was tested in GEAE Cell A19. This facility is used for large-combustor testing and can accommodate combustors up to 92-in diameter. Drawings of the turbocooler test rig are presented in Figures 90 and 91. The main combustor supply air, pressurized and heated to the appropriate temperature, is housed in a separate facility. The turbocooler system is mounted on a separate skid adjacent to the main combustor installation. Combustor inlet air is supplied to the turbocooler through the single bleed port on the combustor case and a F–18 pressure regulating shutoff valve (PRSOV). In the exhaust nozzle cooling mode configuration, the turbocooler discharge air is designed to be returned to the nozzle cooling manifold. The test facility simulates the exhaust nozzle cooling manifold characteristics by installing a back-pressure valve at the ACM turbine exit to control the discharge pressure. Figure 92 is a photograph of the test facility; a photograph of the skid is shown in Figure 93, and a schematic of the adjacent turbocooler skid is shown in Figure 94.

4.3.1 Description of Key Components

The design and features of the primary components specifically for the turbocooler test are described in Sections 3.2 through 3.4. However, additional components were used in support of the rig test, including: an F404 full-annular combustor, ACM start bypass and bearing cooling restoration, fuel filter, air filters, and pressure-regulating valves.

4.3.1.1 F404 Full-Annular Combustor Rig

The F404–GE–400 combustion system comprises a machined-ring, annular-flow-type combustor and annular step diffuser; 18 pressure-atomizing fuel nozzles (modified for the ACEP program); and a single capacitive-discharge igniter. The fuel injection system has 18 pressure-atomizing, dual-orifice fuel nozzles with integral air shrouds. Final fuel atomization is completed in the combustor dome swirler/venturi.

The fuel is delivered to each fuel nozzle by a single manifold with 18 individual pigtails to accommodate differential thermal expansion (see Figure 95). All of the manifold, pigtail, and fuel nozzle fittings were modified for the ACEP program to incorporate a local braze joint. Fuel is delivered to the manifold through a single inlet connection on the bottom centerline of the combustor rig. Uniform fuel distribution is achieved through the use of flow-divider valves that are integral parts of each fuel nozzle assembly. The flow-divider valve schedules flow to the secondary orifice as a function of fuel pressure, and the valve-cracking point occurs during acceleration to ground idle at sea level. In an aircraft installation, a check and drain valve is located between the main fuel control and the nozzle manifold to drain the fuel manifold at engine shutdown. The check and drain valve is not used for combustor rig testing.

Bleed air for the turbocooler is extracted uniformly around the combustor outer annulus immediately downstream from the step diffuser. This air is collected in a 360° internal manifold and ducted through the fan stream by a single port located on the engine/ combustor rig bottom vertical centerline (see Figure 96).

4.3.1.2 ACM Start Bypass and Bearing Cooling Restoration

The details of the ACM are described in Section 3.2. Two features that need clarification for the integrated systems test are the start bypass valve and restoration of the bearing cooling to the ACM

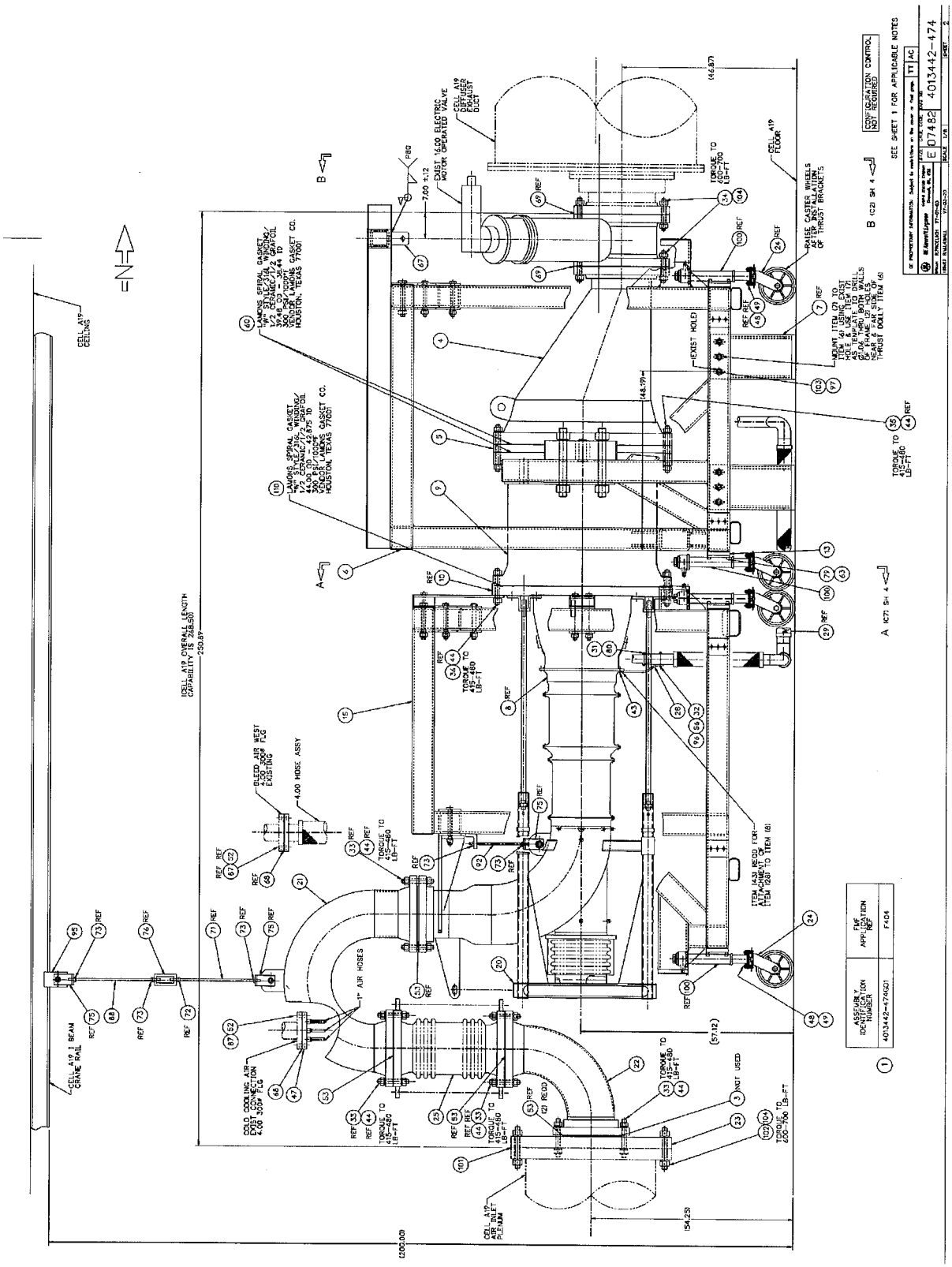

Figure 90. Cross Section of the Turbocooler Test Facility

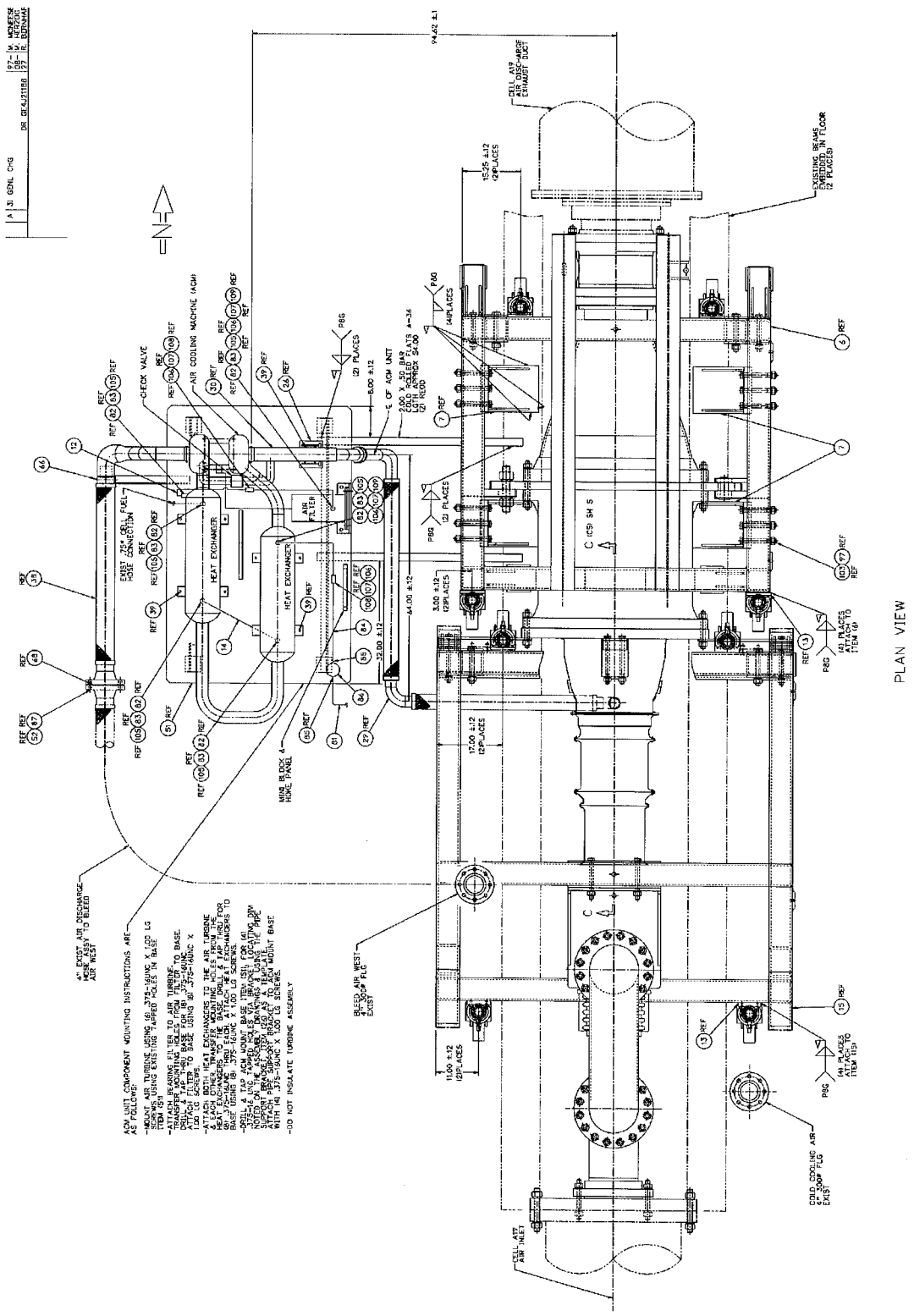

Figure 91. Plan View of Turbocooler Rig Test Facility

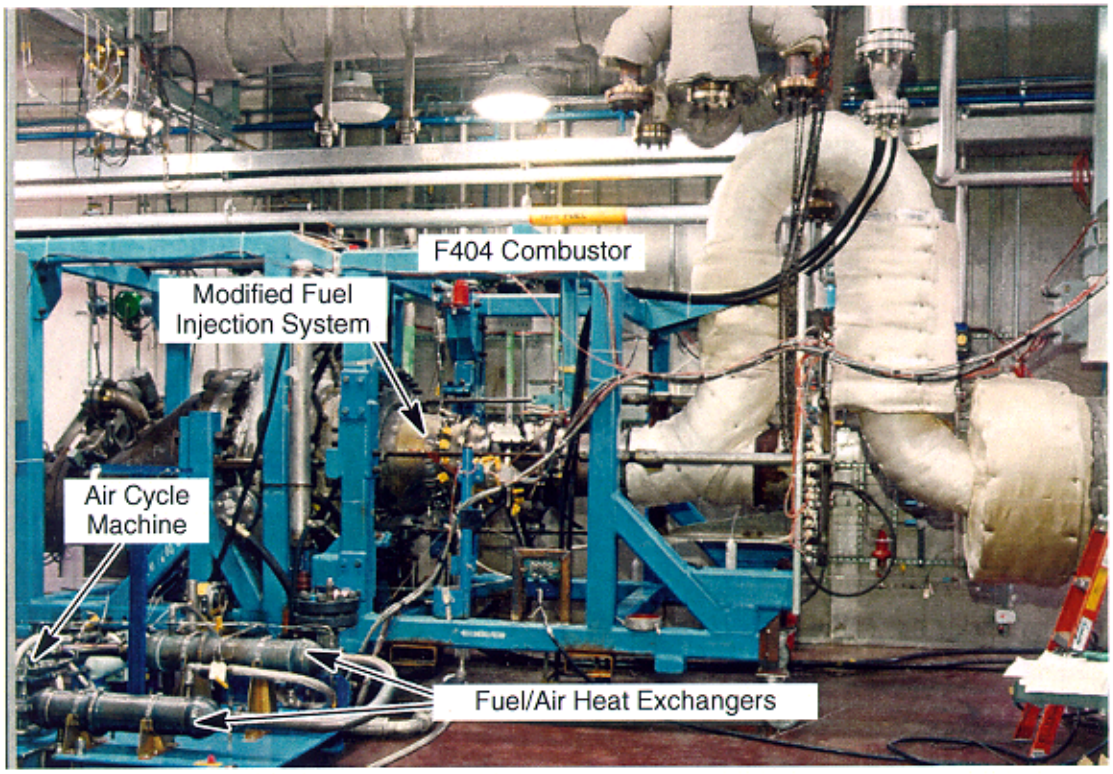

Figure 92. GEAE Cell 19A *Overall test facility includes F404 full-annular combustor and turbocooler.*

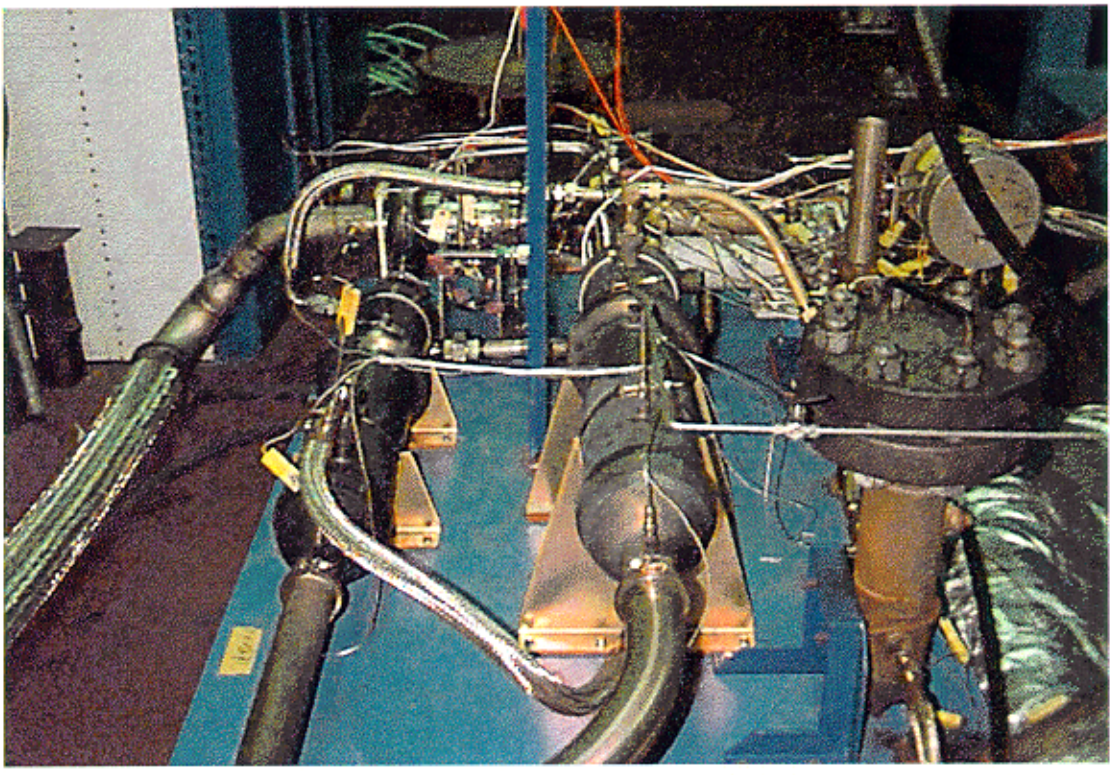

Figure 93. Turbocooler Installation

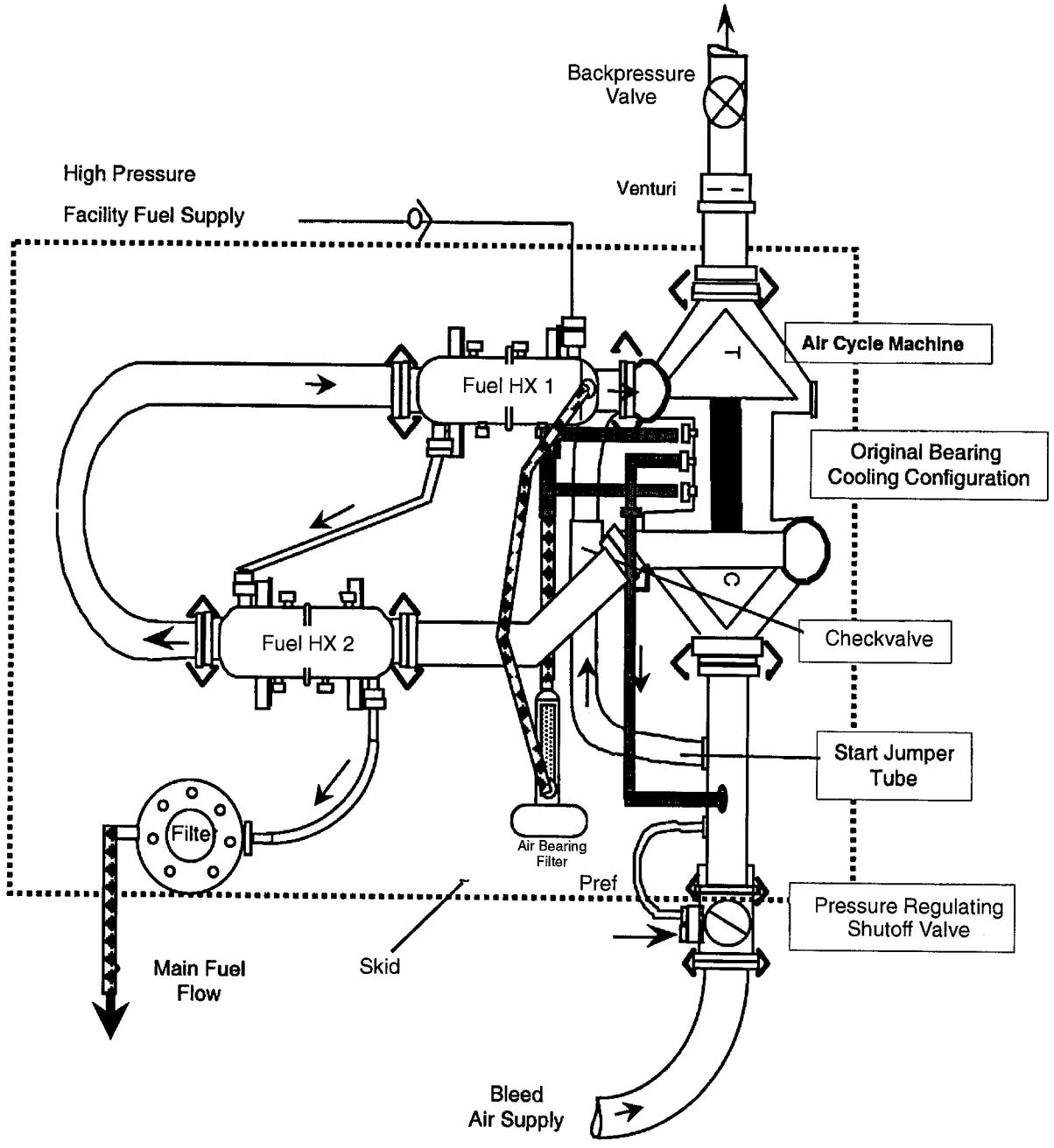

Figure 94. Turbocooler Skid Layout

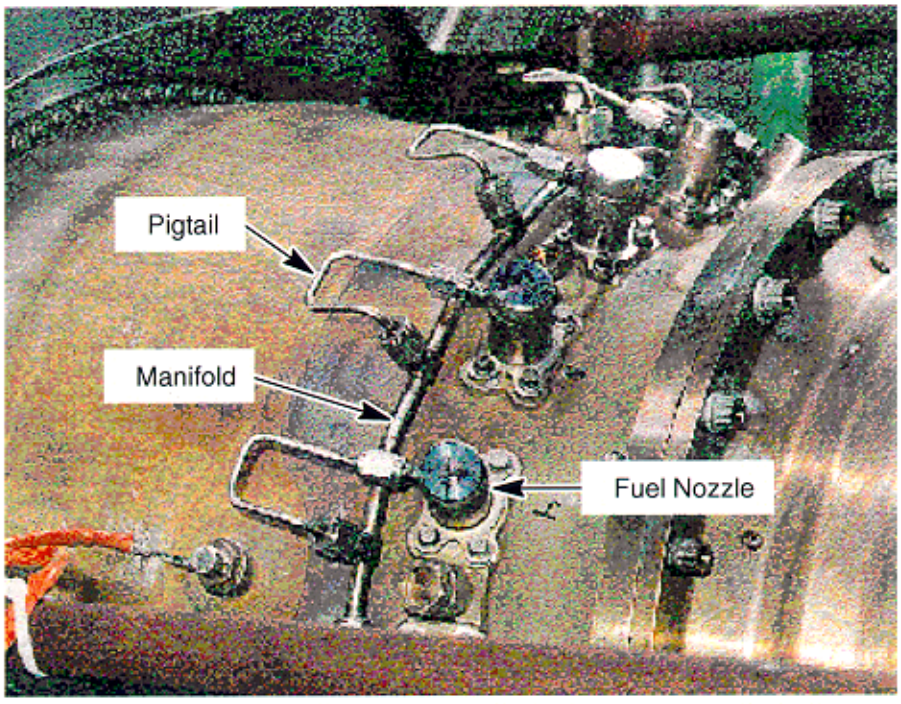

Figure 95. Fuel Manifold *A single manifold supplies fuel to the 18 fuel nozzles; pigtails connect the fuel nozzles to the manifold.*

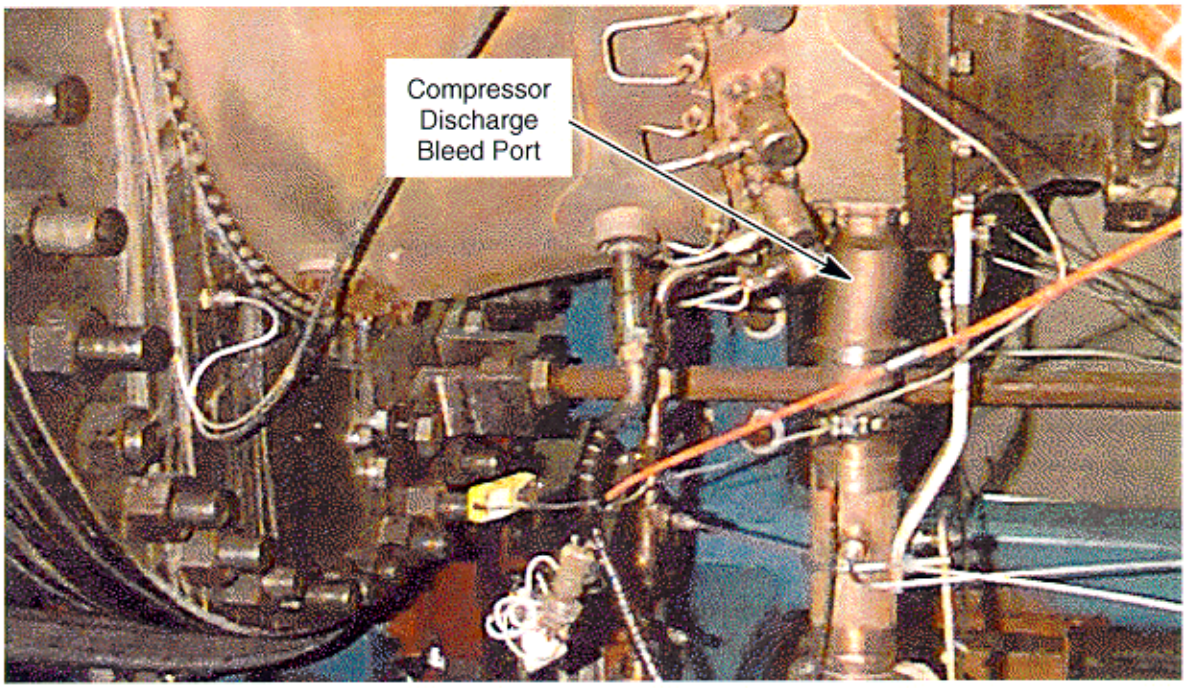

Figure 96. Combustor Discharge Bleed Port

compressor inlet. A turbine inlet bypass line (from compressor inlet duct to the turbine torus inlet) was incorporated to increase available pressure at the turbine inlet during start (see Figure 97). During the ACM start sequence, the inlet pressure (and airflow) is increased at the compressor inlet. With the bypass line installed, similar conditions are seen at the turbine inlet — facilitating ACM rotation as the pressure increases. Once the ACM begins to rotate, the compressor discharge pressure increases, driving the checkvalve in the bypass line closed.

Bearing cooling air is extracted upstream of the turbine inlet, filtered, and delivered to ports on either side of the thrust bearing. Most of the bearing cooling air is collected at the thrust bearing exit port and restored to the compressor inlet via an external line (see Figure 97).

4.3.1.3 Air Bleed Valves

Combustor Bleed Valve – The purpose of this valve is to regulate the pressure and flow of the combustor bleed air supply to the air cycle machine (see Figure 98). The ACEP bleed valve is an F–15 environmental control system (ECS) pressure regulating/shutoff valve (PRSOV) that has been modified to accommodate pneumatic actuation input supply for controlling the downstream pressure (ACM inlet). In the event of loss of control pressure, the bleed valve fails-closed, terminating air flow to the turbocooler. The operation of the valve was verified in a separate component test.

ACM Backpressure Valve – The purpose of this valve is to regulate the exit pressure of the ACM turbine discharge air in order to simulate predicted exhaust nozzle cooling manifold characteristics. The valve is part of the Cell A19 test facility. This valve also provides a secondary means of shutting off airflow to the turbocooler. A choke plate is incorporated near the ACM turbine discharge to prevent an overspeed from occurring in the event of a backpressure valve failure (full open); the choke plate also serves as a means to calculate turbine discharge flow.

4.3.1.4 Filters

High-Temperature Fuel Filter – When petroleum fuels are heated, they undergo chemical changes that result in precipitation of solid matter (insoluble gum, etc.), depending upon fuel quality and conditions of heating. Precipitation of solid matter in hot fuel need not be detrimental to engine operation if the particulate can be passed into the combustor without accumulating or depositing in the fuel system. The ACEP fuel nozzles, like most GEAE pressure-atomizing fuel nozzles, contain a mechanical, variable-orifice, flow-divider valve that distributes fuel to the primary (low-power operation) and secondary circuits (high-power operation). The flow-divider valve will be retained in order to maintain cold-fuel operation consistent with the production engine. A high-temperature barrier filter was used to mitigate downstream propagation of suspended particulates to the fuel nozzles and flow divider valves (see Figure 99). The fuel filter element was removed half way through the test (because of an erroneous pressure measurement) without any adverse effects. Similar experience was obtained on related single-cup combustor testing with hot fuel.

Air Filter – On today's aircraft environmental control systems, engine bleed air is fairly free of entrained particulates that could be detrimental to the ACM air bearings. However, some applications employ particle separators to protect the ACM turbomachinery and air bearings. Because the bleed port is at the six o'clock position and the turbocooler will be run in an test cell that might contain some debris, an air bearing filter is used to protect the ACM air bearings as a precaution (see Figure 100). Only the air extracted from the turbine inlet that is used to cool the air bearing is filtered.

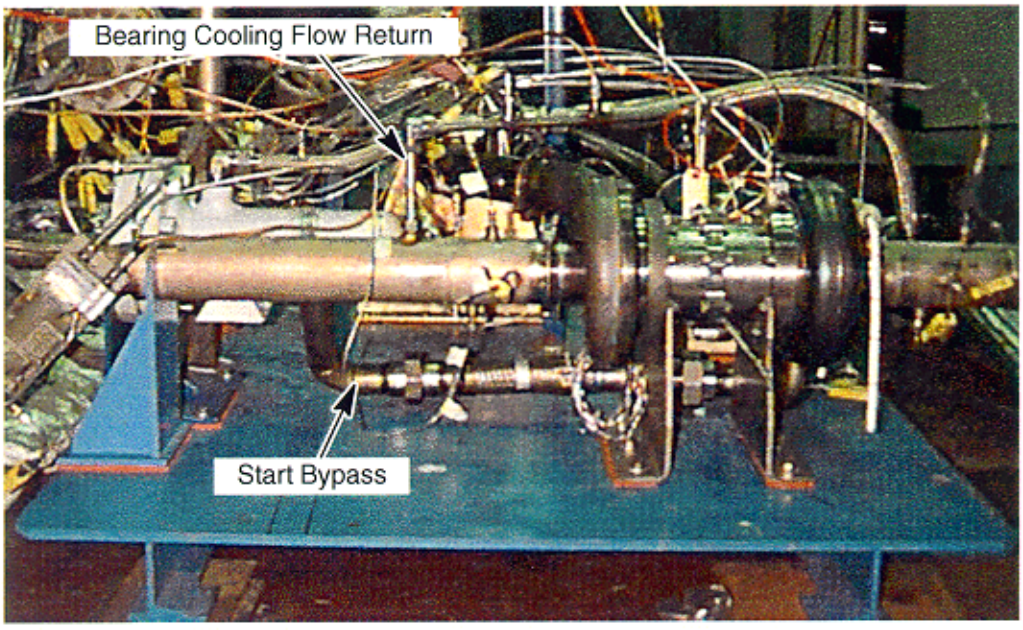

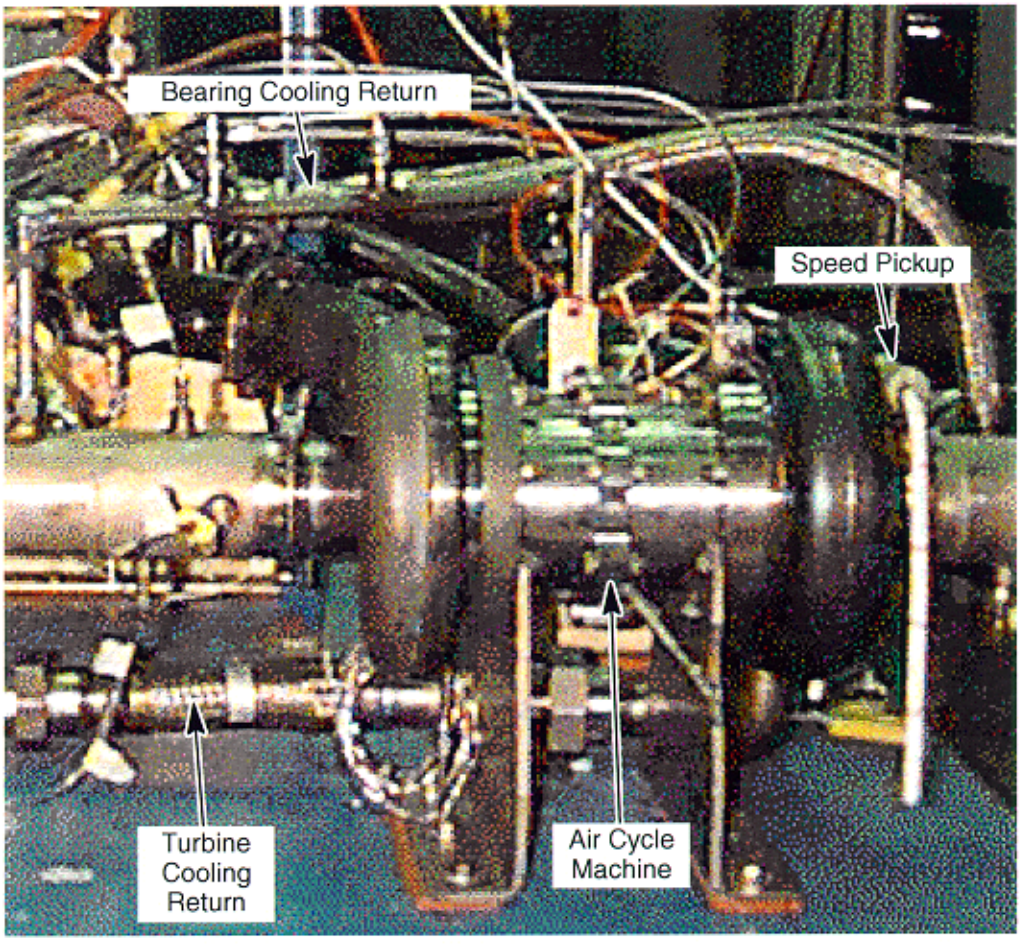

Figure 97. Test Rig and Closeup *Turbine inlet bypass enhances ACM starting; bearing cooling flow is returned to the cycle at the compressor inlet.*

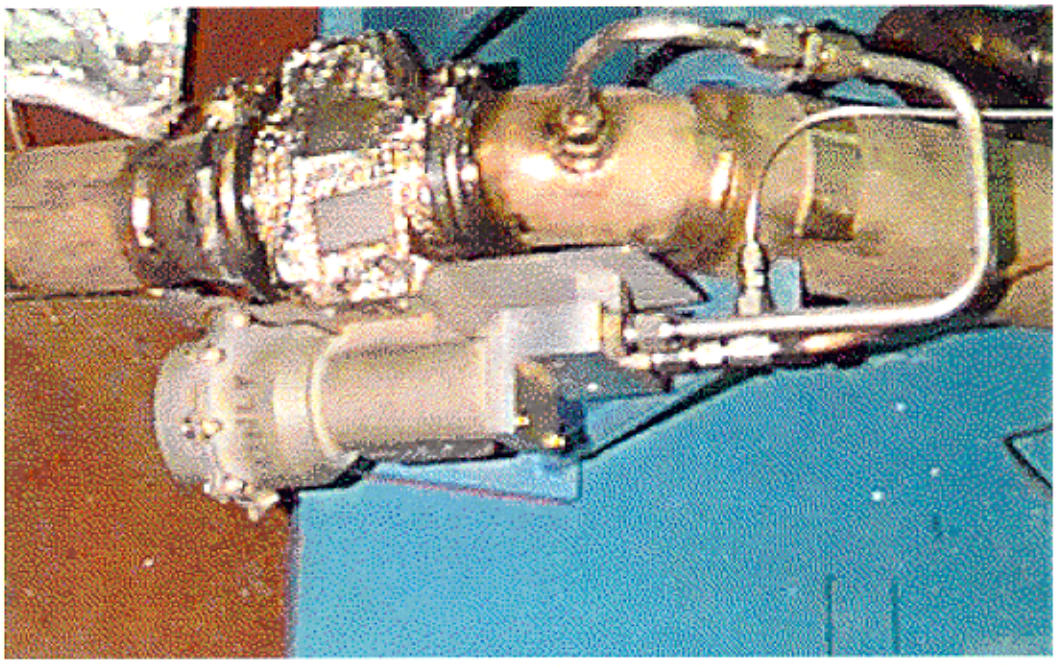

Figure 98. Turbocooler Bleed Air Control Valve *A Modified F–15 ECS bleed valve was used to regulate airflow into the turbocooler system.*

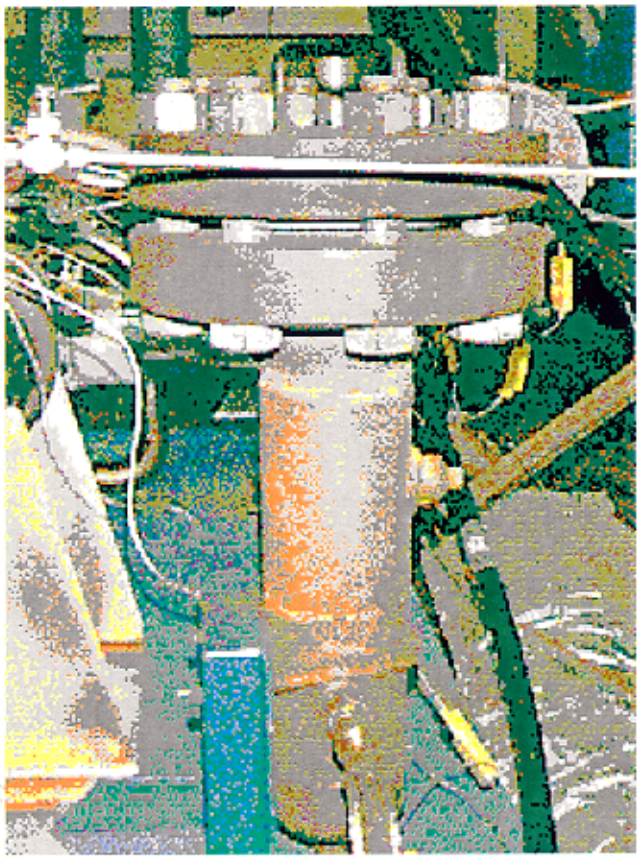

Figure 99. High-Temperature Fuel Filter Installed Downstream of the Fuel Heat Exchangers

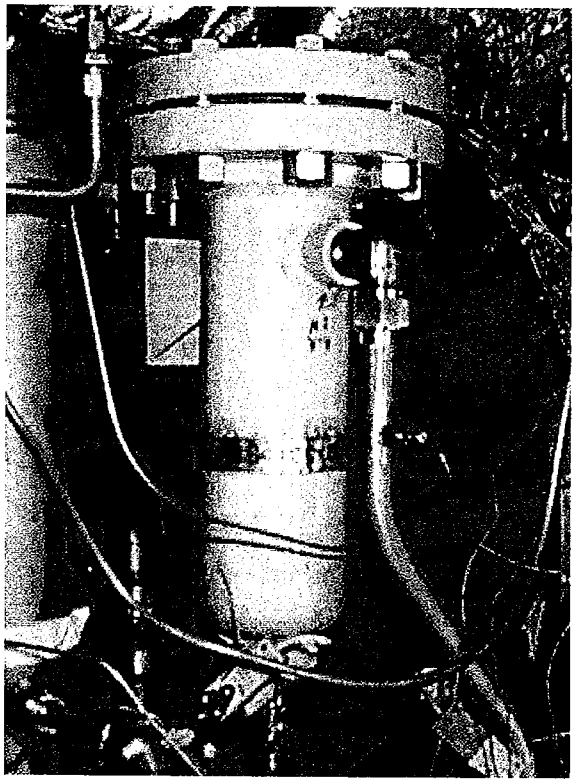

Figure 100. Barrier Filter Used to Protect the ACM Air Bearings from Potential Entrained Debris

4.3.1.5 Connectors

Air Side – All of the air-side connectors, starting with the combustor bleed port, are rigid V-band couplings and mating machined flanges used with resilient, all-metal, E seals. These type of interfaces are used on most commercial and military engine bleed systems and other high-temperature, high-pressure applications.

Fuel Side – Two types of fuel-side connectors are used. For the fuel/air heat-exchanger fuel and inspection ports, a standard AN-type fitting is used that incorporates a C seal. The C seal is to provide added protection from external fuel leaks. The second type of fuel fitting, used exclusively on the fuel manifold, pigtails, and fuel nozzles, is similar to typical AN connectors with the exception that a local braze joint can be applied (and removed) to form a leak-free connection.

4.3.2 Test Instrumentation

Figure 101 is a schematic identifying the principle turbocooler, combustor, and related facility instrumentation. The specific transducer parameter names, descriptions, ranges, and units are listed in Appendix B.

Turbocooler Skid, Air Side – Inlet and exit pressure and temperature sensors are installed to help assess component performance. Turbocooler airflow is measured at the turbine discharge. The bearing cooling flow air filter ΔP is monitored throughout the test. ACM internal instrumentation was operational during a portion of the test series. In addition to the standard instrumentation, the ACM was equipped with external accelerometers and a speed pickup (see Figure 102). The speed pickup detects a one-per-revolution signal from a magnetized washer at the turbine discharge.

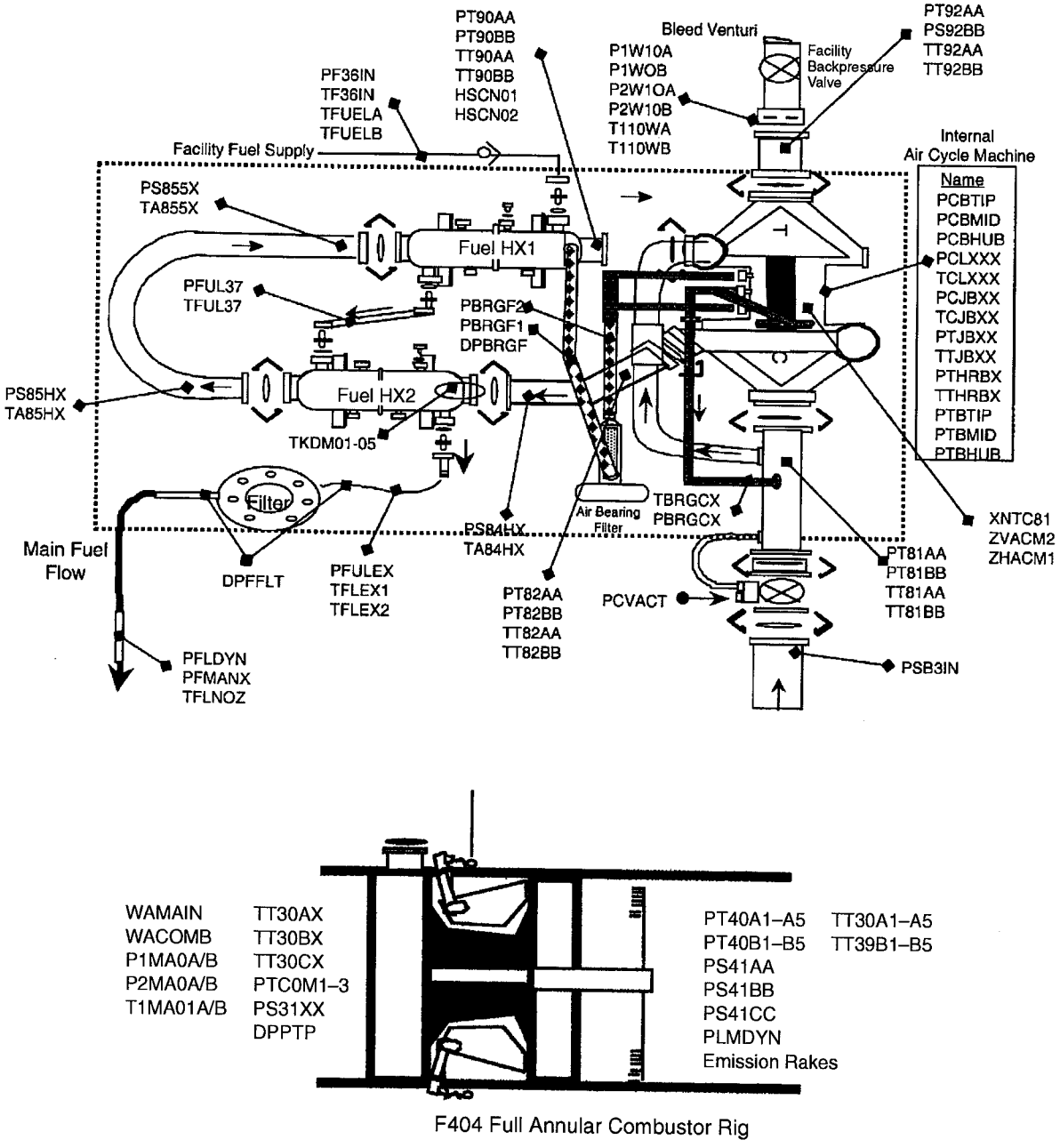

F404 Full Annular Combustor Rig

Figure 101. Turbocooler Instrumentation

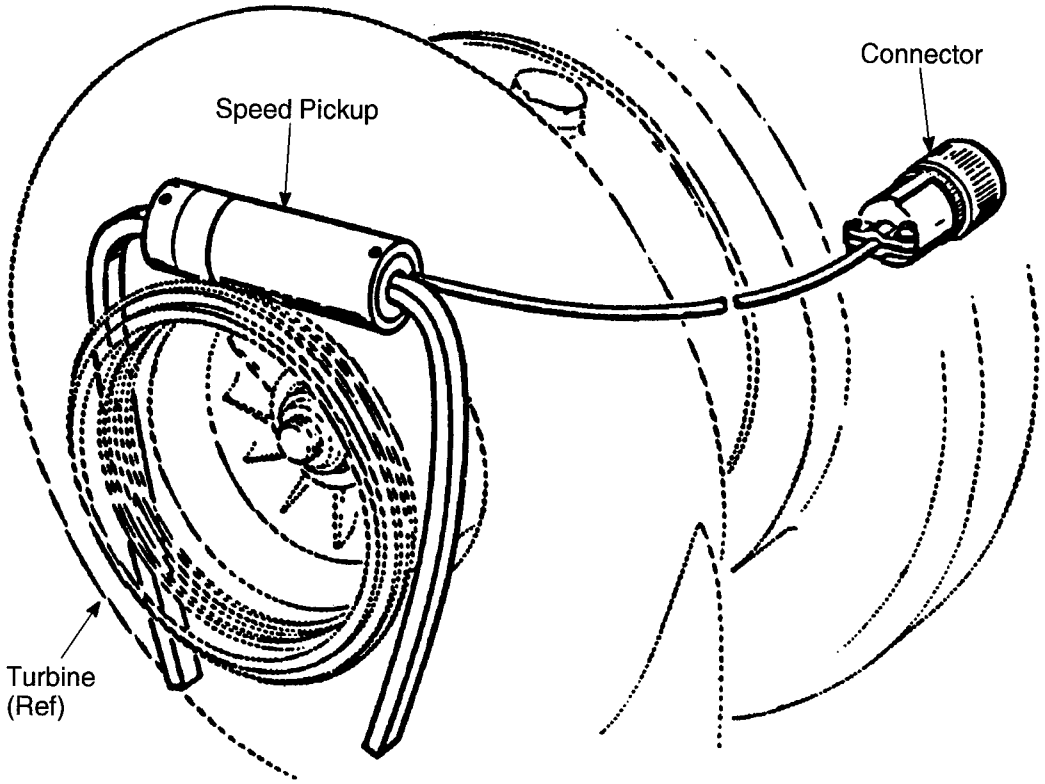

Figure 102. Air Cycle Machine Rotor Speed Sensor

Turbocooler Skid, Fuel Side – Inlet and exit pressure and temperature sensors are installed on the fuel system to help assess component performance. Fuel flow is measured at the pump discharge. Heat exchanger and fuel filter ΔP's are monitored throughout the test. Thermocouples are also installed axially along the outer dome of the fuel/air heat exchanger immediately downstream of the ACM compressor to detect potential adverse thermal differentials (see Figure 103). Fuel system dynamic pressure was measured at the fuel manifold to detect potential fuel system instabilities. It should be noted that the heat exchangers were not insulated, so it was possible to visually monitor for leaks during the test. Heat exchanger performance calculations were adjusted accordingly.

Combustor – Inlet and exit pressure and temperature sensors are installed to evaluate combustor performance. Combustor airflow is measured at the inlet section. Combustor dynamic pressure is measured to detect any combustor instabilities. Thermocouples are installed on the upper and lower combustor liners as shown in Figure 104. The F404 combustor rig is designed with an internal rotating-rake assembly that is used to measure combustor discharge temperature. A photograph of the rotating rake assembly is presented in Figure 105. Two rakes are located 180° apart with five temperature elements on each rake. The rake assembly is capable of rotating 360° for the ACEP program the rotation will be limited to approximately 180° because the two static emission rakes are installed near the 12 o'clock and 6 o'clock position. The temperature rake assembly is rotated between the emission rakes. Each emission rake contains five elements. Each element can be measured separately of ganged together as a single sample. One emission rake is located circumferentially between two fuel injectors, and the second emission rake is located along a fuel injector

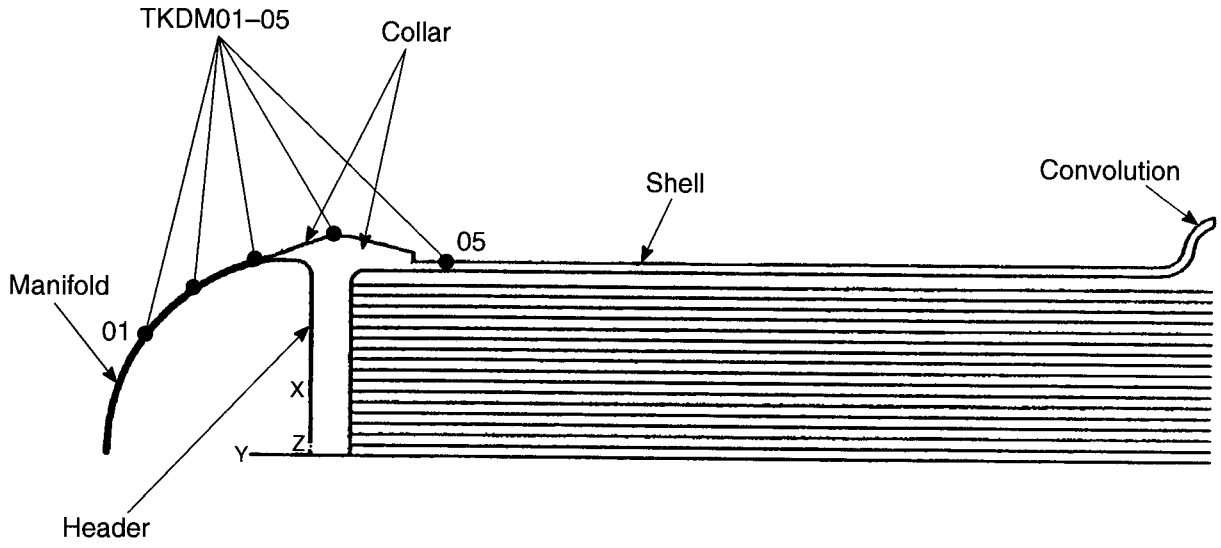

Figure 103. Heat Exchanger No. 2 Surface-Mounted Thermocouples

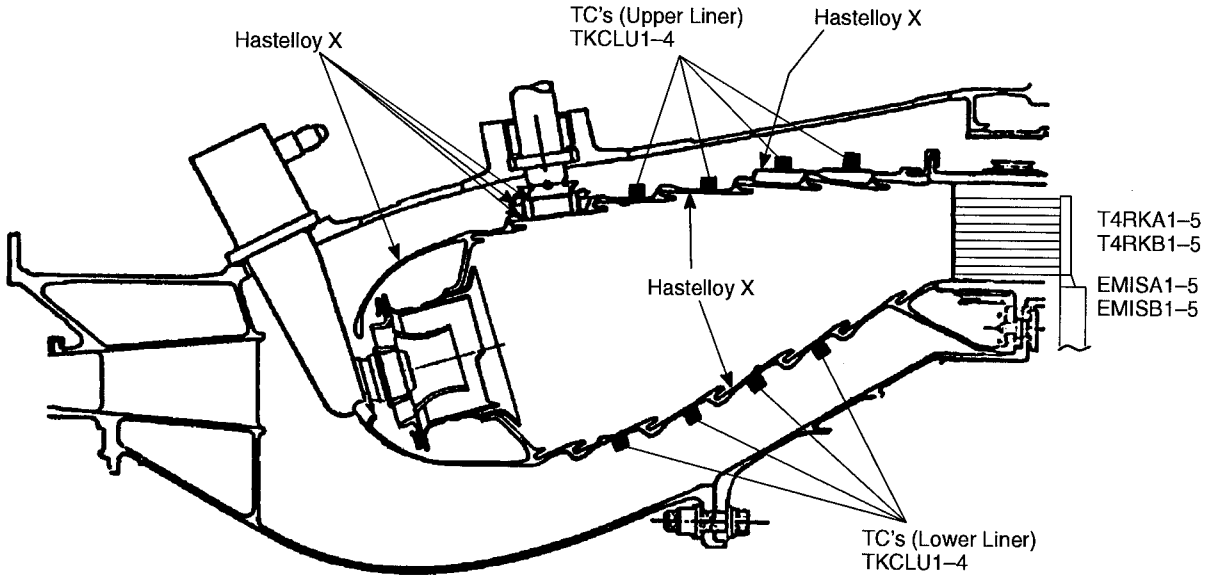

Figure 104. Combustor Liner Thermocouples

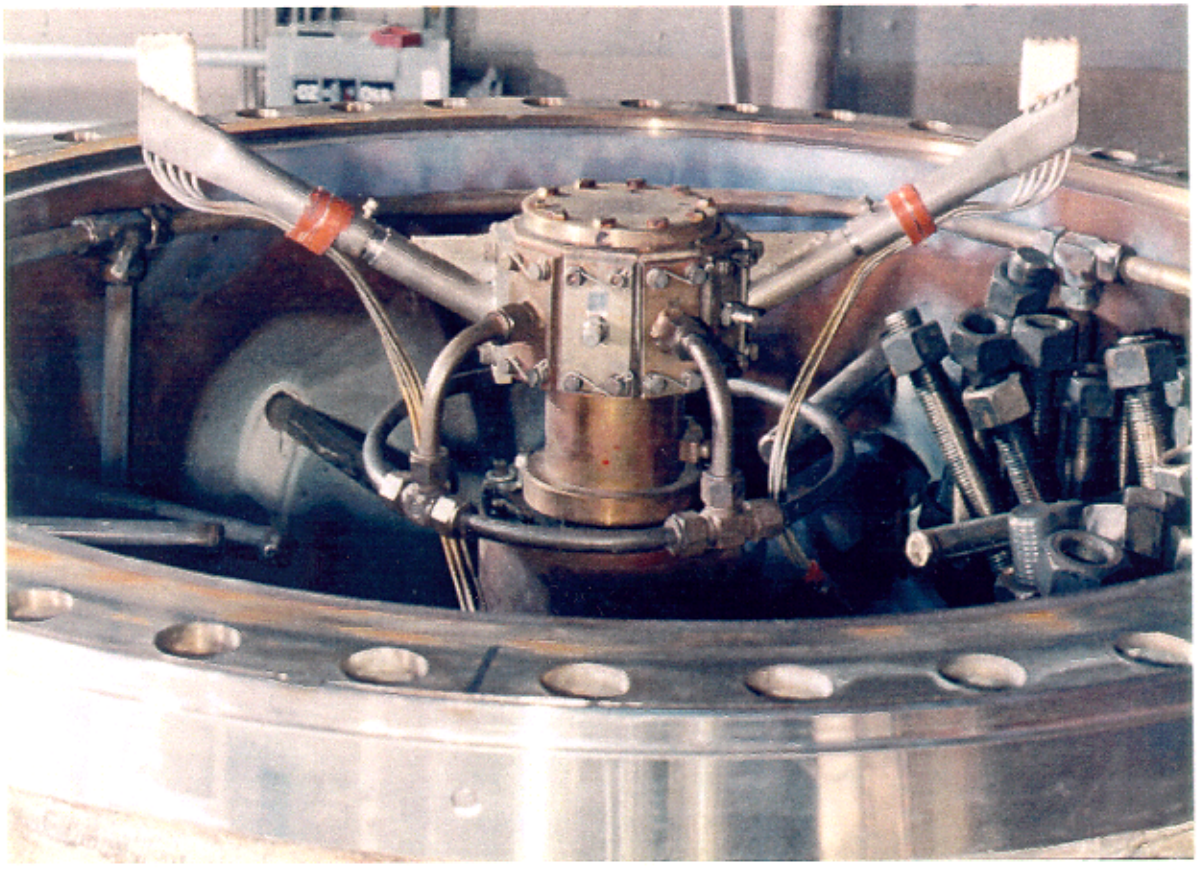

Figure 105. Combustor Exit Rotating Rake Assembly with Temperature and Emission Probes

centerline. The rotating rake assembly is typically used at operating pressures below 8 atmospheres and proved particularly troublesome (failed to consistently rotate) during the turbocooler test.

Turbocooler Control Parameters and Limits – The basic operation of the test rig is controlled through the operation of the parameters defined in Table 24. Parameters that require automatic alarm and/or limit trips are defined in Table 25 along with the recommended action. It should be noted that two hydrocarbon leak detectors were installed in the turbocooler test facility. The HC detectors monitored the quality of the airflow into the ACM turbine to determine if the fuel/ air heat exchanger was leaking fuel (into the air stream).

4.3.3 Data Acquisition

The combustor test facility records and stores all steady-state sensor, emission, and performance calculations defined in the Phase I analysis program. All engineering units and specific performance calculations can be monitored in real time. ACEP component performance parameters are calculated on-line from measured data. Combustor discharge temperature contours are processed off-line from the recorded rotating-rake instrumentation. Transient recordings of predefined parameter sets are available on request.

Table 24. Turbocooler Rig Control Parameters

Parameter			Range		Units	Comments
Name		Description	Low	High		
Air Side	PACTIN	Actuator Supply Pressure	Ambient	400	psia	Controls bleed valve position
	PT81AA	ACM Compressor Inlet	Ambient	300	psia	Set by bleed valve position
	PT90AA	ACM Turbine Exit	Ambient	100	psia	Set by ACM backpressure valve
Fuel Side	WF36MV	Main Fuel Flow	0	8000	pph	Set by pump pressure
	WF36VV	Fuel FLow Rate Verification	0	8000	pph	Set by pump pressure
Combustor	FARCOM	Combustor Fuel/Air Ratio	0	0.033		Set by pump pressure or airflow
	PSCMU1	Main Airflow Oriface Pressure	Ambient	350	psia	Facility controlled
	PSCMU2	Main Airflow Oriface Pressure	Ambient	350	psia	Facility controlled
	PTCOM1	Combustor Inlet Total Pressure	Ambient	350	psia	Facility controlled
	TTCOM1	Combustor Inlet Total Temp	Ambient	1000	°F	Facility controlled
	DPCOMB	Combustor ΔP	0	0	psig	Combustor backpressure valve

Table 25. Turbocooler Rig Alarm and Trip Parameters

Parameter			Limits		Alarm / Action
Name		Description	Yellow	Red	
Air Side	PT82AA	ACM Compressor Exit P_T (psia)	380	400	Close bleed valve 10%, reduce PCNTRL
	TT90AA	ACM Turbine Inlet T_T (°F)	300	400	
	TT92AA	ACM Turbine Exit T_T (°F)	40	32	Close backpressure valve 10%
	DPBRGF	Air Bearing Filter ΔP (psid)	4	5	Change filter element
	XNTC81	ACM Shaft RPM	80,000	110,000	Close backpressure valve 10%
	ZHACM1	Horizontal ACM Vibration (mils)	3	10	
	ZVACM2	Vertical ACM Vibration (mils)	3	10	
	HCSN01–2	HC Sniffer at Turbine Inlet (% LEL CH_4)	50	50	Close bleed valve, shut–off fuel
	PCNTRL	ACM Bleed Valve Control	65	71	Reduce regulation pressure
Fuel Side	PF36IN	Fuel Inlet Pressure to HX1 (psia)	1100	1200	Reduce fuel temperature; close bleed valve ➧ reduce PCNTRL
	PFLDYN	Dynamic Fuel Pressure at Nozzle (P–P)	3	5	
	DPFULF	Fuel Filter ΔP (psid)	10	25	Change filter element
Combustor	FARCOM	Combustor Fuel/Air Ratio	0.03	0.035	Reduce fuel/air ratio
	TKCLU1–5	Upper Liner Temperature (°F)	1400	1600	
	TKCLL1–5	Lower Liner Temperature (°F)	1400	1600	
	PTCOM1	Inlet Total Pressure (psia)	350	400	Reduce facility supply
	TTCOM1	Inlet Total Temperature (°F)	1000	1200	
	T4RKA1–5	Exit Temperature (°F)	2600	3200	Reduce fuel/air ratio
	T4RKB1–5	Exit Temperature (°F)	2600	3200	
	PCMDYN	Dynamic Pressure (P–P)	3	5	Reduce fuel temperature; close bleed valve ➧ reduce PCNTRL

Appendix A – Heat Exchanger Analysis

Temperature Distributions: Start-Up Transient Analysis

The ACEP turbocooler heat exchanger thermal-network model is shown below. The following pages, replicated from the AlliedSignal report, superpose transient temperature distributions onto a half cross section (perpendicular to the coolant-fuel flow) of the symmetrical ACEP turbocooler heat exhanger — section B–B on the left-hand side (section A–A) of the drawing below.

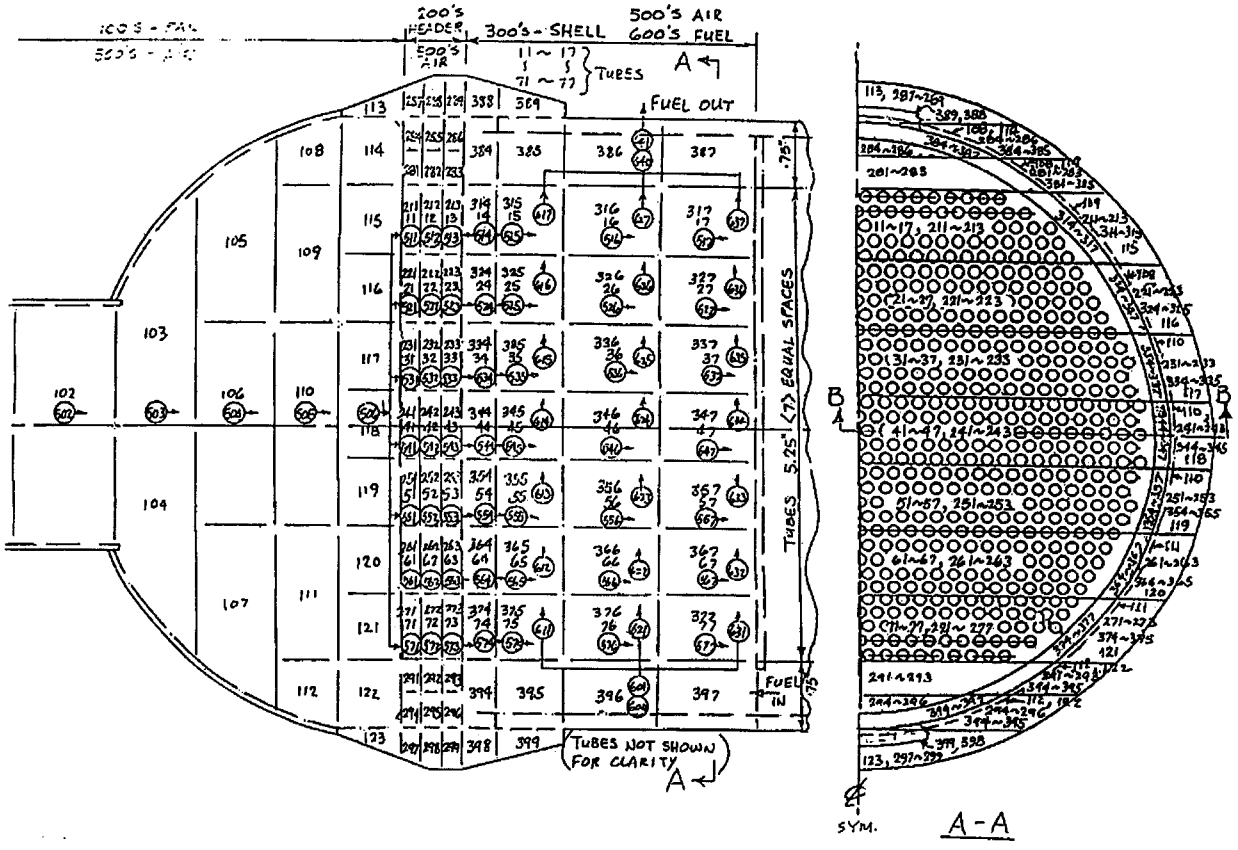

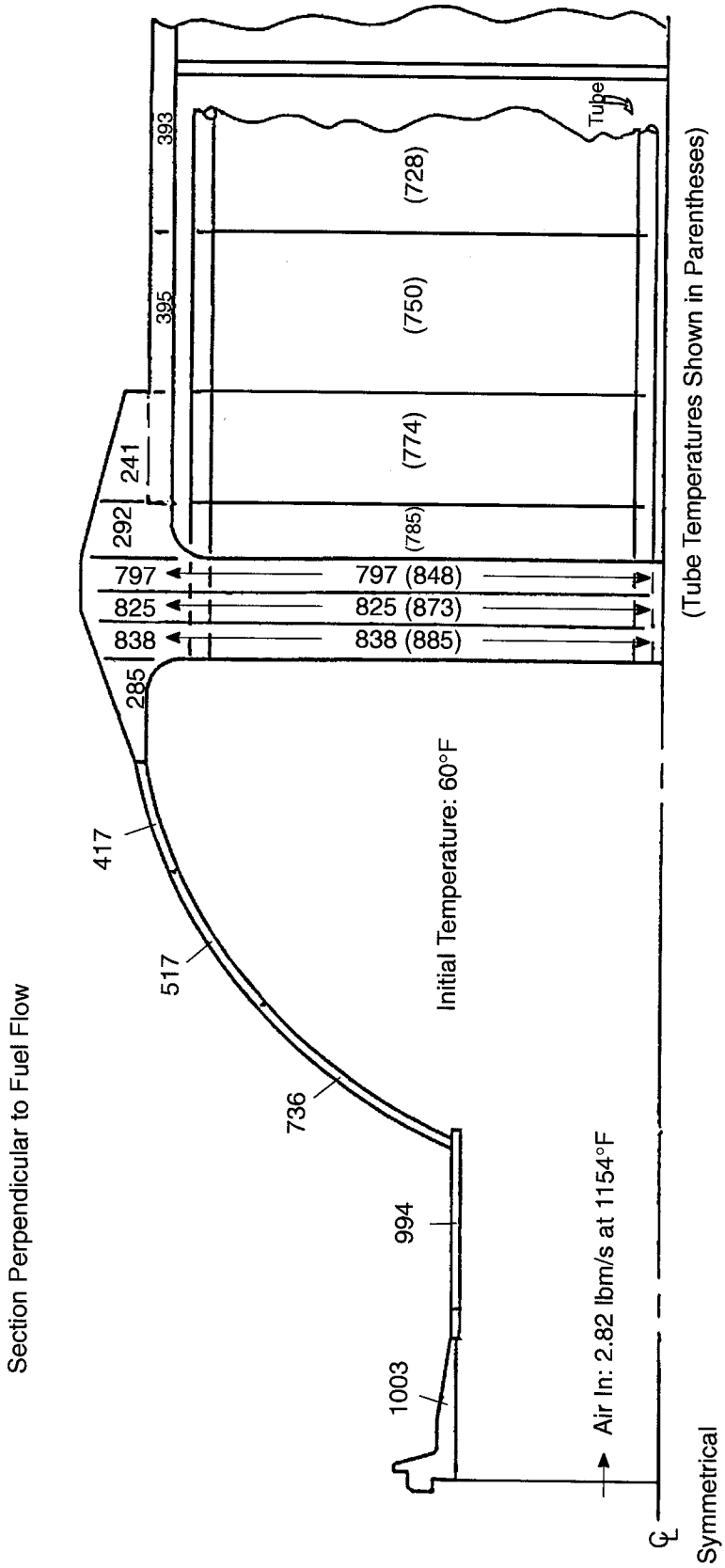

ACEP Turbocooler Heat Exchanger Start-Up Transient Temperature Distribution (°F) at 30 Seconds

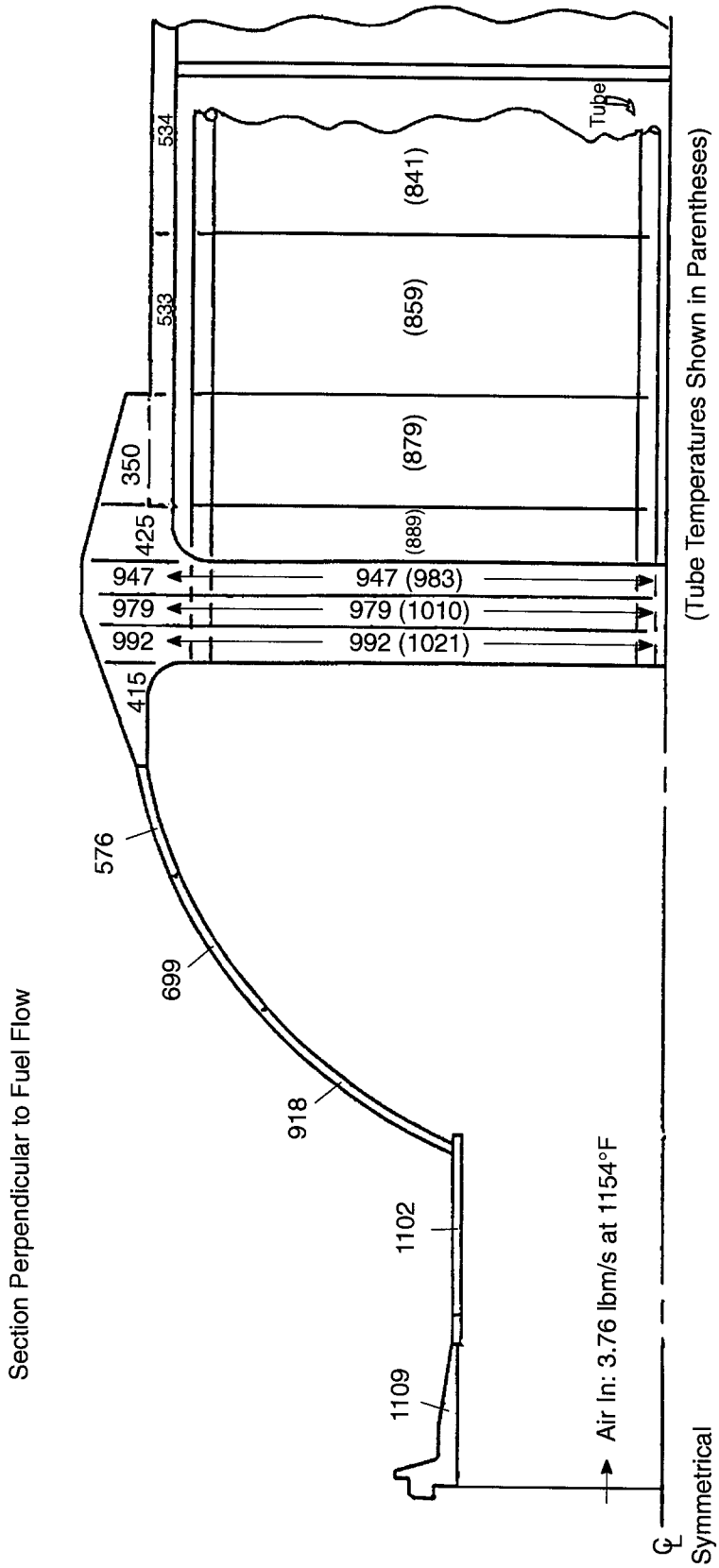

ACEP Turbocooler Heat Exchanger Start-Up Transient Temperature Distribution (°F) at 40 Seconds

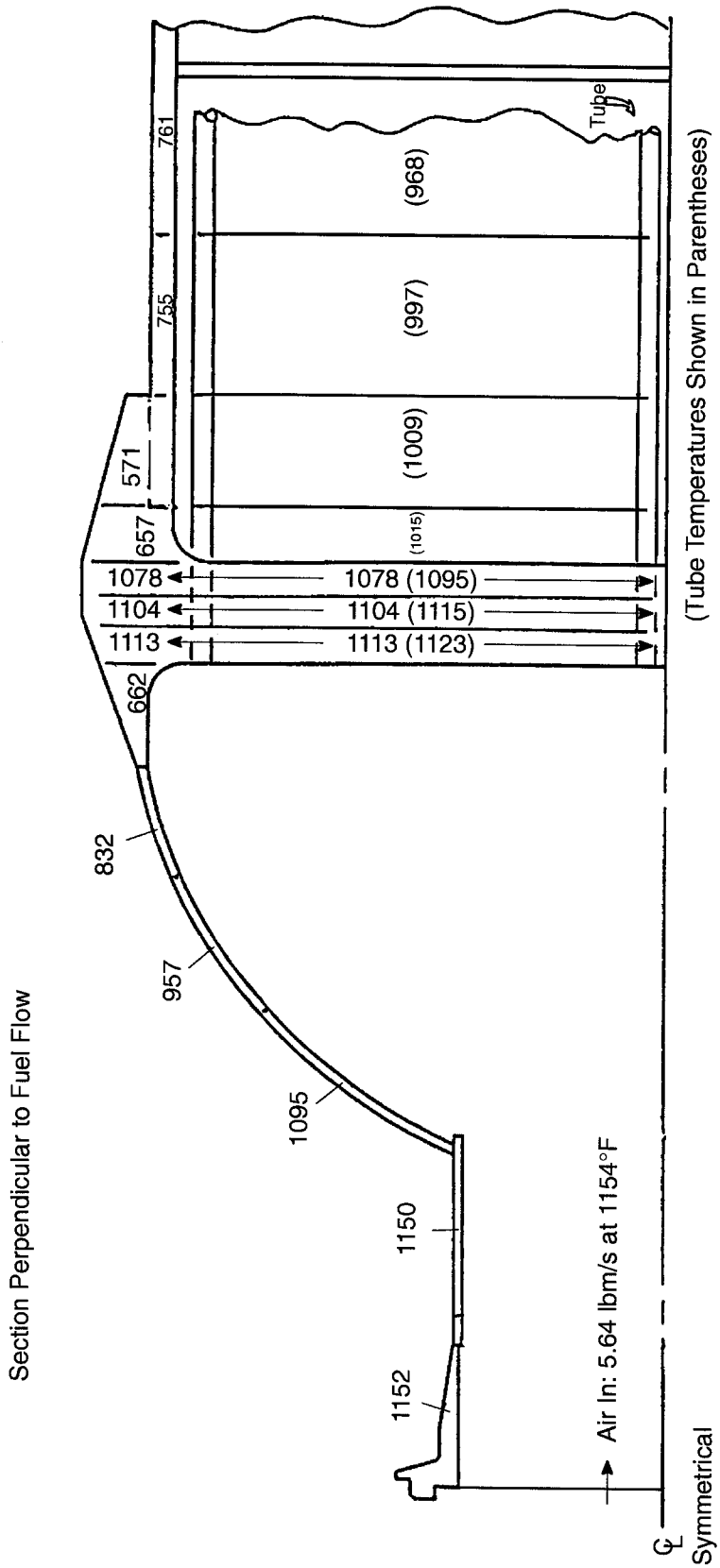

ACEP Turbocooler Heat Exchanger Start-Up Transient Temperature Distribution (°F) at 60 Seconds

Transient Temperature Distributions: LCF Analysis

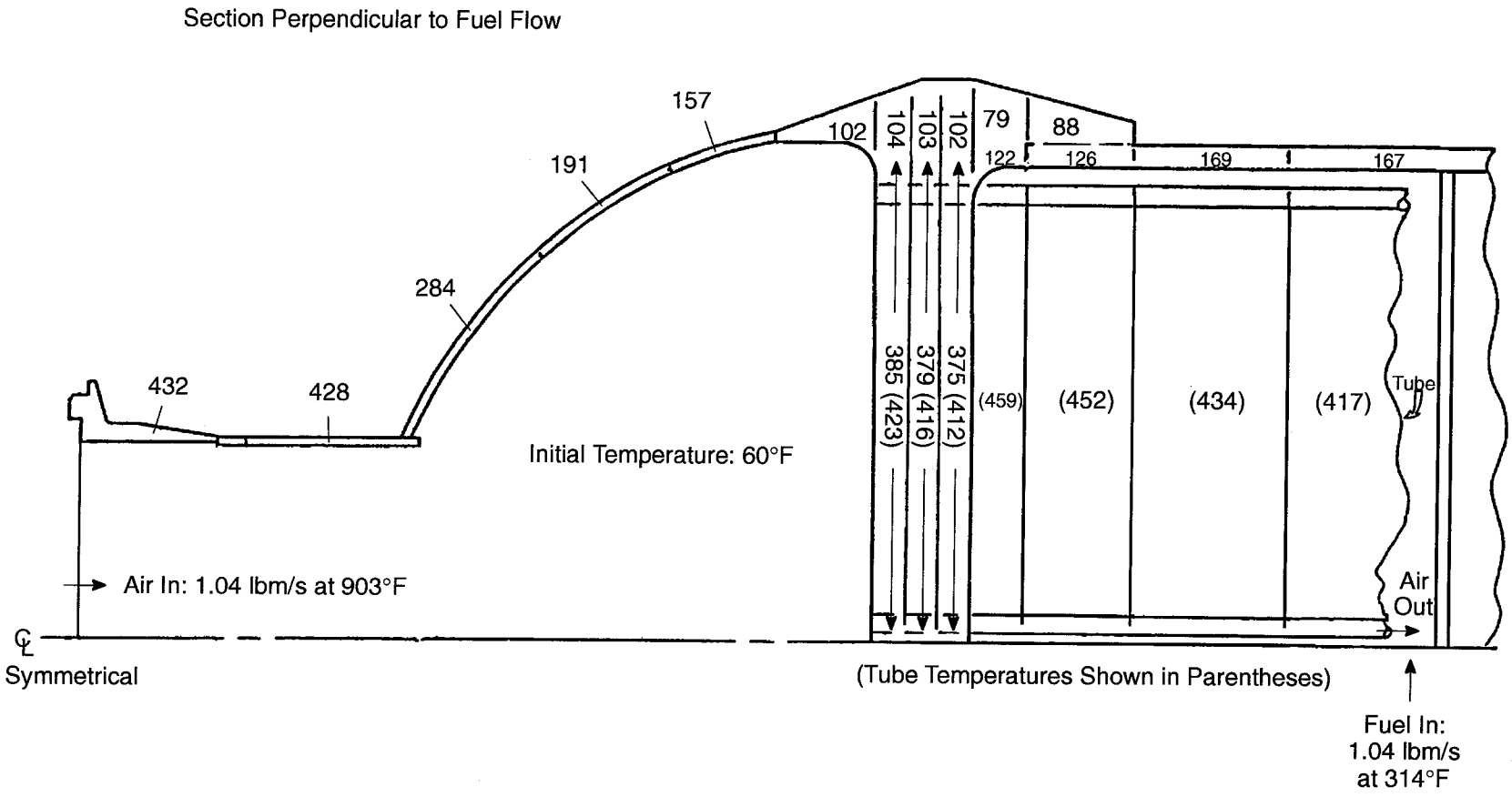

ACEP Turbocooler Heat Exchanger LCF Analysis Transient Temperature Distribution (°F) at 20 Seconds

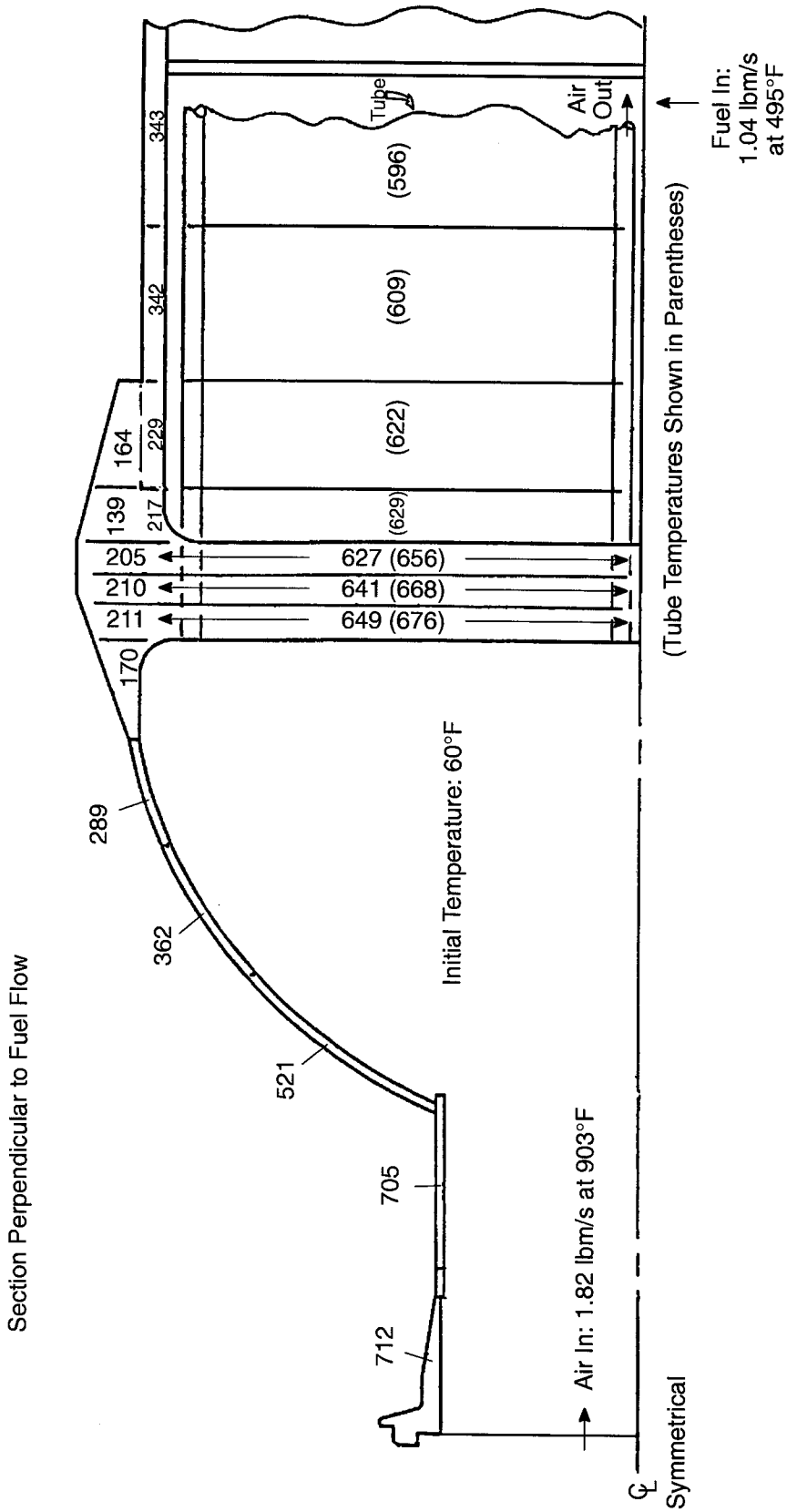

ACEP Turbocooler Heat Exchanger LCF Analysis Transient Temperature Distribution (°F) at 35 Seconds

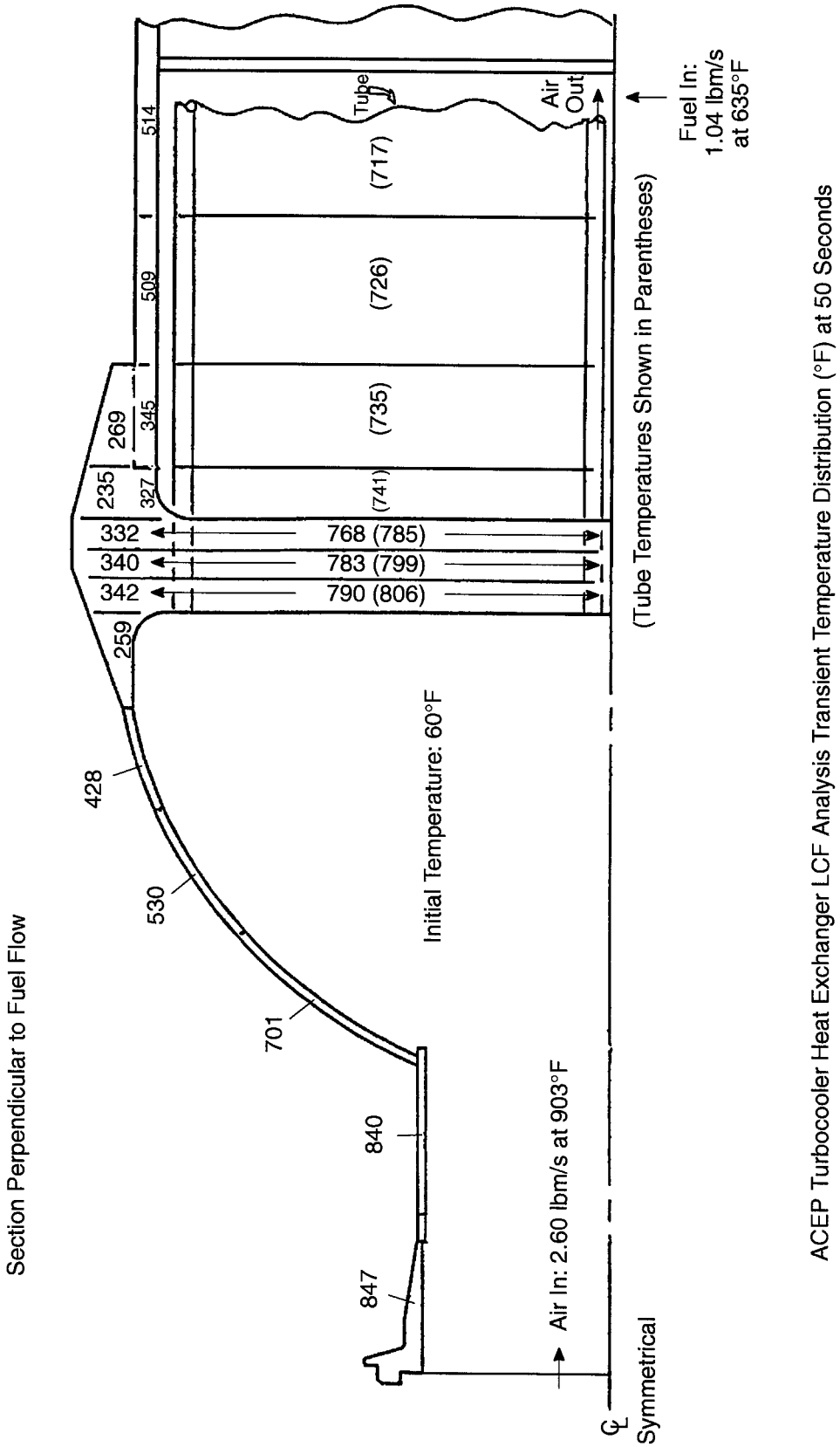

ACEP Turbocooler Heat Exchanger LCF Analysis Transient Temperature Distribution (°F) at 50 Seconds

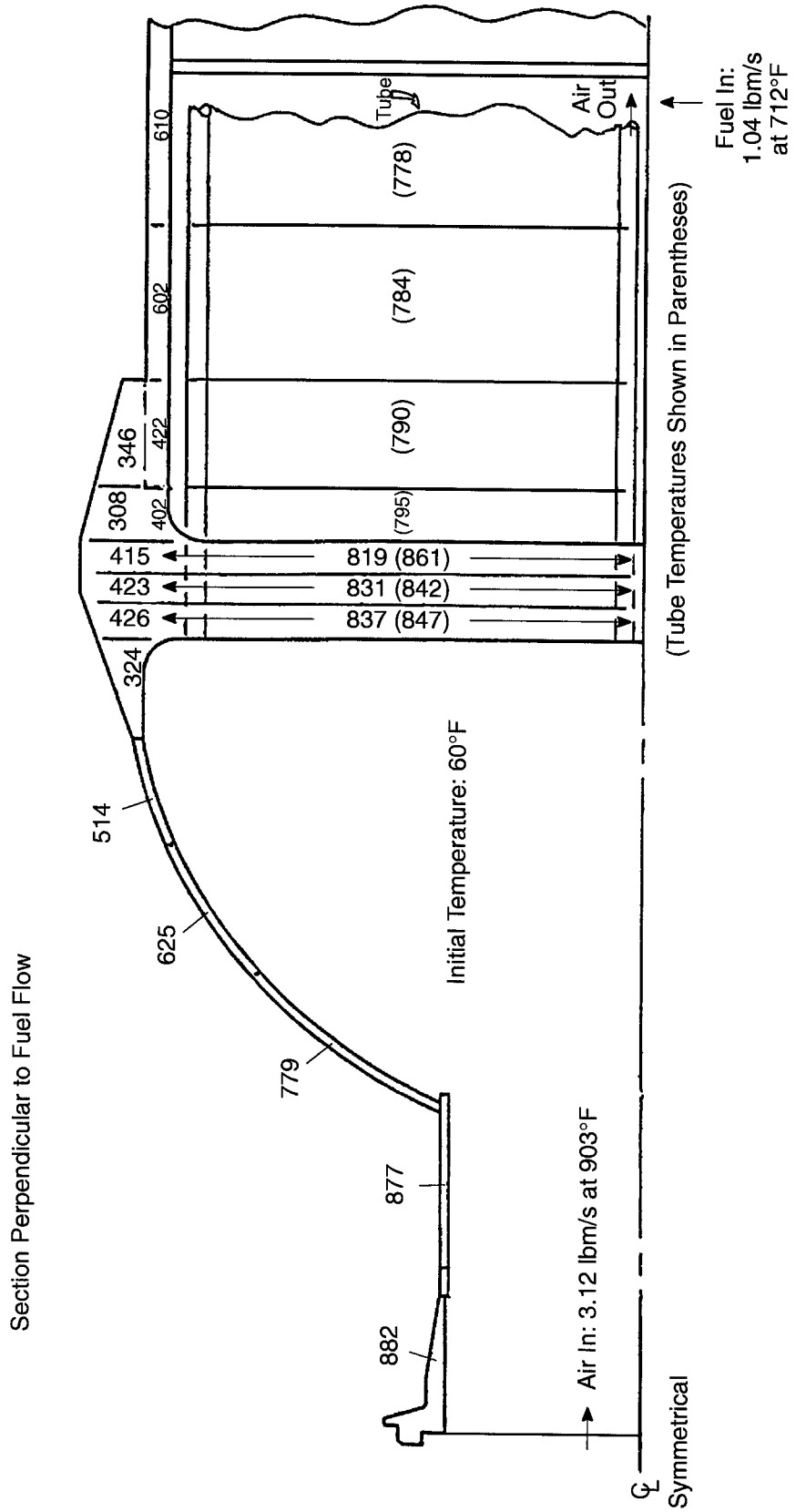

ACEP Turbocooler Heat Exchanger LCF Analysis Transient Temperature Distribution (°F) at 60 Seconds

Stesses and Temperature Plots: LCF Analysis

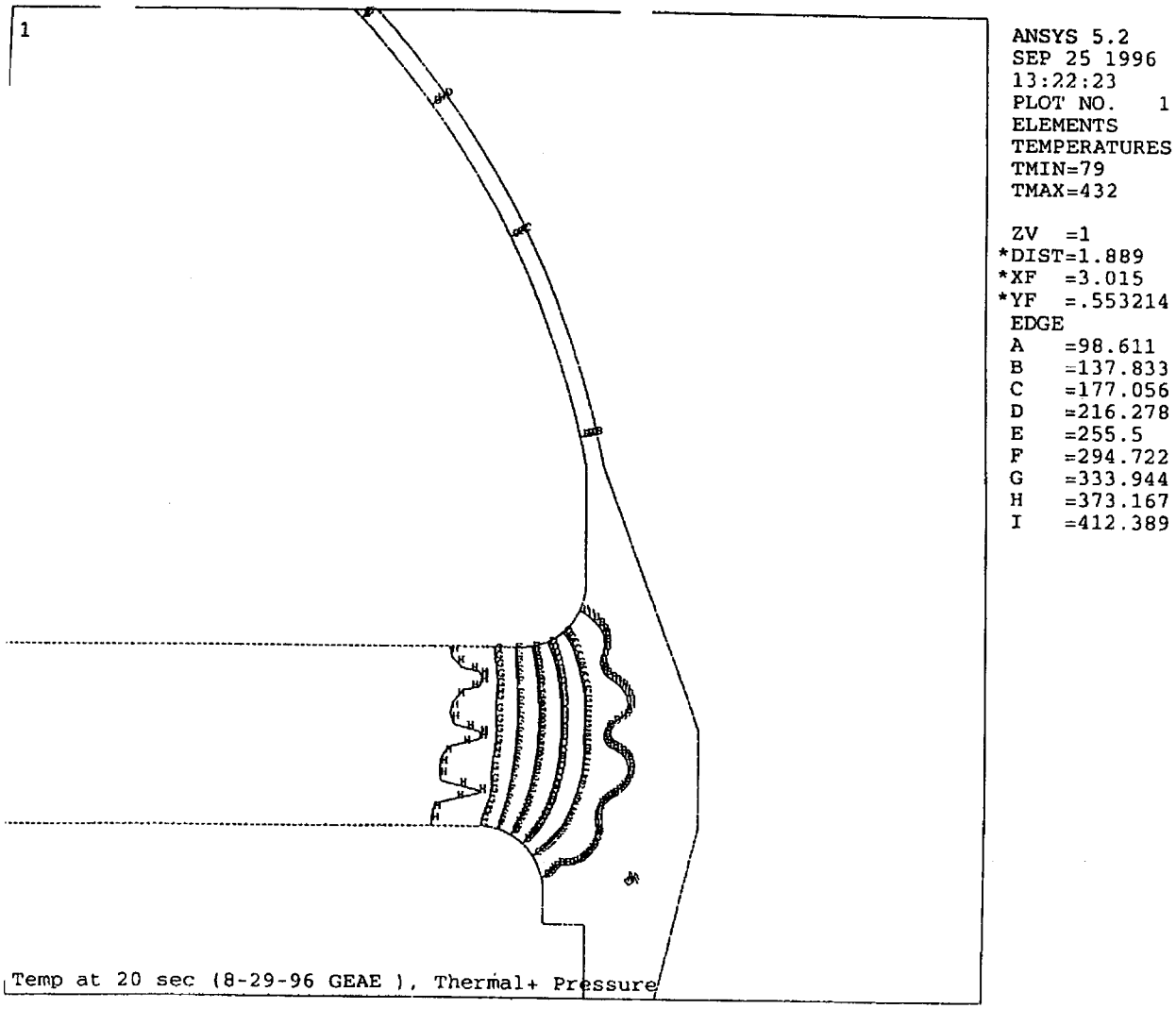

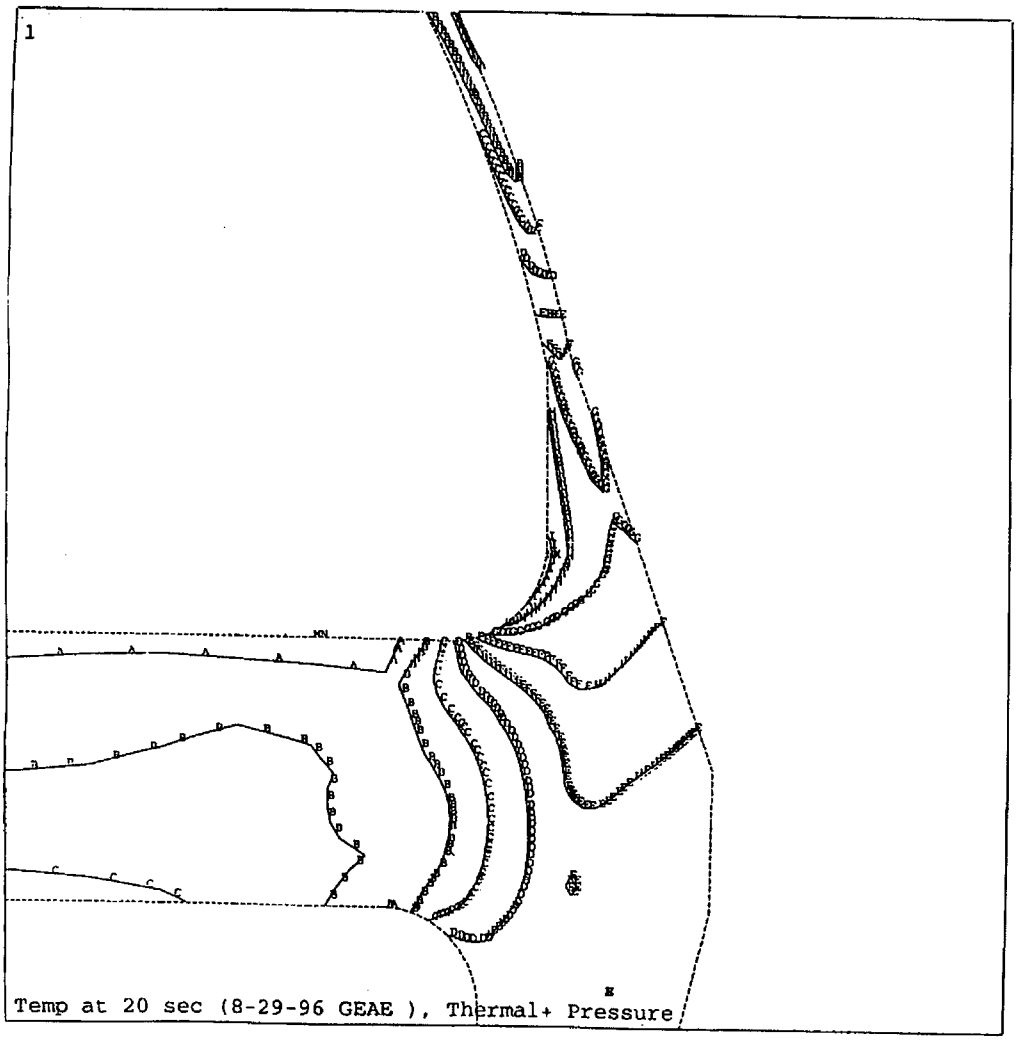
1
Temp at 20 sec (8-29-96 GEAE), Thermal+ Pressure
ANSYS 5.2
SEP 25 1996
08:38:21
PLOT NO. 2
NODAL SOLUTION
STEP=1
SUB =1
TIME=1
SEQV (AVG)
DMX =.056993
SMN =2598
SMNB=639.502
SMX =62970
SMXB=64735
A =5952
B =12660
C =19368
D =26076
E =32784
F =39492
G =46200
H =52908
I =59616

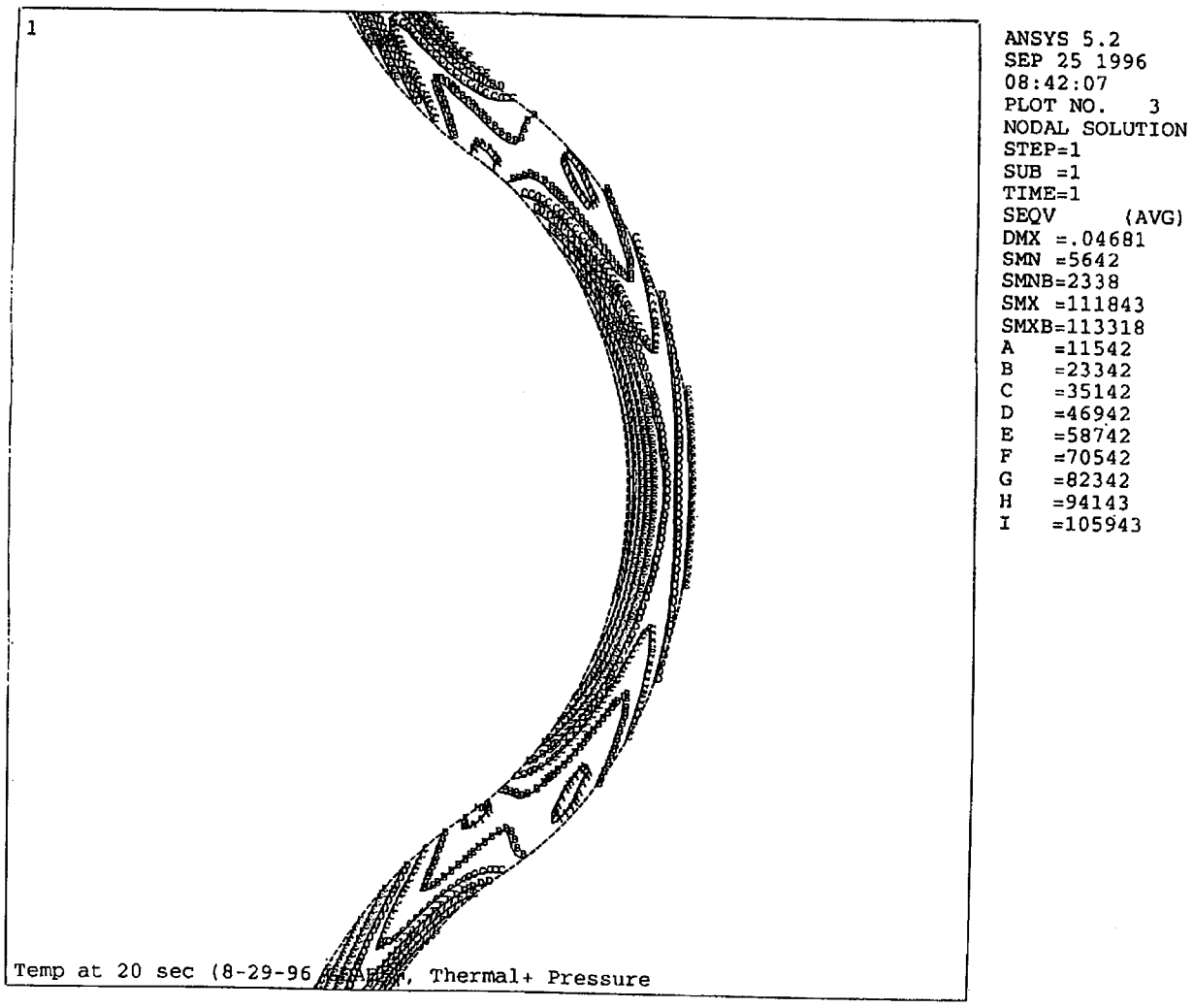
1
ANSYS 5.2
SEP 25 1996
08:42:07
PLOT NO. 3
NODAL SOLUTION
STEP=1
SUB =1
TIME=1
SEQV (AVG)
DMX =.04681
SMN =5642
SMNB=2338
SMX =111843
SMXB=113318
A =11542
B =23342
C =35142
D =46942
E =58742
F =70542
G =82342
H =94143
I =105943
Temp at 20 sec (8-29-96
, Thermal+ Pressure

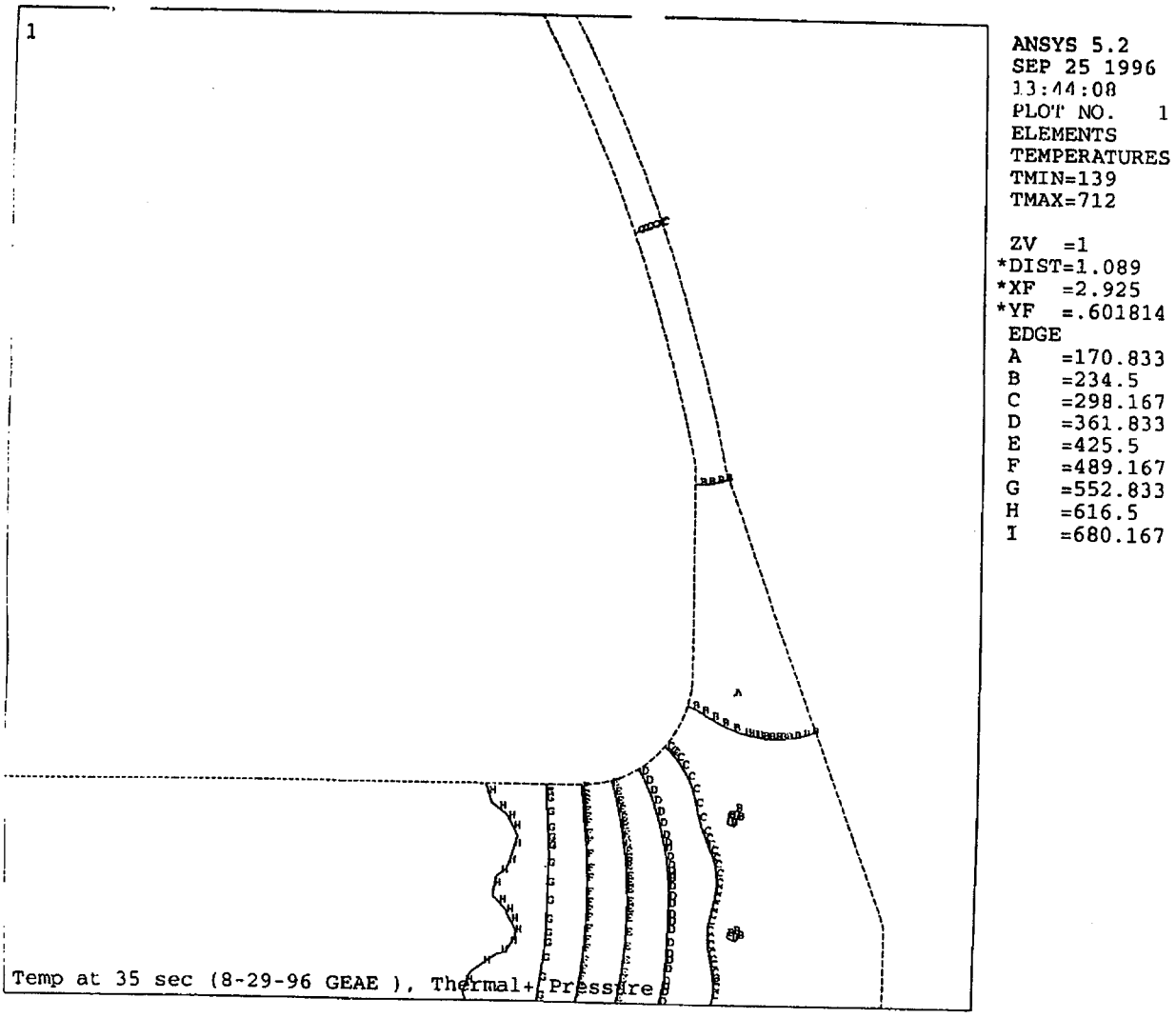
1
ANSYS 5.2
SEP 25 1996
13:44:08
PLOT NO. 1
ELEMENTS
TEMPERATURES
TMIN=139
TMAX=712
ZV =1
*DIST=1.089
*XF =2.925
*YF =.601814
EDGE
A =170.833
B =234.5
C =298.167
D =361.833
E =425.5
F =489.167
G =552.833
H =616.5
I =680.167
Temp at 35 sec (8-29-96 GEAE), Thermal+ Pressure

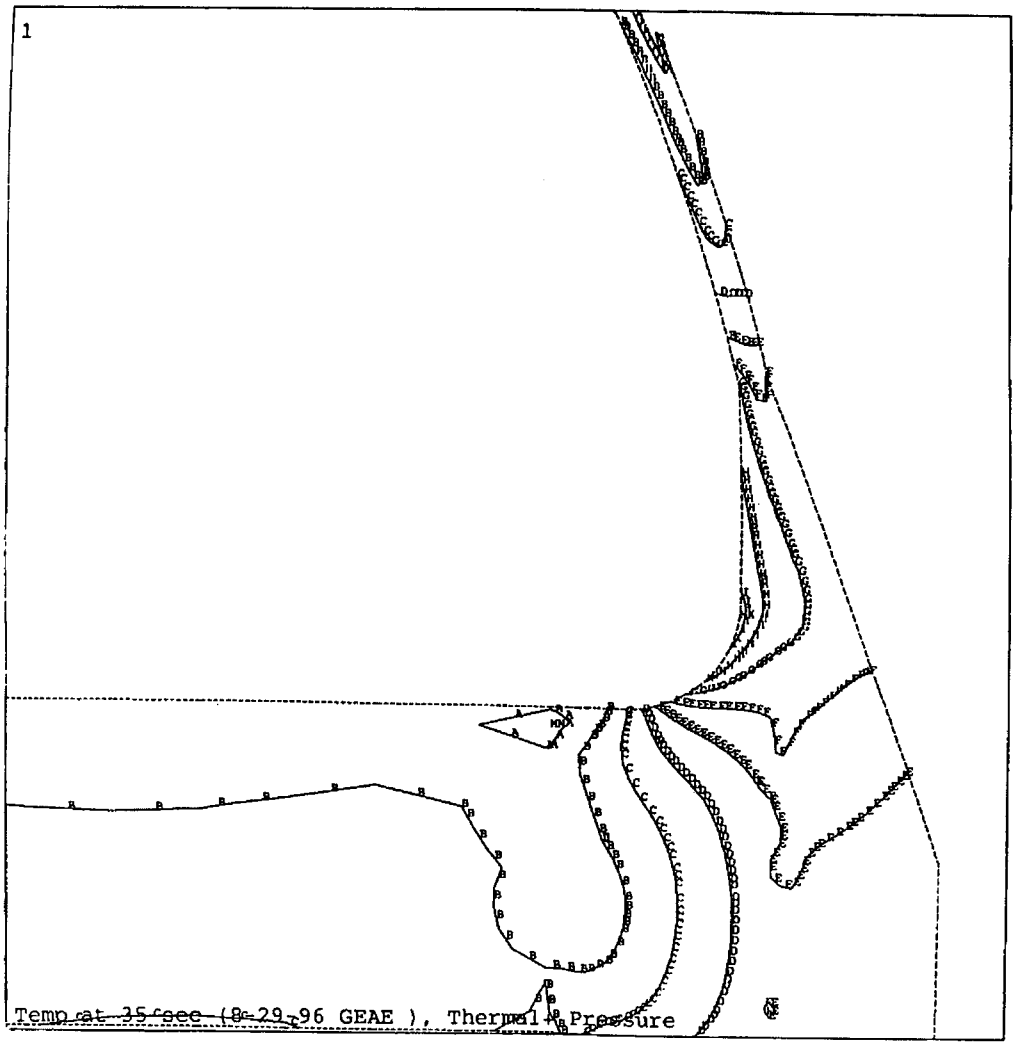
1
ANSYS 5.2
SEP 25 1996
13:44:38
PLOT NO. 2
NODAL SOLUTION
STEP=1
SUB =1
TIME=1
SEQV (AVG)
DMX =.066474
SMN =2043
SMX =106546
SMXB=108963
A =7848
B =19460
C =31071
D =42683
E =54294
F =65906
G =77517
H =89128
I =100740
Temp at 35 sec (8-29-96 GEAE), Thermal + Pressure

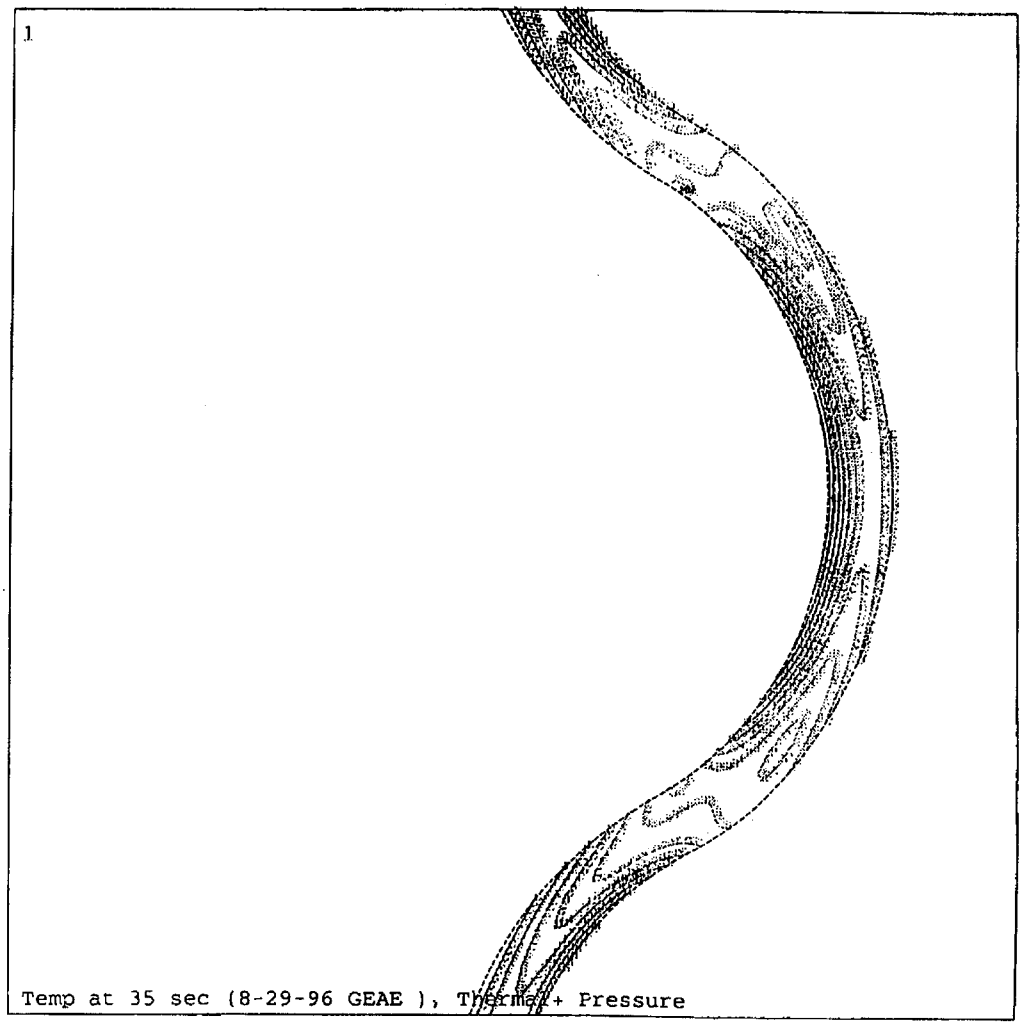
1
ANSYS 5.2
SEP 25 1996
13:36:22
PLOT NO. 1
NODAL SOLUTION
STEP=1
SUB 1
TIME=1
SEQV (AVG)
DMX =.049944
SMN =5516
SMNB=2881
SMX =84226
SMXB=85394
A =9889
B =18602
C =27380
D =36125
E =44871
F =53616
G =62362
H =71107
I =79853
Temp at 35 sec (8-29-96 GEAE), Thermal+ Pressure

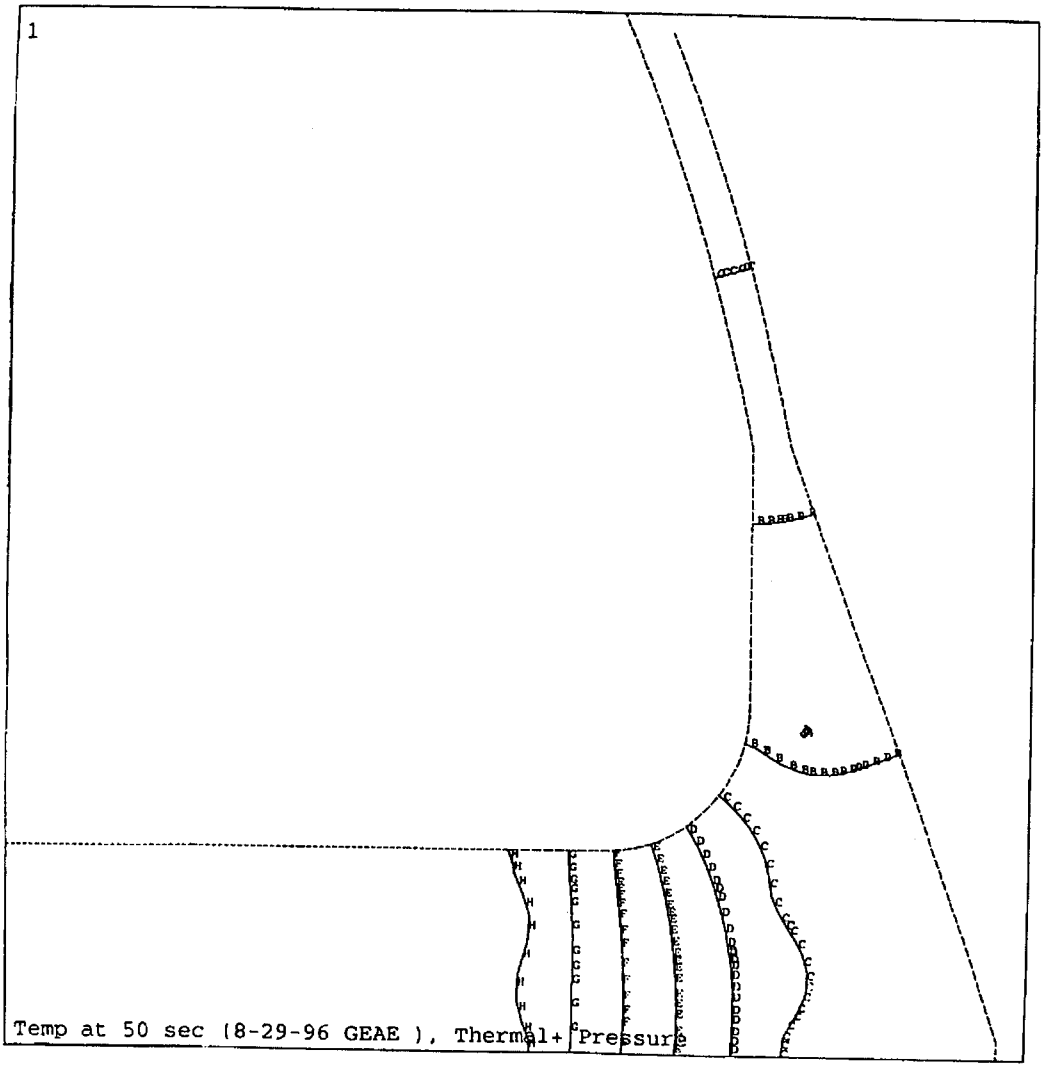
1
ANSYS 5.2
SEP 25 1996
13:51:42
PLOT NO. 1
ELEMENTS
TEMPERATURES
TMIN=235
TMAX=847
ZV =1
*DIST=.890955
*XF =2.969
*YF =.546815
EDGE
A =269
B =337
C =405
D =473
E =541
F =609
G =677
H =745
I =813
Temp at 50 sec (8-29-96 GEAE), Thermal+ Pressure

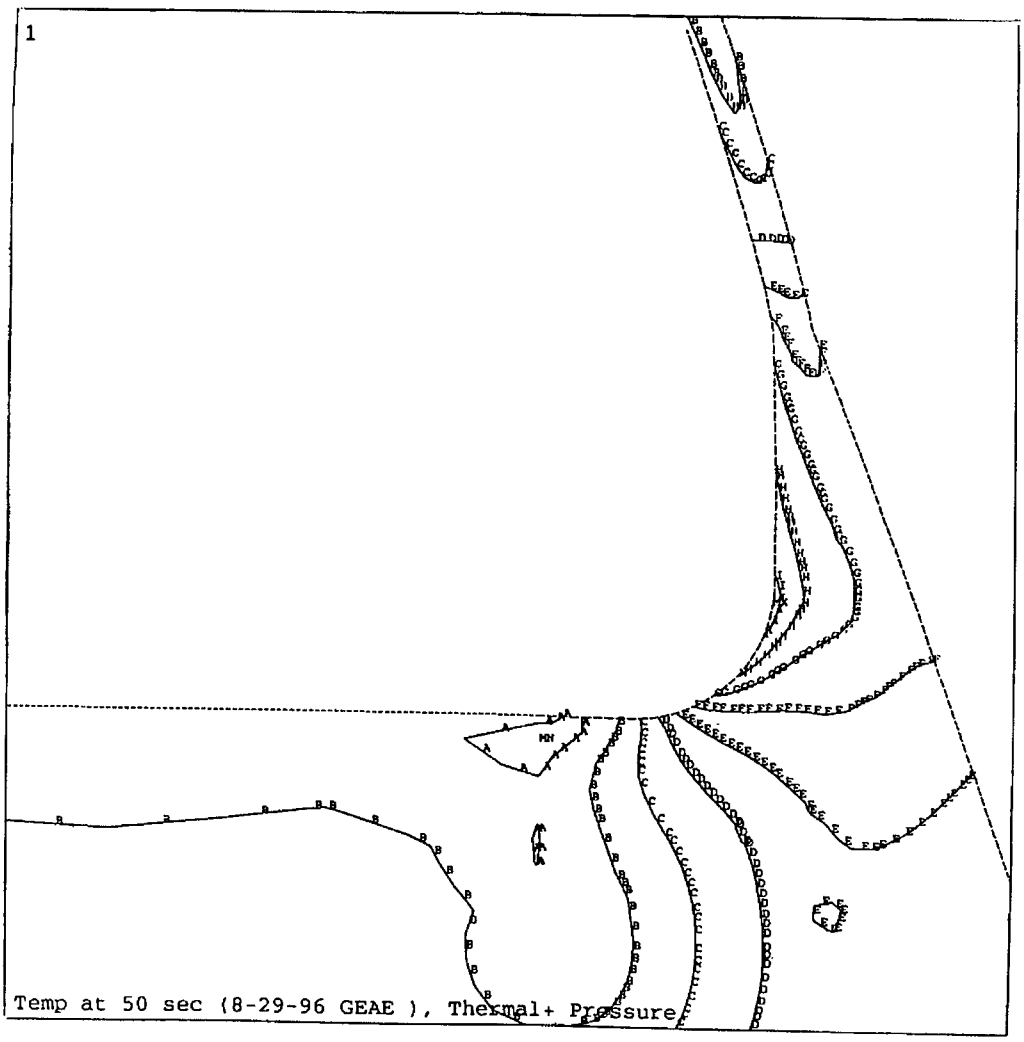
1
ANSYS 5.2
SEP 25 1996
13:52:13
PLOT NO. 2
NODAL SOLUTION
STEP=1
SUB =1
TIME=1
SEQV (AVG)
DMX =.075288
SMN =4098
SMNB=446.484
SMX =111288
SMXB=113732
A =10053
B =21963
C =33873
D =45783
E =57693
F =69603
G =81513
H =93423
I =105333
Temp at 50 sec (8-29-96 GEAE), Thermal+ Pressure

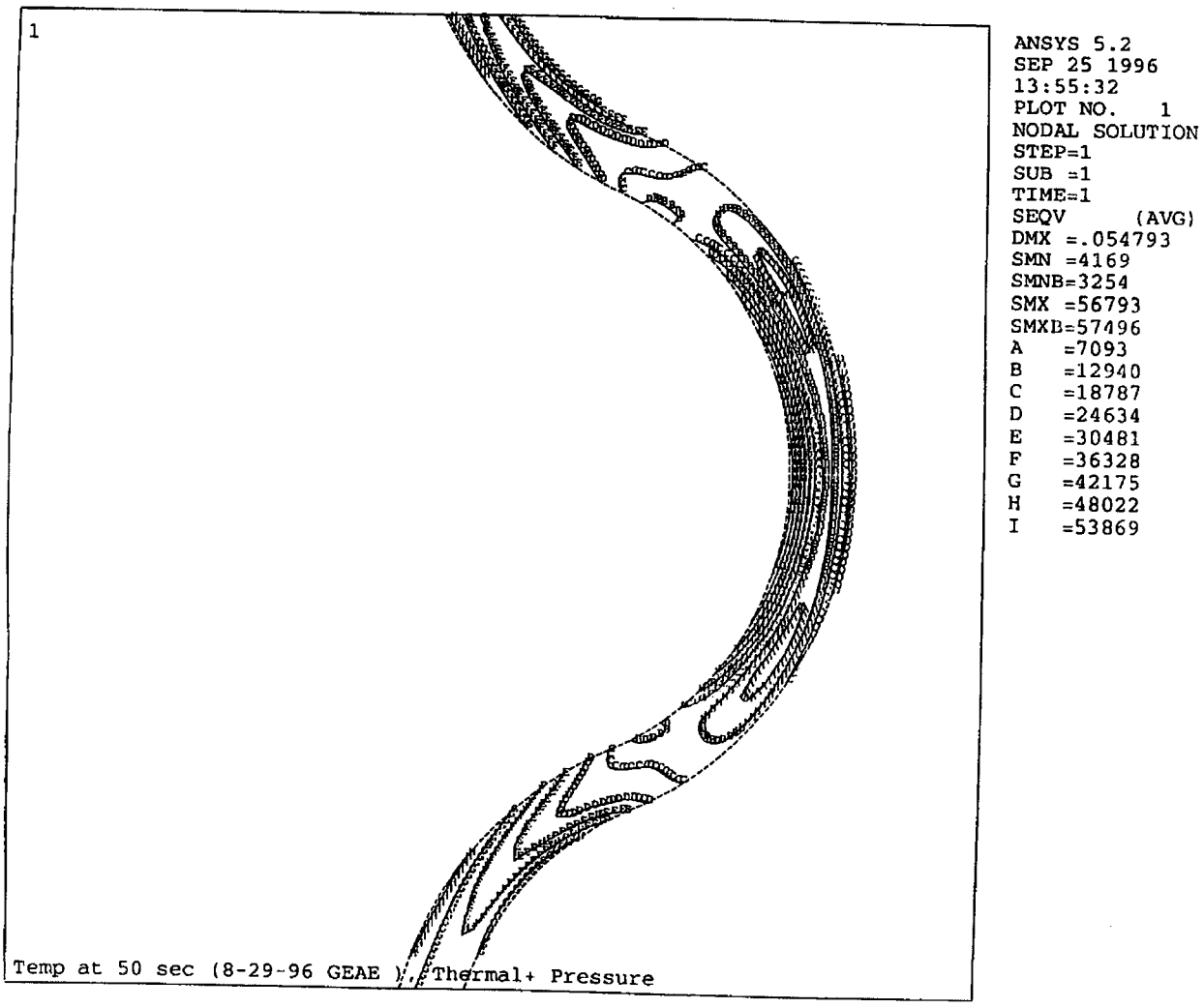
1
ANSYS 5.2
SEP 25 1996
13:55:32
PLOT NO. 1
NODAL SOLUTION
STEP=1
SUB =1
TIME=1
SEQV (AVG)
DMX =.054793
SMN =4169
SMNB=3254
SMX =56793
SMXB=57496
A =7093
B =12940
C =18787
D =24634
E =30481
F =36328
G =42175
H =48022
I =53869
Temp at 50 sec (8-29-96 GEAE) Thermal+ Pressure

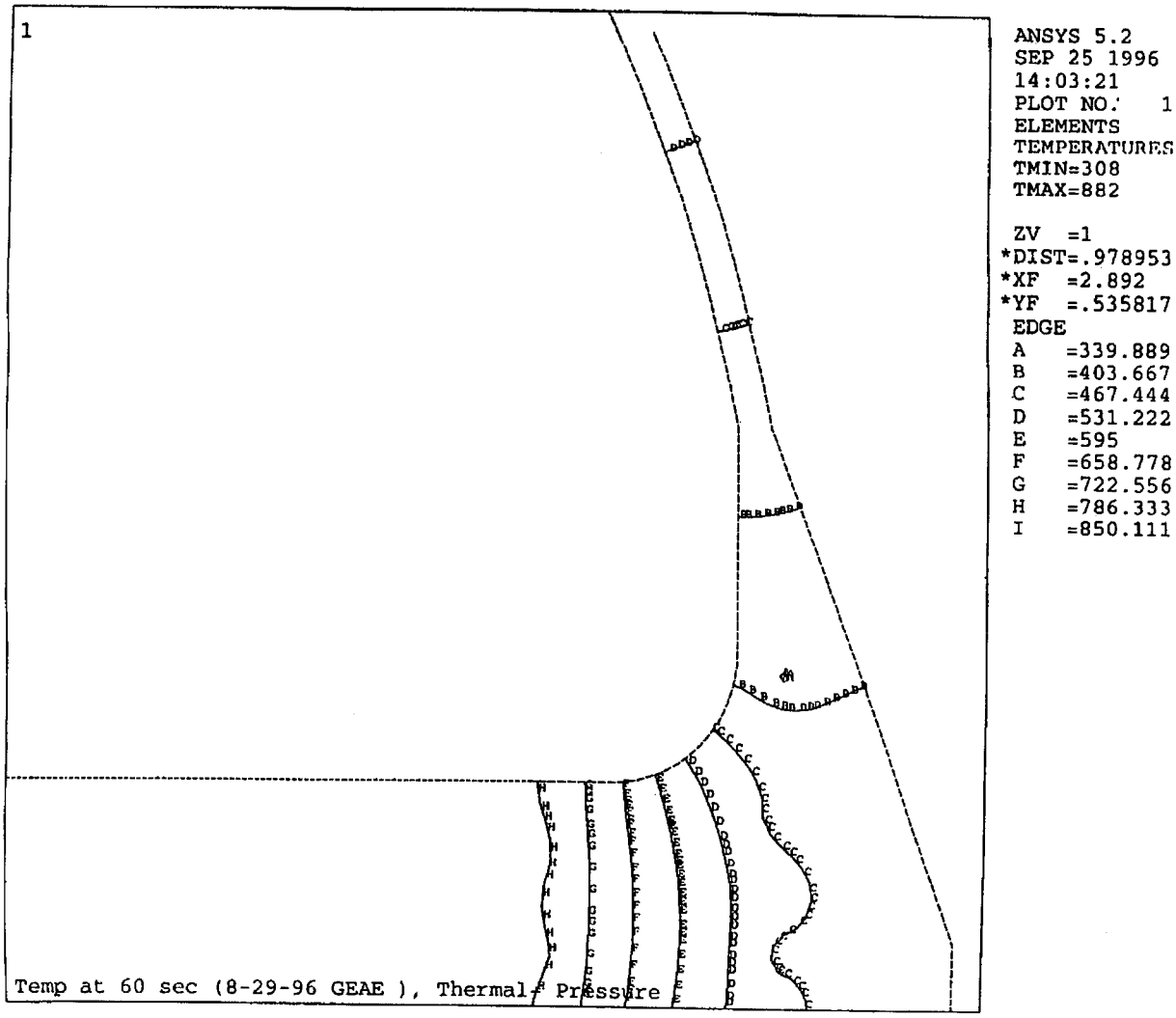
1
ANSYS 5.2
SEP 25 1996
14:03:21
PLOT NO. 1
ELEMENTS
TEMPERATURES
TMIN=308
TMAX=882
ZV =1
*DIST=.978953
*XF =2.892
*YF =.535817
EDGE
A =339.889
B =403.667
C =467.444
D =531.222
E =595
F =658.778
G =722.556
H =786.333
I =850.111
Temp at 60 sec (8-29-96 GEAE), Thermal Pressure

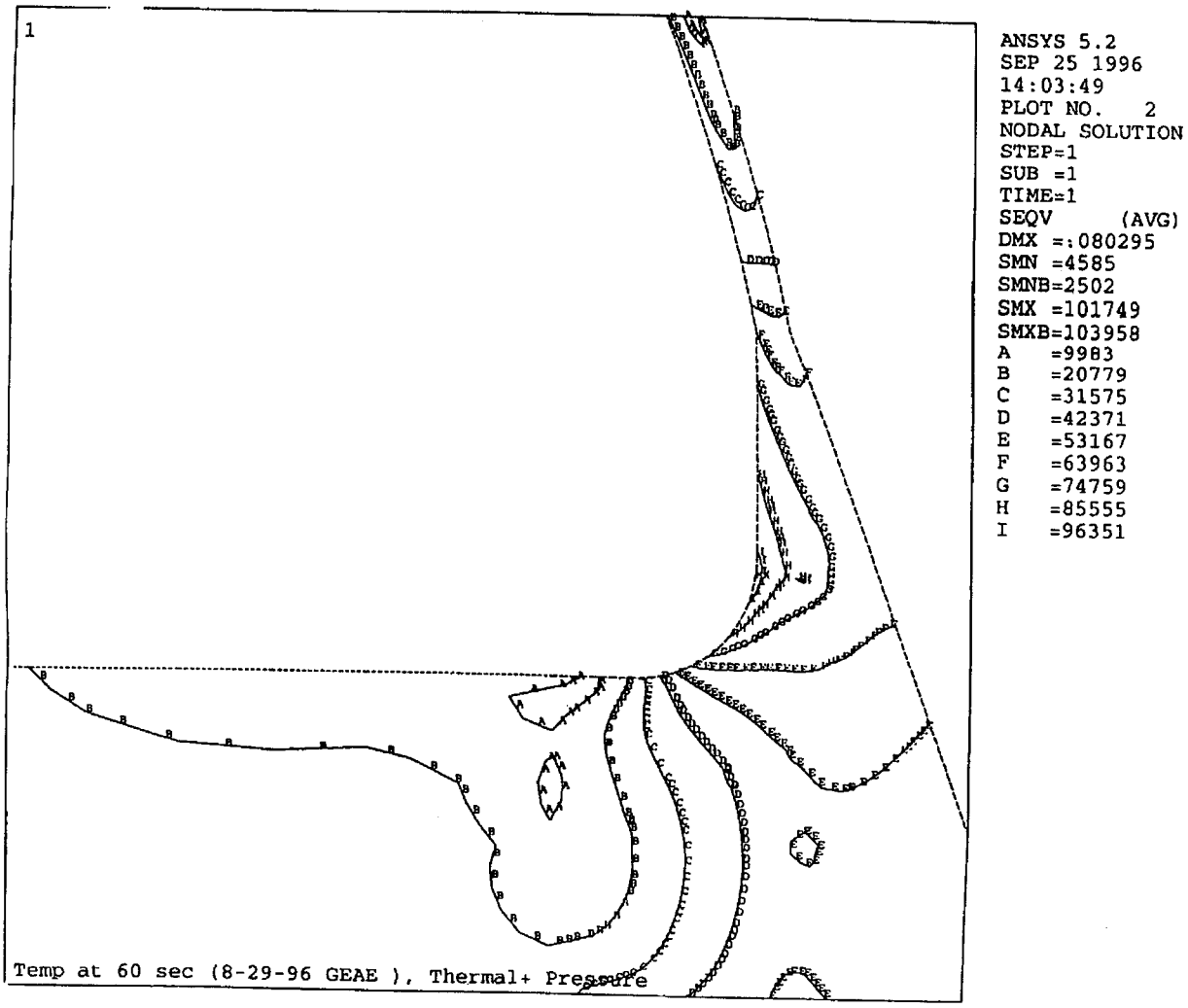
1
ANSYS 5.2
SEP 25 1996
14:03:49
PLOT NO. 2
NODAL SOLUTION
STEP=1
SUB =1
TIME=1
SEQV (AVG)
DMX =.080295
SMN =4585
SMNB=2502
SMX =101749
SMXB=103958
A =9983
B =20779
C =31575
D =42371
E =53167
F =63963
G =74759
H =85555
I =96351
Temp at 60 sec (8-29-96 GEAE), Thermal+ Pressure

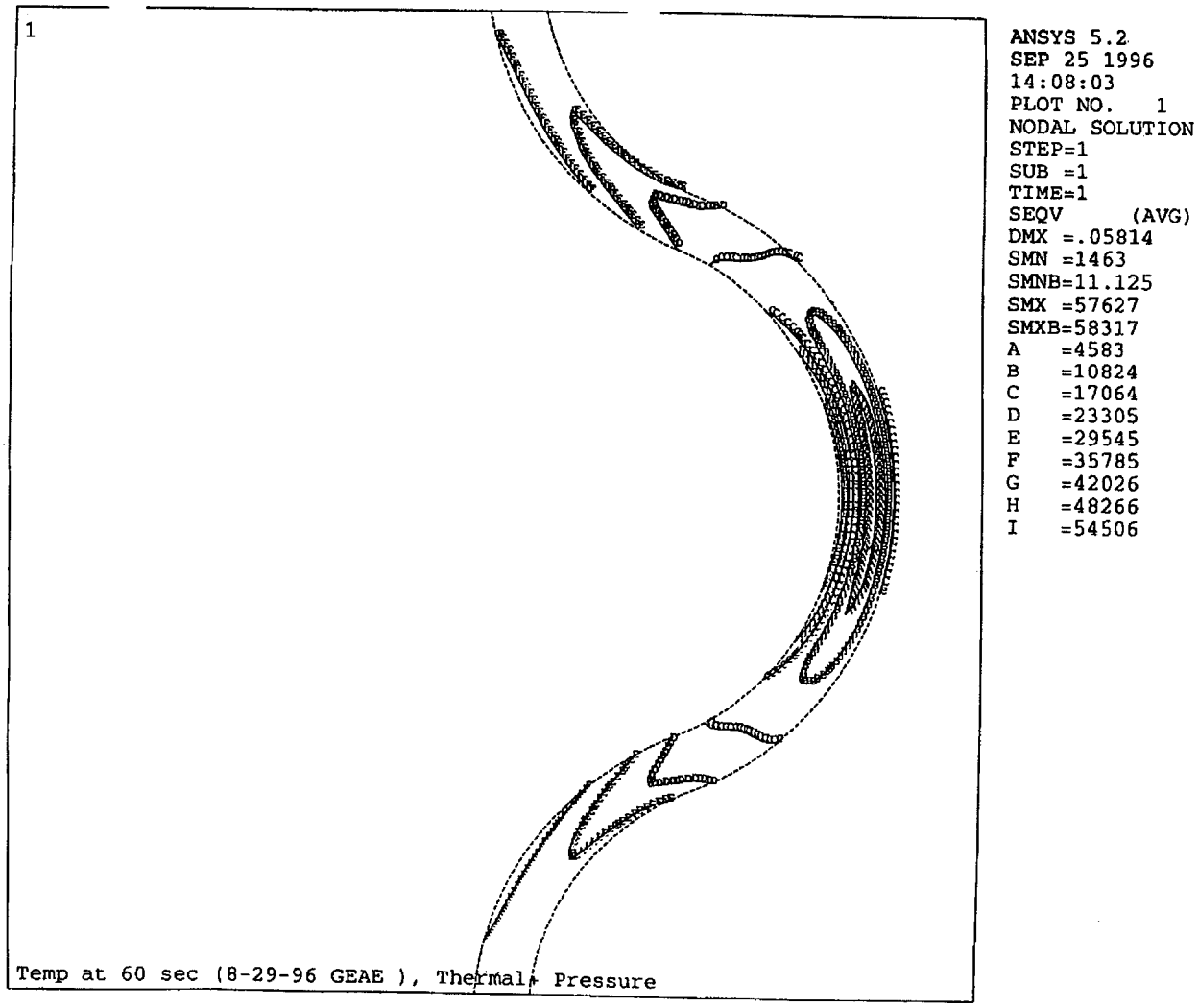
1
ANSYS 5.2
SEP 25 1996
14:08:03
PLOT NO. 1
NODAL SOLUTION
STEP=1
SUB =1
TIME=1
SEQV (AVG)
DMX =.05814
SMN =1463
SMNB=11.125
SMX =57627
SMXB=58317
A =4583
B =10824
C =17064
D =23305
E =29545
F =35785
G =42026
H =48266
I =54506
Temp at 60 sec (8-29-96 GEAE), Thermal Pressure

Acceptance Test Procedure

Procedure AT2341330 is reproduced from AlliedSignal report 97–69390, with permission. These scanned raster images are unedited — except for cropping to remove the original headers, footers, and pagination. Thus Table and Figure numbers and citations are in the original form and not reindexed to the sequence of this Final Report.

ACCEPTANCE TEST PROCEDURE
FUEL/AIR COOLER
2341330-1
GENERAL ELECTRIC

ACTIVE COOLING FOR ENHANCED PERFORMANCE
TURBOCOOLING SYSTEM

AT2341330 March 14, 1997

DATA TYPE II

DEPT	NAME		DATE	DEPT	NAME		DATE
93055	PREP		3-14-97		QUAL ASSUR		3-24-97
93055	EDIT		3-26-97	90100	MFG		3-24-97
	PROJECT		3/16/97		OTHER		3/14/97
93051	PROJECT		3/18/97	94100	OTHER		3-18-97
	MATLS ENGRG				CONFIG MGMT		

PRODUCTION

COMPUTER-PREPARED DOCUMENT. CHANGES MUST BE INCORPORATED VIA THE COMPUTER SYSTEM.

AlliedSignal Aerospace Equipment Systems	CAGE CODE	DOCUMENT NO	REV LTR	PAGE
	70210	AT2341330	-	1 OF 12

Form I-1531 (10/95)

1. SCOPE

This document specifies the tests to be conducted on each research unit of the Fuel/Air Cooler 2341330-1. Only those units which meet all of the test requirements shall be accepted for delivery to the customer.

2. GENERAL TEST REQUIREMENTS

2.1 TEST LOCATION

All tests described herein will be performed at the AlliedSignal Aerospace Equipment Systems (AES), Torrance, California.

2.2 AMBIENT CONDITIONS

Unless otherwise specified in an individual test description, all testing shall be conducted with the test unit at the ambient pressure and temperature existing in the test area at the time of the test.

2.3 TEST SURVEILLANCE AND WITNESSING

The tests required herein shall be conducted under the surveillance of the AES quality assurance department. Authorized customer representatives(s) may witness any or all testing.

2.4 TEST FACILITIES REQUIREMENT

The following special test equipment, or its equivalent, shall be used to conduct the test described in this document:

(a) Hydrostatic Test Stand

(b) Helium Leakage Test Stand

2.5 INSTRUMENTATION SELECTION AND CALIBRATION

Instrumentation shall be provided to measure the test parameters as listed in each test procedure below. The instrumentation shall be appropriate for the parameter being measured. The accuracy of the instruments shall be verified and certified or verified and calibrated periodically in accordance with the applicable government, commercial, and AES-Torrance specifications and procedures. Any certified or verified and calibrated instrument may be used providing the accuracy requirements are met. Standard conversion factors shall be used to convert parameter values when the selected instrumentation units of measurement differ from those presented in the test procedure. The parameters to be measured, nominal test values and required accuracy at the test values are given in Table 1.

2.6 TEST TOLERANCES

The test tolerances for test conditions and requirements are specified within the applicable paragraphs. The test tolerances are independent of the instrumentation accuracy.

2.7 FAILURE REPORTING

2.7.1 Failure Criteria

A failure is defined as any malfunction or combination of malfunctions that degrades any performance parameter to a level outside its specified performance limit. Every instance of performance outside of a performance limit, including intermittent operation, is considered a failure unless sufficient supportive data are provided to reclassify the occurrence as an incident. Test failures considered for reclassification as an incident will be demonstrated to be the direct result of: (1) accidents, (2) operator error, and (3) test equipment or test facility malfunction.

2.7.2 Failure Reporting and Closeout

Should a failure occur, the test shall be stopped and the failure recorded on the applicable data sheet in the acceptance test procedure and coordinated with the responsible engineer.

TABLE 1

INSTRUMENTATION ACCURACY REQUIREMENTS

Test Description	Parameter Measured	Nominal Test Value or Range	Required Accuracy at Test Value
Fuel circuit			
Proof Pressure	Pressure	2339 psig	±10 psig
	Time	5 minutes	±5 sec
	Displacement (sight gauge)	1 cm^3	±.10 cm^3
Leakage	Helium leakage	1.0×10^{-5} scc/sec	1.0×10^{-8} scc/sec
	Time	1 minute	±5 sec
Air circuit			
Proof Pressure	Pressure	812 psig	±5 psig
	Time	5 minutes	±5 sec
	Displacement (sight gauge)	1 cm^3	±.10 cm^3
Leakage	Pressure	812 psig	±5 psig
	Time	5 minutes	±5 sec
Both circuits drying	Temperature	250°F	±3°F
	Time	2 hours	±5 min

2.8 TEST SEQUENCE

(a) Before test examination

(b) Fuel side proof pressure

(c) Air side proof pressure and leakage

(d) Fuel side internal leakage

(e) Fuel side external leakage

(f) After-test examination

2.9 DATA RECORD

Test data shall be recorded by the test technician on the data sheets provided in the back of this document. As each test is performed, the test technician shall observe and record the data using black ink (erasures are not permitted). Each completed data sheet shall be signed and dated by the performing test technician, and stamped as either accepted or rejected by qualified personnel. If the data sheet is stamped as rejected, a statement describing the discrepancy shall be written in the REMARKS column.

3. TESTS

Records of satisfactory completion of any required assembly operations, inspections, weighing, or tests not covered by this ATP are provided on the Assembly Operation and Inspection Record (AOIR), Assembly Inspection Traveler (AIT), or other traveler. Procedures are specified, as applicable, in documents such as the Manufacturing Operations and Tooling (MOT) and Quality Assurance procedures.

3.1 BEFORE TEST EXAMINATION

Before performing the tests described herein, the test technician shall examine the unit for any evidence of physical damage such as cracks, dents, harmful scratches, etc., and record the results on the data sheet

3.2 FUEL SIDE PROOF PRESSURE AND LEAKAGE

CAUTION: DURING ANY HIGH PRESSURE TEST, CARE MUST BE TAKEN TO PROTECT PERSONNEL AND SURROUNDINGS AGAINST EXPLOSION HAZARD.

3.2.1 Setup

Connect one -16 fuel port to a static pressure fitting and plug all other fuel ports. Connect the static pressure fitting to a hydrostatic pressure source. Fill the air circuit with water and seal all air side bosses and flanges except the one which will be connected to a sight gage. See Figure 1. Place the unit in a safety enclosure or completely immerse it in a safety water bath.

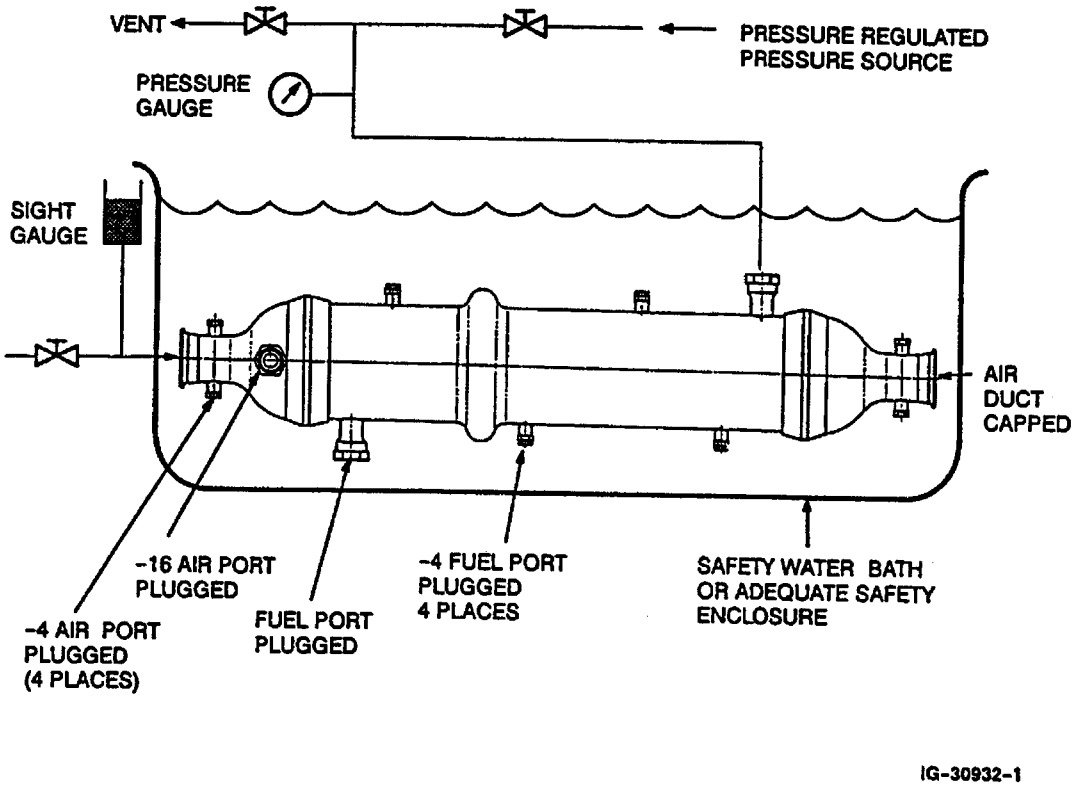

Figure 1. Fuel Circuit Proof Pressure Setup

3.2.2 Procedure

Hydrostatically pressurize the fuel side to 2339 (+24, -0) psig. Close off the pressure source at a point as close to the unit as practical and hold for 5 minutes minimum. Observe the air side sight gauge for displacement indicating leakage.

After release of the applied pressure, there shall be no evidence of permanent deformation (bulging or buckling). If the unit exhibits any pressure decay, external leakage, or sight gauge displacement, a pneumatic pressure test at 100 (+10, -0) psig may be conducted to detect the exact location of the leakage.

3.2.3 Acceptance Criteria

There shall be no visible external leakage, no pressure decay due to leakage, and no sight gauge displacement. To accommodate temperature related expansion or contraction of fluid volume, a minute sight gauge displacement, not to exceed 1 cc per minute of test duration (not to be interpreted as a rate, but rather a maximum), is permissible. In addition, minor variations in pressure gauge readings (less than .25% of the applied pressure) are permissible in either direction.

3.2.4 Drying

Dry the unit within 24 hours in an oven at 250 ±25°F for at least 2 hours. Leave all ports open to allow free circulation of air.

3.3 AIR SIDE PROOF PRESSURE AND LEAKAGE

This test is to be conducted hydrostatically.

CAUTION: DURING ANY HIGH PRESSURE TEST, CARE MUST BE TAKEN TO PROTECT PERSONNEL AND SURROUNDINGS AGAINST EXPLOSION HAZARD.

3.3.1 Setup

Seal one air flange, four -4 air side bosses, and one -16 air side boss. Connect the other air flange to a hydrostatic pressure source. Fill the fuel circuit with liquid, seal all fuel side bosses except one which will be connected to a sight gauge. See Figure 2.

3.3.2 Procedure

Apply a hydrostatic pressure of 812 (+10, -0) psig. Close off the pressure source at a point as close to the unit as practical and hold for 5 minutes minimum. Observe the fuel side sight gauge for displacement indicating leakage.

3.3.3 Acceptance Criteria

There shall be no visible leakage, no pressure decay due to leakage, and no sight gauge displacement. A minute sight gauge or pressure gauge movement as defined in paragraph 3.2.3 is permissible to accommodate temperature related changes in fluid volume.

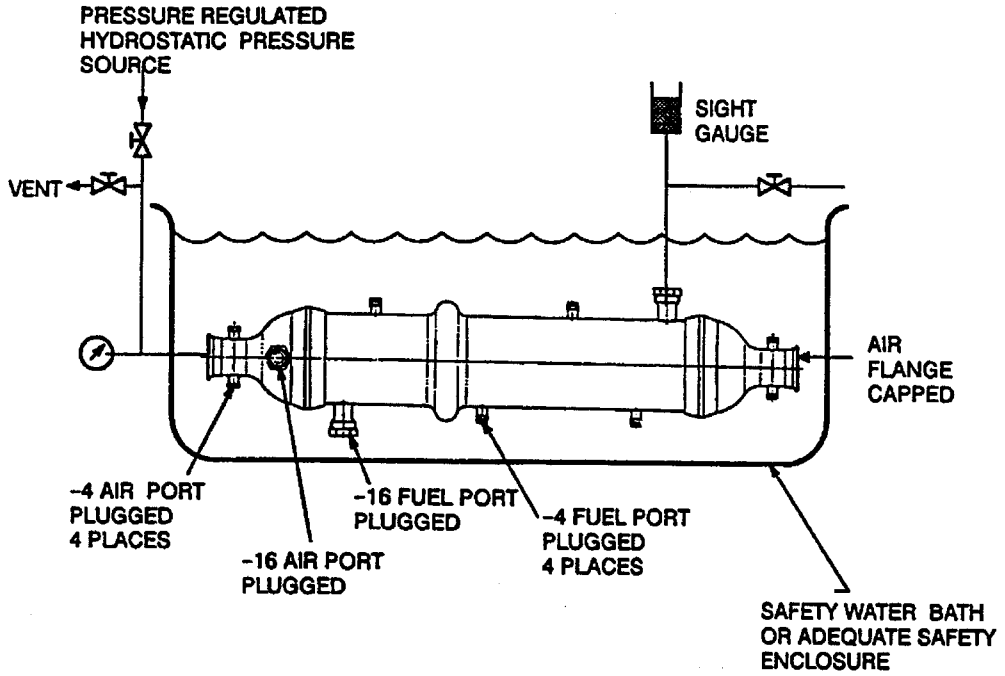

Figure 2. Air Circuit Proof Pressure and Leakage Setup

After release of the applied pressure, there shall be no evidence of permanent deformation (bulging or buckling). If the unit exhibits any pressure decay, external leakage, or sight gauge displacement, a pneumatic pressure test at 100 (+10, -0) psig may be conducted to detect the exact location of the leakage.

3.3.4 Drying

Dry the unit within 24 hours in an oven at 250 ±25°F for at least 2 hours. Leave all ports open to allow free circulation of air.

3.4 FUEL SIDE INTERNAL LEAKAGE

NOTE: **PRIOR TO PERFORMING THIS HELIUM LEAKAGE TEST, CLEAN THE UNIT INTERNALLY TO REMOVE ALL RESIDUE.**

3.4.1 Test Setup

Plug one -16 and four -4 fuel ports. Connect the remaining -16 fuel port to a helium mass spectrometer leak detector. On the air side, cap one air flange, plug four -4 air ports, plug one -16 air port, and connect the remaining air flange to a regulated helium source. See Figure 3.

3.4.2 Test Procedure

Using the leak detector vacuum roughing pump, evacuate the fuel circuit until the leak detector can be switched to the test mode. Apply helium at atmospheric pressure, ±.5 psi, to the air circuit. Measure the leakage rate for a minimum of 1 minute.

3.4.3 Success Criterion

The leakage rate shall not exceed 1.0×10^{-5} scc/sec for a minimum of 1 minute.

3.5 FUEL SIDE EXTERNAL LEAKAGE

3.5.1 Test Setup

Plug one -16 and four -4 fuel ports. Connect the remaining -16 fuel port to a helium mass spectrometer leak detector. On the air side, all flanges and ports shall remain open to allow the flow of helium into the cooler air circuit. Insert entire unit into an enclosure (plastic bag will suffice) capable of containing a regulated helium environment. See Figure 4.

3.5.2 Test Procedure

Using the leak detector vacuum roughing pump, evacuate the fuel circuit until the leak detector can be switched to the test mode. Apply helium at atmospheric pressure, ±.5 psi, to the enclosure surrounding the unit. Measure the leakage rate for a minimum of 1 minute.

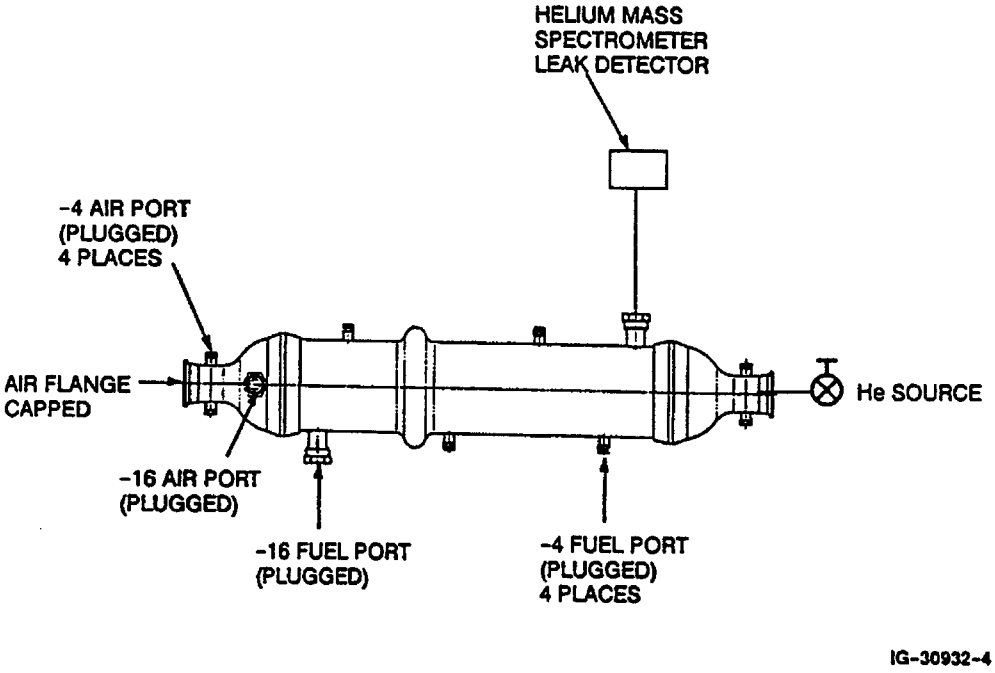

Figure 3. Fuel Circuit Internal Leakage Setup

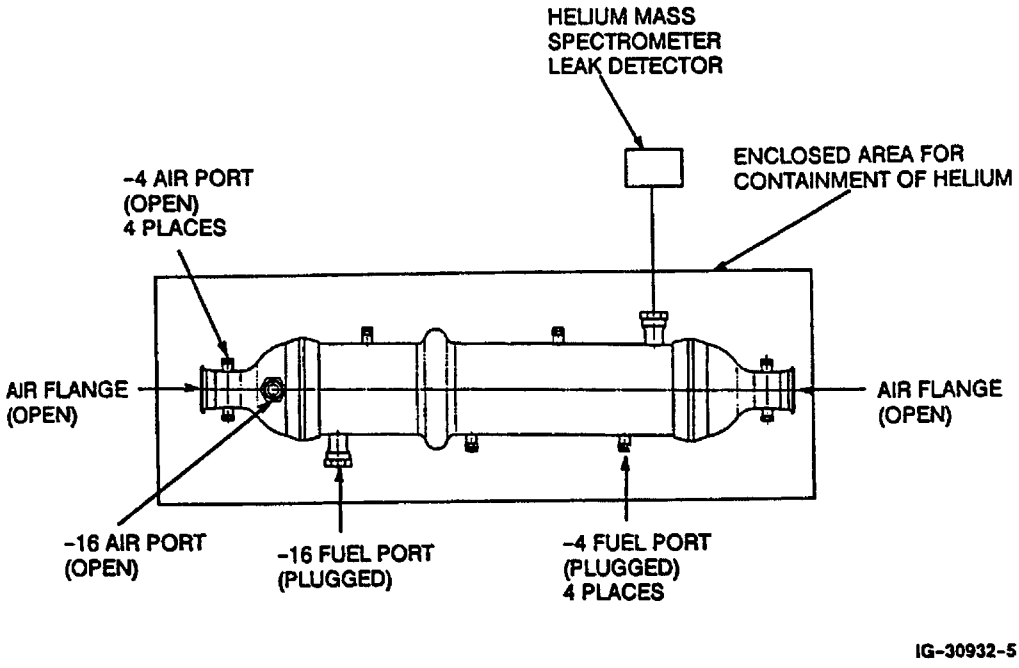

Figure 4. Fuel Circuit External Leakage Setup

3.5.3 Success Criterion

The leakage rate shall not exceed 1.0×10^{-5} scc/sec for a minimum of 1 minute. The difference between the internal leakage rate as measured in para 3.4, and the leakage rate measured in this section, will determine the presence of external leakage, and its corresponding rate.

3.6 CLEANLINESS

At the conclusion of all acceptance tests, flush each circuit for 5 minutes minimum with an aqueous solution of duraclean 212, followed by a de-ionized water flush for 5 minutes minimum. Dry unit within 24 hours in an oven at 250°F ±25°F for 2 hours minimum. Leave all ports open to allow free circulation of air.

3.7 AFTER-TEST EXAMINATION

After all tests have been completed, the test technician shall visually examine the unit for any evidence of physical damage such as cracks, dents, harmful scratches, etc. Record the results on the final data sheet.

DATA SHEET	PART NAME Fuel/Air Cooler	MFG SERIAL NO.
PAGE 1 OF 1	PART NO. 2341330	NAMEPLATE SERIAL NO.

Para.	Measurement or Observation	Required Min	Required Max	Actual
3.1	BEFORE TEST EXAMINATION	Accept ____		Reject ____
3.2	FUEL SIDE PROOF PRESSURE			
	Applied pressure, psig	2339	2363	
	Duration, minute	5	—	
	Sight gauge displacement	None		
	Visible deformation	None		
	Drying: 250 ±25°F for 2 hr	Technician's Initials ____		
3.3	AIR SIDE PROOF PRESSURE			
	Applied pressure, psig	812	822	
	Duration, minute	5	—	
	Sight gauge displacement	None		
	Visible leakage, interpassage	None		
	Visible leakage, external	None		
	Visible deformation	None		
	Drying: 250 ±25°F for 2 hr	Technician's Initials ____		
3.4	FUEL SIDE INTERNAL LEAKAGE			
	Duration, minutes	1	—	
	Leakage rate, scc/sec, helium	—	1.0×10^{-5}	
3.5	FUEL SIDE EXTERNAL LEAKAGE			
	Duration, minutes	1	—	
	Leakage rate, scc/sec, helium	—	1.0×10^{-5}	
3.6	CLEANLINESS	Technician's Initials ____		
3.7	AFTER-TEXT EXAMINATION	Accept ____		Reject ____

Appendix B – Instrumentation List

ACM Cart PS Parameters

TERM POS	COMP NAME	PARAMETER	AVG	RANGE
2	PT81AA	COMP INLT PT	A01	"
3	PT81BB	"	"	"
4	PT82AA	COMP EXIT PT	"	400A
6	PS84HX	HX2 AIR INLT PS	——	400A
7	PS85HX	HX2 INTRM AIR PS	——	"
8	PS855X	HX1 AIR INLT PS	——	"
9	PT90AA	ACM TRBN INLT PT	A01	350A
11	PT92AA	ACM TRBN EXIT PT	"	100A
12	PT92BB	"	"	"
13	PBRGF1	AIR BRNG FLTR P1	——	350A
14	PBRGF2	" P2	——	"
15	PCVACT	BLEED CV ACTUATOR PS	——	100A
16				
17				
18				
19				
NA	DPFFLT	FUEL FLTR DP	——	25D
NA	PFULEX	FUEL FROM HX2	——	1200A
NA	PFUL37	INTERM FUEL PS	——	1200A
NA	PF36IN	FUEL INLT TO HX1	——	1200A
NA	DPBFLT	AIR BRNG FLTR DP	——	5D
	ZVACM2	VERT ACM VIBE	——	10MIL
	ZHACM1	HOR ACM VIBE	——	10MIL
	XNTC81	ACM SHAFT SPEED	——	120K RPM

ACM Cart MB A Parameters

TERM POS	COMP NAME	PARAMETER	AVG	RANGE
MB A1	REF	MB REFERANCE	——	
2	TT81AA	ACM COMPR INLT TT	A03	1000F
3	TT81BB	"	"	"
4	TT82AA	" EXIT TT	"	"
6	TA84HX	HX2 AIR INLT TT	——	400F
7	TA85HX	HX2 INTERM AIR TT	——	800F
8	TA855X	HX1 AIR INLT TT	——	800F
9	TT90AA	ACM TRBN INLT TT	A03	400F
11	TT92AA	ACM TRBN EXIT TT	"	100F
12	TT92BB	"	"	"
14	TKDM01	HX2 AIR INLT DOM TSRF–1	——	1200F
15	TKDM02	" TSRF–2	"	"
16	TKDM03	" TSRF–3	"	"
17	TKDM04	" TSRF–4	——	"
18	TKDM05	" TSRF–5	——	"
20	TFUL37	INTRM FUEL TT	——	700F
21	TFLEX1	FUEL EXIT FROM H2X	R05	1000F
25	REF	REFRENCE		
	PFLDYN	DYN FUEL PS AT CMBSTR MAN.	——	TBD
	HSCN01	HC SNIFFER @ TRBN INLT	——	TBD
	HSCN02	HC SNIFFER @ ACM CART	——	"

Combustor Vehicle PS

TERM POS	COMP NAME	PARAMETER	AVG	RANGE
HOK B1	PSB3IN	BLEED PORT ADAPT PS	———	350A
2	PTCOM1	COMB INLT PT	R01	350A
3	PTCOM2	"	"	"
4	PTCOM3	"	"	"
5	PS41AA	COMB DISCH PS	A03	350
6	PS41AB	"	"	"
7	PS41AC	"	"	"
8	PT40A1	COMB DISCH PT, GAS SAMP RAKE	A05	350
9	PT40A2	"	"	"
10	PT40A3	"	"	"
11	PT40A4	"	"	"
12	PT40A5	"	"	"
13	PT40B1	"	"	"
14	PT40B2	"	"	"
15	PT40B3	"	"	"
16	PT40B4	"	"	"
17	PT40B5	"	"	"
18	PS31XX	Diffuser dnstrm Ps.	———	"
19				
20				
21				
22				
23				
24				
	HSCN03	HC SNIFFER AT FUEL MAN.	———	
	PCMDYN	COMB KULITE	———	10psi ptp
	PFMANX	COMB FUEL MAN PS	———	1000A

Combustor Vehicle MB B

TERM POS	COMP NAME	PARAMETER	AVG	RANGE
MB B1	REF	REFERENCE		
2	TKFMAN	FUEL MAN SKIN TC	——	1000F
3	TKCLU1	COMB UPR LNR SKIN TC	——	1600F
4	TKCLU2	COMB UPR LNR SKIN TC	——	1600F
5	TKCLU3	COMB UPR LNR SKIN TC	——	1600F
6	TKCLU4	COMB UPR LNR SKIN TC	——	1600F
7		Delete		
8	TKCLL1	COMB LWR LNR SKIN TC	——	1600F
9	TKCLL2	COMB LWR LNR SKIN TC	——	1600F
10	TKCLL3	COMB LWR LNR SKIN TC	——	1600F
11	TKCLL4	COMB LWR LNR SKIN TC	——	1600F
12		Delete		
13	TT30AX	COMB INLET TT	A05	1000F
14	TT30BX	"	"	"
15	TT30CX	"	"	"
16	TTHUBX	TRAV HUB COOLING TEMP	——	250F
17	TTMTR1	TRAV MOTOR 1 TEMP	——	"
18	TT3BIN	BLEED HOSE ADPTR TT	——	900F
19	TFLNOZ	FUEL MANIFOLD TT	——	1000F
20	TKTERM	ACTUATOR TERM STRIP TEMP	——	
21	TKARM1	TRAV RAKE ARM TC	——	
22	TKARM2	"	——	
23	TKARM3	"	——	
24	TTMTR2	TRAV MOTOR 2 TEMP	——	

Combustor Venicle Traverse

TERM POS	COMP NAME	PARAMETER	AVG	RANGE
NA	TT39A1	COMB DISCH TRAV RAKE TT R10	A10	3200F
NA	TT39A2	COMB DISCH TRAV RAKE TT R10	A10	3200F
NA	TT39A3	COMB DISCH TRAV RAKE TT R10	A10	3200F
NA	TT39A4	COMB DISCH TRAV RAKE TT R10	A10	3200F
NA	TT39A5	COMB DISCH TRAV RAKE TT R10	A10	3200F
NA	TT39A6	COMB DISCH TRAV RAKE TT R10	A10	3200F
NA	TT39B1	COMB DISCH TRAV RAKE TT R10	A10	3200F
NA	TT39B2	COMB DISCH TRAV RAKE TT R10	A10	3200F
NA	TT39B3	COMB DISCH TRAV RAKE TT R10	A10	3200F
NA	TT39B4	COMB DISCH TRAV RAKE TT R10	A10	3200F
NA	TT39B5	COMB DISCH TRAV RAKE TT R10	A10	3200F
NA	TT39B6	COMB DISCH TRAV RAKE TT R10	A10	3200F

Facility PS

TERM POS	COMP NAME	PARAMETER	AVG	RANGE
	P1MAOA	MAIN AIR ORF	A01	400A
	P1MAOB	"	"	"
	P2MAOA	"	A03	400A
	P2MAOB	"	"	"
	P1W10A	WEST 10" BLD ORF	A01	100A
	P1W10B	"	"	"
	P2W10A	"	A03	"
	P2W10B	"	"	"
	PTRVCL	TRAV COOLING, COLD CA SPLY	——	400A
	PSQNRN	PS QUENCH, RING	——	1000A
	PSQNBR	PS QUENCH, BARS	——	1000A
	PSPURG	FAC PURGE MANIFOLD	——	500A
	PSQNHB	PS QUENCH, HUB/RAKES	——	1000A
	PSEXHD	EXHAUST DUCT PS	——	20A

Facility Temperatures

TERM POS	COMP NAME	PARAMETER	AVG	RANGE
	T1MAOA	MAIN AIR ORF TT	A03	1000F
	T1MAOB	"	"	"
	T110WA	WEST 10" BLD ORF TT	R03	100F
	T110WB	"	"	"
	TSEVEN	BLAST GATE TT (T7)	———	500F
	TTEXHD	EXHAUST DUCT TT	———	500F

Facility Fuel

TERM POS	COMP NAME	PARAMETER	AVG	RANGE
	CPSMAN	FUEL FLOW METER, FM3066	———	900pph
	CPSVER	", FM3067	"	"
	PFMANA	FLOW METER PS	A05	1200A
	PFMANB	"	"	"
	TFUELA	FUEL TT AT FLOWMETER	R05	AMB
	TFUELB	"	"	"

Appendix C – Phase I Performance Calculations

This appendix presents a listing of the Phase I performance calculations program together with a test case.

```
C*****************************************************************
C      PROGRAM ACEP
C*****************************************************************
C     Created for ACEP Test Program in CA19.
C     -----------
C     | PURPOSE |
C     -----------
C
C     PHASE I CALCULATIONS BASED ON MEASURED EU'S, CALCULATED AVG'S
C
C
C     ---------------
C     | ADS SECTION |
C     ---------------
C
C
C     PROCEDURE FOR RUNNING A TEST CASE:
C
C        embedded test case
C        external test case
C
C
C     PROCEDURE FOR EXECUTION:
C
C         PROGRAM RUNS UNDER AUTOPROCESSING.
C
C
C     ----------------------
C     | SUBROUTINE SECTION |
C     ----------------------
C
C     LIBRARIES:
C     FULL FUEL THERMO ROUTINES NOT INCLUDED
C
C
C     SPECIAL  :
C
C     -----------
C     | COMMONS |
C     -----------
C
C     GLOBAL        :  NONE
C
C
C     PRIVATE SHARED:  NONE
C
C
```

```
C     ------------------------
C     | SPECIAL INSTRUCTIONS |
C     ------------------------
C     UNITS TABLE DEFINITIONS:
C
C          1 = CUBIC IN
C          2 = INCHES
C          3 = CUBIC FT
C          4 = FEET
C          5 = SQ IN
C          6 = FT/SEC
C          7 = PERCENT
C          8 = LBS
C          9 = LB/HR
C         10 = LB/SEC
C         11 = LB/HR/LB
C         12 = BTU/LB
C         13 = PPH
C         14 = SCFM
C         15 = PSIG
C         16 = PSI
C         17 = PSIA
C         18 = PSID
C         19 = RPH/PSIA
C         20 = GRAINS
C         21 = UNITS
C         22 = DEGREES
C         23 = DEG F
C         24 = DEG R
C         25 = RPM
C         26 = GPM
C         27 = MPH
C         28 = VDC
C
C
C
C   TYPEFL - TYPE OF FUEL AND VISCOSITY DATA REFERENCE
C
C                1.0----JP4              - ESSO *
C                2.0----JP4, JET B       - CRC **
C                3.0----JP5,             - ESSO
C                4.0----JP5, JET A, JP-8 - CRC
C                5.0----JP7              - CRC
C                6.0----MARINE DIESEL    - GE TM 81-315, SHAYESON
C
C          * ESSO = DATA BOOK FOR DESIGNERS
C                   Aviation Fuels and Lubricating Oils
C                   Complied by ESSO Standard Oil Company
C                   December 1, 1956
C
C          ** CRC = HANDBOOK OF AVIATION FUEL PROPERTIES
C                   COORDINATING RESEARCH COUNCIL
C                   CRC REPORT NO. 530
C                   May 1984
```

```
C
C
C SPECIAL NOTES:
C
C
C    --------------------------------
C    | DEFINITION OF MAJOR VARIABLES |
C     --------------------------------
C
C         MAJOR VARIABLES FOLLOW DATA BASE CODE DEFINITION.
C
C
$I,EU
       PSB3IN          256.11
       PSB3EX        196.08
       PS84HX        309.31
       PS85HX          290.46
       PS855X        290.5
       PBRGF1          350.0
       PBRGF2        345.0
       PFULEX           547.41
       PFUL37            551.54
       TA84HX            1050.1
       TA85HX         664.
       TA855X          664.
       TKDM01           1050.
       TKDM04          1050.
       TFUL37           538.
       PFMANX          930.
       CPSMAN         679.64
       CPSVER               679.64
       PFMANA                930.
       PFMANB               930.
       TFUELA         100.
       TFUELB               100.
       XNTC81            66145.
       PF36IN               554.76
       PSEXHD          15.0
       PBARO1         14.4
       TFLNOZ           873.5
$
$I,CON
       BCRC81           1.03
       BCRC91             0.985
       BCRC84           1.045
       DIA91             4.75
       GRAV            32.2
       CJ             778.16
       GAM            1.33
       CPAIR          0.24
       CPFUL1          0.52
        CPFUL2         0.8357
       HV              18200.0
       PFLOW          20.0
```

```
       PFHIGH              1500.0
       PFTOL                  5.0
        TFLOW             -10.0
       TFHIGH              120.0
         TFTOL              10.0
        MAODIA            5.875
        MAOPIP            11.75
        MAOTYP           1.0
        WBODIA              4.0
       WBOPIP               8.0
       WBOTYP           1.0
       CONXN           1.0
       BYPCON              0.7978
$
$I,MA
        SGFUEL               0.81
       TFSG01                68.0
       TYPEFL              1.0
         RUNNUM             1.0
        POINT               2.0
$
$I,AVG
       AVPT81                 196.08
       AVPT82           309.96
       AVPT90            276.69
        AVPT92            53.08
        AVTT81            859.
       AVTT82              1050.1
        AVTT90             294.1
       AVTT92          52.
        RTFLEX              873.5
       RPTCOM          275.43
        AVPS41           255.75
        AVPT40           255.45
       AVTT30         859.
       AVTT39         2563.3
       AVP1MA           366.1
       AVP2MA                275.43
       AVP1W1             53.08
        AVP2W1           49.81
       AVT1MA          859.0
       RT110W           52.0
       RTFUEL         100.0
$
$B,BANNER
       RUNNUM
       POINT
$
$O,CAL1
      WAMAIN           <10>
      WAACM               <10>
      WF36AV              <9>
       WACOMB          <10>
        DTCOMB            <23>
```

```
        FARCOM          <RAT>
        ETACOM
        WFULNZ         <9>
        DPFNOZ            <18>
       FNDPSY
        FNNOZ
       DPCOMB          <18>
        DPCOMP         <7>
        FFCOMB
       AECOMB      <5>
       DPEXHD        <18>
       PRACM          <RAT>
      DPACM          <18>
      DPBFLT           <18>
       DPFFLT         <18>
       EFCTHX             <RAT>
      P84DQ8           <RAT>
       H4RK
       DPFLXQ           <RAT>
       AVPT39
       WCOMB
       AVGWF
       WAR
       AVFUEL
       T4RKAV          <23>
       SWT4RK
       DPPTP               <7>
$
$O,CAL2
      THT81
      DLT81
      WCOR81          <10>
      P82Q81
      T82Q81
      XNR81            <25>
       ETA81
      PW81              <HP>
      T81CF         <23>
      T82CF          <23>
      PW81C         <HP>
      ETA81C        <RAT>
      WR81CM          <LBM/MIN>
      XNR81C         <25>
      SMW81           <7>
$
$O,CAL3
      WCOR90           <10>
      P92Q90
      P90Q92
      ETA90
      UTIP90             <6>
      XNR90           <25>
      PW90                 <HP>
      ETAMEC
```

```
      FV90
      T92CF          <23>
      ETA90C        <RAT>
      PW90C        <HP>
$
$O,CAL4
       EFFHX1
       QAIR85              <B/SEC>
       WCAP85         <B/SEC/DEG>
       DPQP85
        TAAVG1         <23>
        QFL85H          <B/HR>
       QFL85S           <B/SEC>
        FCAP85         < B/SEC/DEG>
        TFAVG1       <23>
        UAHXM1         <B/HR/DEG>
        CMNHX1           <B/SEC/DEG>
        CRHX1
       XNUTM1
        ARG1
        EFHXM1
$
$O,CAL5
      EFFHX2
        QAIR84            <B/SEC>
        WCAP84        <B/SEC/DEG>
        DPQP84
        TAAVG2          <23>
        QFL84H       <B/HR>
       QFL84S            <B/SEC>
        FCAP84        <B/SEC/DEG>
        TFAVG2          <23>
        UAHXM2         <B/HR/DEG>
        CMNHX2        <B/SEC/DEG>
        CRHX2
        XNUTM2
        ARG2
        EFHXM2
        PQM3
       DTHDR            <22>
$END
C
C
      REAL*4 MAODIA,MAOPIP,MAOTYP,MAODPQ
C
C     PROGRAM CONSTANTS
      INCLUDE 'constx'
C
C
      CHARACTER*6 CVWFMN /'CVWFMN'/
      CHARACTER*6 CVWFVF /'CVWFVF'/
C
C     JFUELX USED BY SUBROUTINE FUELX
      INTEGER   JFUELX(10)
```

```
C
C     JHUMBA USED BY SUBROUTINE HUMBAR
      INTEGER JHUMBA(10)
      $DBI
C
      CALL PUTLAB(0,'ENGINEERING UNITS')
      $P,EU
       CALL PUTLAB(0,'AVERAGES')
      $P,AVG
       CALL PUTLAB(0,'CONSTANTS')
      $P,CON
      CALL PUTLAB(0,'MANUAL INPUTS')
      $P,MA
C
C                          CALCULATIONS:
C
C     FUEL FLOW CALCULATIONS FOR VOLUMETRIC METERS
C
C     ITEST,SGFUEL,TFSG01,TYPEFL,PFLOW,PFHIGH,PFTOL,TFLOW,
C     TFHIGH,TFTOL are config constants and manual inputs
C
C **** FACILITY TOTAL fuel flowmeters
C
      CALL FUELX(ITEST,SGFUEL,TFSG01,TYPEFL,CPSMAN,TFUELA,
     &           PFMANA,CPSVER,TFUELB,PFMANB,CVWFMN,CVWFVF,
     &           PFLOW,PFHIGH,PFTOL,TFLOW,TFHIGH,TFTOL,
     &           TFMTOT,TFVTOT,TFUELT,DTFTOT,PFMTOT,PFVTOT,
     &           PFMQVF,WFMAIN,WFVERI,GPMTTM,GPMTTV,SG6060,
     &           PSCM,PSCV,JFUELX)
C
C                Average of fuelflows for main and verif. meters
      AVWFTT = (WFMAIN + WFVERI) * 0.5
       TF36IN=RTFUEL
C
      WFTTDF = ABS( 100. * (1.-(WFMAIN/WFVERI)) )
      IF (WFTTDF .GT. 5.0) THEN
      WRITE(IERMSG,1001) PROGID
      WRITE(IERMSG,1004)PROGID,WFTTDF
      END IF
 1001 FORMAT(A10,6X)
 1004 FORMAT(A10,6X,'***** WARNING : WFMAIN vs WFVERI DEVIATION(%)=',
     &F15.5,'  *****')
      IF(JFUELX(4) .NE. 0.0) THEN
      WRITE(IERMSG,1001) PROGID
      WRITE(IERMSG,1200) PROGID,DTFTOT
 1200 FORMAT(A10,6x,'WARNING : TOTAL FUEL FLOWMETER TEMP. SPREAD =',
     &F10.3,'DEG F')
      END IF
C
C                      AIR FLOW CALCULATIONS
C
C         MAOPIP = Pipe dia.
C         MAODIA = Orifice dia.
C         MAOBET = Orifice Beta ratio
```

```
C
C
      WAMAIN = 0.0
       MAODPQ=(AVP1MA-AVP2MA)/AVP1MA
C
      CALL AIRFLO(AVP1MA,AVP2MA,AVT1MA,MAOPIP,MAODIA,MAOTYP,WAMAIN)
      IF(MAODPQ .GT. 0.35)THEN
      WRITE(IERMSG, 1300)PROGID
       END IF
 1300 FORMAT(/2X,"WARNING: MAO DP/P EXCEEDS 0.35")
      CALL AIRFLO(AVP1W1,AVP2W1,RT110W,WBOPIP,WBODIA,WBOTYP,WAACM)
      WBODPQ=(AVP1W1-AVP2W1)/AVP1W1
      IF(WBODPQ .GT. 0.35)THEN
      WRITE(IERMSG, 1310)
 1310 FORMAT(/2X,"WARNING: WBO DP/P EXCEEDS 0.35")
       END IF
       IF(WBODPQ .LE. 0.01)THEN
       WAACM = 0.0
       END IF
C
C
C
C               ACM COMPRESSOR:
C
       THT81=(AVTT81+C459)/518.7
         DLT81=AVPT81/14.696
        WCOR81=WAACM*SQRT(THT81)/DLT81*BCRC81
       P82Q81=AVPT82/AVPT81
        T82Q81=(AVTT82+C459)/(AVTT81+C459)
          XNR81=XNTC81/SQRT(THT81)
       H82D8S = HT(TCSTP(AVTT81+C459,P82Q81))-HT(AVTT81+C459)
      H82D81 = HT(AVTT82+C459)-HT(AVTT81+C459)
       ETA81 = 999.
       IF (H82D81.NE.0.0)  ETA81 =  H82D8S/H82D81
       PW81=WAACM*BCRC81*H82D81*1.4148
       PQM3=PSB3IN/AVPT81
       T81QM=(1.+((BCRC81-
     &  1.)*(AVTT90+C459)+4.3/(WAACM*0.245))/(AVTT81+C459))/BCRC81
      T81CR=(AVTT81+C459)*T81QM
      TDJC=1.71/(WAACM*0.245*(BCRC84-BCRC81))
       T82QM=(BCRC84-(AVTT90+C459+TDJC)*(BCRC84-
     & BCRC81)/(AVTT82+C459))/BCRC81
      T82CR=(AVTT82+C459)*T82QM
      H82DC=HT(T82CR)-HT(T81CR)
      H82DCS=HT(TCSTP(T81CR,P82Q81))-HT(T81CR)
      ETA81C= -999.
      IF(H82DC.GT.0.0) ETA81C=H82DCS/H82DC
      PW81C=WAACM*BCRC81*H82DC*1.4148
      XNR81C=XNR81/SQRT(T81QM)
      WR81CM=WCOR81*SQRT(T81QM)*60.
      PQ81S=(2.79E-4*WR81CM+2.94E-2)*WR81CM+0.827064
      SMW81=(PQ81S/P82Q81-1.)*100.
C
```

```
C             ACM TURBINE:
C
        WCOR90=WAACM*SQRT(AVTT90+C459)/AVPT90*BCRC91
       P92Q90=AVPT92/AVPT90
       P90Q92 = 1./P92Q90
       H90D9S = HT(AVTT90+C459) - HT(TCSTP(AVTT90+C459,P92Q90))
       H90D92 = HT(AVTT90+C459) - HT(AVTT92+C459)
        ETA90 = 999.
       IF (H90D9S.NE.0.) ETA90 = H90D92/H90D9S
        UTIP90=XNTC81*DIA91/229.2
       XNR90 = XNTC81/(SQRT((AVTT90+C459)/518.7))
       FV90 = UTIP90/SQRT(2.*GRAV*CJ*H90D9S)/0.707
       PW90=WAACM*BCRC91*H90D92*1.4148
       T92QM=(1.-(1.-BCRC91)*(AVTT90+C459+TDJC)/(AVTT92+C459))/BCRC91
       T92CR=(AVTT92+C459)*T92QM
       H90DC=HT(AVTT90+C459)-HT(T92CR)
       ETA90C= -999.
       IF(H90D9S.GT.0.) ETA90C=H90DC/H90D9S
       PW90C=WAACM*BCRC91*H90DC*1.4148
       ETAMEC=PW81C/PW90C
       PRACM=AVPT81/AVPT92
       DPACM=AVPT81-AVPT92
       DPBFLT=PBRGF1-PBRGF2
C
C        HEAT EXCHANGER 1, FUEL INLET:
C
        WF36AV=AVWFTT
        EFFHX1=(TA855X-AVTT90)/(TA855X-TF36IN)
       QAIR85=WAACM*BCRC84*(HT(TA855X+C459)-HT(AVTT90+C459))
        WCAP85=WAACM*BCRC84*CT(TA855X+C459)
       IF (TA855X.NE.AVTT90)   WCAP85=QAIR85/(TA855X-AVTT90)
         DPQP85=(PS855X-AVPT90)/PS855X
        TAAVG1=(TA855X+AVTT90)/2.0
     CALL J50PTX(PF36IN,TF36IN,0.,HFULIN,SFULIN,DUM1,CPFIN,DNFIN,DUM2,
    &   PRNFIN,DUM3,THCFIN,DUM4,VSCFIN)
     CALL J50PTX(PFUL37,TFUL37,0.,HFUL37,SFUL37,DUM1,CPF37,DNF37,DUM2,
    &   PRNF37,DUM3,THCF37,DUM4,VSCF37)
      QFL85H=WF36AV *(HFUL37-HFULIN)
       QFL85S= QFL85H/3600.0
        FCAP85= WF36AV*CPFIN/3600.
      IF (TFUL37.NE.TF36IN) FCAP85= QFL85S /(TFUL37-TF36IN)
      TDAF11 = TA855X-TFUL37
      TDAF12 = AVTT90-TF36IN
      TDLX1 = MAX(0.5*(TDAF11+TDAF12),1.0)
      TFAVG1 = (TF36IN + TFUL37)/2.
      IF (TDAF11.NE.TDAF12.AND.TDAF11.NE.0.0.AND.TDAF12.NE.0.0)
    &                      TDLX1 = (TDAF11-TDAF12)/ALOG(TDAF11/TDAF12)
       UAHXM1=QAIR85/TDLX1*3600.
      CMNHX1=MAX(0.1,MIN(WCAP85,FCAP85))
      IF (WCAP85.EQ.CMNHX1) CRHX1 = WCAP85/FCAP85
      IF (FCAP85.EQ.CMNHX1)  CRHX1 = FCAP85/WCAP85
         XNUTM1= UAHXM1/(CMNHX1*3600.)
       ARG1=EXP(XNUTM1*(CRHX1-1))
        EFHXM1=(1-ARG1)/(1-CRHX1*ARG1)
```

```
C
C             HEAT EXCHANGER 2, HOT FUEL:
C
      EFFHX2=(TA84HX-TA85HX)/(TA84HX-TFUL37)
       TAAVG2=(TA85HX+TA84HX)/2.0
       CP8485=CT(TAAVG2+C459)
       QAIR84= WAACM*BCRC84*(HT(TA84HX+C459)-HT(TA85HX+C459))
       WCAP84=WAACM*BCRC84*CT(TA85HX+C459)
       IF (TA84HX.NE.TA85HX) WCAP84= QAIR84/(TA84HX-TA85HX)
        DPQP84=(PS84HX-PS85HX)/PS84HX
       CALL J5OPTX(PFULEX,RTFLEX,0.,HFULEX,SFULEX,DUM1,CPFEX,DNFEX,DUM2,
     & PRNFEX,DUM3,THCFEX,DUM4,VSCFEX)
       QFL84H= WF36AV*(HFULEX-HFUL37)
        QFL84S= QFL84H/3600.
       FCAP84 = WF36AV*CPF37/3600.
         IF (RTFLEX.NE.TFUL37)  FCAP84= QFL84S/( RTFLEX-TFUL37)
        TFAVG2=(RTFLEX+TFUL37)/2.0
       TDAF21 = TA84HX-RTFLEX
       TDAF22 = TA85HX-TFUL37
       TDLX2 = MAX(0.5*(TDAF21+TDAF22),1.0)
       IF (TDAF21.NE.TDAF22.AND.TDAF21.NE.0.0.AND.TDAF22.NE.0.0)
     &                       TDLX2 = (TDAF21-TDAF22)/ALOG(TDAF21/TDAF22)
         UAHXM2= QAIR84/TDLX2*3600.
          CMNHX2= MAX(0.1,MIN(WCAP84,FCAP84))
       IF (WCAP84.EQ.CMNHX2) CRHX2 = WCAP84/FCAP84
       IF (FCAP84.EQ.CMNHX2)  CRHX2 = FCAP84/WCAP84
          XNUTM2= UAHXM2/(CMNHX2*3600.)
         ARG2=EXP(XNUTM2*(CRHX2-1.0))
         EFHXM2=(1.-ARG2)/(1.-CRHX2*ARG2)
       DPFFLT = PFULEX - PFMANX
       DTHDR=TA84HX-TKDM04
C
C   OVERALL HEAT X PERFORMANCE, COOLING EFFECT & DP.
C
       EFCTHX = (TA84HX- AVTT90)/(TA84HX-TF36IN)
       P84DQ8=(PS84HX-AVPT90)/PS84HX
       DPFLXQ=(PF36IN-PFULEX)/PF36IN
C              COMBUSTOR:
C
        WACOMB=(WAMAIN-WAACM)*BYPCON
        DTCOMB=AVTT39-AVTT30
        FARCOM=WF36AV/(WACOMB*3600.)
       T4RKAV=AVTT30+0.15*(TFLNOZ-
     &   120.)+(0.9875*FARCOM*18400.)/((0.244+2.184*FARCOM)*(1.+FARCOM))
       SWT4RK=(AVTT39-T4RKAV)/T4RKAV
       HF36 = 172.2 + HFULEX
       H30 = HT(AVTT30+C459)
       H4RK = HTF(AVTT39+C459,FARCOM)*(1.+FARCOM)
        ETACOM=((H4RK-H30) / FARCOM - HF36)/HV
        DPCOMB=RPTCOM-AVPS41
         DPCOMP=100.*DPCOMB/RPTCOM
         FFCOMB=WACOMB**2.0*(AVTT30+C459)/RPTCOM**2.0
        DPEXHD=PSEXHD-PBAR01
      AECOMB=(WACOMB/1.098)*SQRT((AVTT30+C459)/(RPTCOM*DPCOMB))
```

```
      AVPT39=AVPT40
      WCOMB=WACOMB
      AVGWF=WF36AV
      WAR=60.0
      AVFUEL=RTFUEL
      DPPTP=100.*(RPTCOM-AVPT40)/RPTCOM
C
C            FUEL NOZZLE:
C
      WFULNZ=WF36AV/18.
       DPFNOZ=PFMANX-AVPS41
        FNNOZ=WFULNZ/SQRT(DPFNOZ)
      FNSF36=.75347+RTFLEX*(-1.706E-3+RTFLEX*2.6853E-6)
      FNDPSY=(72.088*ALOG(WFULNZ)-97.698)*MAX(FNSF36,0.75)
      T81CF=T81CR-C459
      T82CF=T82CR-C459
      T92CF=T92CR-C459
C
C                PRINTOUT SECTION
C
$PAGE
C
$DBO
      CALL PUTLAB(0,'OVERALL & COMBUSTOR CALCS.')
      $P,CAL1
       CALL PUTLAB(0,'COMPRESSOR CALCS.')
      $P,CAL2
      CALL PUTLAB(0,'TURBINE CALCS.')
      $P,CAL3
      CALL PUTLAB(0,'HEAT X1 CALCS.')
      $P,CAL4
      CALL PUTLAB(0,'HEAT X2 CALCS.')
      $P,CAL5
       STOP
      END
C
C            AIR THERMO FUNCTIONS:
C
       FUNCTION GT(T)
C    GAMMA FOR AIR
       C=CT(T)
       C=14.584356*C
       GT=C/(C-1)
       RETURN
       END
C
       FUNCTION CT(T)
C    SPECIFIC HEAT FOR AIR
       DATA A1,A2,A3,A4,A5,A6,A7,A8/1.0115540E-25,-1.452677E-21,
     &7.6215767E-18,-1.5128259E-14,-6.7178376E-12,6.5519486E-08,
     &-5.1536879E-05,2.5020051E-01/
       CT=((((((A1*T+A2)*T+A3)*T+A4)*T+A5)*T+A6)*T+A7)*T+A8
       RETURN
       END
```

```
C
      FUNCTION HT(T)
C ENTHALPY FOR AIR
      DATA B1,B2,B3,B4,B5,B6,B7,B8,B9/1.2644425E-26,-2.0752522E-22,
     & 1.2702630E-18,-3.0256518E-15,-1.6794594E-12,2.1839826E-08,
     & -2.5768440E-05,2.5020051E-01,-1.7558886E00/
      HT=(((((((B1*T+B2)*T+B3)*T+B4)*T+B5)*T+B6)*T+B7)*T+B8)*T+B9
      RETURN
      END
C
      FUNCTION TCSTP(T,PR)
C TEMPERATURE FOR ISENTROPIC PROCESS
      A=ALOG(PR)
      G=GT(T)
      U=T*EXP(A*(G-1.)/G)
      G=GT(.5*(T+U))
      U=T*EXP(A*(G-1.)/G)
      TCSTP=U*(1.+(ST(T)+A*.068566621-ST(U))/CT(U))
      RETURN
      END
C
      FUNCTION ST(T)
C ENTROPY FUNCTION FOR AIR - TEMPERATURE PART ONLY
      DATA C0,C1,C2,C3,C4,C5,C6,C7,C8/2.5020051E-01,1.4450767E-26,
     &-2.4211288E-22,1.5243153E-18,-3.7820648E-15,-2.2392790E-12,
     &3.2759743E-08,-5.1576879E-05,4.5432300E-02/
      ST=C0*ALOG(T)+((((((C1*T+C2)*T+C3)*T+C4)*T+C5)*T+C6)*T+C7)*T+C8
      RETURN
      END
C
      FUNCTION HF(T)
C ENTHALPY FOR COMBUSTION PRODUCTS
      DATA E1,E2,E3,E4,E5,E6,E7,E8,E9/
     &9.0848388E-26,-1.9050949E-21,1.7021525E-17,-8.4102208E-14,
     &2.4921698E-10,-4.5906332E-7,6.129315E-4,7.3816638E-2,3.058153E+1/
      HF=(((((((E1*T+E2)*T+E3)*T+E4)*T+E5)*T+E6)*T+E7)*T+E8)*T+E9
      RETURN
      END
C
      FUNCTION HTF(T,F)
C ENTHALPY FOR AIR AND PRODUCTS OF COMBUSTION
      H = HT(T)
      HTF = H + (HF(T)-H)*F/(1.+F)
C       FOLLOWING IS EMPIRICAL CORRECTION FOR DISSOCIATION
C       APPLICABLE  FOR EXPECTED RIG OPERATING LINE
      DIS = AMIN1(1.008 - 1.37952E-5*HTF, 1.000)
      HTF = HTF/DIS
      RETURN
      END
C
C      END OF AIR THERMO FUNCTIONS.
```

REPORT DOCUMENTATION PAGE

Form Approved
OMB No. 0704-0188

1. AGENCY USE ONLY (*Leave blank*)	2. REPORT DATE	3. REPORT TYPE AND DATES COVERED
	January 2001	Final Contractor Report

4. TITLE AND SUBTITLE

Design, Fabrication, and Testing of an Auxiliary Cooling System for Jet Engines

5. FUNDING NUMBERS

WU–529–40–14–00
NAS3–27395

6. AUTHOR(S)

Kevin Leamy, Jim Griffiths, Paul Andersen, Fidel Joco, and Mark Laski

7. PERFORMING ORGANIZATION NAME(S) AND ADDRESS(ES)

GE Aircraft Engines
One Neumann Way
Cincinnati, Ohio 54215–6301

8. PERFORMING ORGANIZATION REPORT NUMBER

E–12402

9. SPONSORING/MONITORING AGENCY NAME(S) AND ADDRESS(ES)

National Aeronautics and Space Administration
Washington, DC 20546–0001

10. SPONSORING/MONITORING AGENCY REPORT NUMBER

NASA CR—2001-210353
R2000AE114

11. SUPPLEMENTARY NOTES

Kevin Leamy and Jim Griffiths, GE Aircraft Engines, One Neumann Way, Cincinnati, Ohio 54215–6301; Paul Andersen, Fidel Joco, and Mark Laski, Honeywell, Inc., 2525 West 190th Street, Torrance, California 90509. Project Manager, Jeffrey S. Balser, Aeropropulsion Research Program Office, NASA Glenn Research Center, organization code 0141, 216–433–5714.

12a. DISTRIBUTION/AVAILABILITY STATEMENT

Unclassified - Unlimited
Subject Categories: 07 and 28 Distribution: Nonstandard

Available electronically at http://gltrs.grc.nasa.gov/GLTRS

This publication is available from the NASA Center for AeroSpace Information, 301–621–0390.

12b. DISTRIBUTION CODE

13. ABSTRACT ***(Maximum 200 words)***

This report summarizes the technical effort of the *Active Cooling for Enhanced Performance* (ACEP) program sponsored by NASA (NAS3–27395). It covers the design, fabrication, and integrated systems testing of a jet engine auxiliary cooling system, or turbocooler, that significantly extends the use of conventional jet fuel as a heat sink. The turbocooler is designed to provide subcooled cooling air to the engine exhaust nozzle system or engine hot section. The turbocooler consists of three primary components: (1) a high-temperature air cycle machine driven by engine compressor discharge air, (2) a fuel/air heat exchanger that transfers energy from the hot air to the fuel and uses a coating to mitigate fuel deposits, and (3) a high-temperature fuel injection system. The details of the turbocooler component designs and results of the integrated systems testing are documented. Industry Version—Data and information deemed subject to *Limited Rights* restrictions are omitted from this document.

14. SUBJECT TERMS

Auxiliary cooling system; Turbocooler; High-temperature fuel

15. NUMBER OF PAGES

189

16. PRICE CODE

A09

17. SECURITY CLASSIFICATION OF REPORT	18. SECURITY CLASSIFICATION OF THIS PAGE	19. SECURITY CLASSIFICATION OF ABSTRACT	20. LIMITATION OF ABSTRACT
Unclassified	Unclassified	Unclassified	